C4R

Capacity for Rail

Towards an affordable, resilient, innovative and high-capacity European Railway System for 2030/2050

Innovative designs and methods for VHST

Submission date: 21/08/2017

Deliverable 12.2

This project has received funding from the European Union's Seventh Framework Programme for research, technological development and demonstration under grant agreement n° 605650








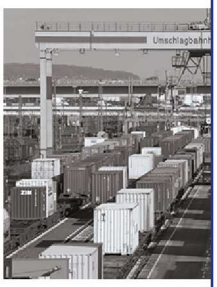

Collaborative project SCP3-GA-2013-60560
Increased Capacity 4 Rail networks through enhanced infrastructure and optimised operations
FP7-SST-2013-RTD-1

Lead contractor for this deliverable:

- KTH Kungliga Tekniska Högskolan

Contributors:

- ADIF
- SYSTRA
- INECO,
- CEDEX

Project coordinator

- International Union of Railways, UIC

Executive Summary

This deliverable presents important aspects of railway bridge dynamics for very high speed lines, comprising analysis, modelling procedures and full scale testing. A state-of-the-art in the subject is also given focusing on the choice models, especially regarding boundary conditions, load distribution and soil-structure interaction.

Parametric studies on common types of beam and portal frame bridges are presented for speeds up to 480 km/h. The results show the importance of considering the effect of train-bridge interaction, the effect of track irregularities and rail surface roughness. Possible solutions for vibrations reduction are presented and discussed.

For verification, a full scale test on a portal frame bridge on Madrid-Lérida high-speed line is presented and results are compared with theoretical models.

The analysis work and the writing of this document has been performed by KTH Royal Institute of Technology in Sweden and Systra in France, as follows:

- KTH: Chapter 1 – Chapter 7, except Section 4.3
- Systra: Section 4.3 and Chapter 7

Appendix A is written by CEDEX and includes a description of the in-situ test campaign performed in November 2015.

Keywords: Railway bridges, dynamics analysis, train models, full scale test, damper, soil-structure interaction, load distribution.

Project team members: ADIF, KTH, SYSTRA, INECO, CEDEX

The authors of this report have used their best endeavours to ensure that the information presented here is of the highest quality. However, no liability can be accepted by the authors for any loss caused by its use.

Table of contents

Abbreviations and acronyms

Abbreviation / Accronym	Description
HSR	High Speed Rail
VHST	Very High Speed Track
SSI	Soil-Structure-Interaction
TBI	Train-Bridge-Interaction
TMD	Tuned Mass Damper
FVD	Fluid Viscous Damper
KTH	Royal Institute of Technology, Stockholm

1. Background

There is an increased demand on the railway sector and much resource is spent on increasing the capacity of the existing network as well as expanding and connecting new lines. The European Commissions is working towards the creation of a Single European Railway Area and has promoted a modal shift from road to rail to achieve more competitive and resource-efficient transport system [1]. The European Commission White Paper [2] outlines the following targets:

- 30% of the road freight over 300 km should shift to other modes such as rail or waterborne transport by 2030 and to more than 50% by 2050.
- Aim to triple the length of the existing high-speed railway (HSR) network by 2030 and complete a European HSR rail network by 2050. By 2050, the majority of medium distance passenger transport should go by rail.
- By 2050, connect all core network airports to the rail network, preferably by HSR and ensure that all core seaports are sufficiently connected to the rail freight.

Hence, a considerable investment will be needed to expand and upgrade the capacity of the rail network infrastructure. To realise these ambitious goals, much effort must be spent on finding viable solutions. This includes:

- Finding methods to prove that a larger share of the existing infrastructure can be upgraded to future demands with sufficient safety margins.
- Finding more cost- and time efficient methods in building new railway infrastructure.
- Finding optimal solutions considering investment, whole life cycle cost and environmental impact.

A substantial share of the infrastructure consists of railway bridges. There are more than 300,000 railway bridges in Europe and a survey covering more than 220,000 of these [3] showed that more than 35% of the bridges are older than 100 years and only 11% are newer than 10 years. Further, 62% of the bridges have a span less than 10 m and only 5% are longer than 40 m. Among the top 10 priority research areas, better assessment tools and verification of dynamic amplification factors were mentioned.

Railway bridges are often subjected to significant dynamic loading due to passing trains. The dynamic response depends on a large number of factors involving the characteristics of the train, the track, the bridge and the substructure. For more than 100 years, dynamic effects have been accounted for in design of bridges by factoring the static response. Early on, this factor resulted in an increase of the design axle load in the range of 30 – 80%. Even the design codes of today (EN 1991-2) stipulate factors that may range up to 70%, both considering equivalent and real train load models. Especially for short and medium span bridges and bridge components, the design codes suggest large dynamic factors. This is likely over-conservative and if the factors can be proven to be smaller, there is great potential in upgrading existing railway bridges to higher loads and to enable more cost-effective new bridge solutions.

At higher train speeds, resonance effects may occur, depending on the natural frequency of the bridge and the axle spacing of the train. This was first observed in the 1980ies when the high-speed line between Paris and Lyon was opened. Large vibrations of the bridges was transmitted to the ballasted track and resulted in track misalignment. This results in dramatically reduced riding comfort and an increased risk of derailment. Consequently, a poorly designed railway bridge may result in increased maintenance cost not only for the bridge but also for the track. In the design of railway bridges for speeds exceeding 200 km/h, a set of dynamic criterions must be fulfilled.

Current design regulations, e.g. Eurocode EN-1990, are only valid for speeds up to 350 km/h and developed for train models envisaged in the late 1990ies. Significantly higher speeds and/or future trains may require an extensive revision of the existing design codes. Further, these design codes do not include requirements for slab tracks. Future developments will require the introduction of “very” high speed track VHST, as the maximum speeds in commercial operation are currently in the range from 300 km/h to 350 km/h. Thus, a study of the influence of very high speeds (up to 480 km/h) on bridges is of high importance.

This report presents important aspects of railway bridge dynamics for very high speed lines, comprising analysis, modelling procedures and full scale testing. Parametric studies on common types of beam and frame bridges are presented for speeds up to 480 km/h. In addition, the efficiency of dampers for vibrations reduction are studied and discussed.

The report is the result of work performed by the Capacity-4-Rail project team members: KTH, ADIF, SYSTRA, INECO, CEDEX. KTH has been responsible for writing Chapter 1 – Chapter 7 (except Section 4.3) and Systra for writing Section 4.3 and Chapter 7.

2. Objectives

The main aim of this study is to investigate the dynamic behaviour and requirements for load bearing structures intended for VHST focusing on common types of railway bridges. Based on previous experience, typical beam and portal frame bridges have been chosen for parametric studies.

The objectives are:

- Investigate bridge deck acceleration levels for speeds up to 480 km/h.
- Investigate the effect of track irregularities and how does it compare against the Eurocode factor.
- Investigate the effect of soil-structure interaction and load distribution on the dynamic response of bridges.
- Investigate the efficiency of damping devices on reducing the level of acceleration on bridges.
- Verify modelling procedure using a full scale test on a portal frame bridge.

3. State-of-the-art

To meet the demands from both the European Commission mentioned in chapter 1, extensive research is needed. Today, within the field of railway bridge dynamics and HSR, countries like China, Japan, Germany, France, Spain and Sweden have great experience and know-how. Some of the major research topics include:

- Determine the real dynamic amplification factor (DAF) to be used in load capacity assessment of bridges on non-HSR lines.
- Development of reliable and efficient structural models for predicting the dynamic response of bridges on HSR lines.
- Scrutinizing the current serviceability design limits for railway bridges on HSR lines as stated in the Eurocodes.
- Real-time monitoring of railway bridges as a tool for conditional assessments and damage detection.
- Finding novel bridge solutions for optimal HSR.

A great deal of research already exists within most of the aforementioned topics. Future challenges consist of progressing beyond the state of the art as well as knowledge transfer between the academia and the industry. The aim is to achieve a safe, reliable and feasible implementation of the research in both assessment of existing railway bridges as well as in the design of new bridges on HSR lines.

This chapter presents some examples of on-going research in both analysis and experimental testing of railway bridges, without any claim of giving a complete overview of the current state of the art.

3.1 Bridge dynamic analysis

3.1.1 Design requirements

For the design of railway bridges for HSR, a set of serviceability criterions regarding traffic safety and riding comfort are to be fulfilled, EN 1990 Annex A2. These criterions consist of limits for vertical deck acceleration, vertical displacements, end rotations and deck twist.

Vertical deck acceleration

In most cases where the bridge is susceptible to dynamic excitation, the vertical bridge deck acceleration will be decisive. This criteria exists to assure a sufficient track alignment and track stability, both from a maintenance and safety perspective. This phenomena was first discovered on the Paris to Lyon high-speed line, where a greater track maintenance than anticipated was required. Experimental testing with test trains at resonance speed showed adverse effects of the ballasted tracks at acceleration levels in the range 0.7 – 0.8g in the bridge deck. Experimental shake table tests were later performed by [4], showing similar results. The effect owes to loss of ballast interlock and loss of contact friction, sometimes described as “floating ballast”. Due to uncertainties in the real behaviour, a safety factor 2 was proposed. As a consequence, the current design limit in EN 1990 is 3.5 m/s^2 for ballasted

tracks. For ballastless tracks, a limit of 5.0 m/s^2 exists, by adopting the safety factor 2 on the ground acceleration g. This is motivated by limiting the risk of loss of rail-wheel contact and hence the risk of derailment. It is important to note that the acceleration is to be evaluated within a limited frequency range, in EN 1990 stated as the greater of 30 Hz, 1.5 times the fundamental mode of vibration and the third mode of vibration. The experimental testing in [4] was done in the range 2 – 20 Hz. Further research is needed on the dynamic behaviour of ballast, what frequency range to include and the influence of transient response. Research is also needed for the case of ballastless tracks, where the current limit of 5 m/s^2 seems as a rather crude simplification with little physical background. As comparison, the Chinese design codes for high-speed railway stipulate a set of running safety indices for the vehicle, as a derailment factor, offload factor, lateral wheel force and an overturn factor. These are used in conjunction with vertical dynamics from traversing train loads and transverse loads from strong wind [5].

Vertical deck displacement

EN 1990 also stipulate limits for vertical bridge deck displacement as an indirect measure to limit the vertical vehicle acceleration and thereby the passenger riding comfort. For bridges on non-high speed lines, the limit is set to L/600 where L is the span length. For higher speeds, the limit depends on the span length, the speed and number of consecutive spans and may range up to L/2600. The Eurocode allows for separate vehicle/bridge interaction analysis if a more refined value for the vertical train acceleration is needed. No detailed information is however given on what vehicle configurations to assume or how the analysis should be performed. A somewhat confusing fact is that the vertical displacement should be determined based on the load model LM 71. In Japan, displacement limits with similar purpose is stipulated in [6], but is evaluated based on the Shinkansen high-speed train. There are some inconsistencies between the two codes, where EN 1990 is stricter for longer spans and [6] is stricter for shorter spans.

Train load models

The above mentioned serviceability criterions are compared to the dynamic response from passing trains, including resonance. Since this is not covered by the DAF-factors, a full dynamic analysis is often required. EN 1991-2 presented a series High-Speed Load Models to be accounted for. Except for simple structures, a total of 10 trains need to be analysed, denoted HSLM A1-A10. The train sets have different configurations with an axle load from 17 – 21 tonnes and a total length of 370 – 400 m. The HSLM load model is designed to account for common high-speed trains in Europe. The resulting envelope may therefore be significantly larger than the response from a single existing train type. This will enable interoperability between different countries but may require a less optimal design. This may also be an obstacle in upgrading existing conventional lines to high-speed standard. Using the so-called train signature method [7] the dynamic load effect of particular trains can be compared, regardless of bridge type.

An example of this is shown in Figure 1, where the wavelength $\lambda = v/f_0$ for the train speed v and the fundamental frequency f_0 of the structure. The train signature parameter S_0 is obtained by a Taylor

series expansion, further explained in [7]. Figure 1 show that the envelope of HSLM-A in many cases far exceeds the load effect from existing real trains in Sweden.

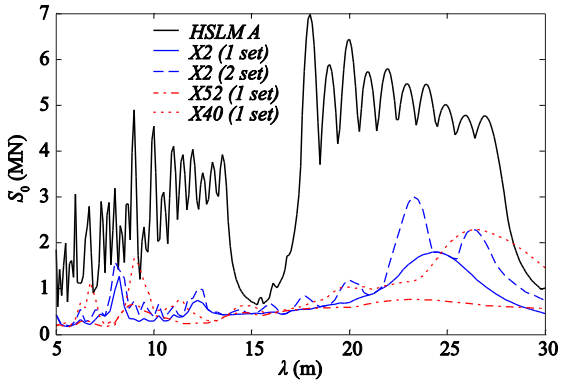

Figure 1. Train signature for train load model HSLM A and common passenger trains in Sweden, reproduced from [8].

3.1.2 Structural Models

To enable realistic predictions of the real dynamic bridge response, the choice of structural model is of paramount importance. Increased level of detail may improve the results, if sufficient input data are available. Since a large set of simulations usually is required, a trade-off between accuracy and computational time is sometimes required. For simply supported 2D Euler-Bernoulli beams on fixed supports, closed form solutions have been developed by [9]. A closed form solution for the dynamic response of continuous beams with variable stiffness on elastic supports is presented in [8] and [10].

Portal frame bridges

The same model as in [10] was used to predict the dynamic response from portal frame bridges, Figure 2. Sufficient agreement was obtained when comparing the response to a full 3D-model [11]. The support conditions were based on 3D-models of the vertical walls, wing walls and foundation slab, see Figure 3. The resulting vertical stiffness k_v and rotational stiffness k_r was included in the simple model. The additional mass from the substructure is included either as a lumped mass m_2 or as a short element L_2 with increased density.

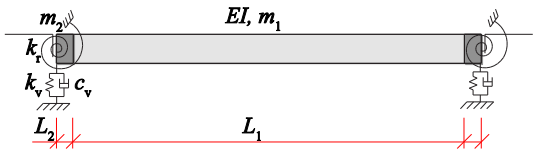

Figure 2. Simple 2D beam model for a portal frame bridge, accounting for SSI, based on [8] except the inclusion of c_v.

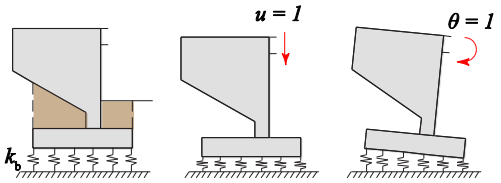

Figure 3. Substructure to determine the support stiffness, reproduced from [12].

The Soil-Structure Interaction (SSI) between the frame bridge and the adjacent backfill material is not trivial. For the case of a slab on a semi-infinite soil, charts of impedance functions were developed by [13]. The resulting stiffness and damping components may be seen as frequency dependent. This concept was used by [14], see Figure 4.

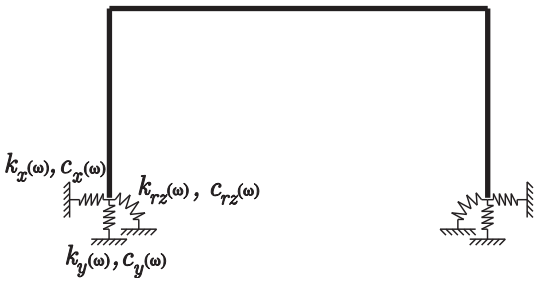

Figure 4. 2D frame model of a portal frame bridge with frequency dependent boundaries, reproduced from [14].

Another approach is to model the surrounding soil directly, Figure 5. Even for a 2D-approach, the computational time increases significantly compared to simple 2D frame/beam models. Great care must also be taken to the boundaries, to avoid unwanted reflecting waves and spurious vibrations. This can be achieved by what is sometimes denoted as silent boundaries. Different strategies exist, e.g. using elements with similar properties as the adjacent soil but with increased material damping, using a set of optimal springs and dashpots, infinite elements or boundary elements. In the case of shallow foundations, Figure 5b, reflecting waves may be expected and fully fixed boundaries may be motived.

If plate modes or other 3D effects are expected, a full 3D model similar to Figure 6 may be required. Accounting for the SSI only as a vertical stiffness under the foundation slab may be a crude simplification. Extending the concept of Figure 5 in 3D usually result in a significant increase in computational time.

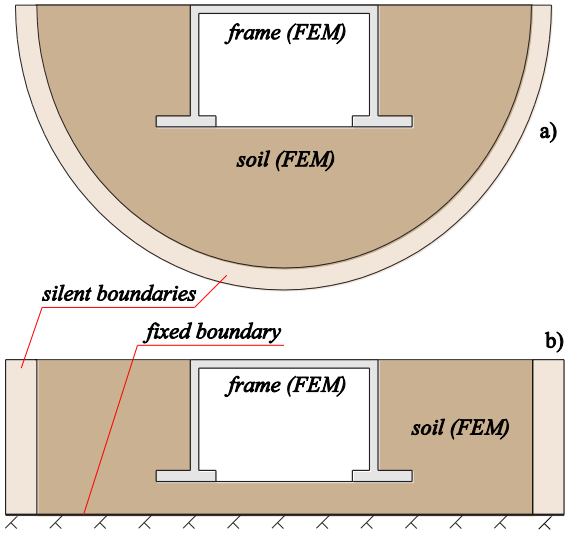

Figure 5. 2D approach for full SSI of a portal frame bridge, a) half-space model for deep foundations, b) vertical constraints for shallow foundations.

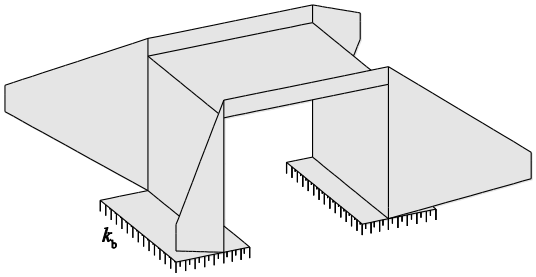

Figure 6. 3D shell model of a portal frame bridge, accounting for foundation support stiffness.

In Figure 7, simulation results from a 6.5 m single track portal frame bridge is presented. The peak vertical deck acceleration from an ICE3-train is calculated at speeds varying from 100 to 400 km/h. A 2D-model similar to Figure 5 was used. A model only accounting for the vertical support stiffness, denoted "no SSI" suffers from resonance at about 325 km/h with a resulting acceleration of 6 m/s^2. For the present case, assuming either a half-space or a shallow foundation depth results in a significant decrease in acceleration. The model in Figure 2 may have been able to produce similar results, provided a suitable value for c_v.

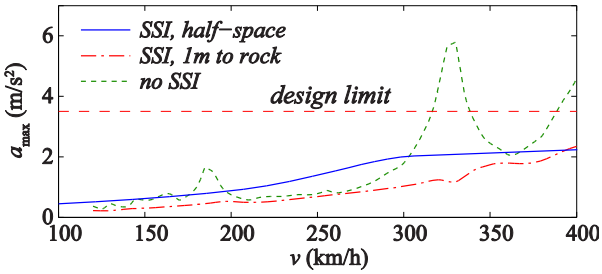

Figure 7. Influence of soil-structure interaction, case of a single track portal frame bridge with a span of 6.5 m. [15]

Live load distribution

In design, the load from the train can be distributed to the deck via three sleepers according to Figure 8. The track may instead be assumed to work as a Winkler bed, or as in the case of Figure 9 as a continuous beam on elastic supports. The support reactions are presented in Figure 10 for a rail seat stiffness of 150 MN/m and a sleeper distance s = 0.65 m. A triangular projection of the load distribution with a length of 3 m is suggested, [8]. The dynamic response from passing trains can in many cases be significantly reduced by accounting for the load distribution of the track, especially for shorter spans.

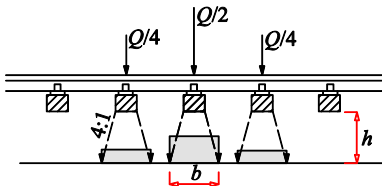

Figure 8. Load distribution from a single axle Q used in design, reproduced from [16].

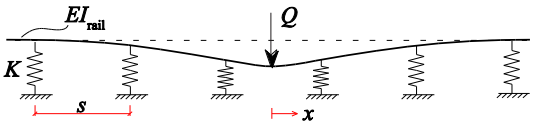

Figure 9. A continuous 2D beam on elastic supports, illustrating the deformed track under a single axle load Q, reproduced from [11].

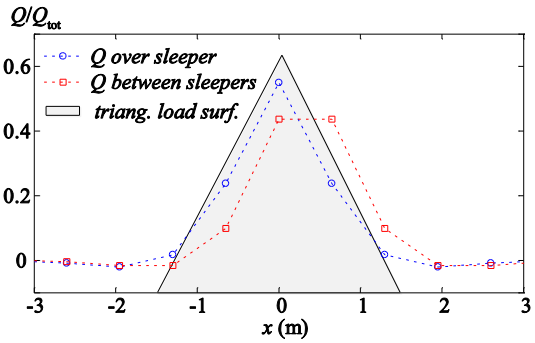

Figure 10. Load distribution from a single axle load, based on a Winkler-bed model with K = 150 MN/m. Reproduced from [11].

Train-Bridge Interaction

Each axle of the train is often simplified as a vertical point load. The Train-Bridge Interaction (TBI) may however mitigate part of the vibrations due to the primary suspension system, Figure 11. This effect was studied in [7]. Including the sprung-mass system of the train increases the level of complexity in the analysis, motivating the need for a simpler approach. The result was to account for the TBI by an additional damping of the structure, $\Delta\zeta$, which is currently included in EN1991-2 [16].

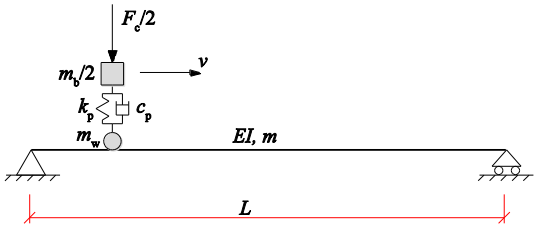

Figure 11. Sprung-mass system of a single axle traversing a simply supported beam, reproduced from [17].

The TBI is illustrated in Figure 12, consisting of a simply supported beam with a span of 10 m, a fundamental frequency of 9.7 Hz and a mass 10 tonnes/m, subjected to an ICE2 train model. Good agreement is found when comparing the result from the sprung-mass model with moving point loads, where the latter includes the additional damping Δζ. Similar results were obtained by [18] for the same case. The formulas in EN 1991-2 are mainly intended for simply supported bridges. A study of the applicability for portal frame bridges was performed by [17], which showed that the additional damping in EN 1991-2 may be non-conservative.

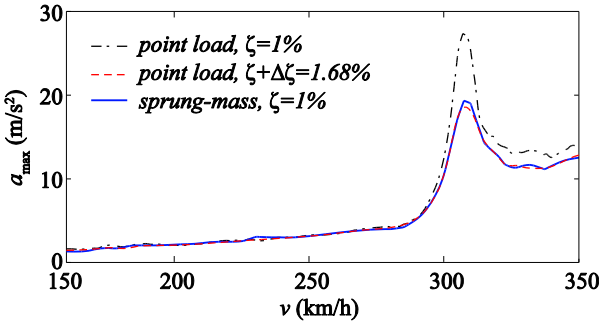

Figure 12. Case of a simply supported bridge, comparison between point loads, additional damping and the sprung-mass model, reproduced from [17].

NONLINEAR BEHAVIOUR

The dynamic design checks for HSR bridges mainly comprise a set of serviceability criteria and the analysis is therefore assumed to be linear. However, in fact, several sources of nonlinearities may still exist and should be accounted for, e.g.:

- concrete cracking [19]
- ballast behaviour [20]
- supports and bearings [21]
- temperature and seasonal variation [22]
- amplitude dependencies [23].

3.2 VERIFICATION BY FIELD TESTS

Most of the existing recommendations are based solely on theoretical models without experimental verification. Many of the bridges that were deemed to exceed the limit for vertical deck acceleration may in reality show significantly less vibrations. To prove that more bridges fulfil the dynamic criterion, extensive experimental testing is required.

Experimental data serve as valuable input in understanding the real structural manner of action of the bridges and for updating or revising the proposed structural models. The main characteristics to be determined consist of natural frequencies, mode shapes and damping ratios. In addition, non-linear effects as listed above in section 2.1.2 may be studied further. In the following, some case studies of experimental testing on railway bridges in Sweden are presented.

3.2.1 CASE STUDY 1 – A PORTAL FRAME BRIDGE

The first case study is a portal frame bridge at Orrvik, Figure 13, located along the Bothnia Line in Sweden. Based on the simple 2D-model, a peak acceleration of 6.0 m/s^2 was calculated at a critical train speed of 286 km/h. The span length is 15.2 m and the first natural frequency was calculated to 5.9 Hz. Experimental results from passing trains are reported in [24], but no clear information on the natural frequencies or damping is presented.

The experiments were performed during high-speed tests with the Green Train [25]. The speed record for the Green train is 303 km/h, but during the bridge test the highest speed was about 280 km/h.

Accelerometers were mounted on top of the edge beams, 1.5 m from mid-span. The peak acceleration during the train passages at different speeds are plotted in Figure 14. The measured acceleration is subjected to a low-pass filter at first 90 Hz and the 30 Hz. A 2D frame model proposed by [24] shows overall reasonable agreement for the case of 90 Hz frequency range. The acceleration magnitude is decreased significantly when using a 30 Hz filter.

Figure 13. The portal frame bridge at Orrvik.

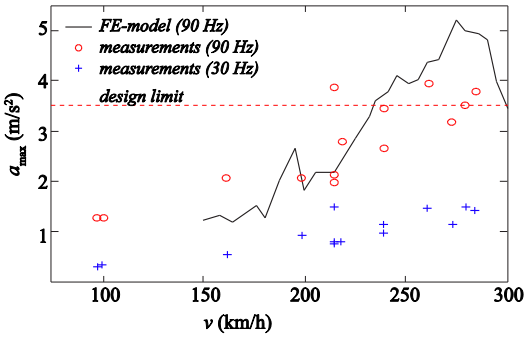

Figure 14. Peak vertical deck acceleration during passage of the test train at different speed (gröna tåget), comparison between experimental testing and simulation results, based on [24]

3.2.2 Case study 2 – Steel-concrete composite bridge

The second case study is a 36 m simply supported single track steel-concrete composite bridge, at Skidträsk, about 190 km North of Umeå. The bridge is designed for freight trains with 25 tonnes/axle but not for high-speed trains. A long-term monitoring system was installed for continuous monitoring of deck acceleration and strain in the steel beams.

Figure 15. The portal frame bridge at Skidträsk, reproduced from [22].

In [22], the change in dynamic properties due to seasonal changes was studied. A significant increase in natural frequency was discovered during the winter period, both for the first vertical bending mode and the first torsional mode, Figure 16.

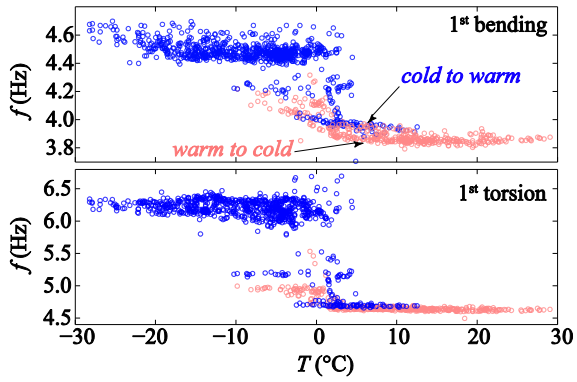

Figure 16. Influence of the temperature on the first bending and torsional mode of the unloaded bridge, reproduced from [22].

A 3D FE-model was developed, including relevant SSI components from both the ballasted track and the substructure. Distribution functions for the variation of concrete stiffness, ballast stiffness and foundation stiffness was assumed and a Bayesian model update technique was used to find plausible matches between the model and the experimental data. The results showed that the change in vertical bending frequency is mainly governed by the foundation stiffness, whereas the change in torsional frequency is mainly governed by the ballast stiffness. The model proposed that the E-modulus of the ballast would increase from 180 MPa in the summer to 1500 MPa in the winter. The corresponding increase in the foundation was from 75 MPa to 110 MPa. The model did not propose any change in E-modulus for the concrete.

The response from passing trains on the same bridge is presented in [23]. Based on the measured free vibrations after train passages, a change in both natural frequency and damping was observed. The ballasted track was believed to be the main source of this non-linear behaviour. Later studies of the mechanism of bearings [21] do however suggest that the hysteresis behaviour of roller bearings may have a significant impact in the response of the bridge. For low amplitude vibrations, the roller bearings are expected to act as fixed.

3.2.3 Case study 3 – Soil-Steel composite bridge

The third case study is a corrugated steel culvert in Märsta, about 40 km North of Stockholm. Corrugated steel culverts are statically designed accounting for composite action with the surrounding soil but its performance during dynamic loading is not readily known. The studied bridge serves as a pedestrian underpass, Figure 17, and has an elliptical section with a horizontal diameter of 3.75 m and a vertical diameter of 4.15 m. The fill height at the crown is about 1.9 m and carried two tracks. The line consists of mixed train traffic with both medium heavy freight trains (max 22.5 tonnes/axle) and various commuter and long distance train (with speeds up to 170 km/h).

Figure 17. The soil-steel composite bridge at Märsta during passage of an X52 train, reproduced from [26].

The bridge was instrumented with displacement transducers, accelerometers and strain gauges. The main aim of the measurements was to gain further understanding of the dynamic behaviour during train passages and if they would be suitable for HSR. A small part of the instrumentation is shown in Figure 18.

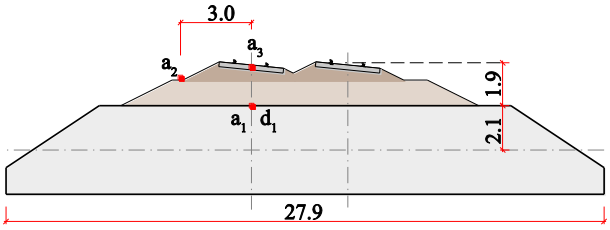

Figure 18. Cross-section of the bridge at the crown, illustrating part of the instrumentation, from [26].

The peak acceleration from a number of passing trains is shown in Figure 19, after applying a 30 Hz low-pass filter. For conventional slab-like bridges, the vertical deck acceleration is an indirect measure of the allowable vibration of the track. It is therefore of interest to investigate the relation between the acceleration of the steel pipe to the acceleration in the track zone. Train model X52, similar to the Green Train, pass the bridge at about 170 km/h in most cases. The acceleration a_1 in the steel pipe appears well correlated to the acceleration a_2 at the ballast shoulder. Acceleration a_3 in the ballast within the track zone does however scatter significantly. Values with a_{max}<0.4 m/s^2 is due to trains passing on the opposite track.

A 3D FE-model of the bridge have been developed as an extension of Figure 5b. A similar version of the model is found in [27]. A comparison between the model and the experimental results are shown in Figure 20. A manual model update is performed, primary focusing on the soil stiffness and the soil-steel interaction. The presented results are based on full contact with no slip between the soil and the steel. Further, E_{soil} = 120 MPa is used. This results in good agreement with the vertical displacement d_1 at the crown, but underestimates the acceleration a_1 and overestimates the acceleration a_3. It shall be noted however, that the measured acceleration scatters significantly.

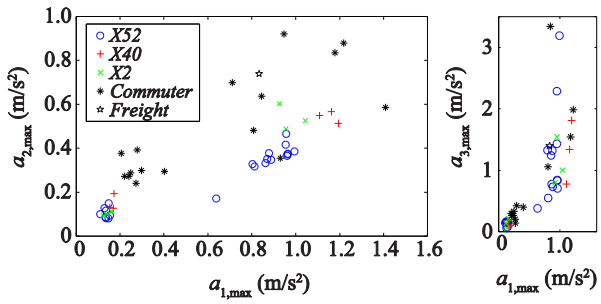

Figure 19. Peak acceleration from passing trains, a1 inside the steel pipe, a2 at the ballast shoulder, a3 in the ballast between the sleepers [26].

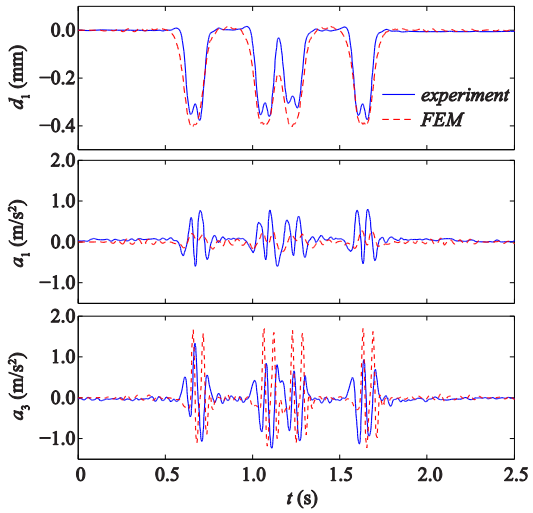

Figure 20. Comparison between measured response and dynamic simulation using a 3D model with full SSI, X52 train at 170 km/h.

3.2.4 Case study 4 – Multi-span concrete slab bridge

The last case study comprise controlled excitation of a three-span two track concrete bridge in Södertälje, 35 km South of Stockholm. The side spans are 11.1 m and the mid-span 18.4 m. The bridge was part of the feasibility study reported in [11]. From the simplified 2D analysis, excessive accelerations were predicted, owing to the integrated back-walls with 3.0 m over-sail. A view of the bridge is shown in Figure 21.

A hydraulic bridge exciter has recently been developed by KTH (as part of the IP2-In2Track European project) and the presented bridge serves as a first full-scale pilot test. The concept of the hydraulic exciter is to apply a constant amplitude load with variable frequency at the bridge soffit. Testing can therefore be performed without closing the track and the mass of the exciter equipment does not influence the bridge response. The system essentially consists of a support plate, a hydraulic load cylinder and a truss frame that is pre-stressed against the bridge soffit. A photo of the system when installed on the bridge is shown in Figure 22. The force is monitored by a load cell at the upper connection to the bridge and an MTS FlexTest SE controller assures that constant load amplitude is achieved. The system is able to account for flexibility in both the test frame and the foundation. The load cylinder has a capacity of 50 kN. The system works in compression, enabling load amplitudes up to 25 kN. The system is designed for a working range up to 50 Hz, but can be increased for lower displacement amplitudes.

Although the load capacity is less than a conventional train axle load, the main advantage is that the excitation can be controlled in both load and frequency. The bridge exciter is expected to enable relatively high amplitude vibrations, since the steady-state response can be obtained. Further, experimental frequency response functions (FRF) can be obtained with high accuracy, serving as

valuable input for model updating and structural identification. Further details on the bridge exciter and the pilot test are presented in [28] and [29].

Figure 21. The beam bridge at Pershagen. [28]

Figure 22. The beam bridge at Pershagen, during testing with the hydraulic exciter, [28]

A 3D FE-model of the bridge have been created, further described in [28]. The experimental testing revealed a total structural damping of 1.7% for the 1st mode and 2.5% for the 3rd mode, which was used in fitting a Rayleigh material damping in the model. However the experiments showed that the 2nd mode was significantly more damped, in the order of 7 – 9%. The reason for this is not readily known. As a consequence, the model will overestimate the response from the 2nd mode. A comparison of the FRF between the experiment and the model is shown in Figure 23. Good match is found for the first mode, both in frequency and amplitude. As expected, the model overestimates the amplitude of the 2nd mode but with good agreement in frequency. A slight shift in frequency is seen for the remaining part of the FRF, which may be refined by additional model updating.

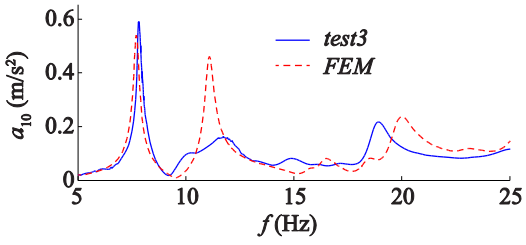

Figure 23. FRF at mid-span, comparison between experimental results and the 3D FE-model. [28]

The FE-model is finally used to predict the dynamic response from passing trains. The envelope of HSLM A1-A10 at different speed is presented in Figure 24. SSI is considered by modelling the soil material in contact with the integrated back wall, assuming E_{soil} = 200 MPa. It is here concluded that the stiffness of the soil has only a minor influence of the natural frequencies.

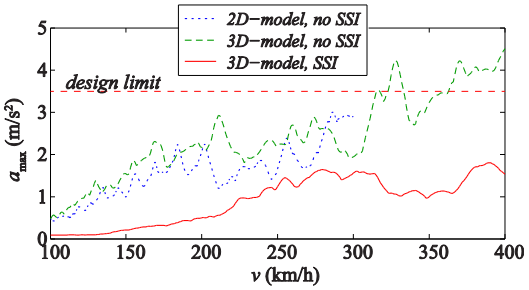

Figure 24. Peak vertical deck acceleration from HSLM A1-A10, comparing different simulation models.

4. Response of bridges at very high speed

4.1 General

The study presented in this chapter focuses on short-span bridges as the dynamic analysis of short-span bridges often results in excessive acceleration levels compared to current standards. The response is often dominated by transient loading due to individual bogies. More detailed models than usual will be proposed, to account for load distribution and stiffness of the track, energy dissipation and stiffness of the foundation, influence of the train mass, etc.

By idealizing the train axle loads as moving forces, the resonance speed for a bridge can be predicted by the well-known formula $v_{cr} = df_n/k$, n = 1, 2, 3, …, k = 1, 2, 3, …, where n is the mode number, v_{cr} is the critical or resonant speed, f_n are the natural frequencies of the beam and d is a characteristic distance between axle loads. From the equation, it can be observed that the most vital bridge parameters are those that influence the bridge frequencies: mass, span length, stiffness and support conditions. In the general case, there is an interaction between these parameters (i.e. a change in stiffness often leads to a change in mass), thus making the dynamic behaviour of bridges complex, and so, difficult to predict. An increase in mass reduces the bridge deck acceleration and reduces the critical speed with no effect on the amplitude of deck displacement. An increase in stiffness decreases the deck displacement and increase the critical speed with no effect on the amplitude of deck acceleration. As the amount of energy dissipation limits the dynamic response, damping is another key parameter in the train–bridge system.

In the work presented here, the bridge dynamic behavior is checked according to the Eurocode requirements and the wheel unloading coefficient is calculated. For the short span beam bridges analyzed by KTH in Section 4.2, the bridge deck acceleration criterion is generally the decisive criterion, instead of deflection/passenger comfort. This is why deck acceleration and wheel-rail forces will be analyzed for these bridges and not passenger comfort.

In section 4.3 Systra has analysed the dynamical behaviour of 4 typical short-span portal frame bridges. The dynamical behaviour of these bridges are checked by the analyses below:

- Rolling stock analyses according to Eurocode EN 1991-2 art. 6.4.6 and Eurocode 0 Annex A2 (High speed line train corresponding to 480 km/h maximum calculation speed)
    - Only one track is modelled
    - Two tracks are modelled
    - Impact of ballast stiffness on results
    - Impact of horizontal stiffness of soil on results
- Deck acceleration and Passenger comfort, under vertical acceleration for French TGV and ICE 2 (2D model for train)
- Passenger comfort, under horizontal acceleration for French TGV (3D model for train)
- Passenger comfort, under vertical and horizontal acceleration for French TGV (3D model for train) with track irregularities in vertical and transversal directions

- The derailment coefficient and wheel unloading coefficient will be calculated for French TGV

The analysis that SYSTRA developed include both vertical and transverse vibrations of the bridge under train loads, although transverse vibrations are not considered in Eurocodes. Rolling stock dynamic characteristics corresponding to French TGV and German ICE trains have been incorporated in the calculation model.

4.2 Beam Bridges

In the following section, beam bridges are studied. The aim and scope of the analyses performed are:

- To determine whether it is possible to find an upper limit for the acceleration level in typical two- and three-span bridges for speeds up to 480 km/h.
- To especially show what happens between high speeds (up to 350 km/h) and very high speeds (up to 480 km/h).
- To investigate the effect of track irregularities and compare the analysis results against the Eurocode factor (1+0.5ϕ'').

The utilized 2D train-tack-bridge analysis tool has been developed by KTH and is implemented in Matlab. More information about this tool is available in [30].

4.2.1 Bridge data

This section presents lists of bridges included in this investigation. Table 1 presents data for five reinforced concrete bridges along the Madrid-Barcelona high-speed line. The Val de Palacin viaduct is a concrete box girder bridge, while the others are voided concrete deck structures. The bridge properties are based on the sectional properties at mid span for the voided decks. The masses indicated in the table include the mass of the track structure. This bridge data is the basis for the analyses presented in the followings sections.

Table 1. Bridge data for reinforced concrete bridges along the Madrid-Barcelona high-speed line, provided by ADIF.

Name	Spans	Span lengths	Tracks	m (kg/m)	E (MPa)	I (m^4)	f_0, field test (Hz)	f_0, model (Hz)
Val del Sordo	2	15.75+15.75	2	32000	35	2.14	10.18	9.49
Barranco Concepcion	3	20+25+20	1	27800	40	2.10	6.24	5.52
Madrid Sur Viaducto 1	4	16+23+23+16	2	42800	40	4.30	6.94	-
Val de Palacin	4	27+33+33+37	2	32200	35	7.48	4.65	-
Valdipuey	5	18+30+30+30+18	2	30400	30	2.60	4.44	-

In order to make a prediction of the dynamic behaviour of typical short two- and three-span bridges, reference bridges have been chosen, and analyses have been performed for a range of variations in the reference properties. With data based on the Val del Sordo viaduct (Table 1), double-track two-span bridges with span lengths 14, 15, 16 and 17 m have been studied. Similarly, single-track three-span bridges with a centre span of 20, 22.5 and 25 m (with side spans 0.8*centre span) were studied based on the Barranco Concepcion viaduct. Additionally, double-track three-span bridges were studied based on the properties of the Madrid Sur Viaducto 1.

The following input data was used:

- The bridge mass was varied +/−20% from the mass of the reference bridge. The bridge mass was assumed to vary with span length according to [32], see Figure 25.
- The bridge stiffness was varied +/−20% from the stiffness of the reference bridge. The resulting bridge frequencies can be seen in Figure 25. All frequencies lie within the frequency range recommended in EN 1991-2 [16].

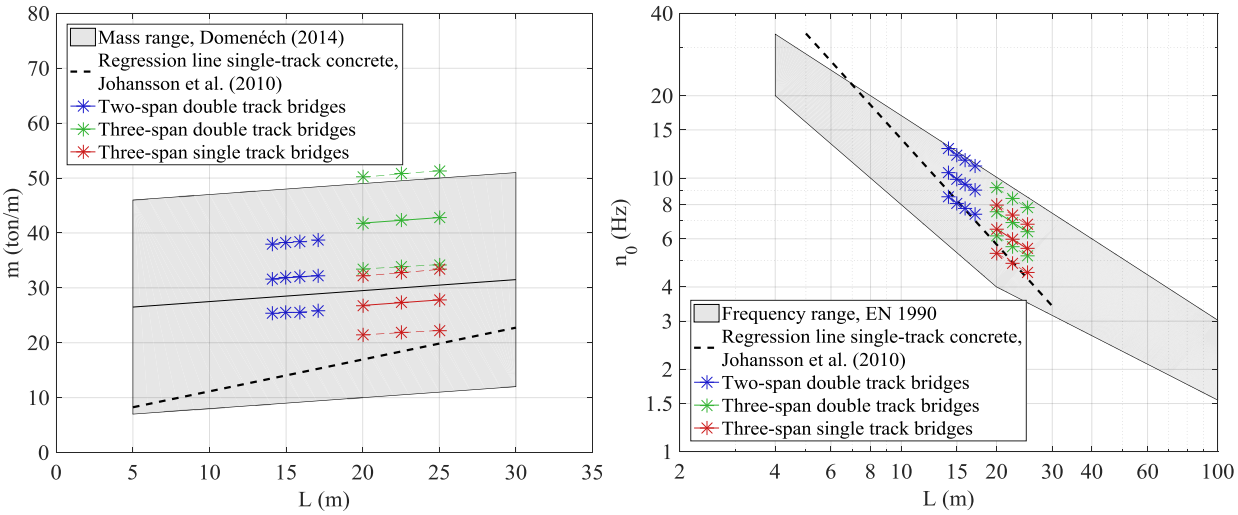

Figure 25. Bridge mass and frequency for the reference case (solid lines) and +/−20% (dashed lines) compared to the ranges given in references [8], [16] and [32].

4.2.2 Modelling aspects

Train-Track-Bridge Model

The analyses were carried out using a 2D train–track–bridge model shown in Figure 26. The bridge and rail are modelled with Euler-Bernoulli beams. In the ballasted track, the sleepers and ballast are modelled as discrete masses connected by vertical springs and dampers. The train load is modelled as a multi-body system with 6 degrees of freedom from the car body and bogies, while the wheel nodes are assumed rigidly connected to the rail. A detailed description of the model can be found in [30]. The coupled train–track–bridge system is solved using direct integration (Newmark β method), with a time step of 0.0005 s. The damping of the bridge follows the EN 1991-2 recommendations [16]. The track properties were chosen according to [31]. The maximum deck response is evaluated from the envelope of all nodes along the bridge.

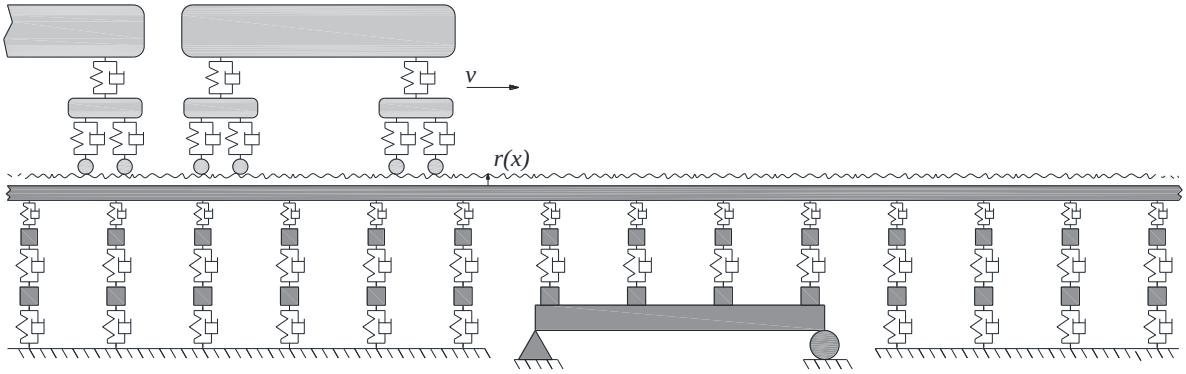

Figure 26. 2D Train–track–bridge model including track irregularities *r(x)*.

TRAIN MODEL

A model of the ICE3 train has been used in the analysis presented in section 4.2 with the properties defined in Table 2. An 8-carriage configuration of the ICE3 train was adopted.

Table 2. Properties of the ICE3 train model.

Item	C1, C8	C2–C3, C6–C7	C4–C5
Carriage length (m)	25.835	24.775	24.775
Bogie distance (m)	17.375		
Bogie wheelbase (m)	2.5		
Car body mass (kg)	47800	47800	41200
Bogie mass (kg)	3500	3500	2800
Wheel mass (kg)	1800		
Car body inertia (kgm^2)	1957888	1957888	1687552
Bogie inertia (kgm^2)	1715	1715	1372
Primary stiffness per axle (kN/m)	2400		
Primary damping per axle (kNs/m)	20		
Secondary stiffness per bogie (kN/m)	700		
Secondary damping per bogie (kNs/m)	40		

TRACK IRREGULARITIES

Track irregularities in the wavelength range around 0.5–150 m and longer are deviations from the ideal track geometry generated from, for example, settlements, the sleeper spacing and irregular track stiffness. EN 13848-5 [35] defines wavelength ranges D1 (3–25 m), D2 (25–70 m) and D3 (70–150 m), where the lower range is more relevant for running safety (wheel-rail forces) and the upper range is more relevant for passenger comfort [30, 35]. As the unsprung axle masses travel over the irregular profile, variations in the wheel–rail forces arise, providing an additional excitation of the TTB system. This increase in load can lead to higher bridge response. For the vehicle, the running safety and passenger comfort is affected. The short wavelengths affect the wheel-rail forces but are effectively filtered out by means of the suspension system, while the longer wavelengths can excite the car body modes of vibration [30]. As an example, the vertical car body frequency (0.5-1 Hz) lies within the range of the frequencies induced by the 70-150 m wavelengths in the speed range 100–400 km/h (0.2–1.6 Hz).

Random track irregularities are often idealized as stationary random processes, described by power spectral density (PSD) functions. Examples are given in Figure 27 and Figure 28. The analysis presented in this section will show the effect of the vertical track irregularities. The aim is to compare the obtained effect with the factors provided in the Eurocode, see Figure 29.

In the present study, track irregularities were considered based on the track quality class A for design speeds 230–300 km/h (standard deviation 0.4 mm in the wavelength range 3–25 m) according to [33], EN 13848-6 (CEN 2014). The German track spectra [34] was used and scaled to obtain the standard deviation 0.4 mm, see Figure 27. Wavelengths 3–150 m were included according to EN 13848-5 [35]. The maximum profile elevation is lower than the alert limits for isolated effects given in EN 13848-5, which means that the results may not reflect the worst allowed condition according to present EN standards, but rather a well maintained high-speed track. It should be noted, however, that here are no current standards for speeds above 300 km/h. Possibly, a higher track quality must be kept for very high speeds.

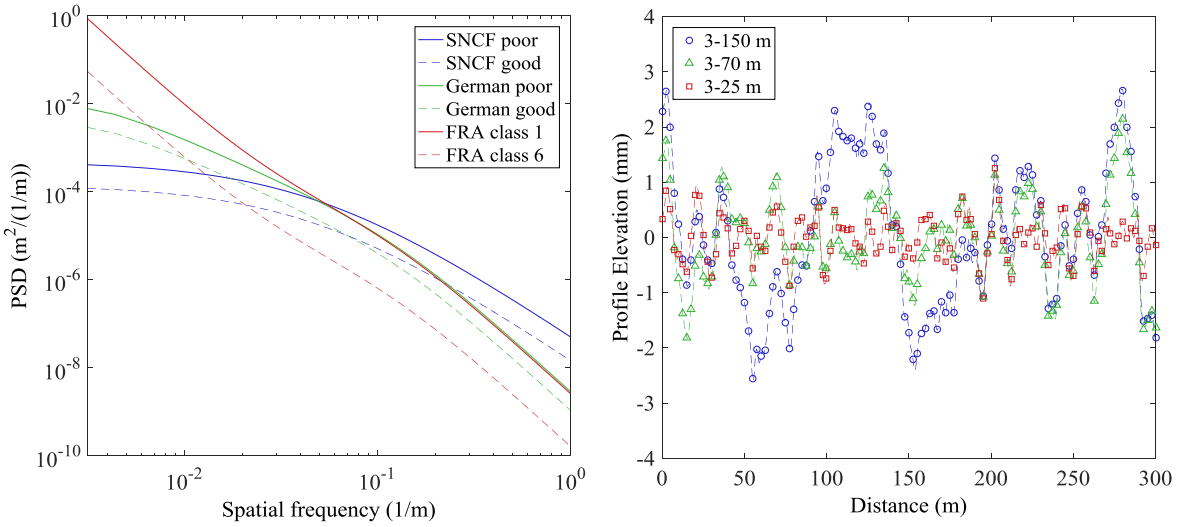

Figure 27. PSD-functions (left) for different track quality, from [31]. Random samples (right) from the German track spectra with standard deviation 0.4 mm in the wavelength range 3-25 m.

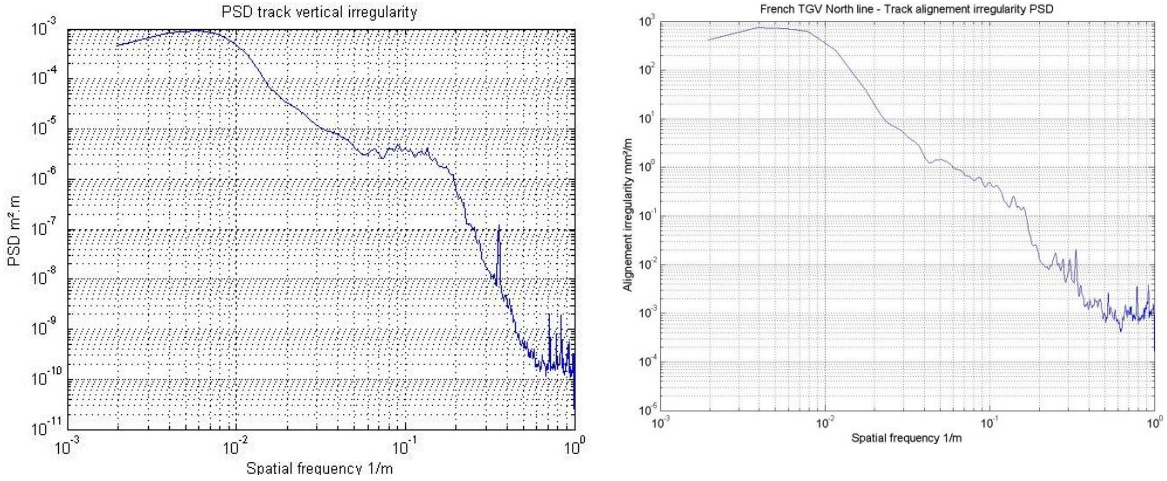

Figure 28. Vertical irregularities and Transverse irregularities used by SYSTRA.

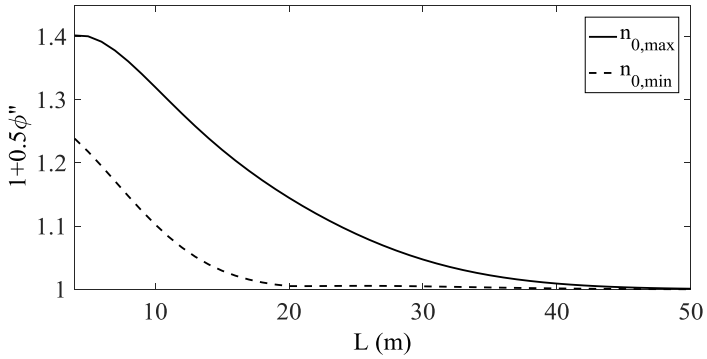

Figure 29. Factor for including the effect of track irregularities according to EN 1991-2 [16].

4.2.3 Analysis Steps

The dynamic characteristics at very high speed were investigated for typical European continuous bridges with bridge properties based on typical examples of continuous reinforced concrete deck bridges. In order to make a prediction of the dynamic behaviour of these types of bridges, analyses were performed for a range of variations in bridge properties, as described in Section 4.2.1.

Examples of bridge deck maximum vertical acceleration are presented for the two-span Val del Sordo viaduct and the three-span Barranco Concepcion viaduct in Figure 30.

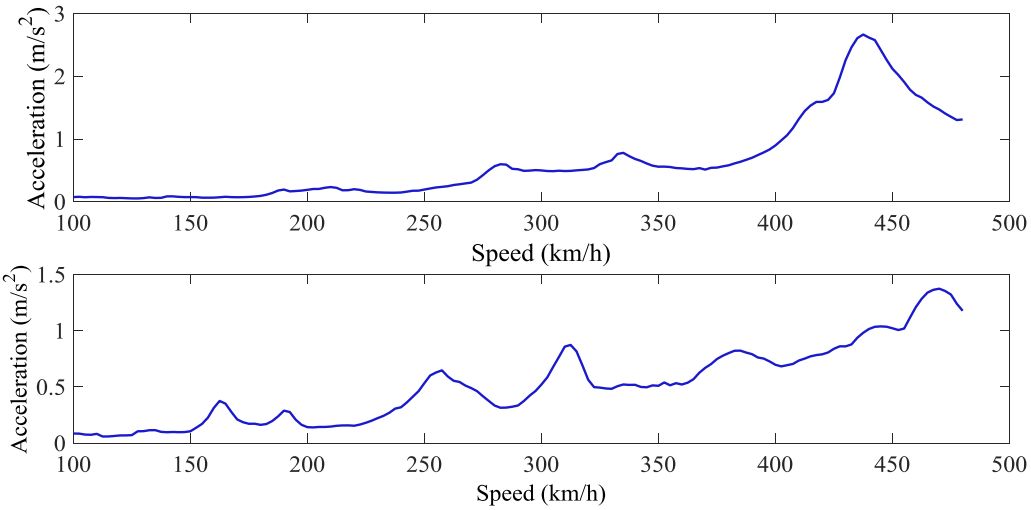

Figure 30. Maximum bridge deck vertical acceleration for the Val del Sordo viaduct (upper figure) and the Barranco Concepcion viaduct (lower figure).

The analyses were carried out in the following steps:

1. For each span length, analyses were carried out for the speed range 100–480 km/h for the four extreme combinations of bridge mass (+/−20%) and bridge stiffness (+/−20), as is exemplified in Figure 31. A perfectly smooth track profile was assumed.
2. For each span length, the critical speed (highest resonance peak) for the most critical combination of bridge mass and stiffness was determined, see again Figure 31. Such a critical speed and parameter combination was determined both for the speed interval 100–480 km/h and 100–350 km/h.
3. The effect of track irregularities was studied at the critical speed for the critical combination of bridge mass and bridge stiffness (as determined in step 2). 400 random track profile

realizations was analysed in a Monte Carlo simulation. The 95-percentile of the results was determined, as is exemplified in Figure 31.

4. The results are shown and analysed in Sections 4.2.4–4.2.6 for two- and three-span bridges. The results for speeds up to 480 km/h are compared to the results for speeds up to only 350 km/h.

5. Filtering of the results at different cut-off frequencies is discussed.

6. The effect of track irregularities is compared to the Eurocode factor (1+0.5ϕ'').

As an example, the results for the two-span 16 m bridge is shown in Figure 31. The maximum bridge deck acceleration for the critical parameter combination is 3.3 m/s^2 (for a smooth track profile). The critical combination for this two-span 16-m bridge is a mass variation of −20% and a stiffness variation of −20%. The acceleration level should be compared to 2.7 m/s^2 for the reference bridge (Figure 30). The unfiltered bridge deck acceleration for the 400 track profiles are also shown in the figure. It can be observed that the unfiltered bridge deck acceleration increase significantly from track irregularities.

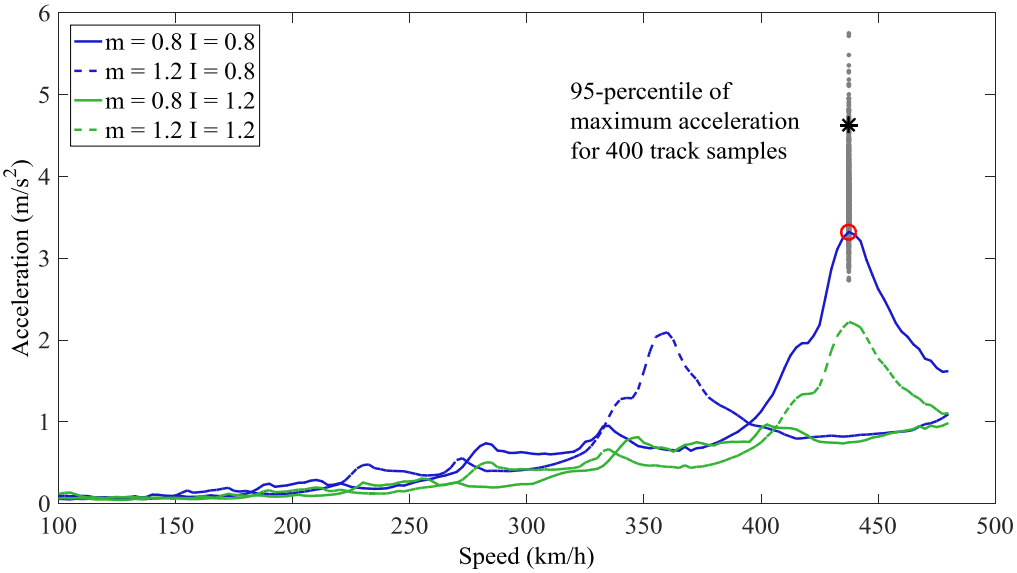

Figure 31. Maximum bridge deck acceleration for the 16+16 m span bridge. The critical speed for the critical combination of bridge mass and bridge stiffness is indicated by the red circle. The results from 400 track samples at this critical speed are seen in grey.

4.2.4 Results and discussions: double-track two-span bridges

The results for two-span bridges are shown in Figure 32 and Figure 33. The following can be observed:

- For very high speeds (up to 480 km/h) the acceleration levels in the studied bridges (14–17-m two-span bridges) are close to the limit value 3.5 m/s^2 even if a perfectly smooth track is assumed.

- For speeds up to 350 km/h only, the acceleration levels are significantly lower (below 2.5 m/s^2).
- For very high speeds, the unfiltered acceleration level is significantly increased at the presence of track irregularities. The cut-off filter has a large effect and for 30 Hz filtering the effect of track irregularities is moderate and compare well with the Eurocode factor (1+0.5ϕ'').
- For speeds up to 350 km/h only, the cut-off filter has smaller effect; hence less high frequency content is present in these results. The effect of track irregularities compare well with the Eurocode factor.

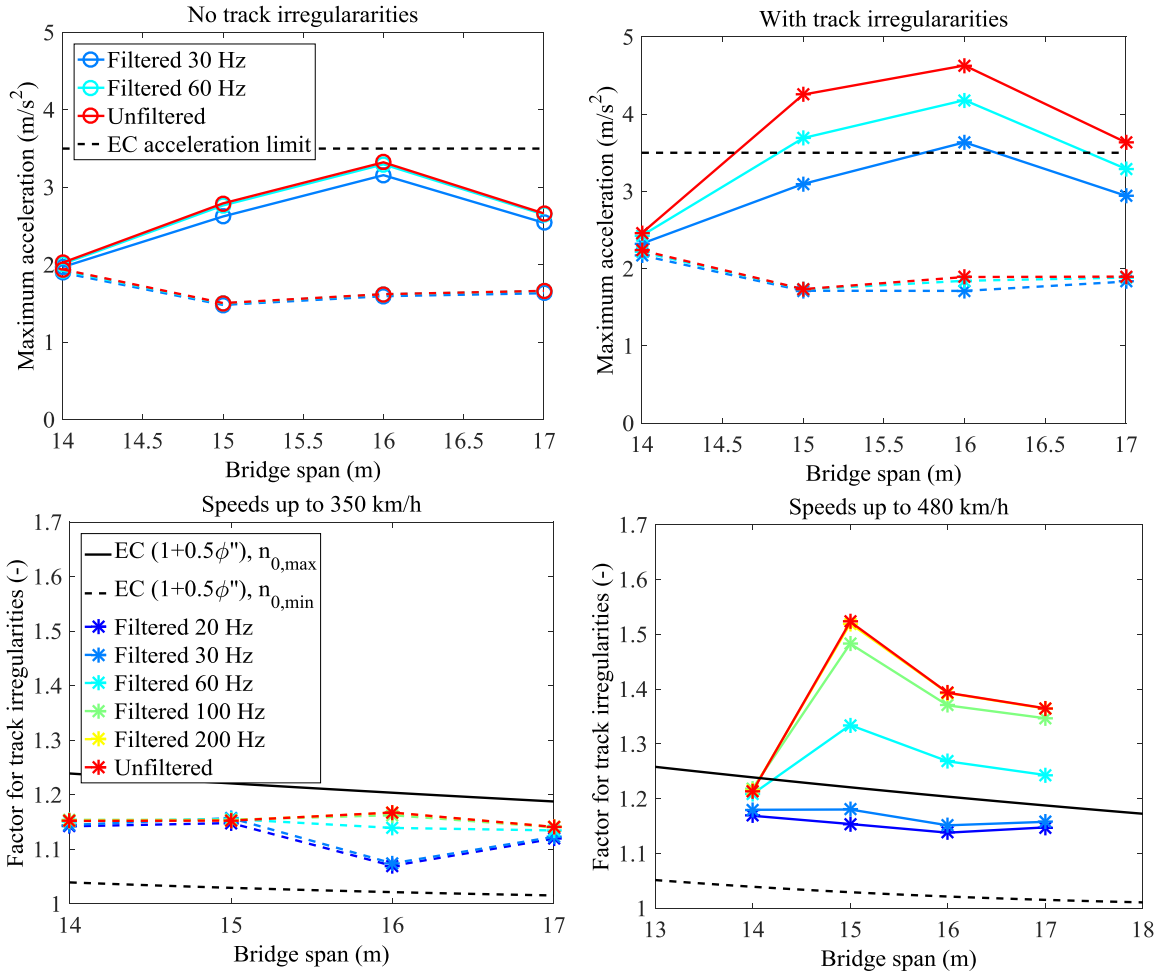

Figure 32. Two-span double-track bridges: maximum bridge deck acceleration (upper row) and factor for track irregularities (lower row) for different cut-off frequencies. Solid lines: speeds up to 480 km/h, dotted lines: speeds up to 350 km/h.

The maximum dynamic wheel unloading factor ($\Delta Q/Q_0$) is given in Figure 33. The results show that the wheel unloading factor increases with speed and with the presence of track irregularities. The wheel-rail forces contain significant high-frequency content and the choice of cut-off frequency in filtering

the results is important. The wheel unloading is well below the suggested limits 0.6 in [36] EN 14363 (CEN 2005) and 0.9 in [37] EN 14067 (CEN 2010) for all choices of cut-off frequency. The wheel unloading for the three-span bridges show similar trends and will not be presented.

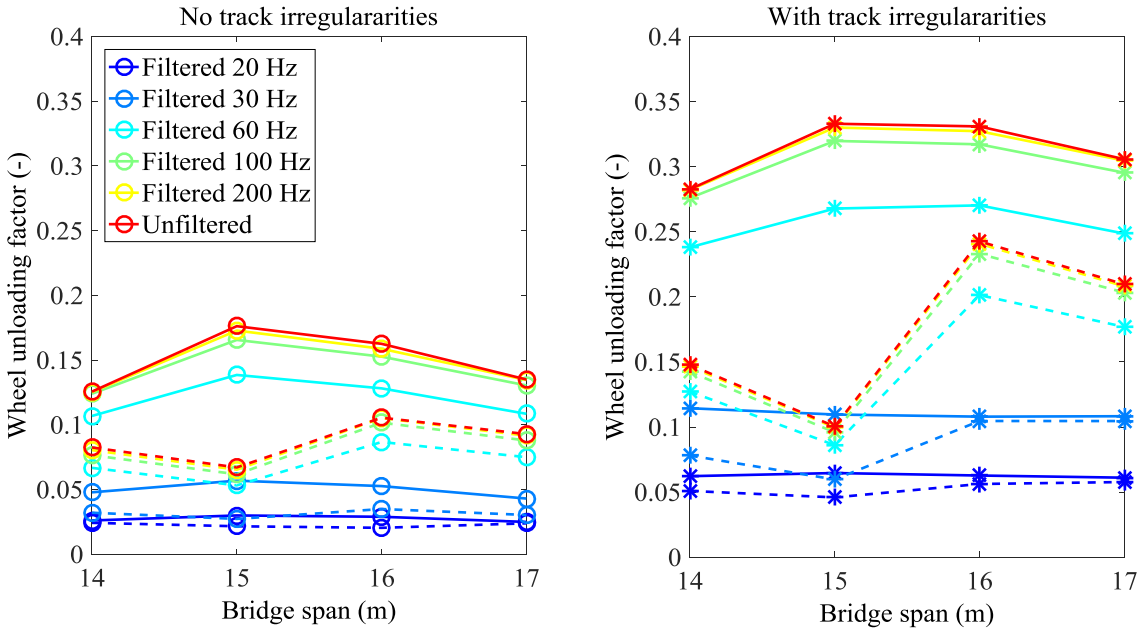

Figure 33. Maximum wheel unloading factor with and without track irregularities for different cut-off frequencies for two-span double-track bridges. Solid lines: speeds up to 480 km/h, dotted lines: speeds up to 350 km/h.

4.2.5 Results and discussions: Single-track three-span bridges

Figure 34 presents the results for the single-track three-span bridges. It can be concluded that:

- For high speeds (up to only 350 km/h), the acceleration level is well below the limit value for all three span lengths.
- For very high speeds, the acceleration level in the 20-m span bridge is far above the Eurocode limit at 3.5 m/s^2 due to that the primary resonance with the fundamental bridge frequency is shifted into the speed range for the critical combination (mass variation +20% and stiffness variation −20%) and lies at 480 km/h. The acceleration level in the 22.5-m span bridge is close to the acceleration limit, while the 25-m span bridge lies well below the limit.
- The additional effect on the acceleration level from track irregularities is moderate and comparable with the Eurocode factor (1+0.5ϕ'') for bridge spans 20 and 22.5 m. The high frequency content is low, as can be seen from the small effect from filtering. For the 25-m span, the effect from track irregularities is larger and the high-frequency content is large for very high speeds. However, it should be noted that the acceleration level for this case is well below the limit value.

As seen from Figure 34 the maximum bridge deck acceleration for the critical parameter combination for the 25-m span bridge is 1.7 m/s^2. This should be compared to the 1.4 m/s^2 for the reference 25-m span bridge (Figure 30).

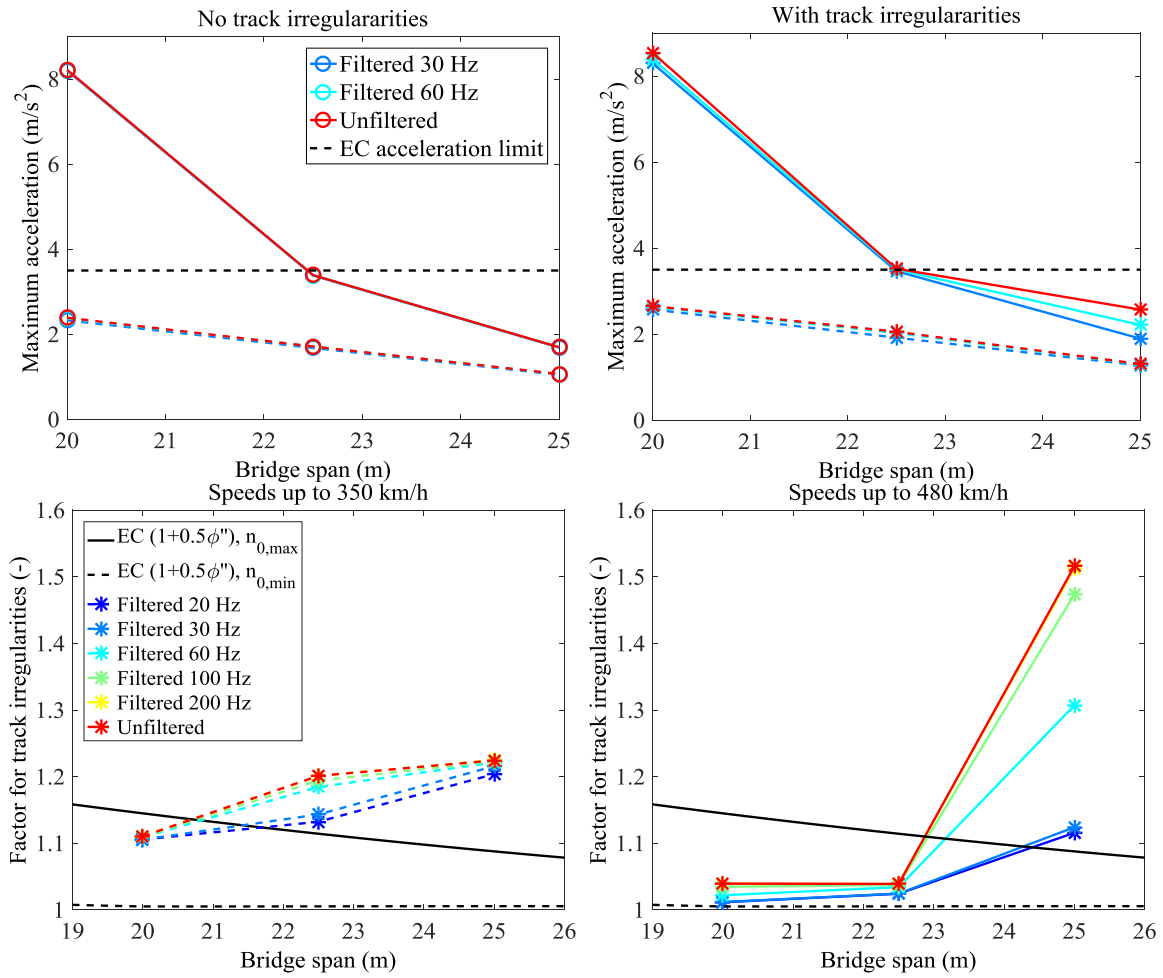

Figure 34. Three-span single-track bridges: maximum bridge deck acceleration (upper row) and factor for track irregularities (lower row) for different cut-off frequencies. Solid lines: speeds up to 480 km/h, dotted lines: speeds up to 350 km/h.

4.2.6 Results and discussions: double-track three-span bridges

Figure 35 present the results for the double-track three-span bridges. It can be concluded that:

- The acceleration level for all three bridge spans lies well below the Eurocode acceleration limit.
- Significant increase in acceleration level between high speeds (350 km/h) and very high speeds (480 km/h) is seen for the 22.5-m span, while the increase in acceleration for the 20-m and 25-m spans is small.

- The unfiltered acceleration level is significantly increased at the presence of track irregularities for spans 22.5 and 25 m, especially so at very high speeds. The cut-off filter has a large effect and for 30 Hz filtering the effect of track irregularities is moderate and compare well with the Eurocode factor (1+0.5ϕ'').

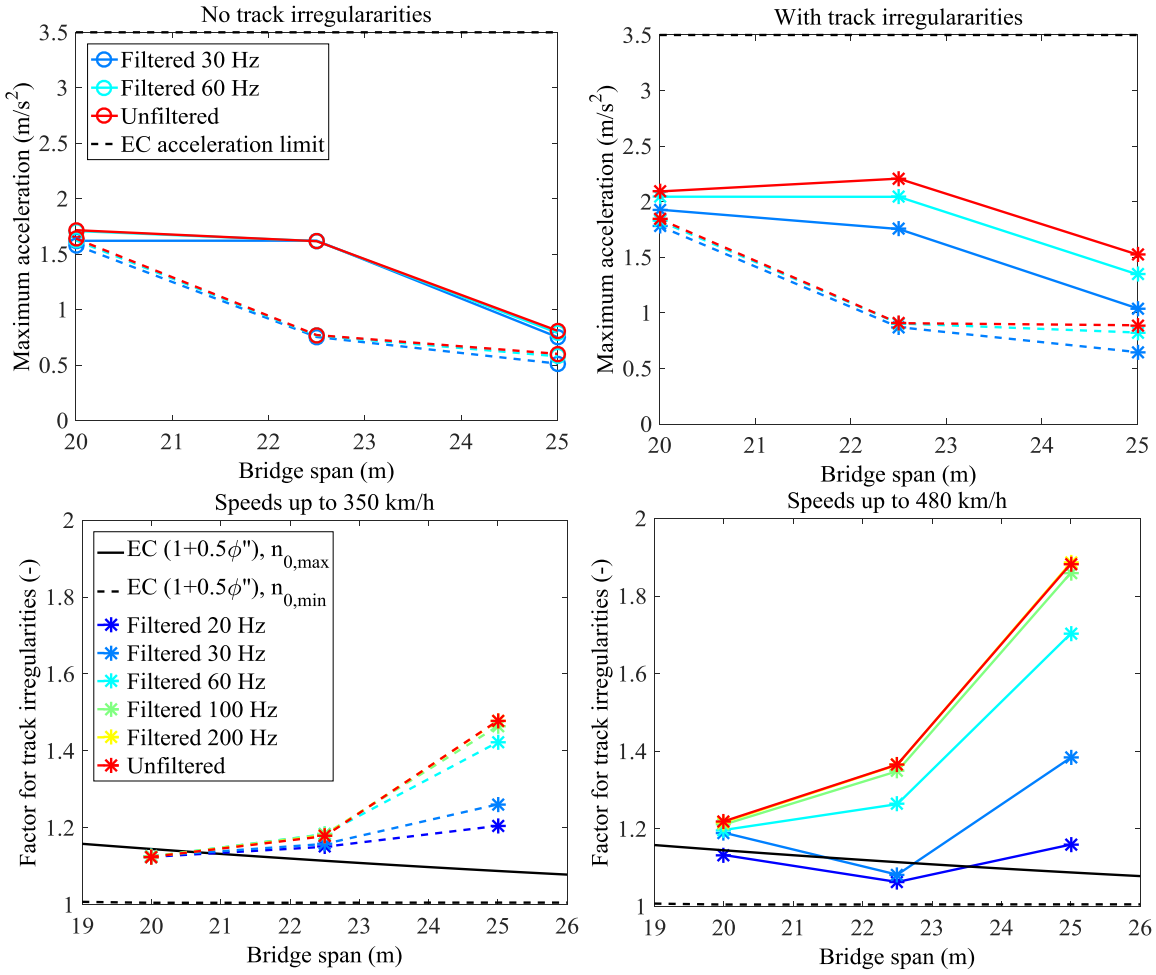

Figure 35. Three-span double-track bridges: maximum bridge deck acceleration (upper row) and factor for track irregularities (lower row) for different cut-off frequencies. Solid lines: speeds up to 480 km/h, dotted lines: speeds up to 350 km/h.

4.2.7 Practical implications

The results from both two-span and three-span bridges show a significant increase in acceleration level between high speeds (up to 350 km/h) and very high speeds (up to 480 km/h). Thus, the dynamics of these railway bridges need to be studied carefully in the speed range between high speeds and very high speeds. The present parametric study shows that double-track two-span bridges, as well as single-track three-span bridges, may have acceleration levels above or close to the Eurocode acceleration limit 3.5m/s^2 for very high speeds. An upper limit for the deck acceleration cannot be determined, as it has been shown to depend largely on whether the primary train-bridge resonance lies within the

speed range or above the upper speed limit. The double-track three-span bridges in this study all have acceleration levels well below the limit value.

At the presence of track irregularities, significant high-frequency content was observed in the bridge deck acceleration for some of the case study bridges, which shows that the choice of cut-off frequency in filtering the results is important.

For low-pass filtered results (30 Hz), the presented additional effects from track irregularities on the bridge deck acceleration compare well with the Eurocode factor (1+0.5ϕ'') for high and very high speeds. When evaluating the Eurocode factor for bridge deck accelerations ERRI D214 [38] generally applied a cut-off frequency of 20 Hz in order to filter out the large high-frequency content in their numerical results. For ballasted bridges, the Eurocode generally recommends that frequencies up to 30 Hz should be considered. There is a need for further research on the behaviour of ballast at different frequencies of vibration in order to give thorough recommendations on the choice of cut-off frequency.

It should be noted that the maximum assumed rail profile elevation is lower than the alert limits for isolated effects given in EN 13848-5, which means that the results may not reflect the worst allowed condition according to present EN standards, but rather a well maintained high-speed track. However, that here are no current standards for speeds above 300 km/h. Possibly, a higher track quality must be kept for very high speeds.

4.3 Portal Frame Bridges

4.3.1 Selected portal frame bridges

Small span portal bridges have been chosen because they are generally critical as far as dynamic behaviour is concerned. In the following section, the following portal frame bridges are studied:

Type	Span Length [m]	Height of side wall [m]
Reinforced concrete open frame	10	5
Reinforced concrete open frame	15	5
Reinforced concrete closed frame	5	5
Reinforced concrete closed frame	10	5

Figure 36. Studied Bridges

We propose the following bridge types, which are very common on high speed lines:

Reinforced concrete open frame

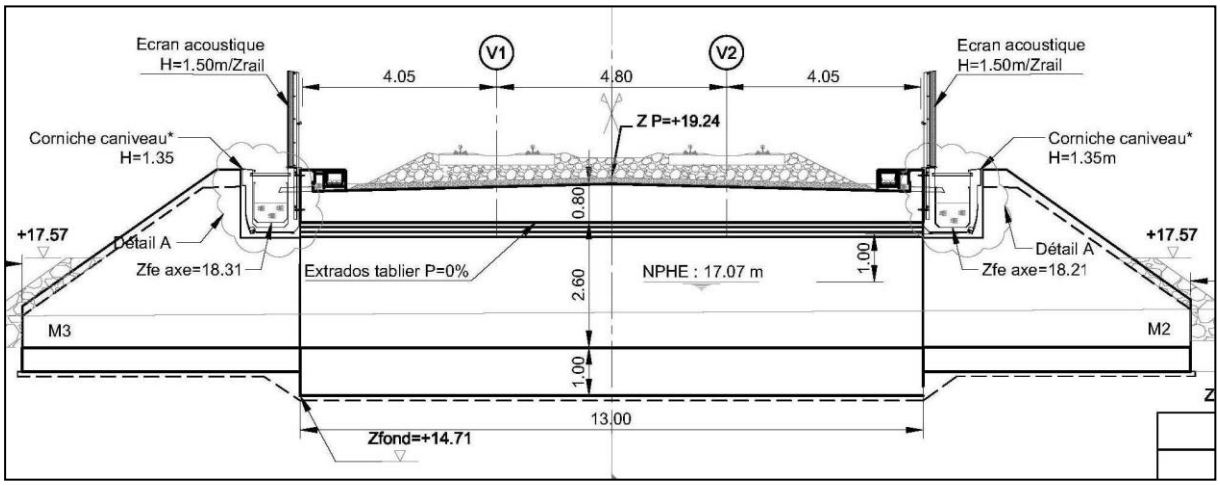

Figure 37. Section of Reinforced Concrete open Frame

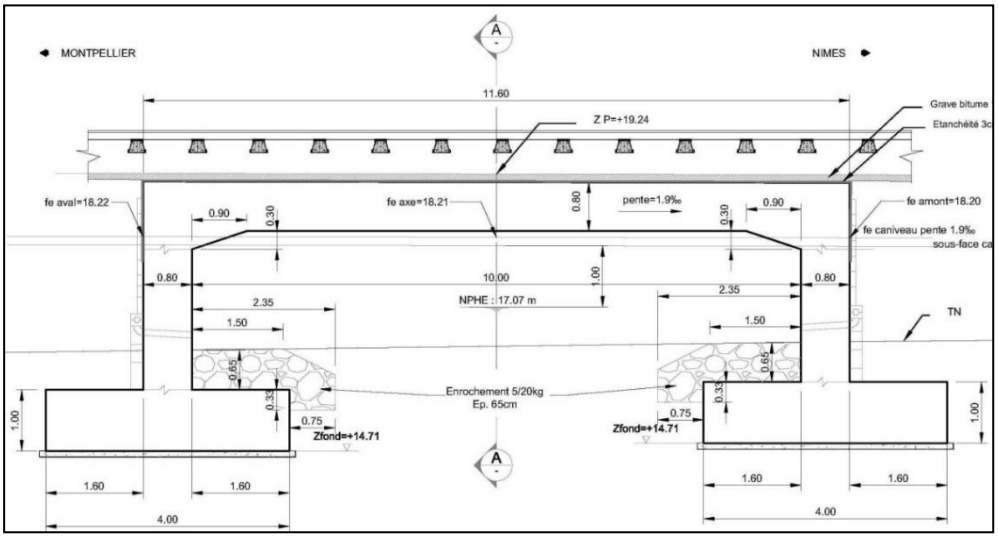

Figure 38. Elevation of Reinforced Concrete open Frame

Two types of reinforced concrete open frames are studied. The main characteristics are shown in the table below:

Type	Span Length [m]	Height of side wall [m]	Side wall thickness [m]	Deck thickness [m]	Width [m]	Foundation	Footing thickness [m]	Footing width [m]	Span Length/Deck thickness
Reinforced concrete open frame	10	5	0.85	0.85	12.9	Footing	1	5.3	12
Reinforced concrete open frame	15	5	1.2	1.2	12.9	Footing	1.1	5.3	13

Figure 39. Main Characteristics of Reinforced Concrete open Frames

REINFORCED CONCRETE CLOSED FRAME

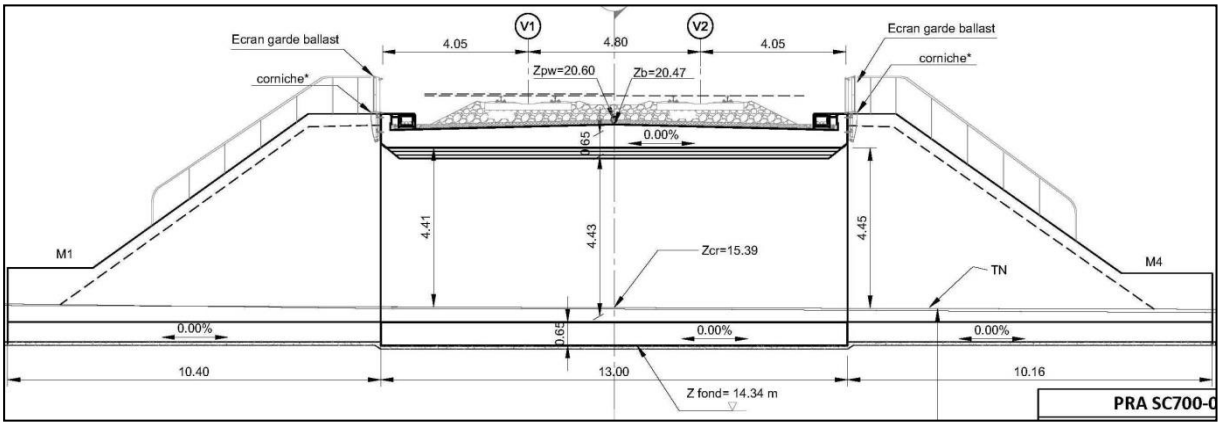

Figure 40. Section of Reinforced Concrete Closed Frame

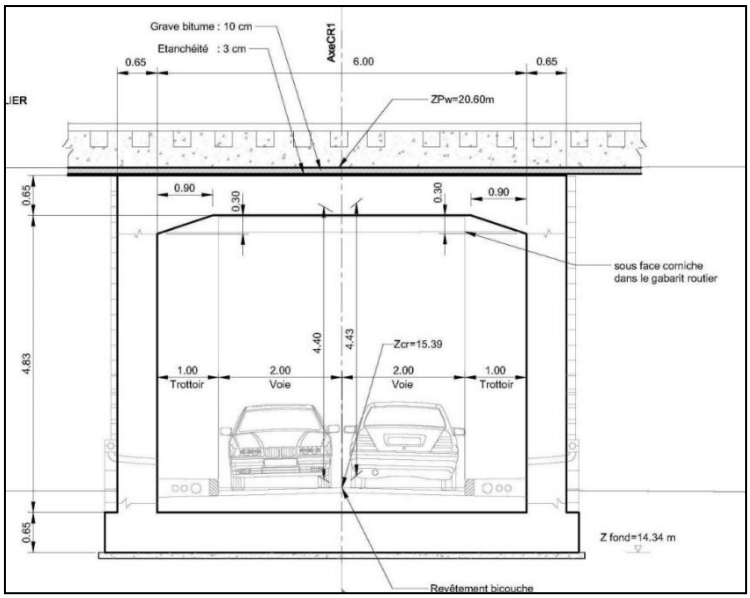

Figure 41. Elevation of Reinforced Concrete Closed Frame

Two types of reinforced concrete closed frames are studied. The main characteristics are shown in the table below:

Type	Span Length [m]	Height of side wall [m]	Side wall thickness [m]	Deck thickness [m]	Width [m]	Foundation	Footing thickness [m]	Footing width [m]	Span Length/Deck thickness
Reinforced concrete closed frame	10	5	1	1	12.9	Footing	1	-	10

Reinforced concrete closed frame	5	5	0.6	0.6	12.9	Footing	0.6	-	8.3

Figure 42. Main Characteristics of Reinforced Concrete Closed Frames

The weights of SIDL applied on these structures are summarized in the table below:

Name	Nominal value(kg/ml)	coef min	coef max	Min value (kN/m)	Max value (kN/m)
ballast barrier h=1,5 m	70	0.8	1.2	0.56	0.84
metal cornice	25	0.8	1.2	0.2	0.3
cable duct	250	0.8	1.2	2	3
drainage channel	75	0.95	1.05	0.71	0.79
TOTAL	420			3.47	4.93
rail weight (for one track)	120.42	0.7	1.3	0.84	1.57

Name	nominal value	minimum value (kg/m²)	maximum value (kg/m²)	Min value (kN/m²)	Max value (kN/m²)
ballast	2000 t/m3	1700*((0.30+0.22)*1.00)	2000*((0.35+0.22)*1.30)	9	15
waterproofing	2200*0.03	vnom*0.80	vnom*1.40	1	1
TOTAL				9	16

Figure 43. Weight of SIDL

4.3.2. Modelling Aspects

4.3.2.1. Bridge models

There are two types of calculations and then two types of modelling:

- Dynamic behaviour of bridge
- Comfort analysis

The dynamic behaviour of bridges, according to Eurocode EN 1991-2 art. 6.4.6 and Eurocode 0 Annex A2 (High speed line train), were carried out using 2D train-bridge with and without track model (see figure below).The bridge is modelled by shell elements, the track, when it is modelled ,by beam elements. Bridge and track are connected by vertical springs. The soil stiffness is considered equal to 15333 kN/m^3. It isn't a coupled system (no interaction between train and bridge). The analysis is solved using direct integration method (Wilson-theta).

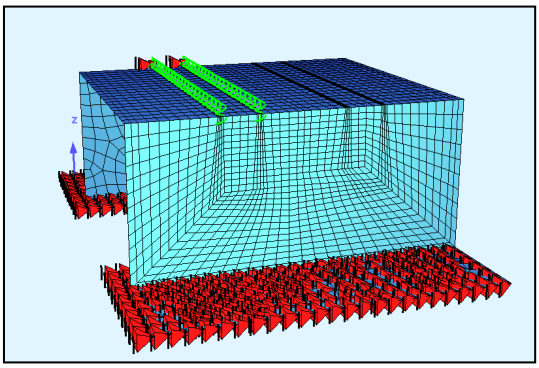

Figure 44. Bridge model - no coupled system

The comfort analyses were carried out using 2D train-bridge without track model (see figure below).The bridge is modelled by shell quadrilateral elements; the train load is modelled by beam and discrete masses connected by vertical springs and dampers. It is a coupled system (interaction between train and bridge). The analysis is solved using direct integration method (Wilson-theta).

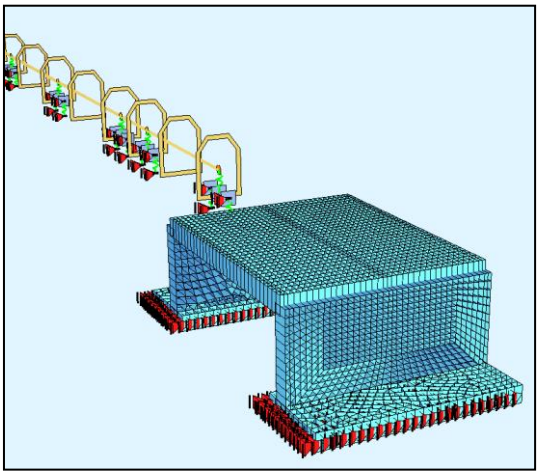

Figure 45. Bridge model - 2D train coupled system

The comfort analyses with track irregularities were carried out using 3D train-bridge without track model (see figure below). The track irregularities were taken into account by using PSD, the detailed description is in paragraph “track irregularities”. The bridge is modelled by shell elements; the train load is modelled by beam and discrete masses connected by vertical springs and dampers. It is a coupled system (interaction between train and bridge). The analysis is solved using direct integration method (Wilson-theta).

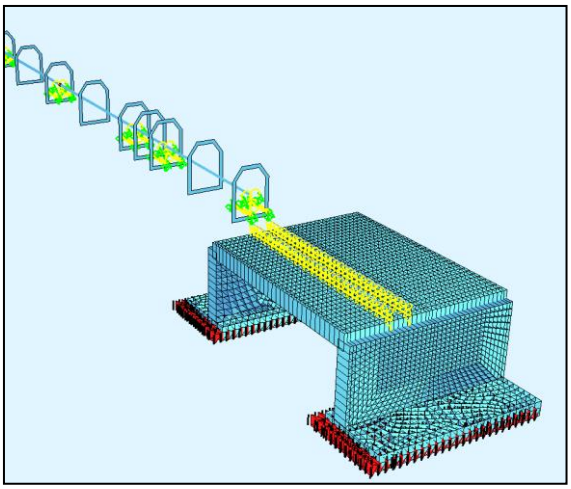

Figure 46. Bridge model - 3D train coupled system

4.3.2.2. Train models

The dynamic and comfort analysis were carried out using:

For dynamic behaviour of bridge: 10 HSLM trains

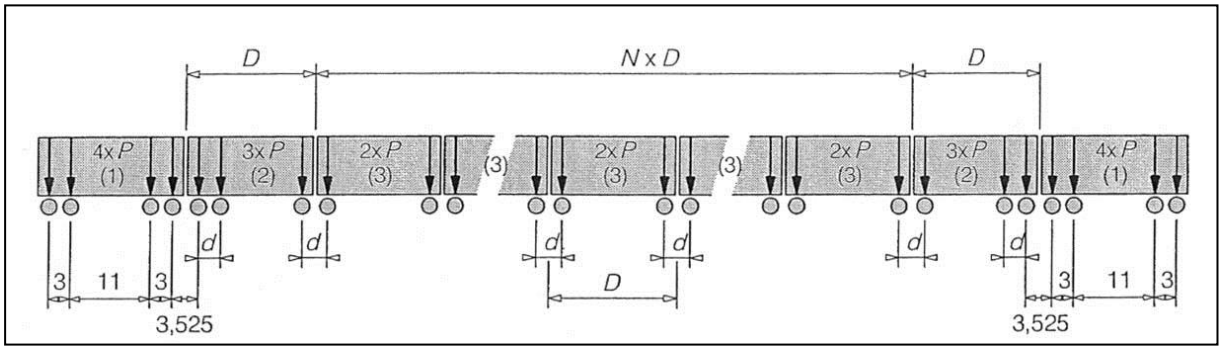

Figure 47. HSLM Trains

Universal Train	Number of intermediate coaches N	Coach length D [m]	Bogie axle spacing d [m]	Point force P [kN]
A1	18	18	2,0	170
A2	17	19	3,5	200
A3	16	20	2,0	180
A4	15	21	3,0	190
A5	14	22	2,0	170
A6	13	23	2,0	180
A7	13	24	2,0	190
A8	12	25	2,5	190
A9	11	26	2,0	210
A10	11	27	2,0	210

Figure 48. HSLM Train Loads

For comfort analysis 2D and 3D model of French TGV was used.

Characteristics of the TGV, French high speed train, are used. Nominal loads and spacing between loads are shown hereafter:

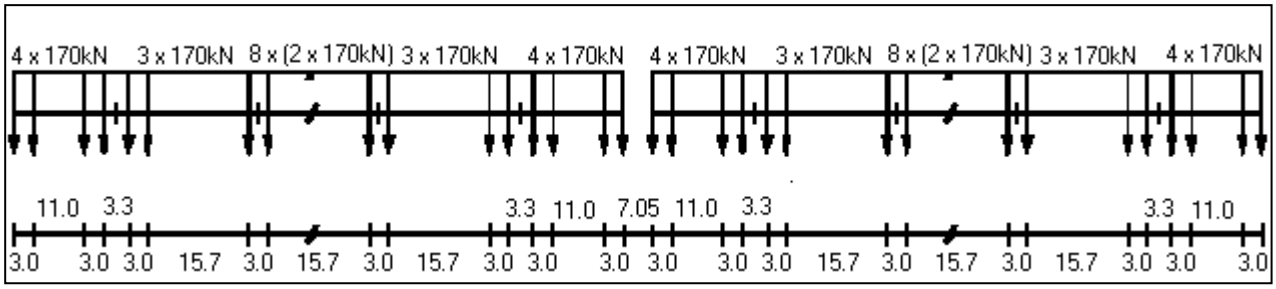

Figure 49. French TGV nominal Loads

French TGV convoy is composed with following car sequence:

[M + R1 + 8 x R2-R9 + R10 + M] + [M + R1 + 8 x R2-R9 + R10 + M]

First train Second train

TGV TRAIN MODEL CHARACTERISTICS

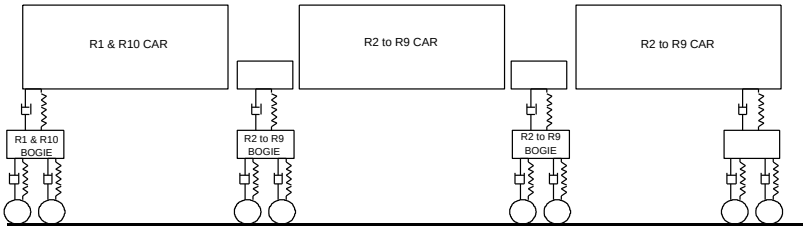

TGV R1 & R10 CAR

			Vertical translation & Transverse axis rotation	Transverse translation & Longitudinal axis rotation
NOMINAL LOAD		kN/wheelset	170	-
MASS				
Car	cog	m	7.93 / bogie axis	1.62 / rail top
	translation	kg	36240	36240
	rotation	$kg.m^2$	1675737	1675737
Bogie	cog	m	-	0.60 / rail top
	translation	kg	3250	3250
	rotation	$kg.m^2$	2773	1138
Wheel	cog	m	-	0.46 / rail top
	translation	kg/wheel	1000	1000
SPRINGS				
Primary	translation	kN / m / bogie	3280	22400
	rotation	kN.m / rad / bogie	7380	3380
Secondary	translation	kN / m / bogie	637	482
	rotation	kN.m / rad / bogie	-	657
DAMPERS				
Primary	translation	kN.s / m / bogie	20	0
	rotation	kN.m.s / rad / bogie	45	20.6
Secondary	translation	kN.s / m / bogie	40	80
	rotation	kN.m.s / rad / bogie	-	41.2
SPACINGS				
Bogie wheel long spacing		m	3	
Bogies axis long spacing		m	18.7	

TGV R2 & R9 CAR

			Vertical translation & Transverse axis rotation	Transverse translation & Longitudinal axis rotation
NOMINAL LOAD		kN/wheelset	170	-
MASS				
Car	cog	m	9.35 / bogie axis	1.62 / rail top
	translation	kg	26350	26350
	rotation	$kg.m^2$	948600	948600
Bogie	cog	m	-	0.60 / rail top
	translation	kg	3200	3200
	rotation	$kg.m^2$	2731	1121
Wheel	cog	m	-	0.46 / rail top
	translation	kg/wheel	1000	1000
SPRINGS				
Primary	translation	kN / m / bogie	3280	22400
	rotation	kN.m / rad / bogie	7380	3380
Secondary	translation	kN / m / bogie	588	482
	rotation	kN.m / rad / bogie	-	606
DAMPERS				
Primary	translation	kN.s / m / bogie	20	0
	rotation	kN.m.s / rad / bogie	45	20.6
Secondary	translation	kN.s / m / bogie	0	80
	rotation	kN.m.s / rad / bogie	-	41.2
SPACINGS				
Bogie wheel long spacing		m	3	
Bogies axis long spacing		m	18.7	

Figure 50.French TGV Train 3D Model Characteristics

The vertical and transverse Eigenvalues are calculated for passenger car of French TGV for the primary and secondary suspension. The values are shown on the table below:

French TGV R2 & R9	vertical translation	transversal rotation	transversal translation	longitudinal rotation
	f (Hz)	f (Hz)	f (Hz)	f (Hz)
car	0.72	0.0	0.68	0.12
bogie	7.53	11.7	18.9	12.9

Figure 51. French TGV Eigenvalues for passenger car

For comfort analysis 2D model of ICE2 was used.

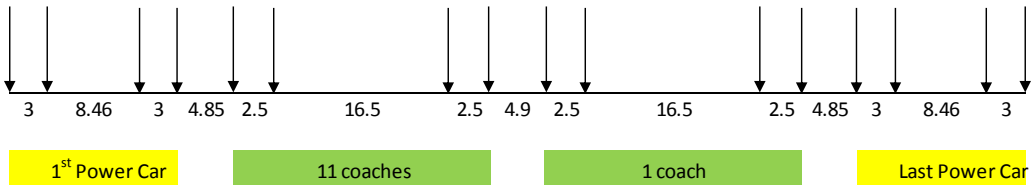

Number of axles, N = 56 — Distance between regularly spaced groups of axles, d = 26.4 m

Axle No k	l_k m	P_k kN	Axle No k	l_k m	P_k kN	Axle No k	l_k m	P_k kN
1	0	195	21	124.91	112	41	256.91	112
2	3	195	22	127.41	112	42	259.41	112
3	11.46	195	23	143.91	112	43	275.91	112
4	14.46	195	24	146.41	112	44	278.41	112
5	19.31	112	25	151.31	112	45	283.31	112
6	21.81	112	26	153.81	112	46	285.81	112
7	38.31	112	27	170.31	112	47	302.31	112
8	40.81	112	28	172.81	112	48	304.81	112
9	45.71	112	29	177.71	112	49	309.71	112
10	48.21	112	30	180.21	112	50	312.21	112
11	64.71	112	31	196.71	112	51	328.71	112
12	67.21	112	32	199.21	112	52	331.21	112
13	72.11	112	33	204.11	112	53	336.06	195
14	74.61	112	34	206.61	112	54	339.06	195
15	91.11	112	35	223.11	112	55	347.52	195
16	93.61	112	36	225.61	112	56	350.52	195
17	98.51	112	37	230.51	112			
18	101.01	112	38	233.01	112			
19	117.51	112	39	249.51	112			
20	120.01	112	40	252.01	112			

Figure 52. ICE2 nominal Loads

Dynamic data of an ICE 2 power car

Type of train	ICE 2 power car		Unit
Car body	mass	60 768	kg
	moment of inertia	$1.344 \cdot 10^6$	kgm²
Bogie	mass	5600	kg
	moment of inertia	21 840	kgm²
Wheelset	mass	2003	kg
Wheelset load		$1.962 \cdot 10^5$	N
Stiffness coefficients	secondary/bogie	$1.76 \cdot 10^6$	N/m
	primary/wheelset	$4.80 \cdot 10^6$	N/m
Damping coefficients	secondary/bogie	$1.52 \cdot 10^5$	Ns/m
	primary/wheelset	$1.08 \cdot 10^5$	Ns/m
Length of the car		20.9	m
Distance between centre of gravity of car body and pivot of leading bogie		5.75	m
Distance between centre of gravity of car body and pivot of trailing bogie		5.75	m
Wheelbase		3.0	m

Dynamic data of an ICE 2 coach

Type of train	ICE 2 coach		Unit
Vehicle body	mass	33 930	kg
	moment of inertia	$2.115 \cdot 10^6$	kgm²
Bogie	mass	2373	kg
	moment of inertia	1832	kgm²
Wheelset	mass	1728	kg
Wheelset load		$1.12 \cdot 10^5$	N
Stiffness coefficients	secondary/bogie	$3.0 \cdot 10^5$	N/m
	primary/wheelset	$1.6 \cdot 10^6$	N/m
Damping coefficients	secondary/bogie	$6.0 \cdot 10^3$	Ns/m
	primary/wheelset	$2.0 \cdot 10^4$	Ns/m
Length of the vehicle		26.4	m
Distance between centre of gravity of vehicle body and pivot of leading bogie		9.5	m
Distance between centre of gravity of vehicle body and pivot of trailing bogie		9.5	m
Wheelbase		2.5	m

Figure 53. ICE2 Train 2D Model Characteristics

The vertical Eigenvalues are calculated for passenger car of ICE2 for the primary and secondary suspension. The values are shown on the table below:

ICE 2 coach	vertical translation
	f (Hz)
car	0.45
bogie	6.11

Figure 54. French TGV Eigenvalues for passenger car

4.3.2.3. TRACK MODELS

Three modelling of track have been considered for the dynamic analysis of bridges:

- Perfect contact between load and bridge

Only one line is modelled by beam elements with a vertical stiffness of ballast equal to 50000 kN/lm

- Two lines are modelled by beam elements with a vertical stiffness of ballast equal to 25000 kN/lm

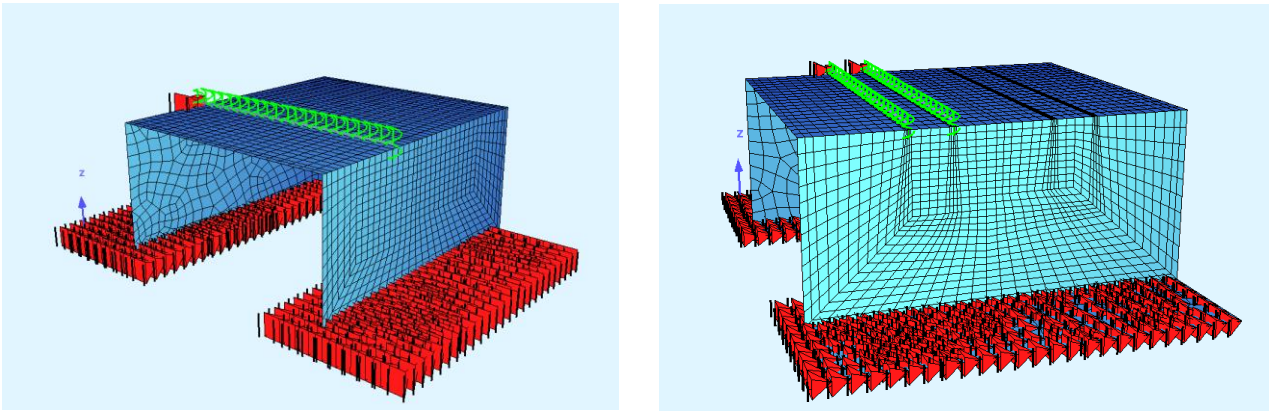

Figure 55. One line and two lines models

The ballast is modelled only in the deck area. Outside the deck area the ballast is not modelled.

In the table below stiffness and damping values of the ballast, considered in the literature, are shown.

Stiffness and damping values of the ballast

SOURCE	BALLAST STIFFNESS (MN/ m)	BALLAST DAMPING (MN.S/ m)	BALLAST SHEAR STIFFNESS (MN/ m)	BALLAST SHEAR DAMPING (MN.S/ m)	ASSUMPTIONS
J.M.Olmos, M.A.Astiz. Analysis of the lateral dynamic response of high pier viaducts under high-speed train travel. Engineering Structures 56 (2013) 1384-1401.	50	0.20	37	0.24	
Mécanique de la voie. SNCF octobre 1981.	100-300				
D.Herron, C.Jones, D.Thompson. Characterising the high-frequency dynamic stiffness of railway ballast. ICSV16, Poland, 5-9 July 2009.	100-500				For a 300mm deep layer of ballast, subject to a preload of 20KN. The value of the stiffness is constant between 0 and 100Hz. Beyond 100Hz it increases
W.M.Zhai, K.Y.Wang, J.H.Lin. Modelling and experiment of railway ballast vibrations. Journal of Sound and Vibration 270 (2004) 673-683	138	0.059	78.4	0.08	Ballast thickness : 0.45 m Sleeper spacing : 0.545 m

Track Stiffness

SOURCE	TRACK STIFFNESS PER RAIL CORRESPONDING TO THE VERTICAL DISPLACEMENT OF 1 TO 2 MM (MN/ m)
UIC Project I/03/U/283 – Ballastless Track – Version 2005-08-02	50-100

Figure 56. Stiffness and damping values of the ballast in the literature

4.3.2.4. TRACK IRREGULARITIES AND RAIL SURFACE ROUGHNESS

The effects of track irregularities in vertical and in horizontal direction are taken into account in dynamic and comfort analysis.

The track irregularities are generated through the power spectra density (PSD). Track irregularity for TGV line is issued from measures on TGV French North line. S_v is for vertical irregularity, S_a is for the horizontal irregularity.

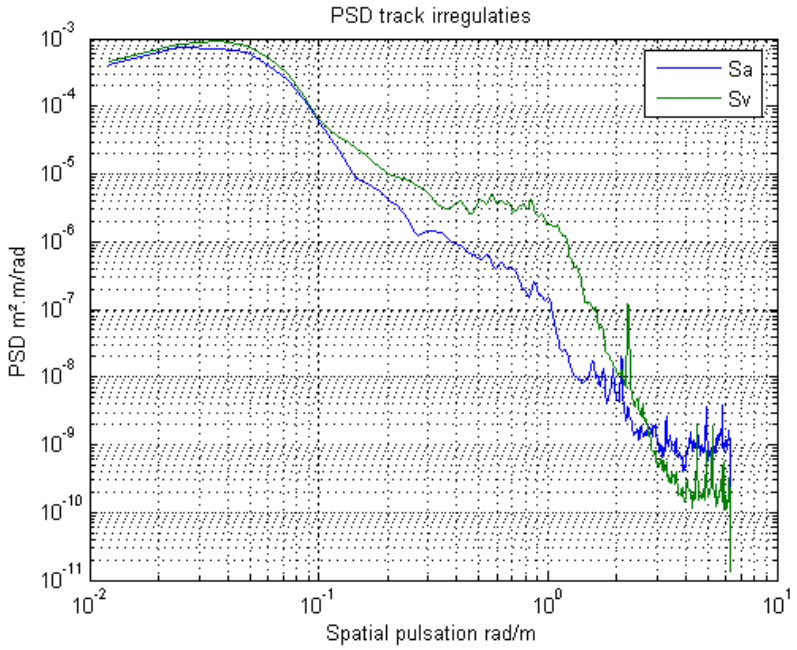

Figure 57. PSD track irregularities (horizontal and vertical)

For a given train speed, trajectory of track due to irregularity is calculated as follow:

$t_v(x) = \Sigma_i A_i \cos(\omega_i t + \varphi_i)$ [m]

$A_i = (2.Sv(\omega_i).\Delta\omega)^{0.5}$ [rad*m]

$t_v(x)$: trajectory of the alignment irregularity [m]

$Sv(\omega)$: power spectral density of vertical irregularity [m²/m/rad],

ω : spatial angular frequency [rad/m]

φ_i : randomly chosen phase

The maximum value of track irregularity is ±4 mm.

The input data of PSD of TGV French North Line were defined in the Sofistik software with the appropriate unit. Therefore the PSD defined by spatial pulsation [rad\m] has been converted to [rad/s].

Ω [rad/m] → to convert → ω [rad/s]

S (Ω) [m²/(rad/m)] → S(ω) [m²/(rad/s)]

For a constant speed: $v = \frac{x}{t}$

Ω*x = ω * t => ω = Ω * v => dω = v*dΩ [rad/s]

S(ω)*dω = S(Ω)*dΩ [m²]

$S(\omega) = S(\Omega) * \frac{d\Omega}{d\omega} = S(\Omega) * \frac{1}{v}$ [m²/(rad/s)]

After this conversion, the PSD is defined in (ω [rad/s], S(ω) [m²/(rad/s)]). This function is defined in Sofistik software with FUNC T= [1/sec] F= [M2/M].

To define the vertical profile of track irregularities the function SIMQ is used. This function allows to superpose the PDS and a typical Intensity function (generally used for seismic accelerograms).

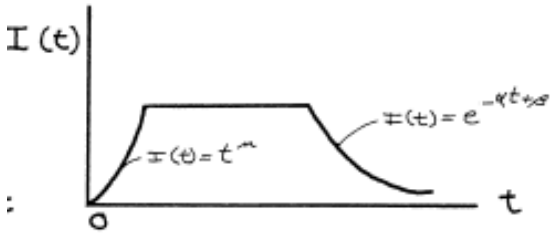

Figure 58. Intensity function

These types of profiles are generated:

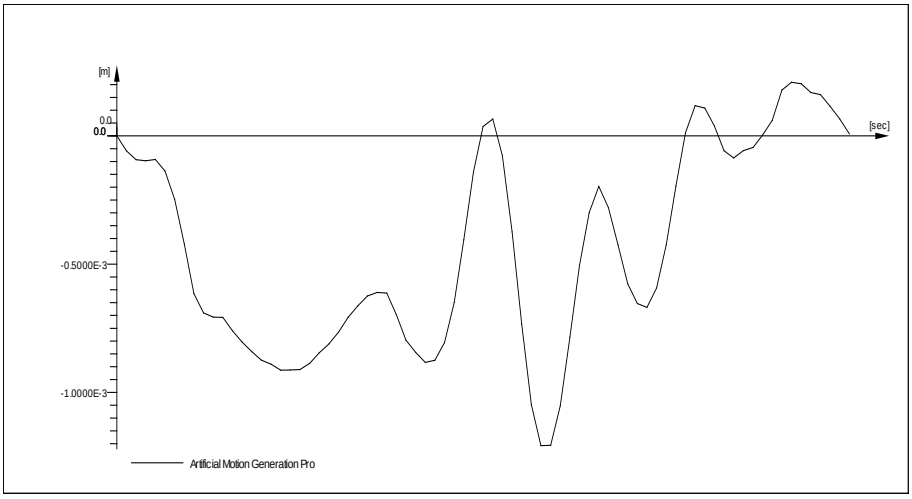

Figure 59. Vertical irregularity track for one speed in function of time.

The Wilson-Theta integration method is used for the time history analysis. Θ is equal to 1.40.

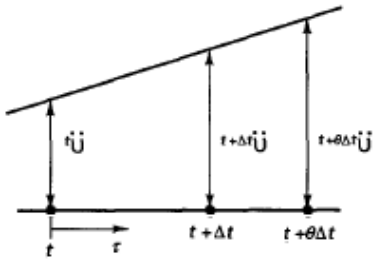

Figure 60. Wilson-theta integration method.

4.3.3. METHODS OF DYNAMIC ANALYSIS

The analysis was performed with Sofistik Software, version 2016. Dynamic and comfort analysis were carried out by direct time-history analysis. The equation of motion has been solved numerically by direct integration. The time step chosen for all calculations is 0.003s or 0.002s.

The time step of 0.003 s corresponds approximatively to a frequency equal to 10 times the maximum frequency (10 x 30 Hz), which is usual practice for time-history analysis.

No filter has been used in this analysis. It should be possible to use filter in order to avoid all frequencies above 30 Hz. (see the UIC 776-4 art A.6.2.4).

The integration method used for calculations is Wilson-theta method. This method is a modification of Newmark method where the numerical damping enlarges the period to a greater extent, but keeps the amplitudes to a higher accuracy.

4.3.4. RESULTS OF DYNAMIC ANALYSIS

4.3.4.1. DAMPING CHARACTERISTICS FOR DYNAMIC ANALYSIS

Present here parameter for dynamic analysis: total considered masses, damping, first vertical frequency, maximal considered frequency for dynamic analysis, Rayleigh damping.

	Open frame 10m	**Open frame 15m**	**Closed frame 5m**	**Closed frame 10m**
Masses [tons]	1104	1702	505	1238
ξ [%]	2.141	1.766	2.508	2.13
Δξ [%]	0.387	0.628	0.128	0.398
Total damping [%]	2.528	2.394	2.636	2.528
f1 (First Vertical Frequency) [Hz]	6.541	5.268	8.722	7.025
f2 (F max) [Hz]	30	30	30	30

Rayleigh Mass proportional damping A	1.706	1.348	2.238	1.808
Rayleigh Stiffness proportional damping B	0.000220	0.000216	0.000217	0.000217

Figure 61. Damping Characteristics for Dynamic Analysis for de Deck behavior

4.3.4.2. Comparison of one loaded line vs two loaded lines (with or without ballast stiffness)

Dynamic analyses were carried out considering four different hypothesis:

- Perfect contact between train and bridge, only one loaded line is considered (one for the whole track)
- Perfect contact between train and bridge, two loaded lines are considered (one per rail)
- Ballast is modelled between rail and bridge. Only one line is modelled. The ballast has a vertical stiffness equal to 50000 kN/lm
- Ballast is modelled between rail and bridge. Two lines are modelled. The ballast has a vertical stiffness equal to 25000 kN/lm for each line.

The 10 HSLM trains are considered.

Speed from 144 km/h to 480 km/h with a speed step equal to 5 km/h.

OPEN FRAME 10M

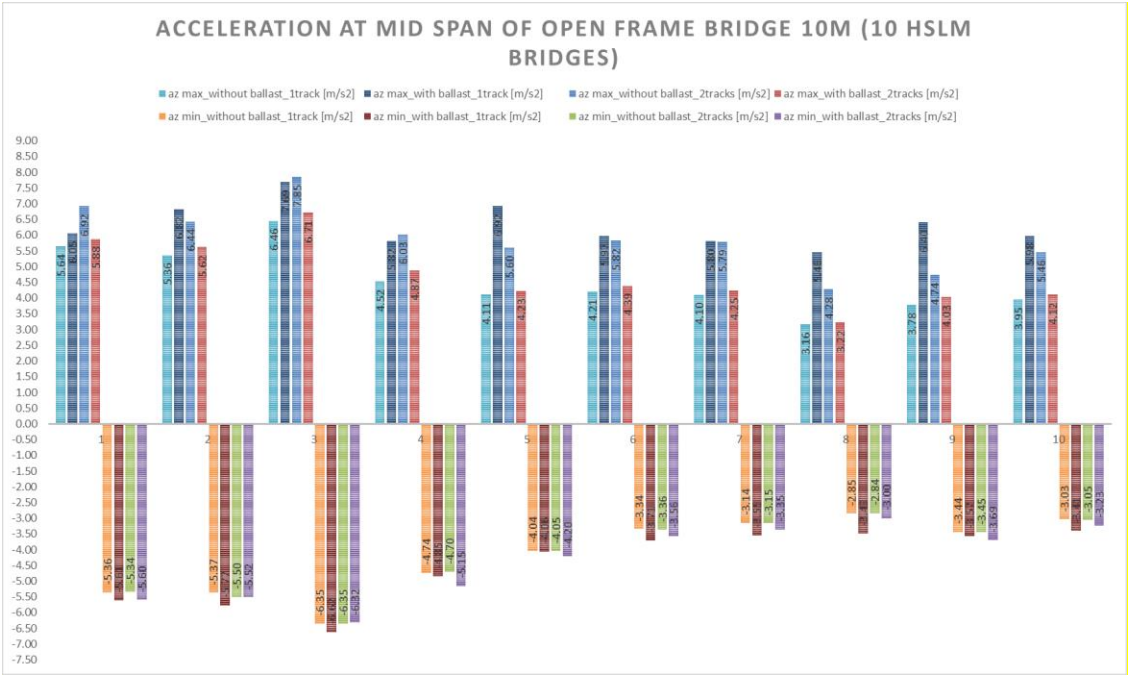

Figure 62. Comparison between one loaded line vs two loaded lines with or without ballast for open frame 10m (Acceleration)

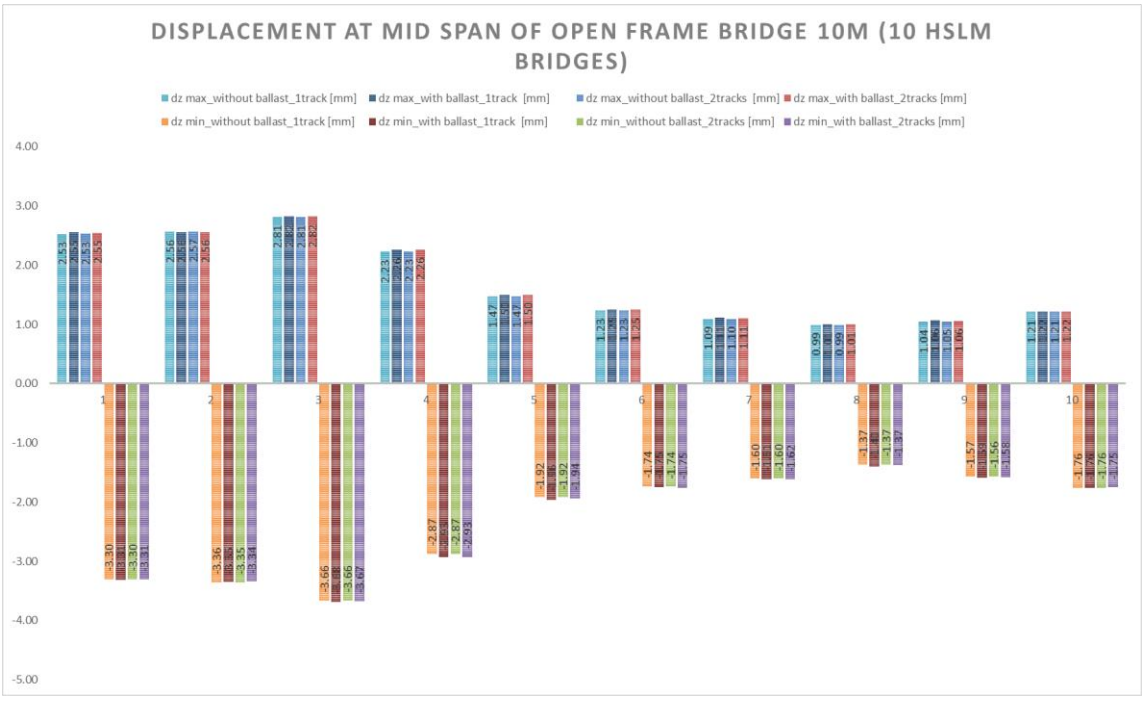

Figure 63. Comparison between one loaded line vs two loaded lines with or without ballast for open frame 10m (Displacements)

OPEN FRAME 15M

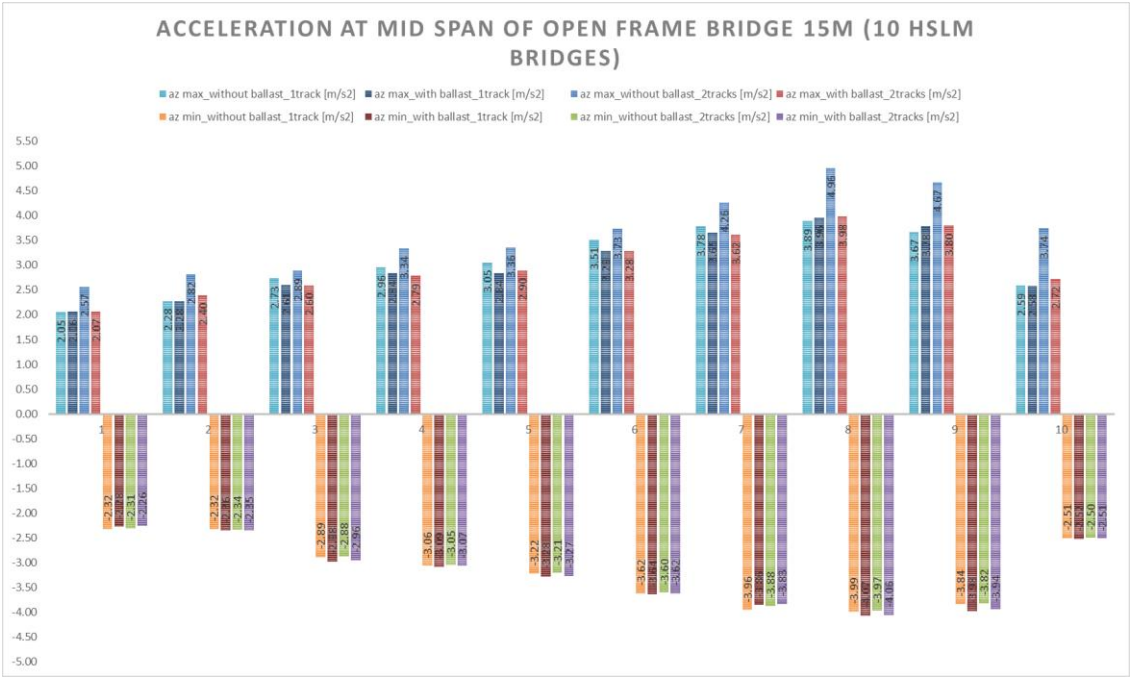

Figure 64. Comparison between one loaded line vs two loaded lines with or without ballast for open frame 15m (Acceleration)

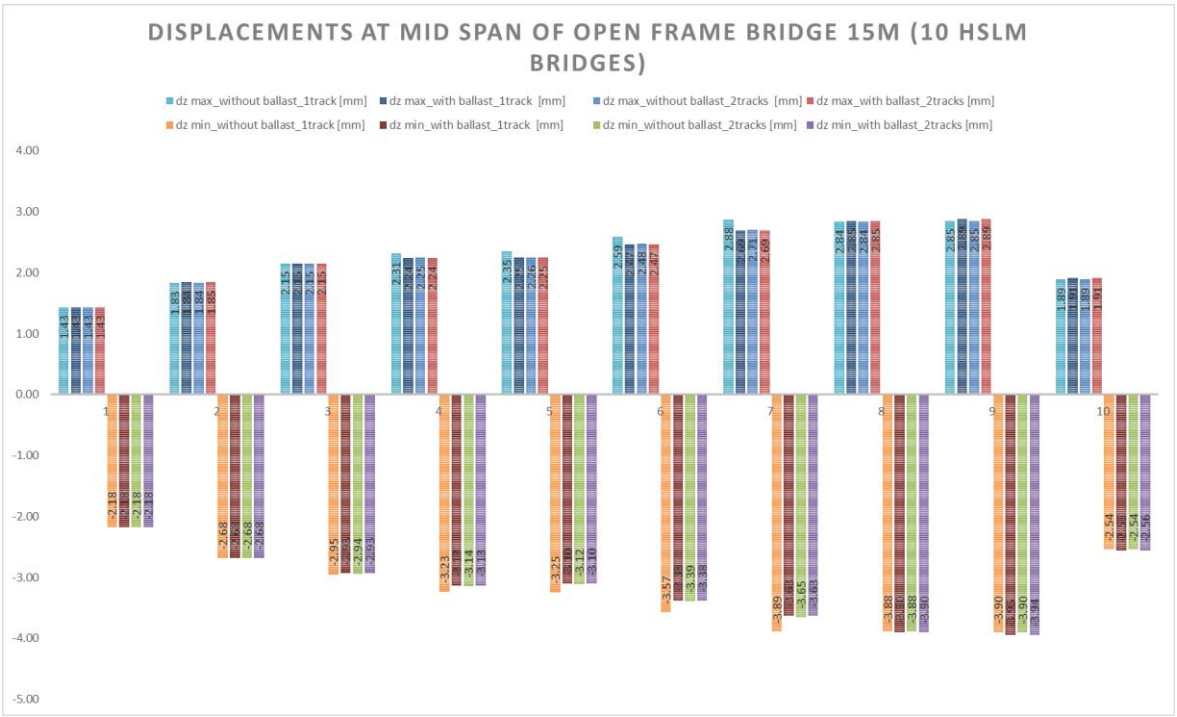

Figure 65. Comparison between one loaded lane vs two loaded lanes with or without ballast for open frame 15m (Displacements)

CLOSED FRAME 5M

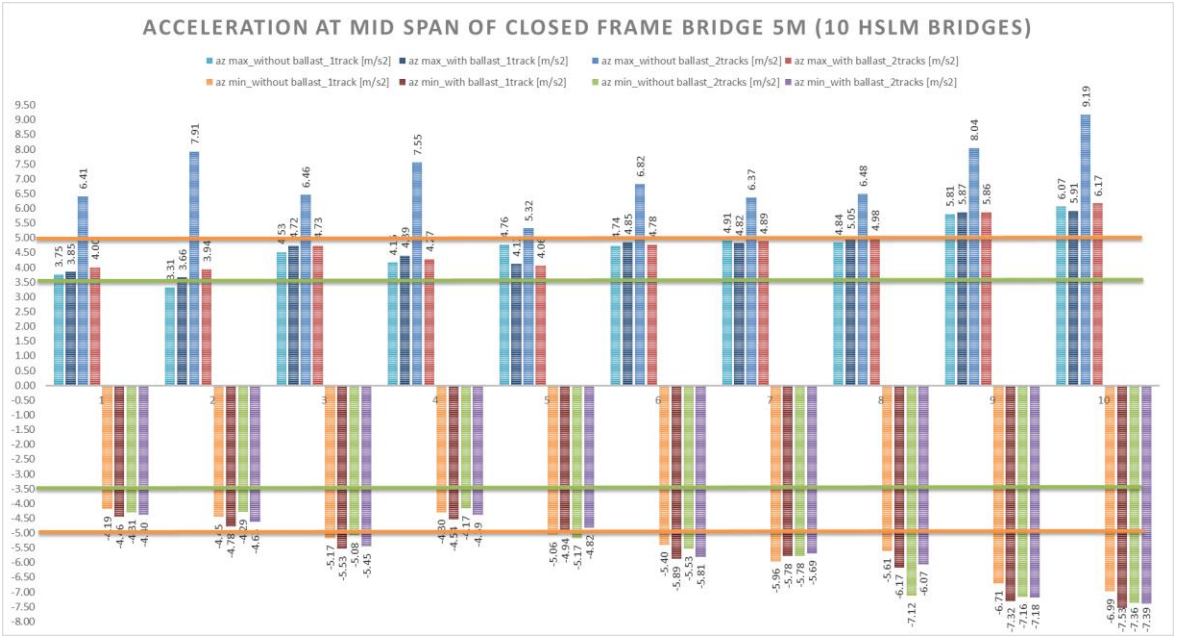

Figure 66. Comparison between one loaded line vs two loaded lines with or without ballast for closed frame 5m (Acceleration)

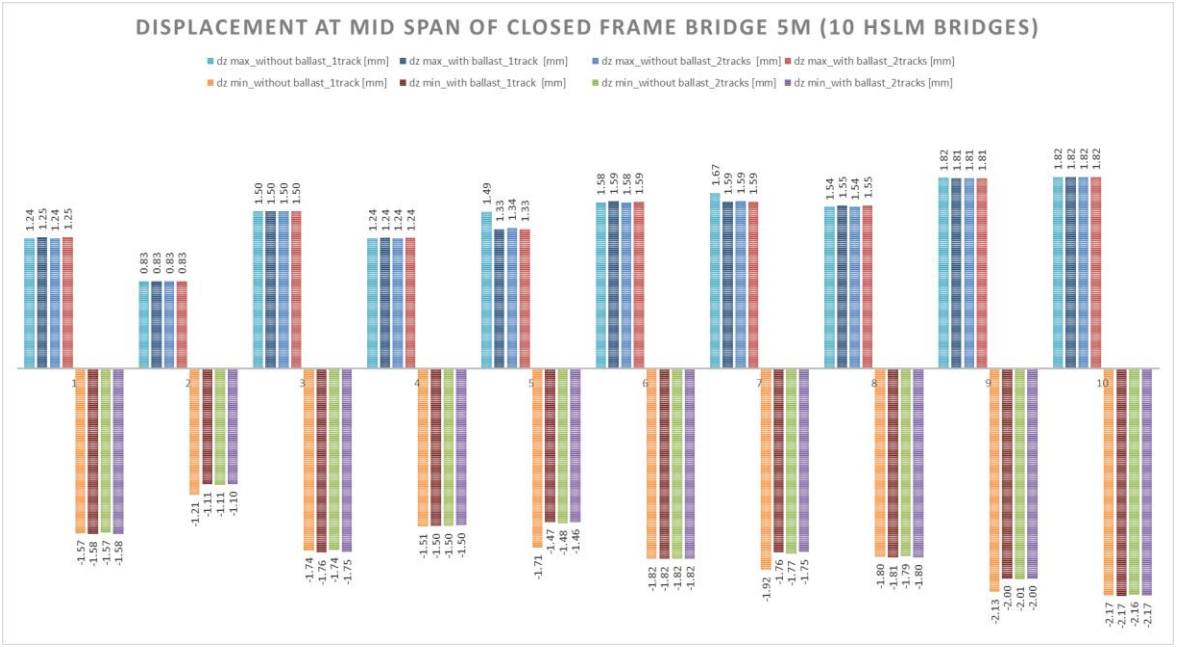

Figure 67. Comparison between one loaded line vs two loaded lines with or without ballast for closed frame 5m (Displacements)

CLOSED FRAME 10M

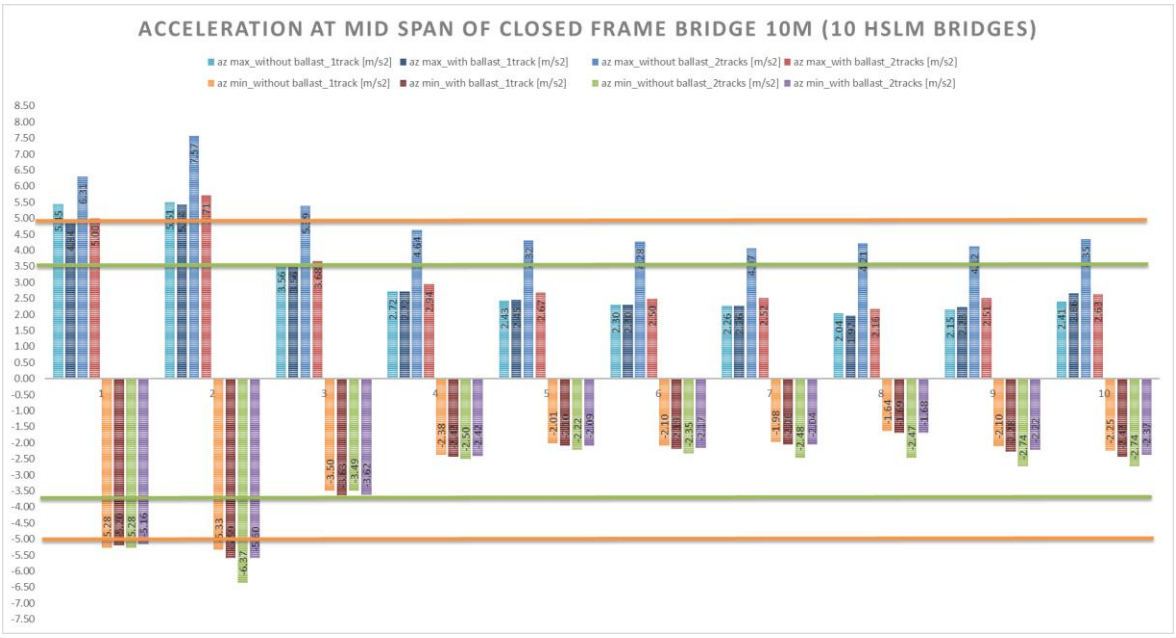

Figure 68. Comparison between one loaded line vs two loaded lines with or without ballast for closed frame 10m (Acceleration)

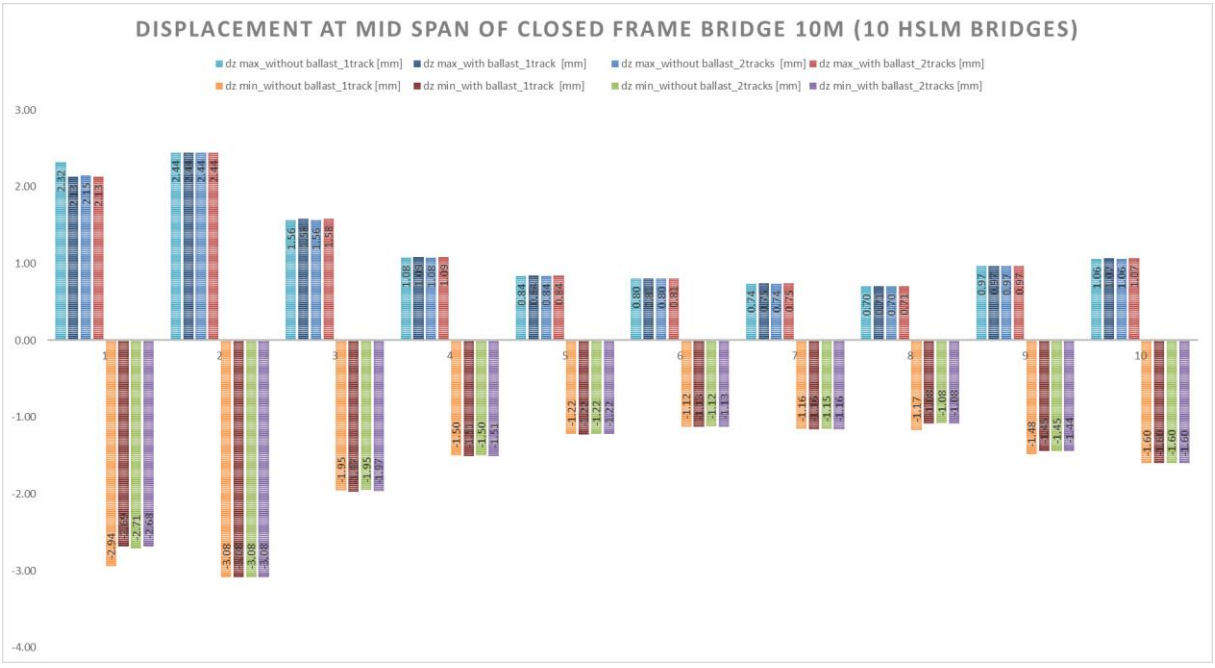

Figure 69. Comparison between one loaded line vs two loaded lines with or without ballast for closed frame 10m (Displacements)

We noted that:

- In the models where only one loaded line is considered, the acceleration at mid span of bridge is higher than in the models where two loaded lines are modelled. This increase corresponds to 10 % - 15 %,
- In the models where only one loaded line is considered, the vertical displacement at mid span of bridge is higher than in the models where two loaded lines are modelled. This increase corresponds to ,10 %,
- In the models where vertical stiffness of ballast is modelled, accelerations and displacements are similar than in the models where ballast is not modelled.
- In the model where vertical stiffness and damping of ballast is modelled, the impact of ballast damping is negligible.

  As the ballast stiffness and ballast damping have no impact on the results, they will be neglected in some of the following studies.

4.3.4.3. MODEL WITH LATERAL STIFFNESS OF SOIL

To evaluate the impact of lateral stiffness of soil on deck acceleration and displacement we model the soil by lateral area springs. The horizontal stiffness is variable linearly in z direction and it follows the law below:

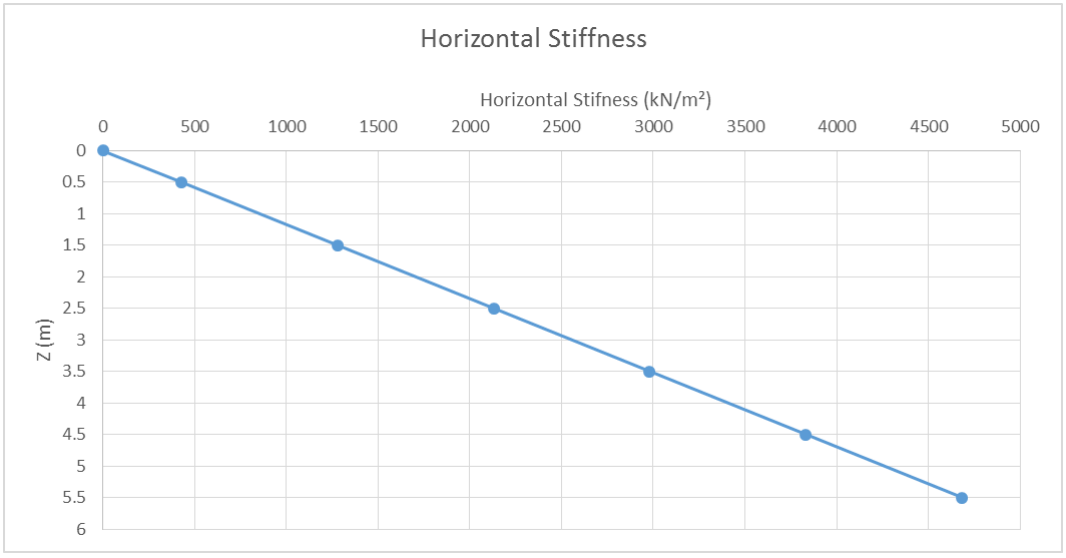

Figure 70. Linear variations in z direction for horizontal stiffness

We have analyzed vertical displacements at mid span and accelerations for closed frame 5m and open frame 10m length, without lateral soil springs and with lateral soil springs.

CLOSED FRAME 5M

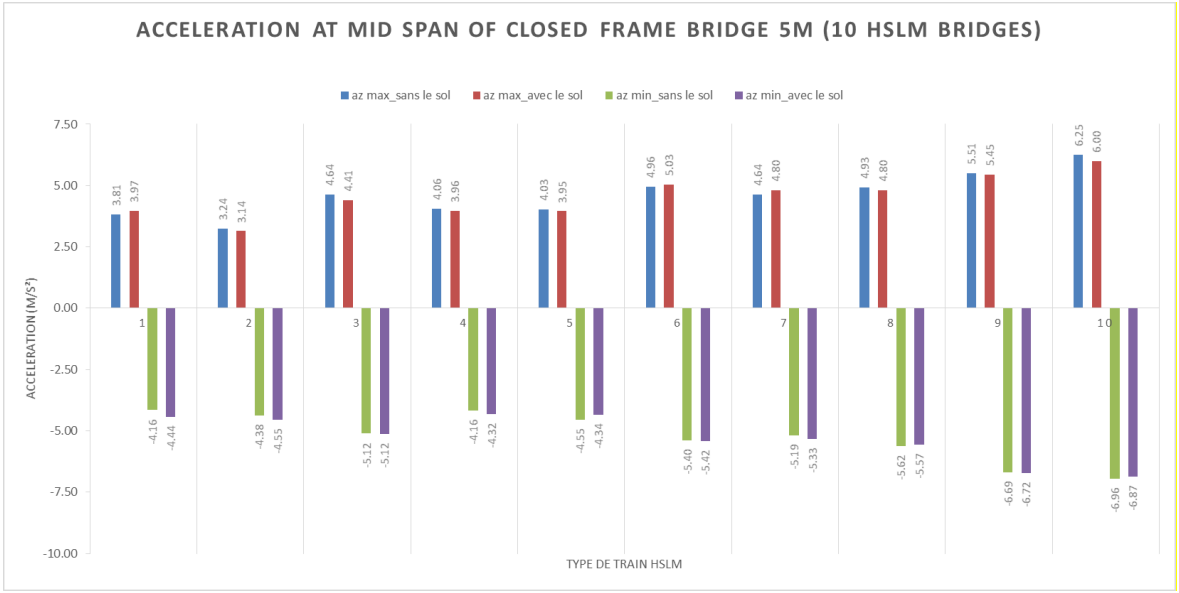

Figure 71. deck acceleration at mid span for closed frame 5m with or without lateral soil model

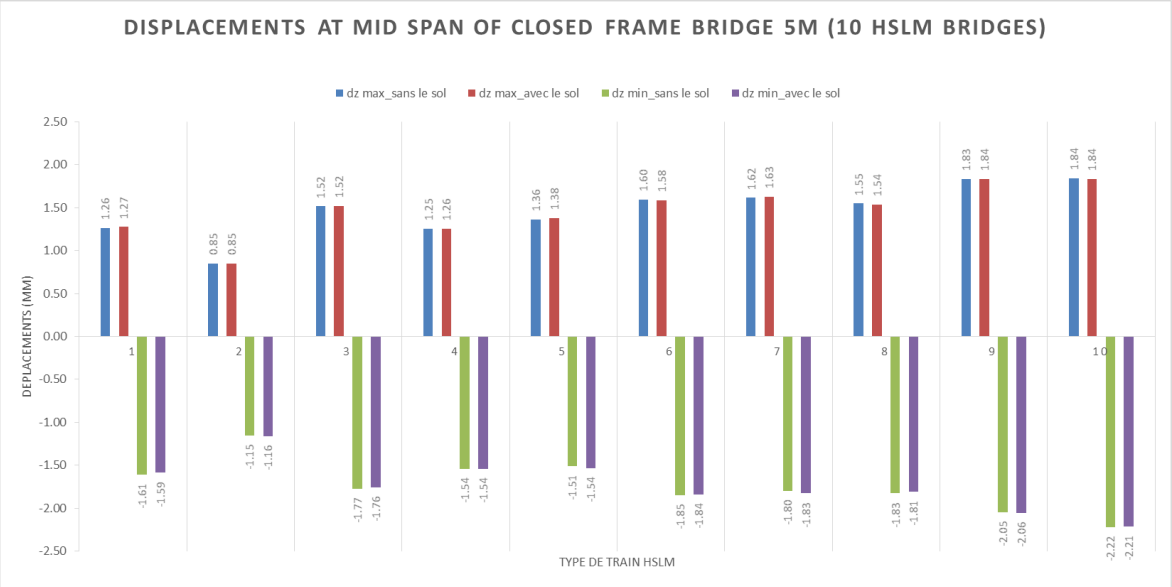

Figure 72. deck displacement at mid span for closed frame 5m with or without lateral soil model

OPEN FRAME 10M

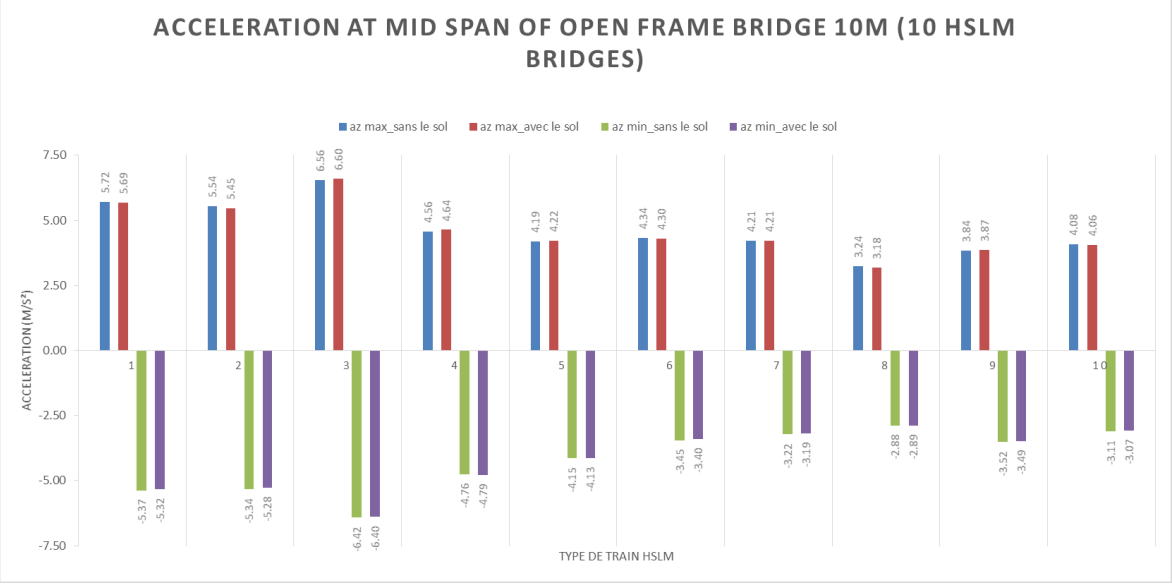

Figure 73. Deck Acceleration at mid span for Open frame 10m with or without lateral soil model

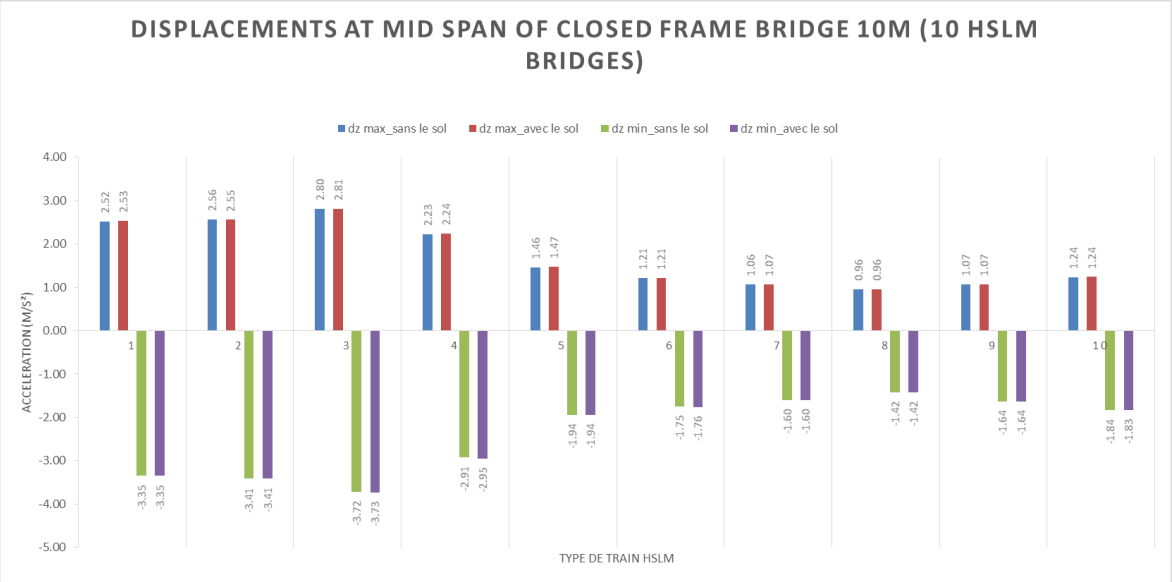

Figure 74. Deck Displacement at mid span for open frame 10m with or without lateral soil model

CONCLUSIONS

We noted that the consideration of lateral stiffness of soil has no significant impact in the results, neither for displacements nor for accelerations.

Therefore, the lateral stiffness of soil will be neglected in all of the following studies.

4.3.4.4. Allowable Speed to match with dynamic criteria for HSLM train

Dynamic analyses were carried out considering two different hypothesis below:

- Perfect contact between train and bridge, two loaded lines are considered (track without ballast)
- Ballast is modelled between rail and bridge. Two lines are modelled. The ballast has a vertical stiffness equal to 25000 KN/lm for each line.

  In both cases:
- The 10 HSLM trains are considered
- Speed from 144 km/h to 480 km/h (1.2*400 km/h) with a speed step equal to 5 km/h.

  According to EN 1990, Annexe A2, Art. A.2.4.4.2.1, allowable vertical deck acceleration is 3.5 m/s^2 with ballast and 5 m/s^2 without ballast.

Open Frame 10m (two ballasted tracks)

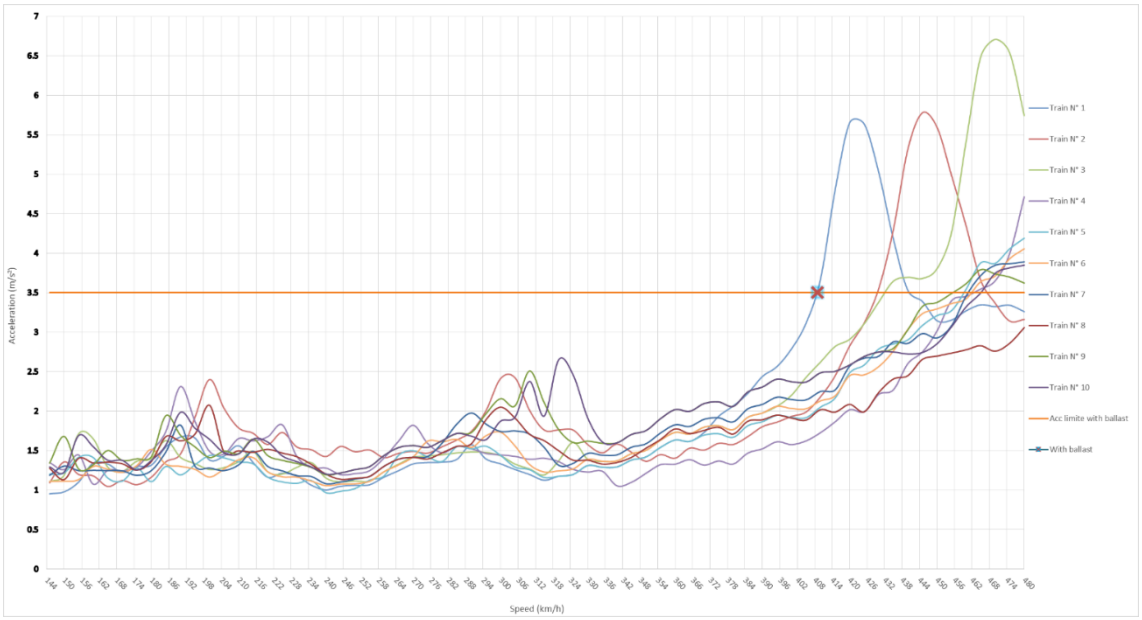

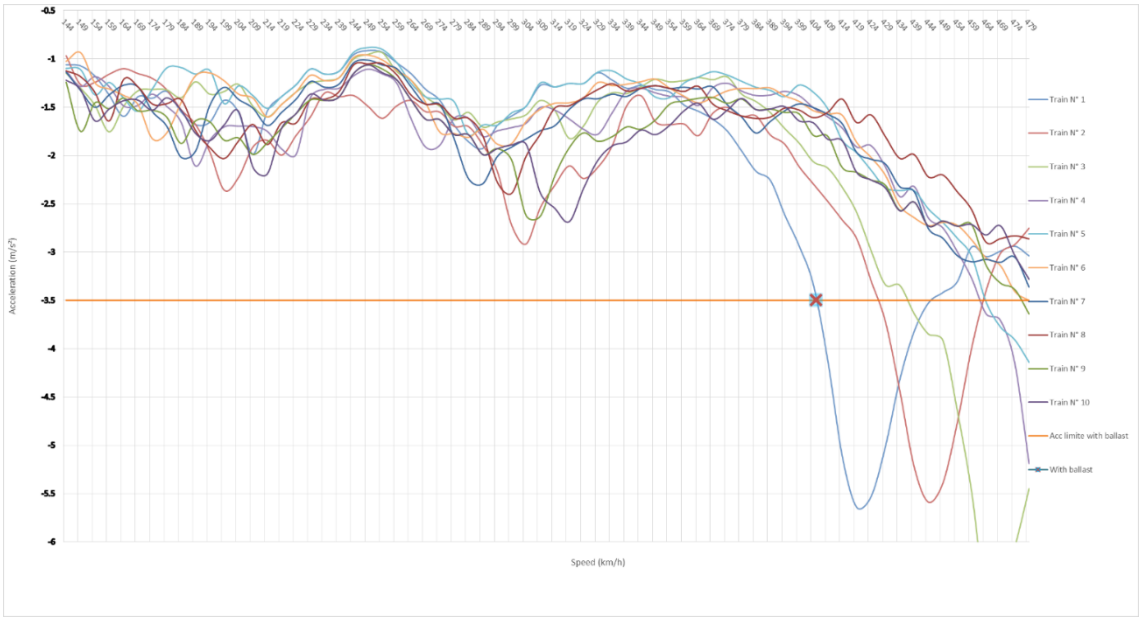

Figure 75. Maximum and minimum Acceleration Results for open frame bridge 10m, 10 HSLM trains, ballasted track

With ballast		With ballast	
Intersection point		Intersection point	
Velocity	409	Velocity	406
Acceleration	3.5	Acceleration	-3.5

Figure 76. Speed equal to acceleration ± 3.5m/s2 (open frame 10m ballasted track)

OPEN FRAME 10M (WITHOUT BALLAST)

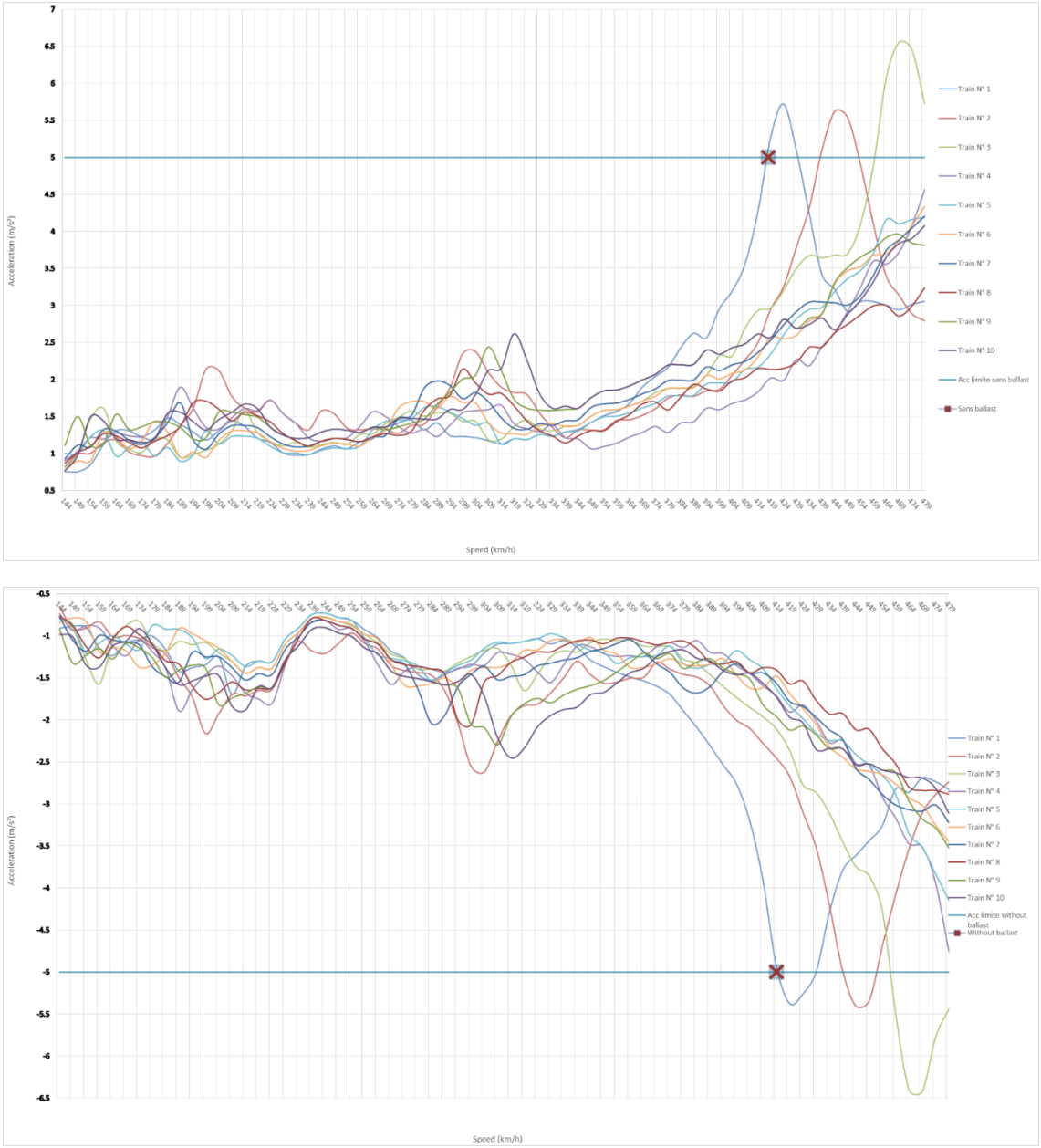

Figure 77. Maximum and minimum Acceleration Results for open frame bridge 10m, 10 HSLM trains, without ballast

Without ballast		Without ballast	
Point d'intersection		Intersection point	
Vitesse	419	Velocity	415
Acceleration	5	Acceleration	-5

Figure 78. Speed equal to acceleration ± 5m/s2(open frame 10m without ballast)

OPEN FRAME 15M (TWO BALLASTED TRACKS)

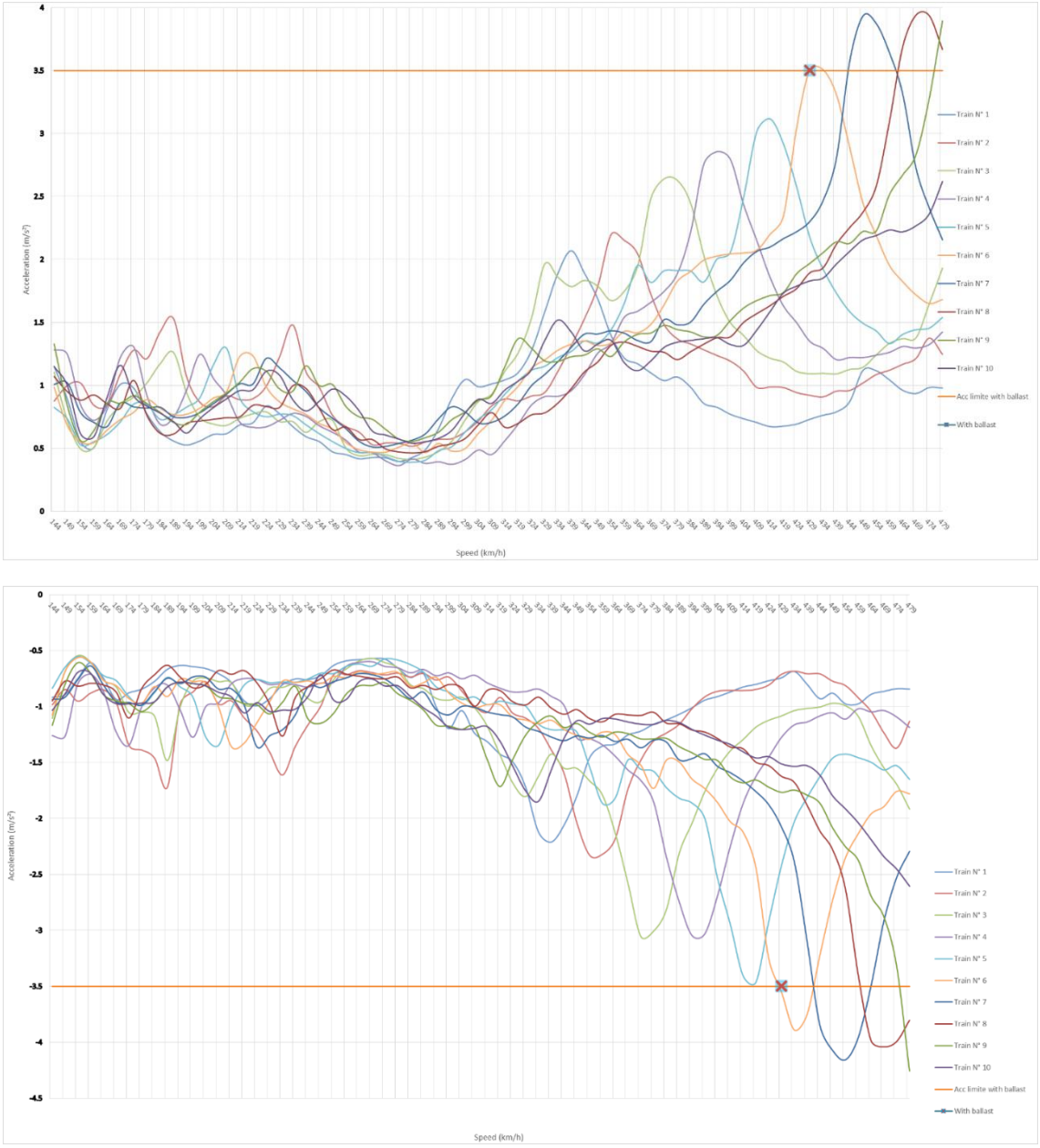

Figure 79. Maximum and minimum Acceleration Results for open frame bridge 15m, 10 HSLM trains, ballasted track

With ballast		With ballast	
Intersection point		Intersection point	
Velocity	430	Velocity	430
Acceleration	3.5	Acceleration	-3.5

Figure 80. Speed equal to acceleration ± 3.5m/s2 (open frame 15m ballasted track)

OPEN FRAME 15M (WITHOUT BALLAST)

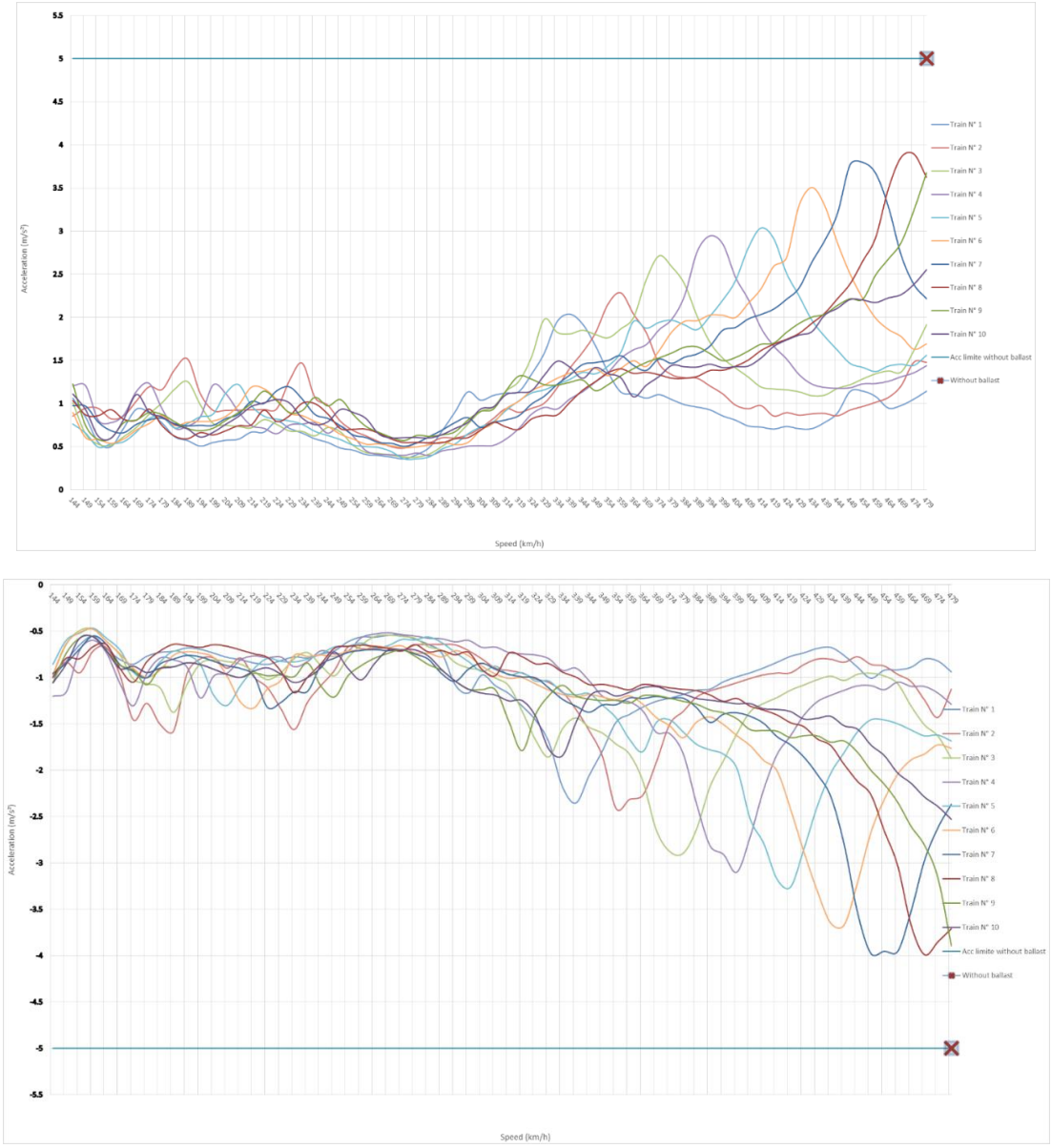

Figure 81. Maximum and minimum Acceleration Results for open frame bridge 15m, 10 HSLM trains, without ballast

Without ballast		Without ballast	
Intersection point		Intersection point	
Velocity	480	Velocity	480
Acceleration	5	Acceleration	-5

Figure 82. Speed equal to acceleration ±5m/s2 (open frame 15m without ballast)

CLOSED FRAME 5M (TWO BALLASTED TRACKS)

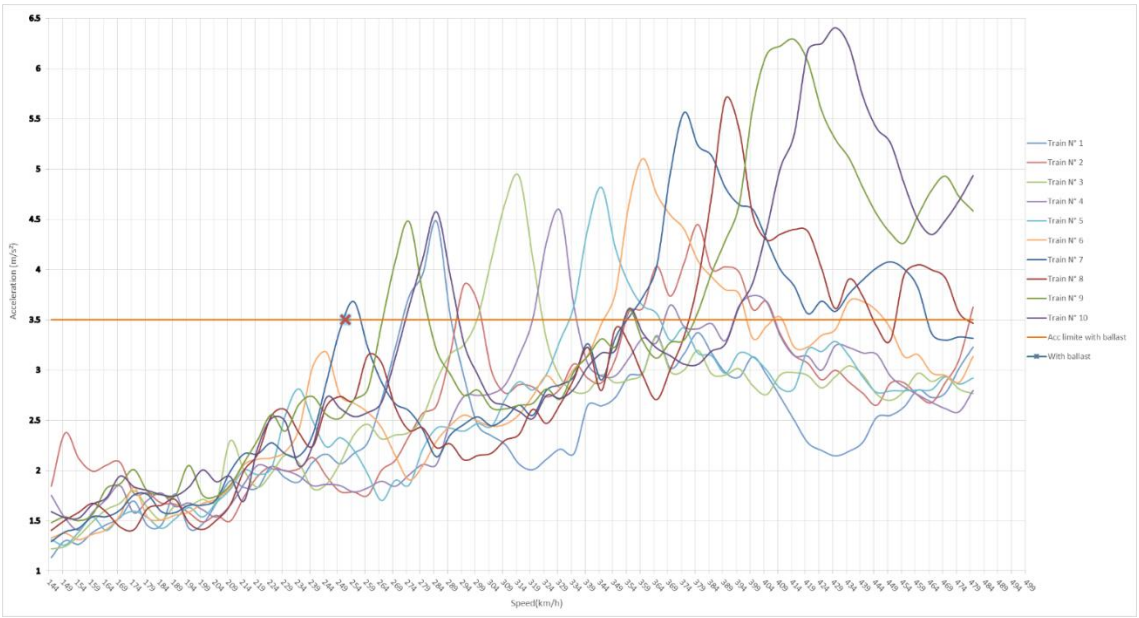

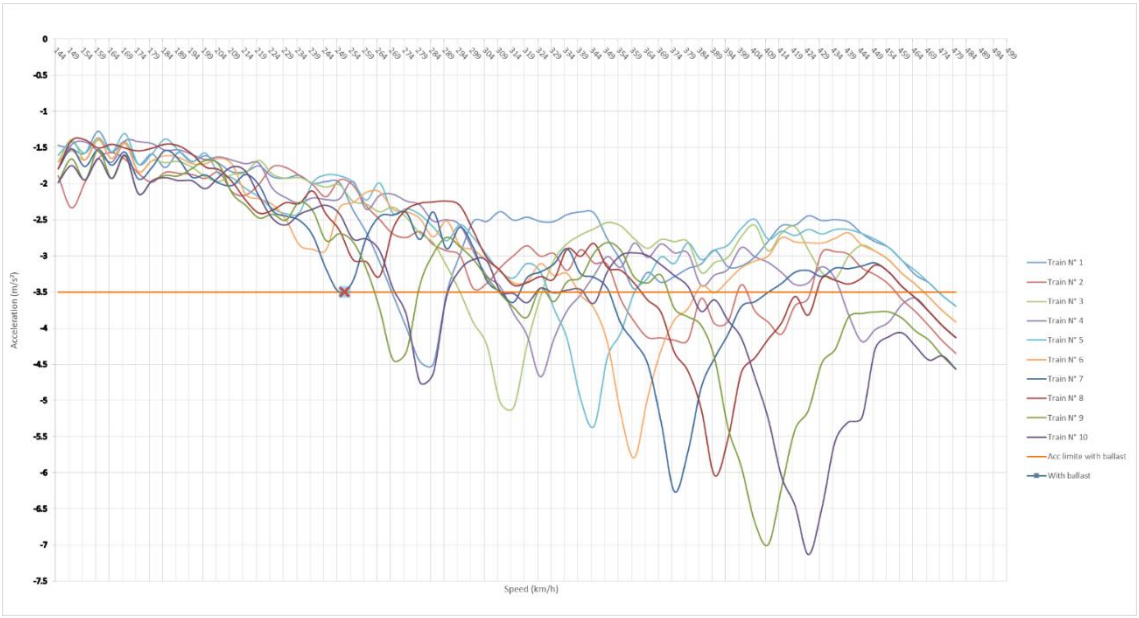

Figure 83. Maximum and minimum Acceleration Results for closed frame bridge 5m, 10 HSLM trains, ballasted track

With ballast	
Intersection point	
Velocity	252
Acceleration	3.5

With ballast	
Intersection point	
Velocity	252
Acceleration	-3.5

Figure 84. Speed equal to acceleration ± 3.5m/s2 (closed frame 5m ballasted track)

CLOSED FRAME 5M (WITHOUT BALLAST)

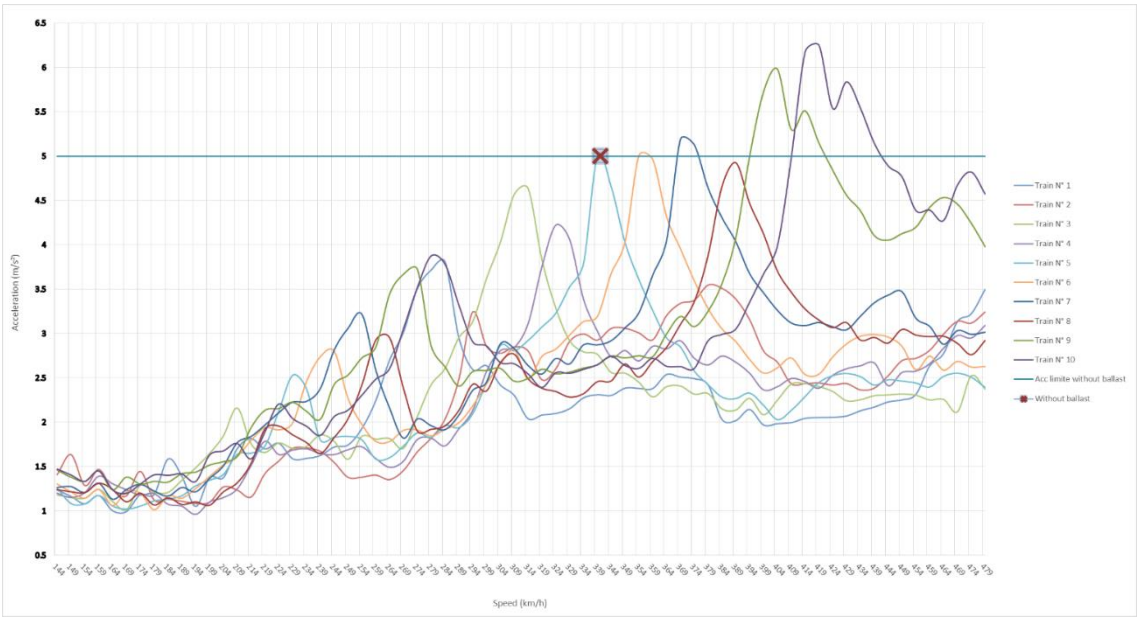

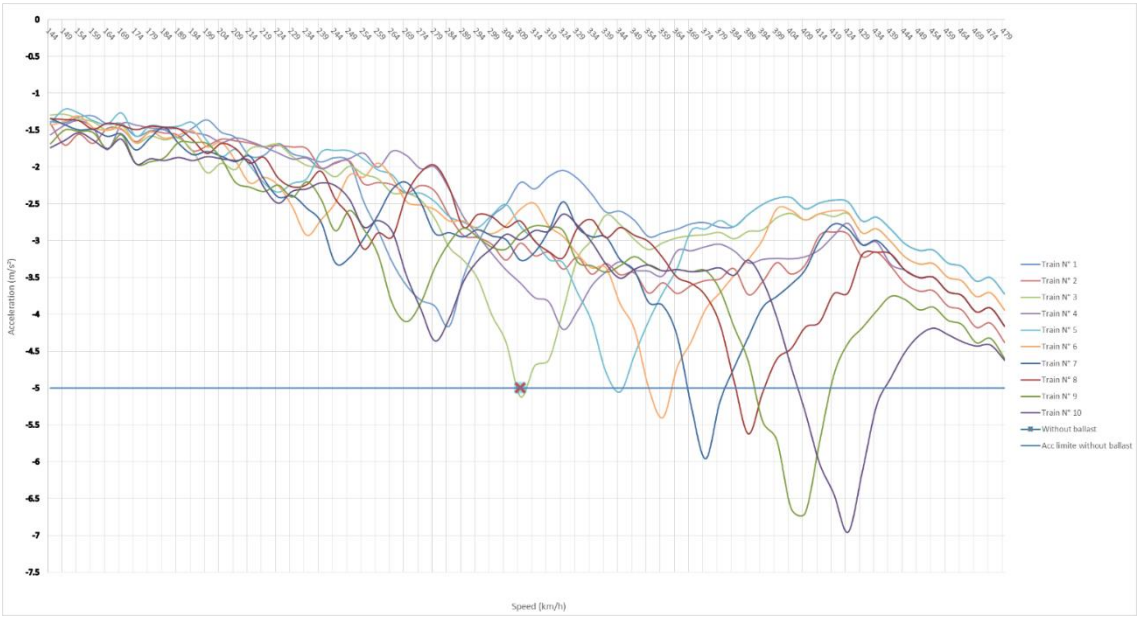

Figure 85. Maximum and minimum Acceleration Results for closed frame bridge 5m, 10 HSLM trains, without ballast

Without ballast	
Intersection point	
Velocity	341
Acceleration	5

Without ballast	
Intersection point	
Velocity	310
Acceleration	-5

Figure 86. Speed equal to acceleration ± 5m/s^2(closed frame 5m without ballast)

CLOSED FRAME 10M (TWO BALLASTED TRACKS)

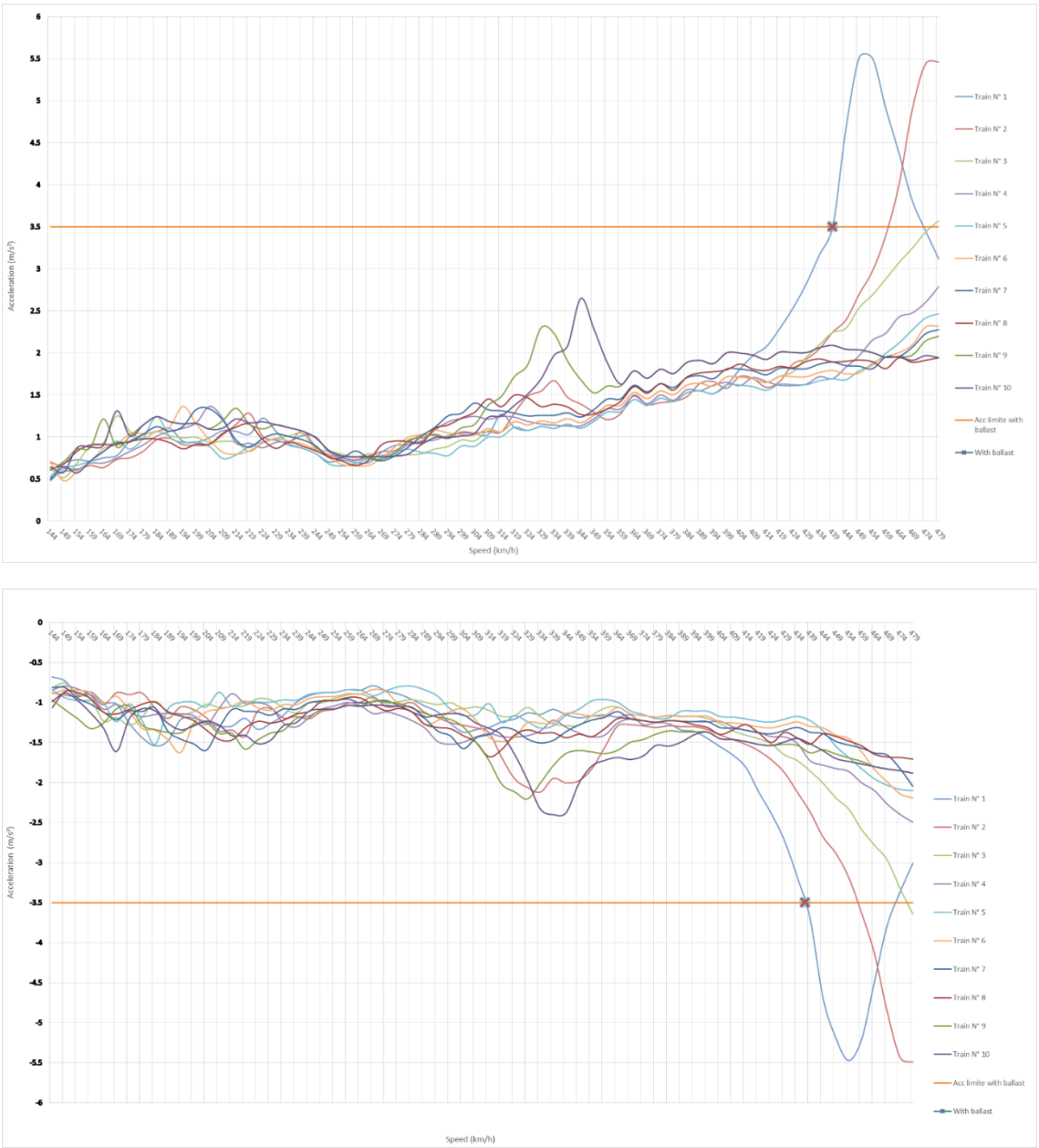

Figure 87. Maximum and minimum Acceleration Results for closed frame bridge 10m, 10 HSLM trains, ballasted track

With ballast		With ballast	
Intersection point		Intersection point	
Velocity	440	Velocity	438
Acceleration	3.5	Acceleration	-3.5

Figure 88. Speed equal to acceleration ± 3.5m/s2 (closed frame 10m ballasted track)

CLOSED FRAME 10M (WITHOUT BALLAST)

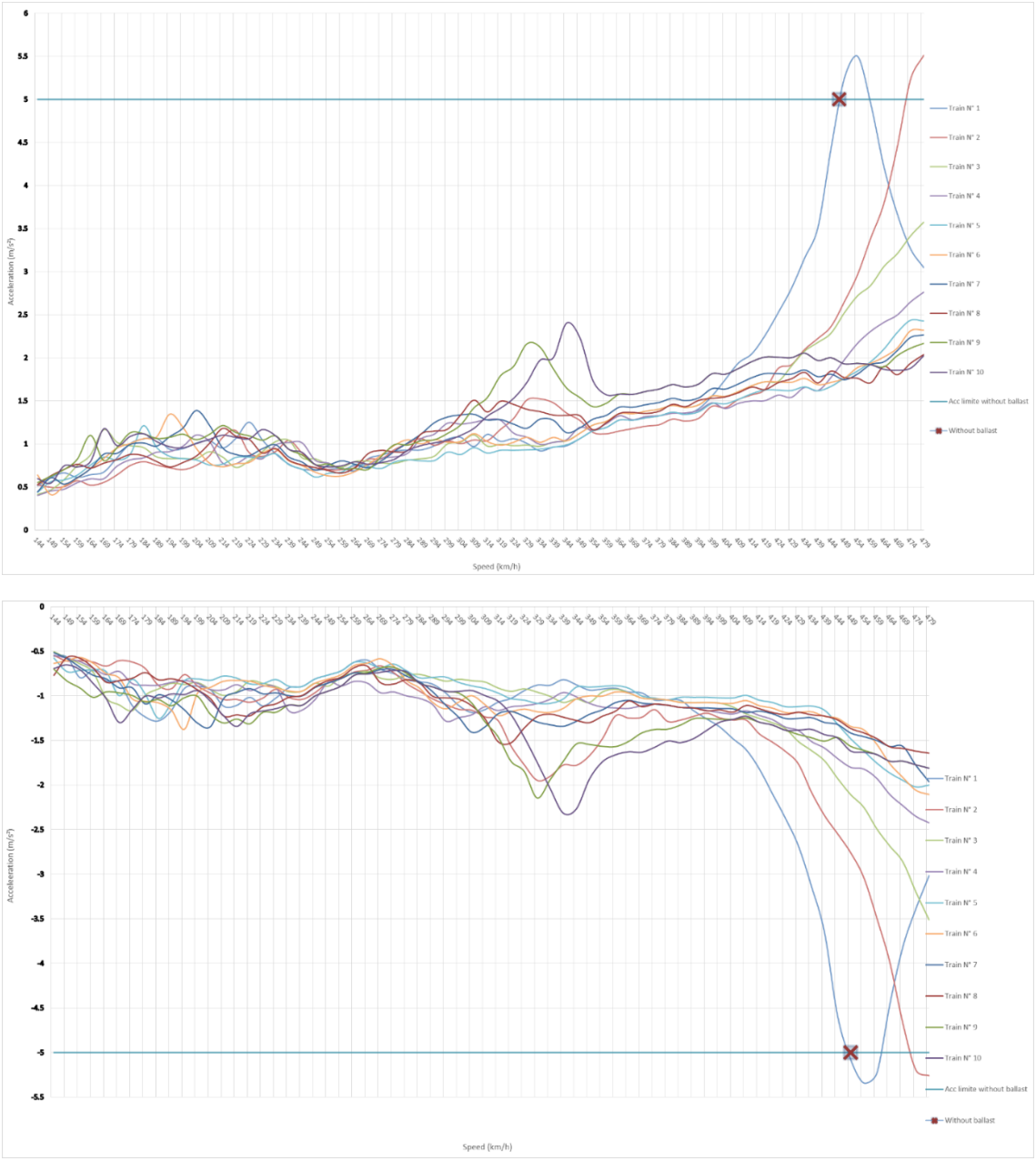

Figure 89. Maximum and minimum Acceleration Results for closed frame bridge 10m, 10 HSLM trains, without ballast

Without ballast		Without ballast	
Intersection point		Intersection point	
Velocity	448	Velocity	450
Acceleration	5	Acceleration	-5

Figure 90. Speed equal to acceleration ± 5m/s2 (closed frame 10m without ballast)

CONCLUSIONS

We noted that:

- For closed frame bridges, the lower is the span length, the higher is the resonance risk for high speed. The vertical acceleration at mid span for 5m closed Frame Bridge is higher than acceleration for 10m closed Frame Bridge.
- For open frame bridges, the lower is the span length, the higher is the resonance risk for high speed. The vertical acceleration at mid span for 10m open frame bridge is higher than acceleration for 15m open Frame Bridge.
- The results of studied bridges are higher than limit of 3.5 m/s2 for ballasted track or 5 m/s2 for track without ballast. To respect these limitations for speed up to 480 Km/h we have redesigned the thickness of deck and increased the value as below:
    - Open frame 10m: from 0.85m to 1.00m
    - Open frame 15m: from 1.20m to 1.30m
    - Closed frame 5m: from 0.60m to 0.85m
    - Closed frame 10m: from 1.00m to 1.15m

The maximum train speeds for which the allowable deck vertical acceleration is reached, are given below.

Type	Open Frame 10m		Open Frame 15m		Closed Frame 5m		Closed Frame 10m	
	With Ballast	Without Ballast	With Ballast	Without Ballast	With Ballast	Without Ballast	With Ballast	Without Ballast
	acc=3.5m/s²	acc=5 m/s²	acc=3.5m/s²	acc=5 m/s²	acc=3.5m/s²	acc=5 m/s²	acc=3.5m/s²	acc=5 m/s²
Speed max (km/h)	**406**	**415**	**430**	**480**	**252**	**310**	**438**	**448**

Figure 91. Maximum speed to check the acceleration limit

In all of the following studies we have considered the original deck thickness:

- Open frame 10m: 0.85m
- Open frame 15m: 1.20m
- Closed frame 5m: 0.60m
- Closed frame 10m: 1.00m

4.3.4.5. Deck acceleration for TGV and ICE2

Dynamic analyses were carried out considering the different hypothesis below:

- Perfect contact between train and bridge, one loaded line is considered without ballast stiffness.
- 2D models for French TGV and ICE2
- Speed from 144 km/h to 480 km/h (1.2*400 km/h) with a step of speed equal to 5 km/h.

Open Frame 10m (one ballasted track, without ballast stiffness, TGV)

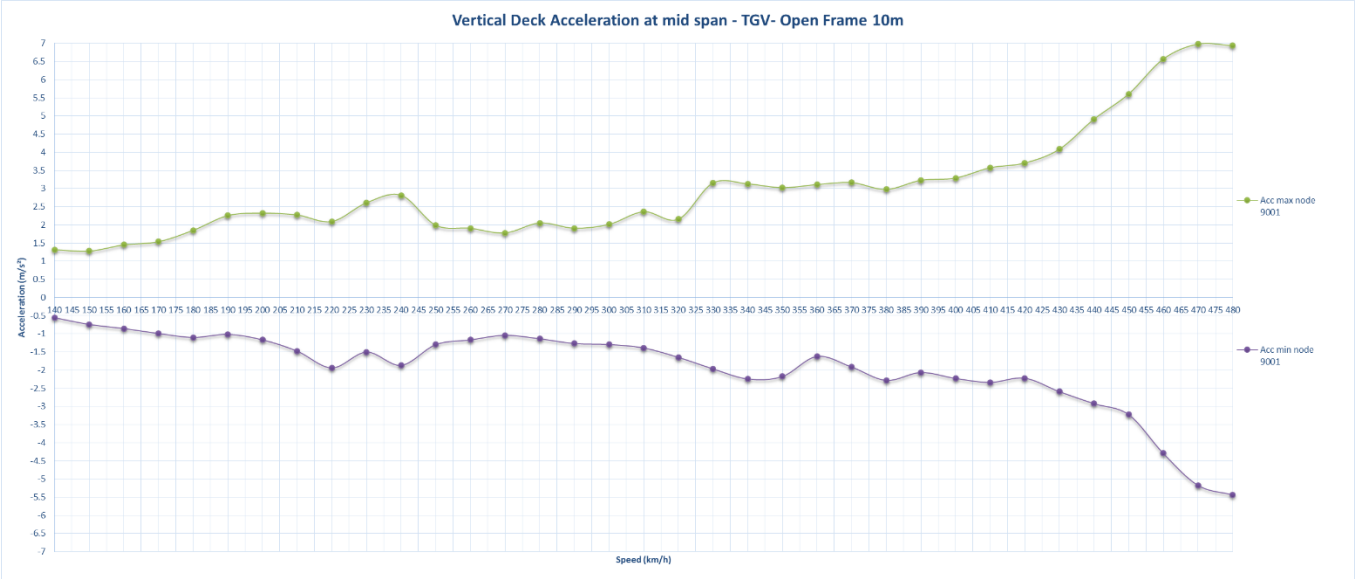

Figure 92. Maximum and minimum Acceleration Results for open frame bridge 10m, TGV, one ballasted track

OPEN FRAME 15M (ONE BALLASTED TRACK, WITHOUT BALLAST STIFFNESS, TGV)

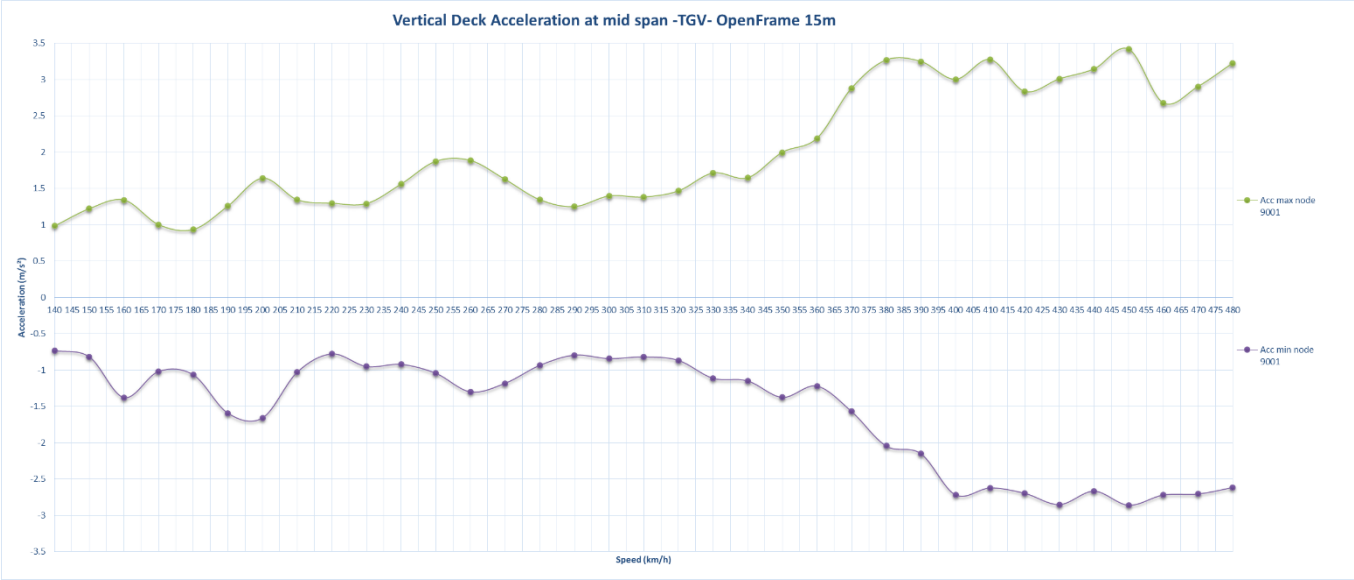

Figure 93. Maximum and minimum Acceleration Results for open frame bridge 15m, TGV, one ballasted track

CLOSED FRAME 5M (ONE BALLASTED TRACK, WITHOUT BALLAST STIFFNESS, TGV)

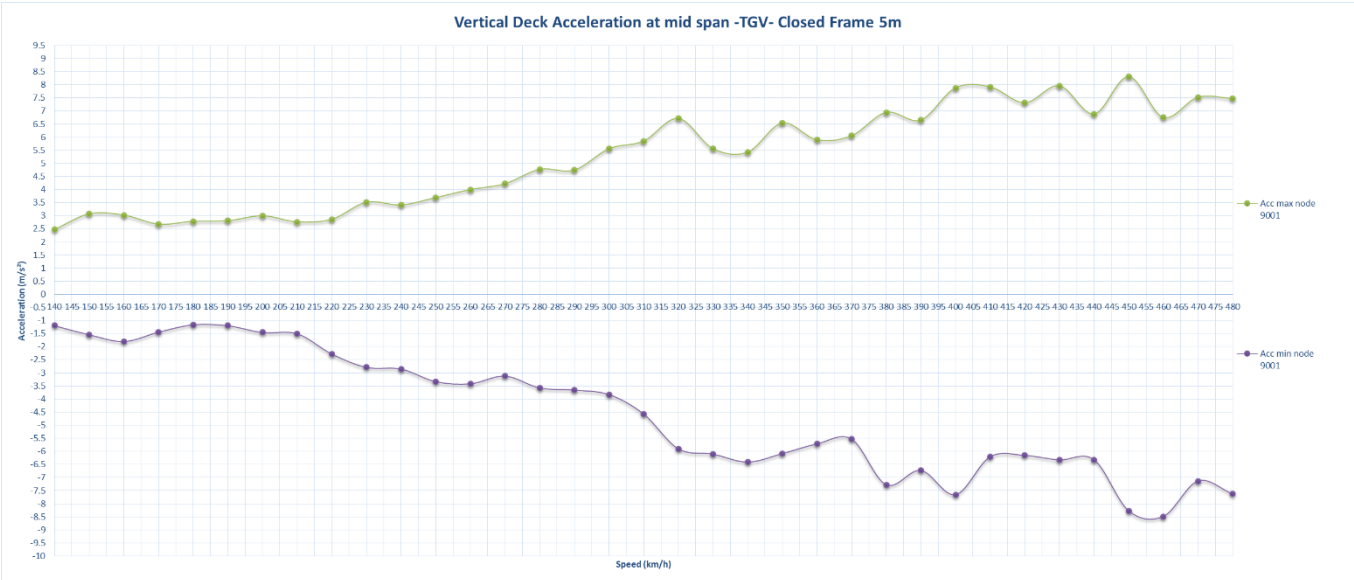

Figure 94. Maximum and minimum Acceleration Results for closed frame bridge 5m, TGV, one ballasted track

CLOSED FRAME 10M (ONE BALLASTED TRACK, WITHOUT BALLAST STIFFNESS, TGV)

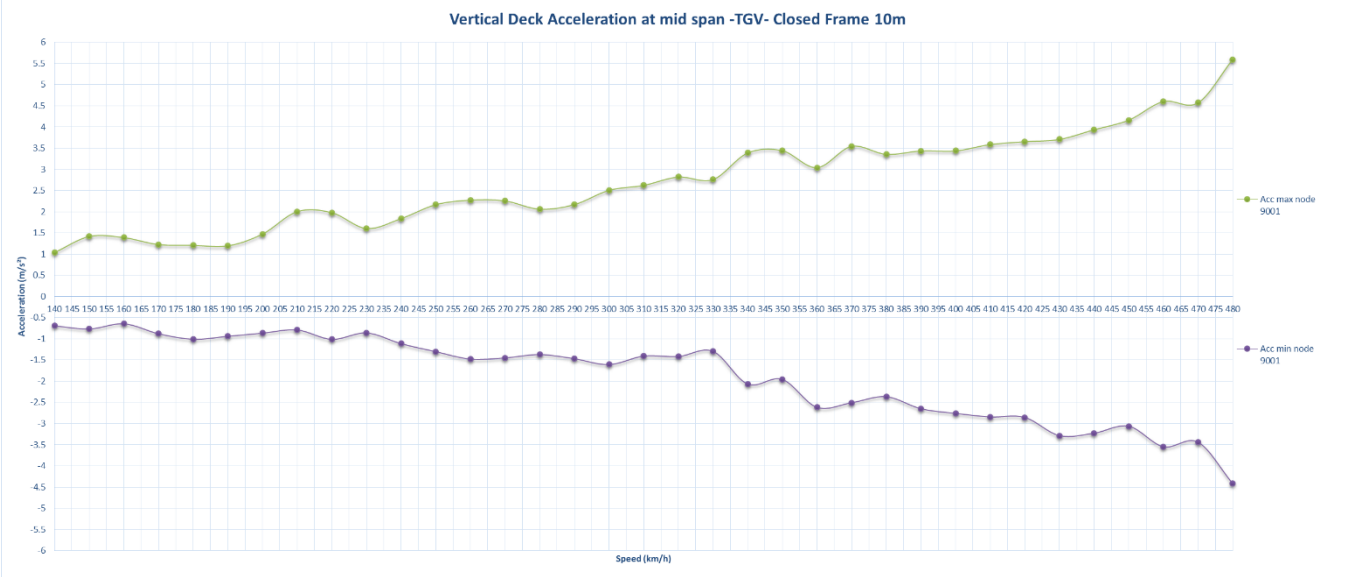

Figure 95. Maximum and minimum Acceleration Results for closed frame bridge 10m, TGV, one ballasted track

OPEN FRAME 10M (ONE BALLASTED TRACK, WITHOUT BALLAST STIFFNESS, ICE2)

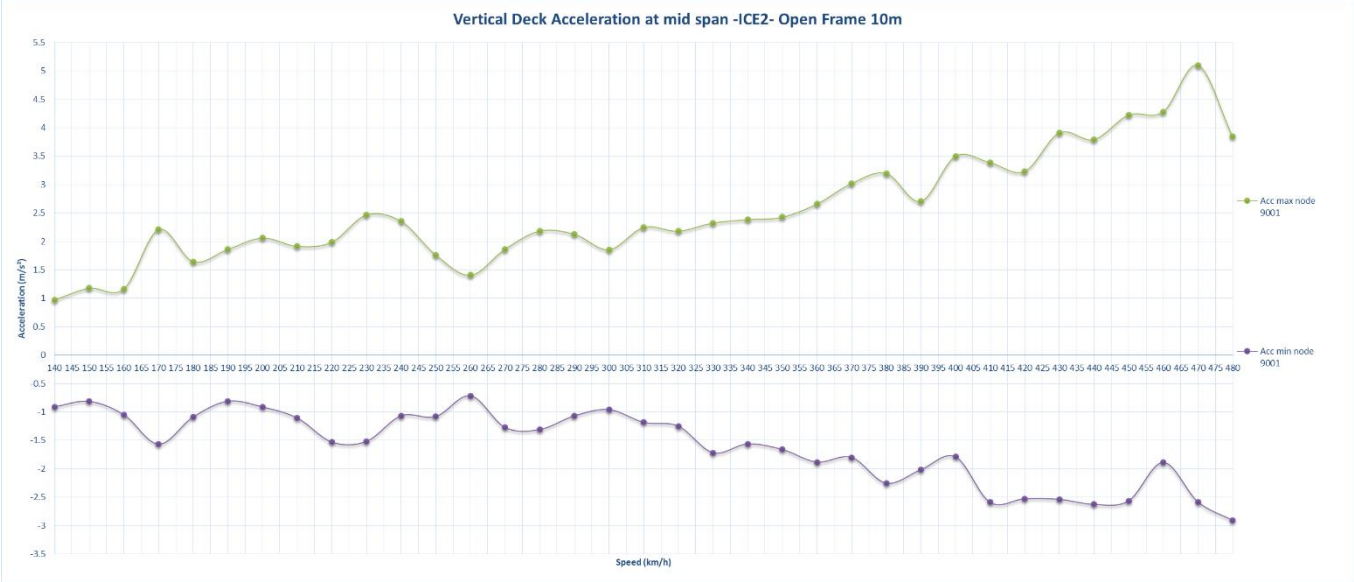

Figure 96. Maximum and minimum Acceleration Results for open frame bridge 10m, ICE2, one ballasted track

OPEN FRAME 15M (ONE BALLASTED TRACK, WITHOUT BALLAST STIFFNESS, ICE2)

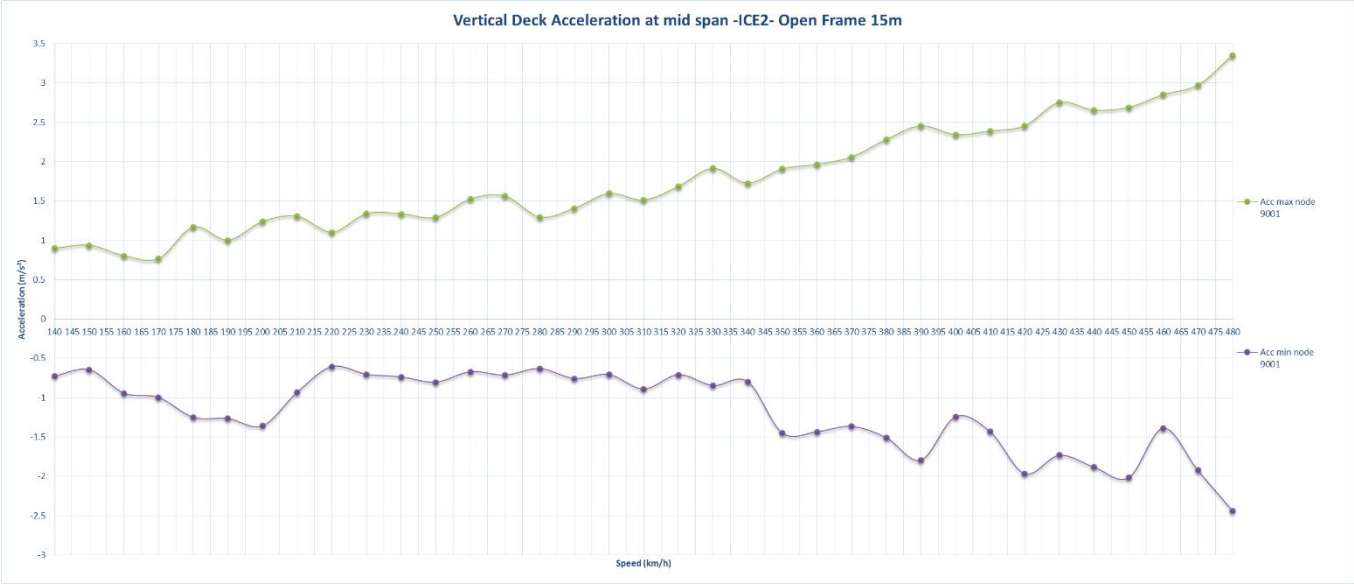

Figure 97. Maximum and minimum Acceleration Results for open frame bridge 15m, ICE2, one ballasted track

CLOSED FRAME 5M (ONE BALLASTED TRACK, WITHOUT BALLAST STIFFNESS, ICE2)

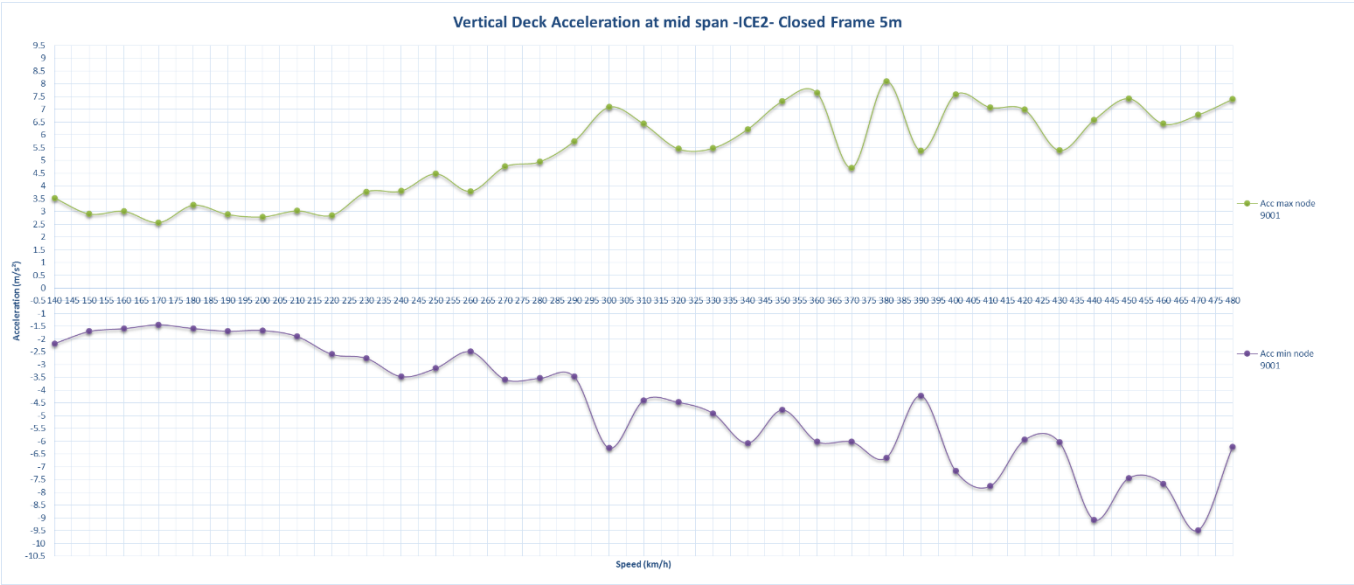

Figure 98. Maximum and minimum Acceleration Results for closed frame bridge 5m, ICE2, one ballasted track

CLOSED FRAME 10M (ONE BALLASTED TRACK, WITHOUT BALLAST STIFFNESS, ICE2)

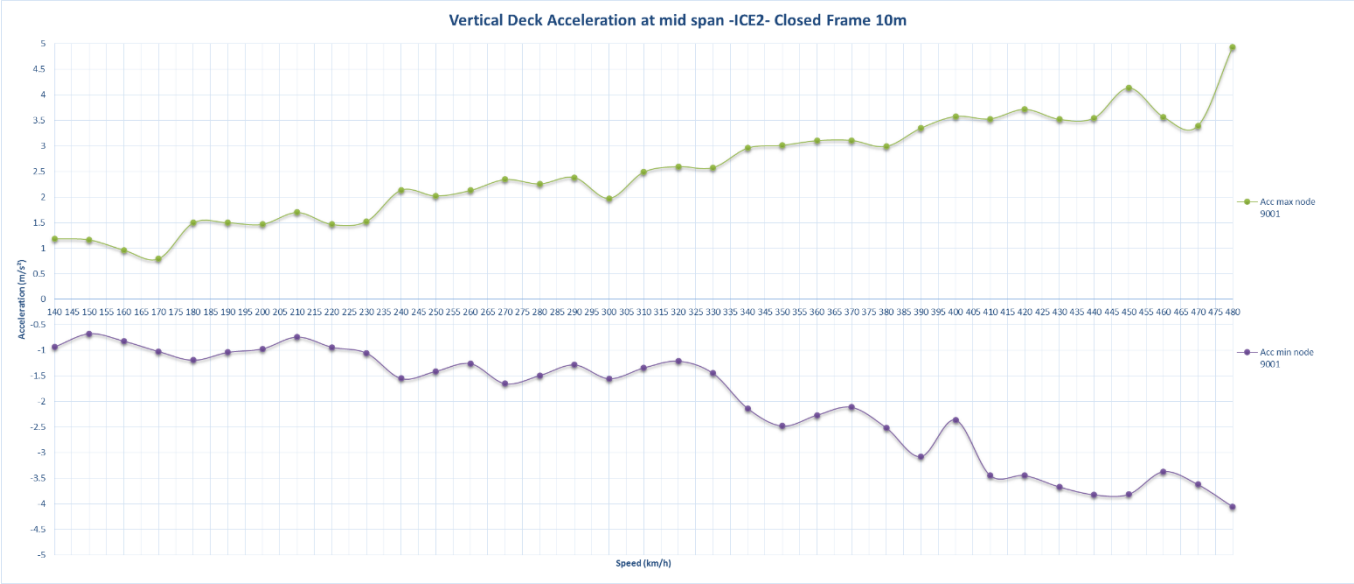

Figure 99. Maximum and minimum Acceleration Results for closed frame bridge 10m, ICE2, one ballasted track

CONCLUSIONS

We noted that:

- For closed frame bridges, the lower is the span length, the higher is the resonance risk for high speed. The vertical acceleration at mid span for 5m closed Frame Bridge is higher than acceleration for 10m closed Frame Bridge.
- For open frame bridges, the lower is the span length, the higher is the resonance risk for high speed. The vertical acceleration at mid span for 10m open frame bridge is higher than acceleration for 15m open Frame Bridge.
- The results of studied bridges are higher than limit of 5 m/s2 for track without ballast. Only the open frame 15m respects the limitations

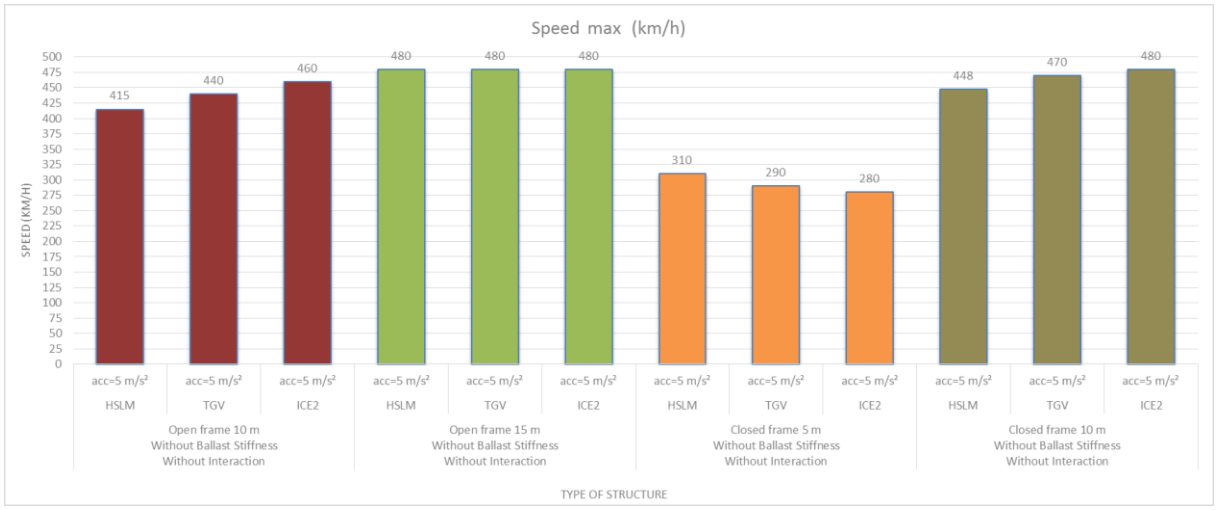

Figure 100. Maximum speed to check the acceleration limit for track without ballast

- The results of studied bridges are higher than limit of 3,5 m/s2 for track with ballast.

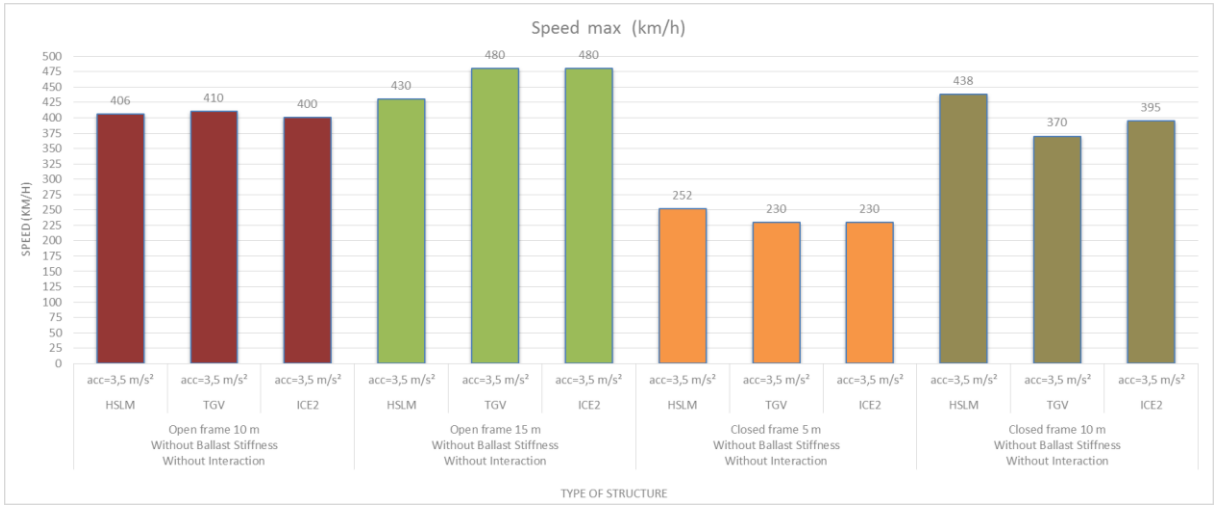

Figure 101. Maximum speed to check the acceleration limit with ballast

-

4.3.4.6. 2D MODEL: COMPARISON DECK VERTICAL ACCELERATION FOR FRENCH TGV WITH AND WITHOUT INTERACTION

Dynamic analyses were carried out considering:

- Perfect contact between train and bridge, only one loaded lane is considered with and without interaction. In models without interaction the damping increment $\Delta\xi$ is considered (following EN1991-2 art 6.4.6.4). However in models with interaction $\Delta\xi$ is not considered.
- 2D models for French TGV
- No track stiffness is modelled
- No track irregularity is considered
- Speed from 144 km/h to 400 km/h with a step of speed equal to 5 km/h
- Time step is 0.003s

OPEN FRAME 10M

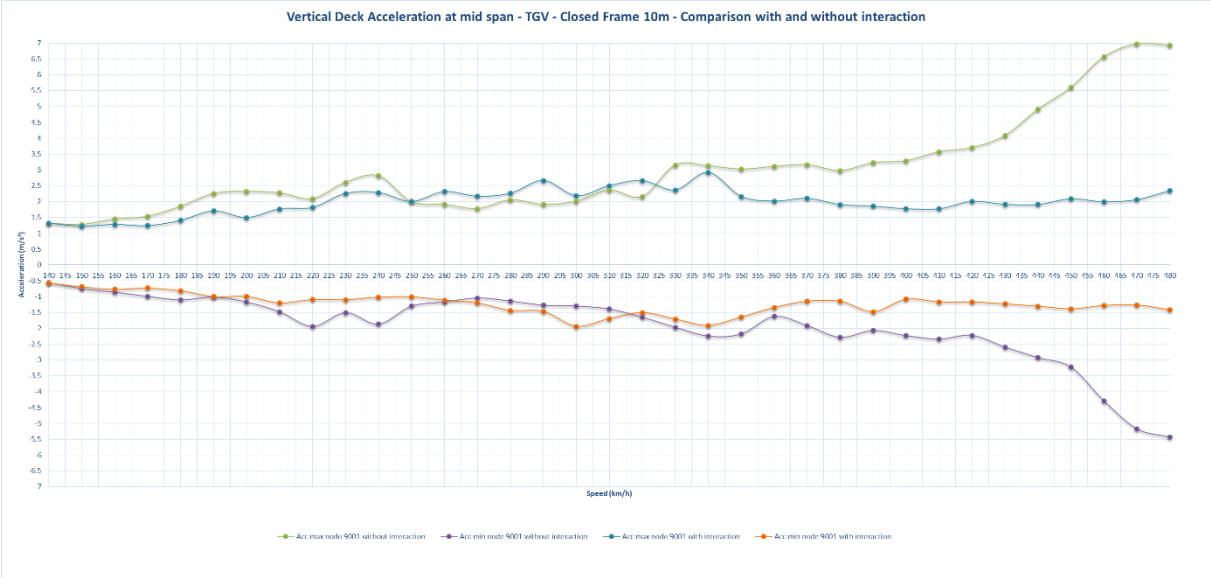

Figure 102. Vertical Deck Acceleration at Mid Span- Results for open frame bridge 10m, TGV, with and without Interaction

OPEN FRAME 15M

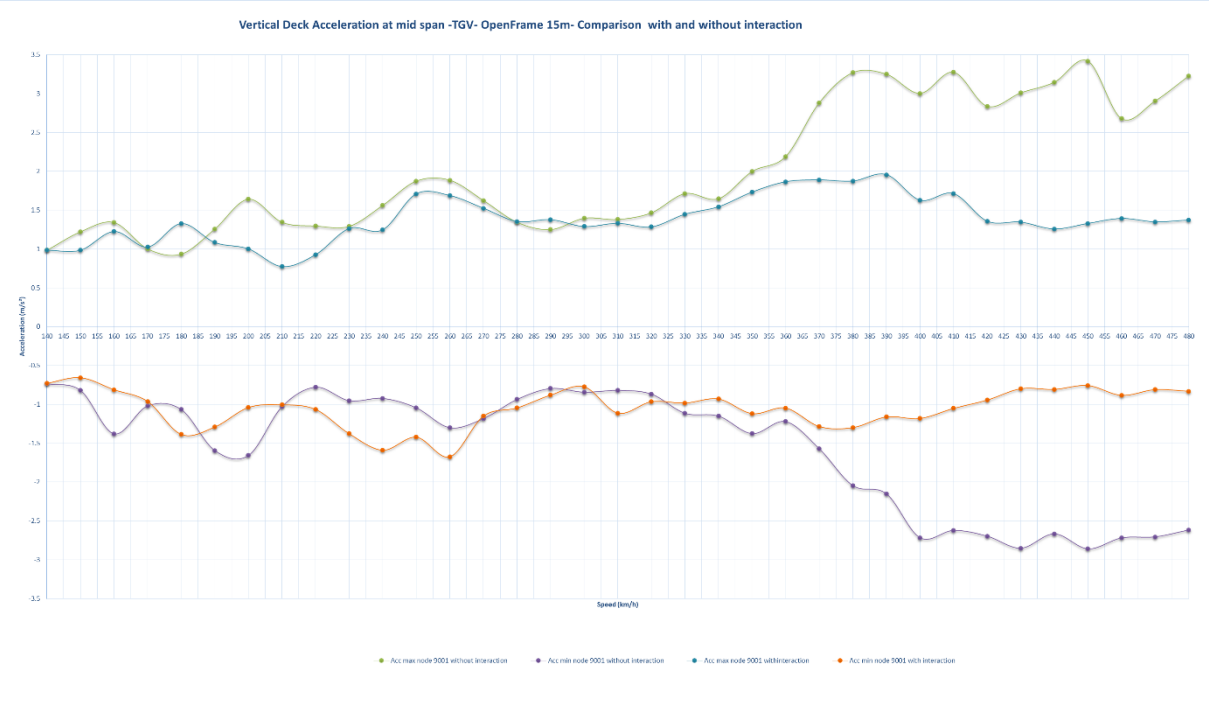

Figure 103. Vertical Deck Acceleration at Mid Span- Results for open frame bridge 15m, TGV, with and without Interaction

CLOSED FRAME 5M

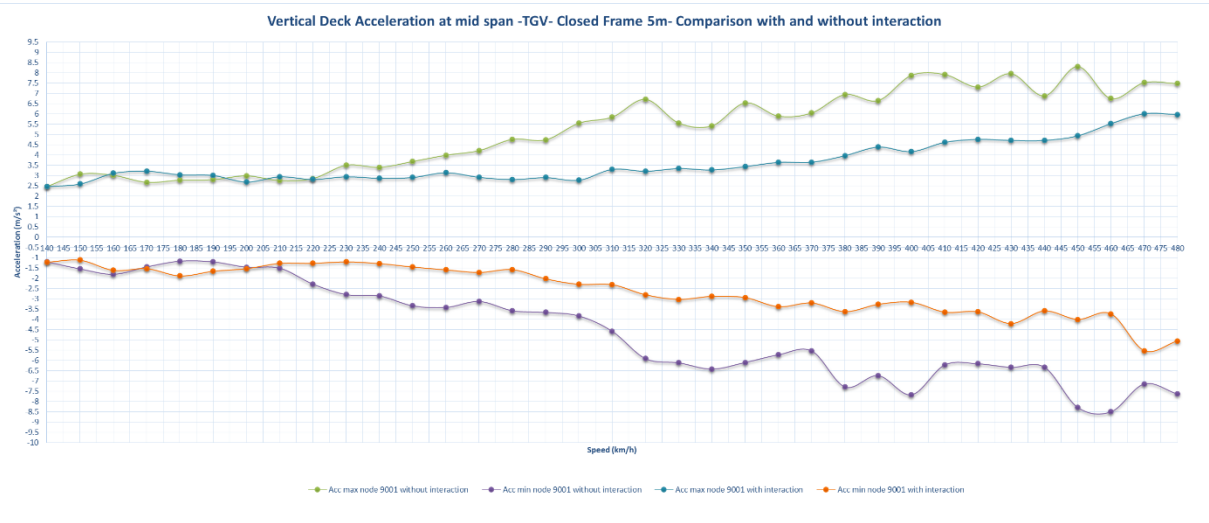

Figure 104. Vertical Deck Acceleration at Mid Span- Results for closed frame bridge 5m, TGV, with and without Interaction

CLOSED FRAME 10M

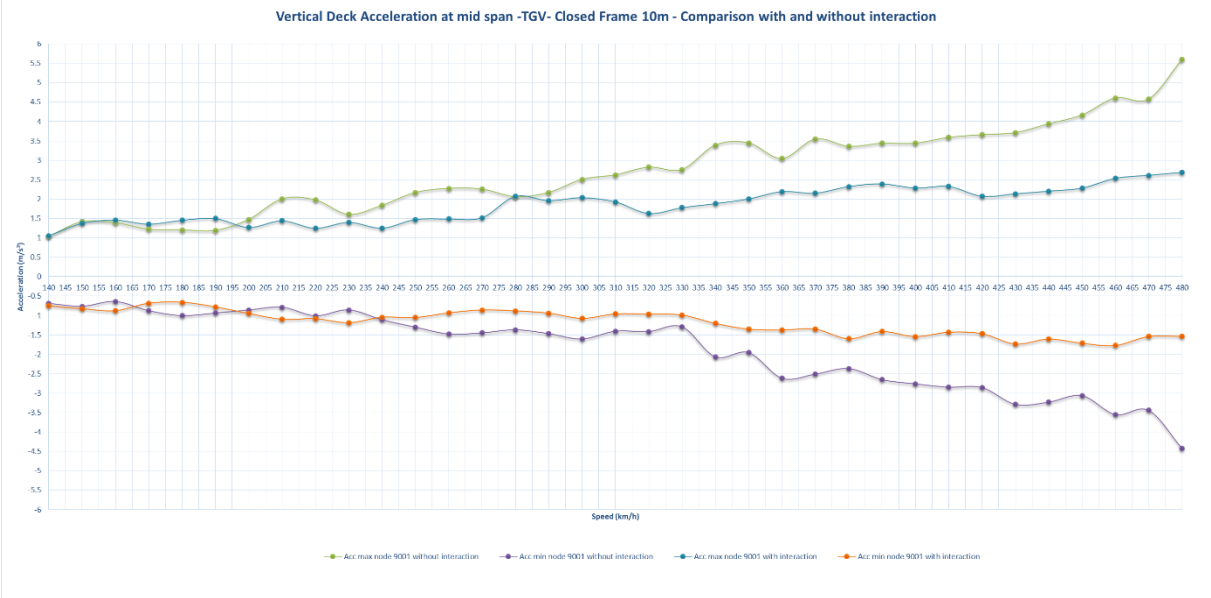

Figure 105. Vertical Deck Acceleration at Mid Span- Results for closed frame bridge 10m, TGV, with and without Interaction

CONCLUSIONS

We noted that:

- The acceleration at mid Span for studied open frames bridges and closed frames bridges calculated with interaction is lower than acceleration calculated without interaction.

In the calculation without interaction the damping increment $\Delta\xi$ is considered (following EN1991-2 art 6.4.6.4), the purpose of this increment is to take into account the interaction between the train and the bridge. We can conclude that the calculation with the incremental damping is conservative because the acceleration calculated considering the real interaction are lower. Therefore to take into account this incremental damping is on the safe side.

4.3.5. RESULTS OF COMFORT ANALYSIS WITHOUT TRACK IRREGULARITIES

4.3.5.1. DAMPING CHARACTERISTICS FOR COMFORT ANALYSIS

	Open frame 10m	Open frame 15m	Closed frame 5m	Closed frame 10m
Masses [tons]	1104	1702	505	1238
ξ %	2.141	1.766	2.508	2.13
f1 (First Vertical Frequency) [Hz]	6.541	5.268	8.722	7.025
f2 (F max) [Hz]	30.000	30	30	30
Rayleigh Mass proportional damping A	1.445	0.994	2.130	1.524
Rayleigh Stiffness proportional damping B	0.000187	0.000159	0.000206	0.000183

Figure 106. DAMPING Characteristic for Comfort Analysis for de Deck behavior

The damping Increment Δξ of EN1991-2 art. 6.4.6.4 has not been considered here, because the purpose of this increment is to take into account the interaction between the train and the bridge.

4.3.5.2. 2D MODEL: COMPARISON VERTICAL ACCELERATION IN PASSENGER CAR FOR FRENCH TGV AND ICE2

Comfort analyses were carried out considering:

- 3D structure geometry of bridge
- Perfect contact between train and bridge, only one loaded line is considered
- 2D models for French TGV and ICE2
- No ballast is modelled
- No track irregularity is considered
- Speed from 144 km/h to 400 km/h (it is not necessary to multiply the design speed by 1.2 for comfort analysis) with a speed step equal to 5 km/h
- Time step is 0.003s

The maximum vertical acceleration at barycentre of various cars of the TGV and ICE2 train are calculated for various speeds.

OPEN FRAME 10M

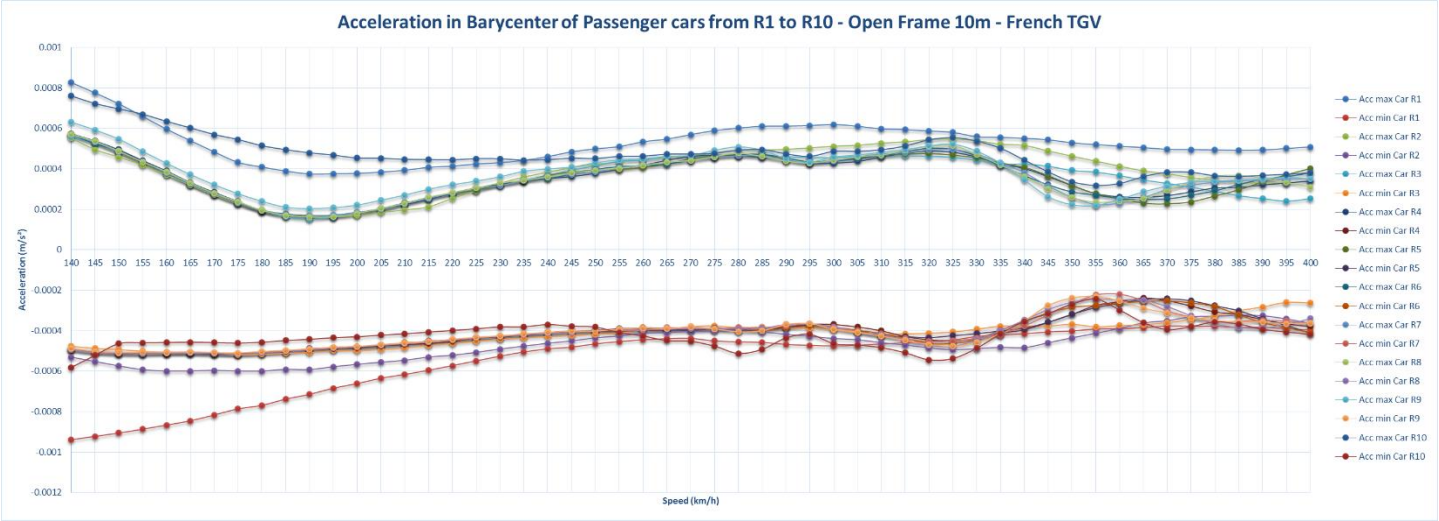

Figure 107. Vertical Acceleration in Barycenter of Passenger cars from R1 to R10 - Open Frame 10m - French TGV

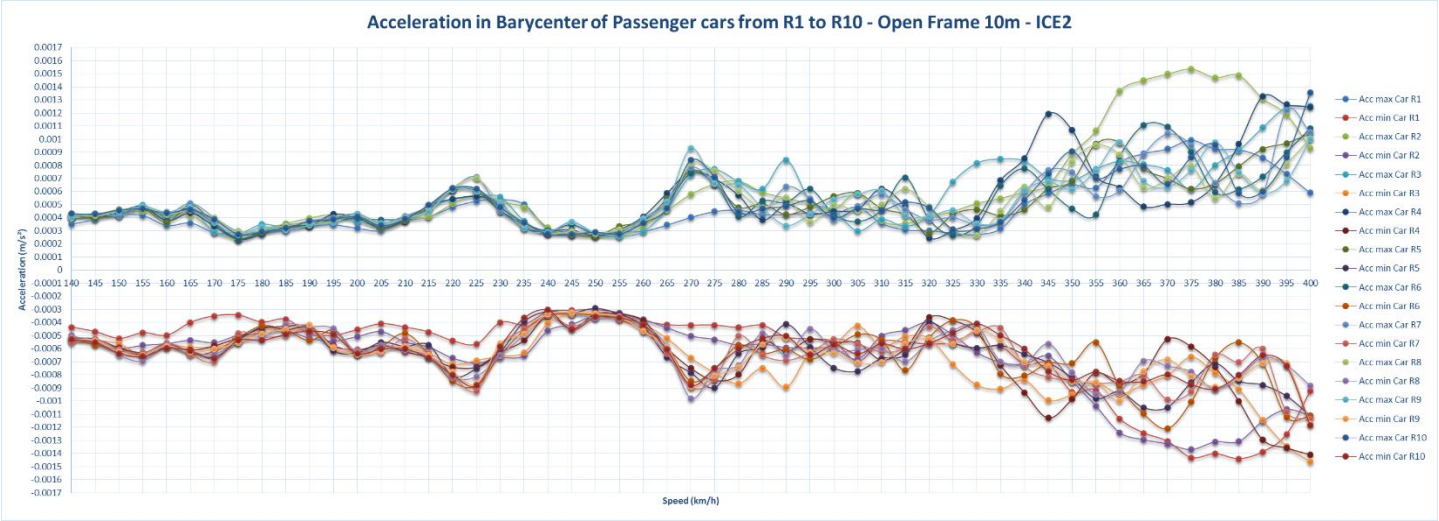

Figure 108.Vertical Acceleration in Barycenter of Passenger cars from R1 to R10 - Open Frame 10m – ICE2

OPEN FRAME 15M

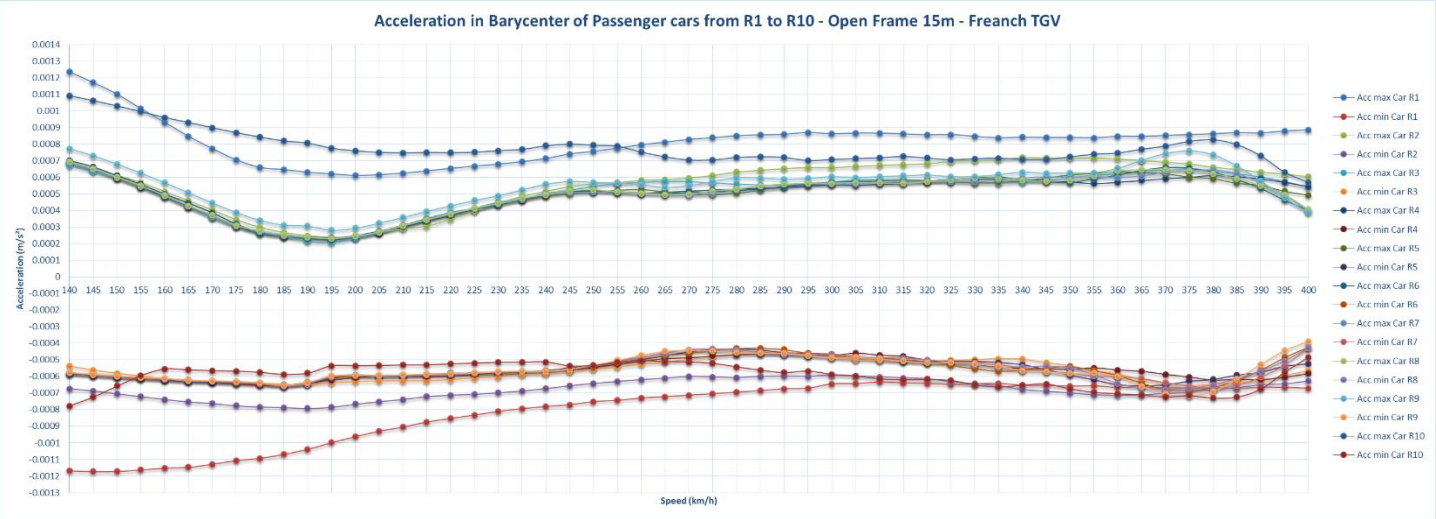

Figure 109. Vertical Acceleration in Barycenter of Passenger cars from R1 to R10 - Open Frame 15m - French TGV

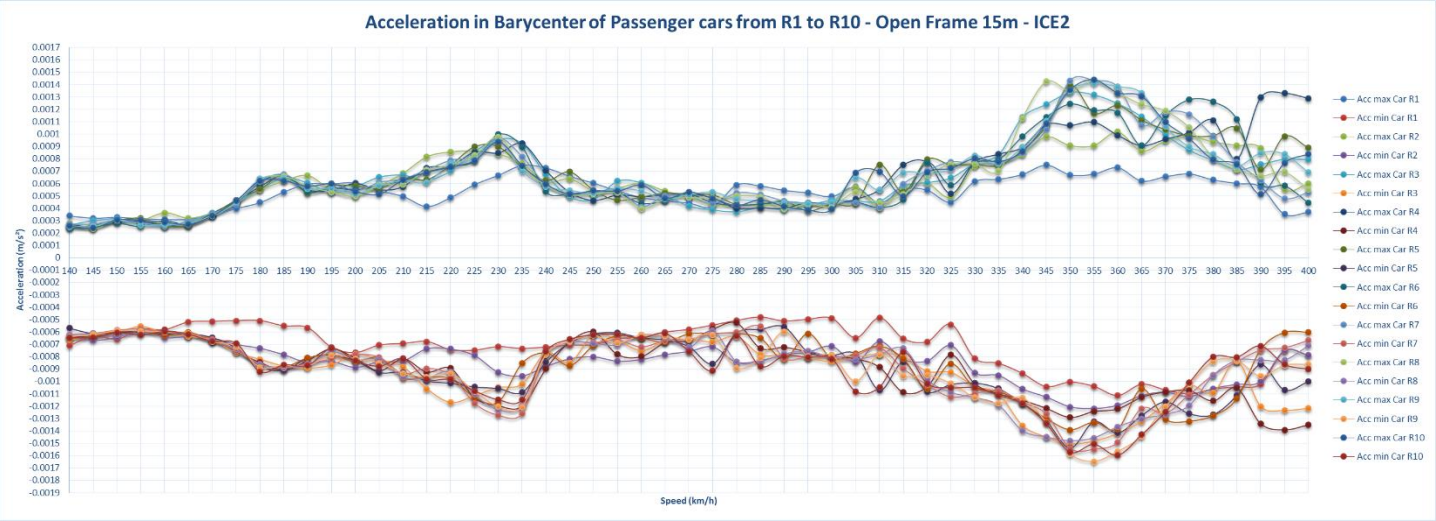

Figure 110.Vertical Acceleration in Barycenter of Passenger cars from R1 to R10 - Open Frame 15m – ICE2

CLOSED FRAME 5M

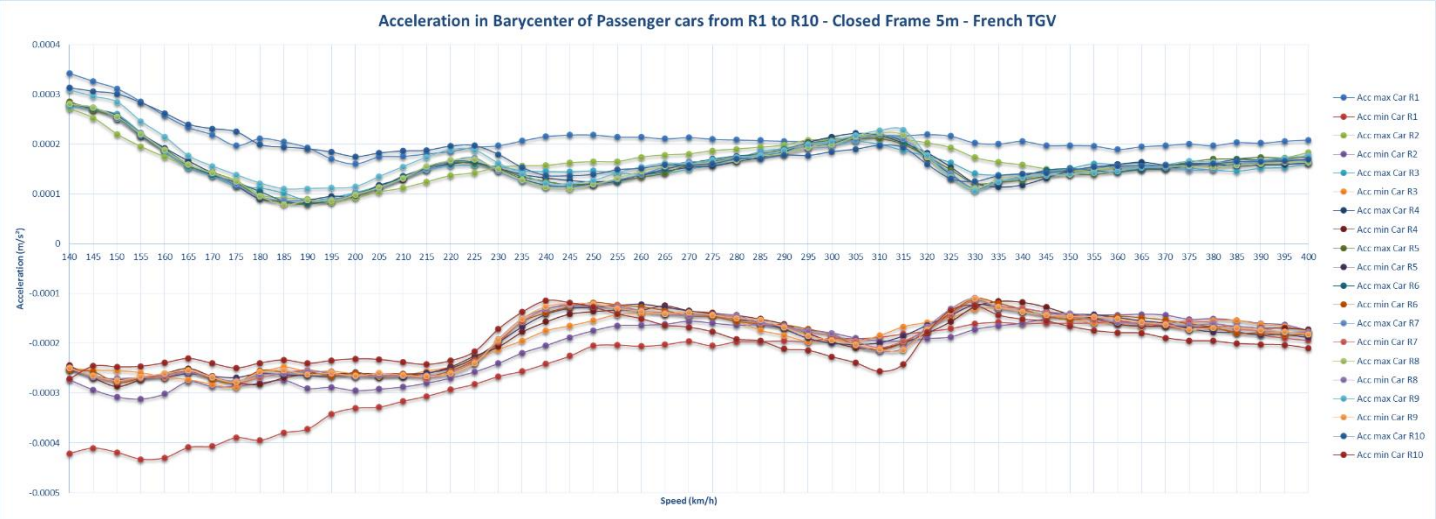

Figure 111. Vertical Acceleration in Barycenter of Passenger cars from R1 to R10 - Closed Frame 5m - French TGV

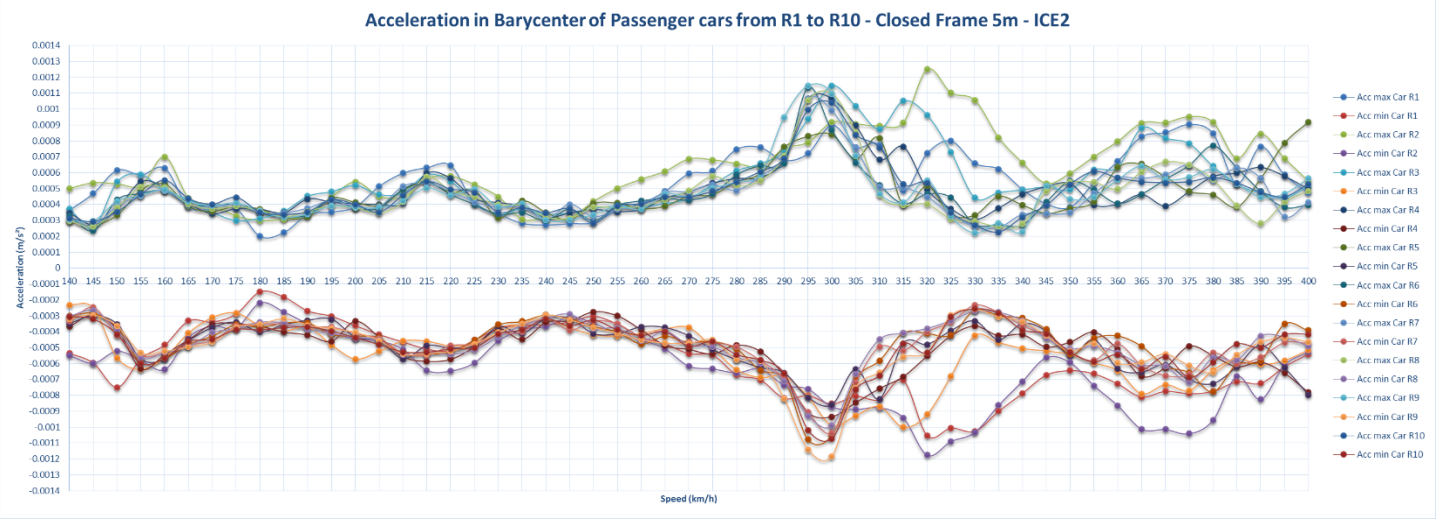

Figure 112. Vertical Acceleration in Barycenter of Passenger cars from R1 to R10 - Closed Frame 5m – ICE2

CLOSED FRAME 10M

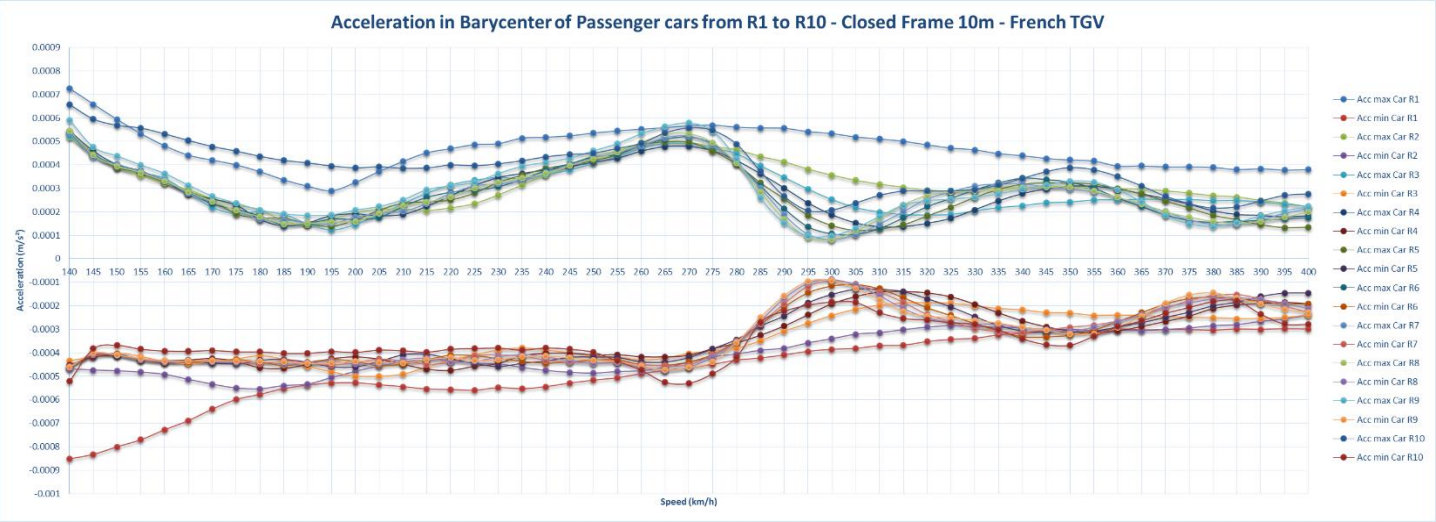

Figure 113. Vertical Acceleration in Barycenter of Passenger cars from R1 to R10 - Closed Frame 10m - French TGV

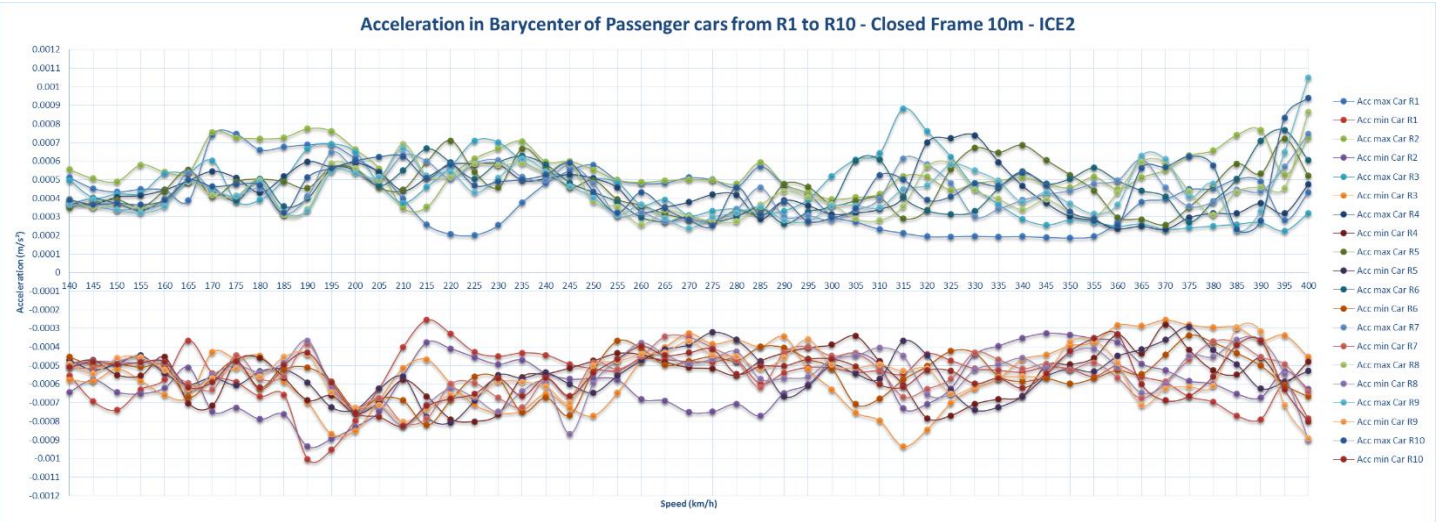

Figure 114. Vertical Acceleration in Barycenter of Passenger cars from R1 to R10 - Closed Frame 10m – ICE2

CONCLUSIONS

We noted that:

- The power cars of French TGV and ICE2 have the most important accelerations.
- The first bogie of power car of French TGV and ICE2 presents the most important acceleration.

- For French TGV the passenger acceleration generally decreases when speed of train increases. This phenomena is not shown for the ICE2.
- The passenger acceleration decreases if the span length decreases, because the deck deflection decreases.
- The passenger acceleration is much lower than 1 m/s^2 (good comfort following Eurocode 0 Annex A2).

az (mm/s^2)	Open frame 10 m	Open frame 15 m	Closed frame 5 m	Closed frame 10 m
TGV	0.94	1.23	0.43	0.85
ICE2	1.50	1.50	1.60	1.30

Figure 115. Comparison vertical acceleration in passenger car for French TGV and ICE2, 2D model

4.3.6. Results of Dynamic analysis and comfort analysis with track irregularities

4.3.6.1. 3D model characteristics

Comfort analyses were carried out considering:

- 3D Structure Geometry of bridge
- 3D train is modelled

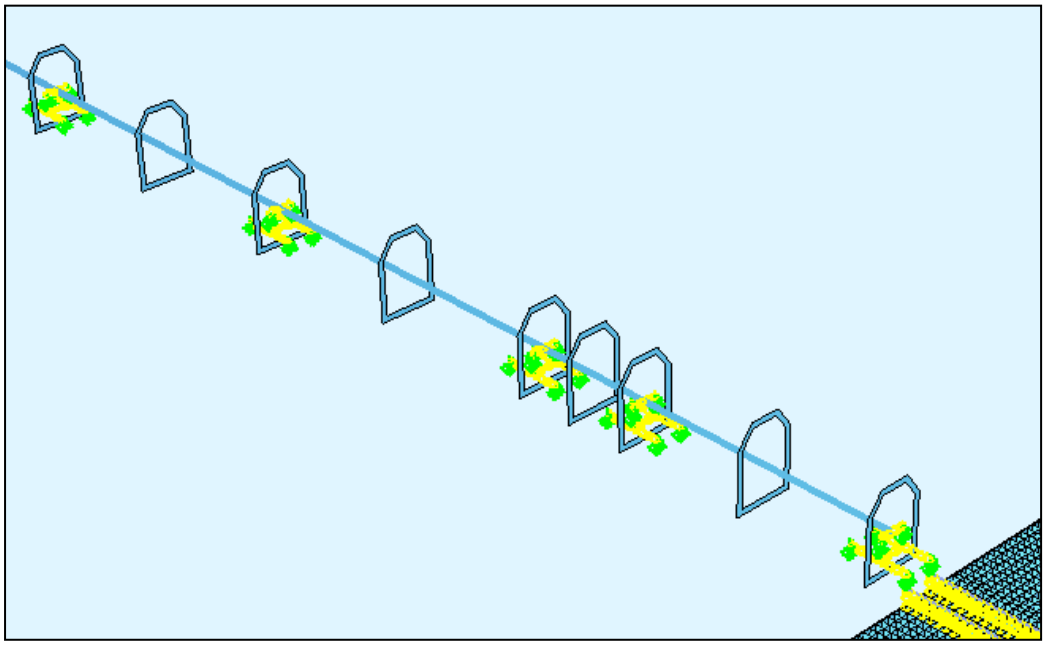

Figure 116. 3D Train model

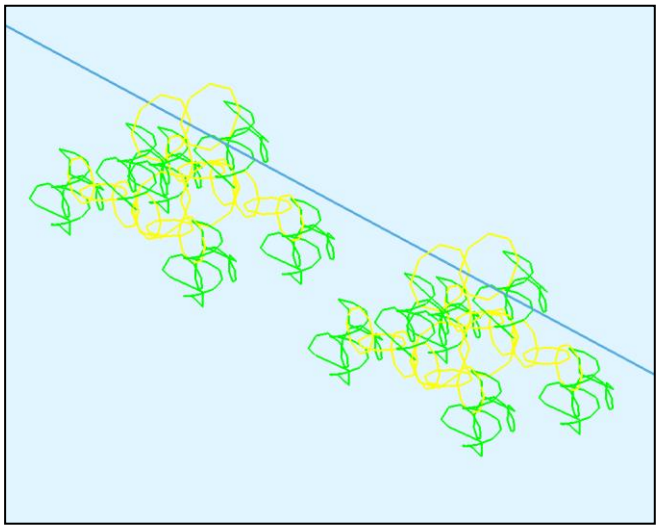

Figure 117. 3D Train model

- No Ballast is modelled between rail and bridge.
- 3D models for French TGV

- 2 cases are studied : with or without Track irregularities. (5 different track irregularities are generated)
- Speed from 144 km/h to 400 km/h with a speed step equal to 5 km/h
- Time step is 0.002s

4.3.6.2. 3D MODEL: VERTICAL DECK ACCELERATION FOR FRENCH TGV WITH OR WITHOUT IRREGULARITIES

OPEN FRAME 10M

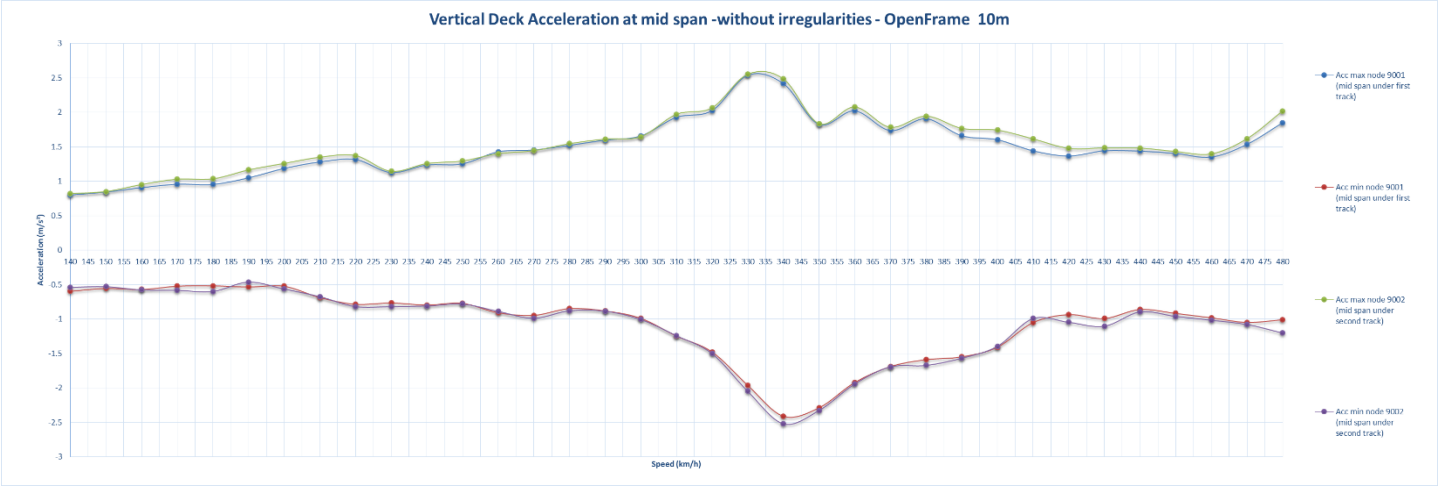

Figure 118. Vertical deck acceleration at mid span – without irregularities –Open Frame 10m

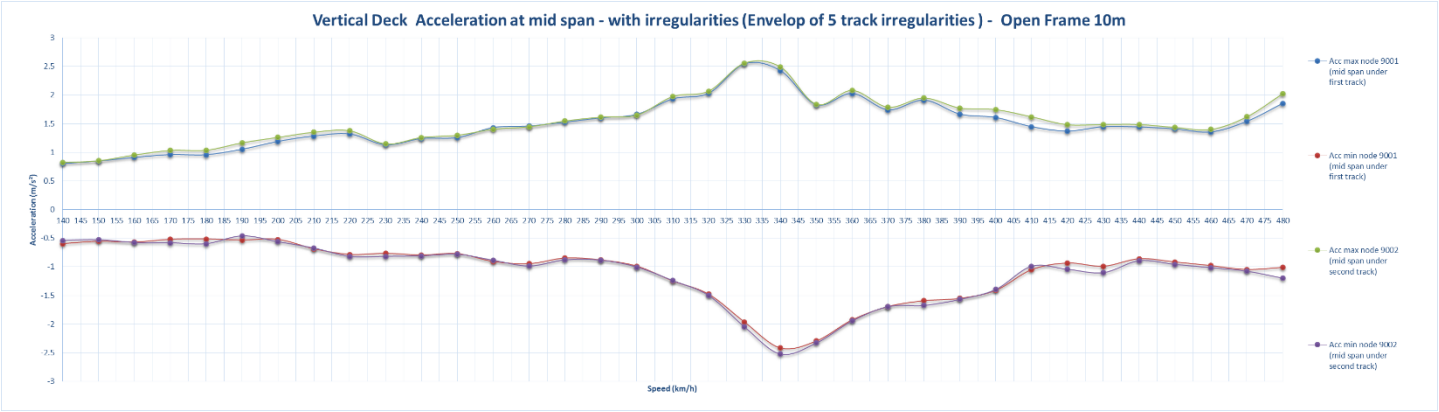

Figure 119. Vertical deck acceleration at mid span – with irregularities –Open Frame 10m

OPEN FRAME 15M

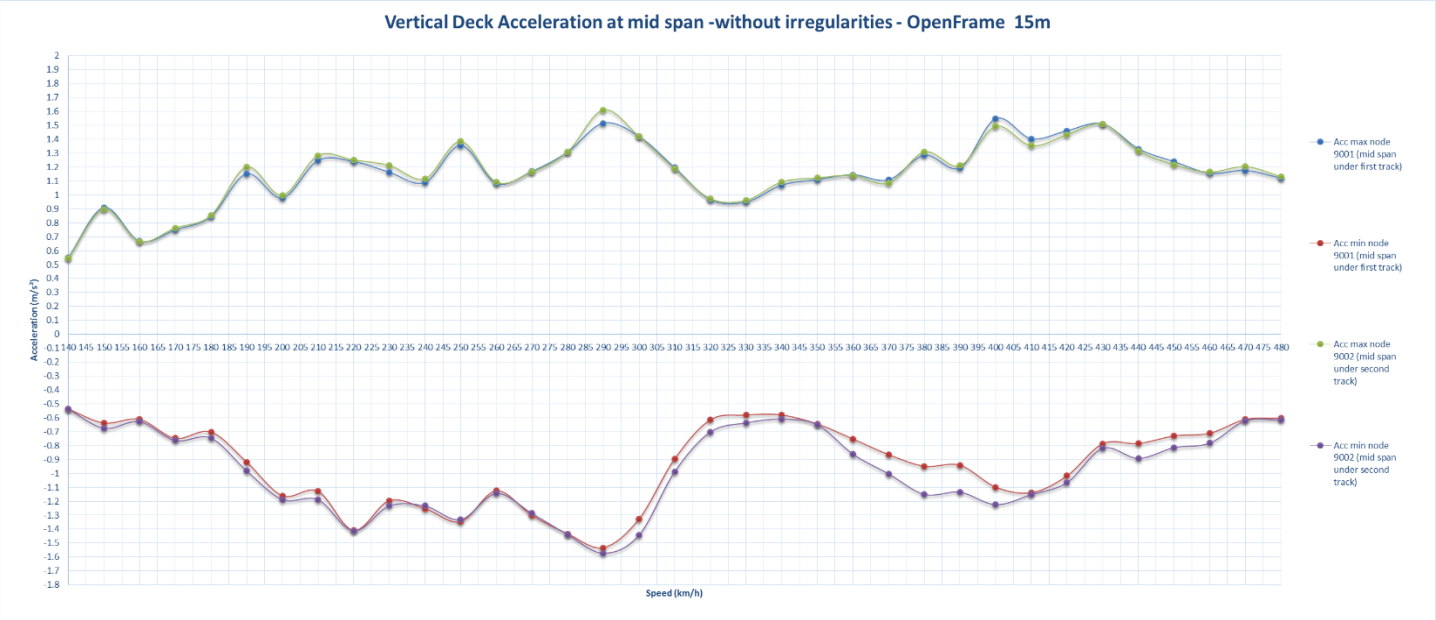

Figure 120. Vertical deck acceleration at mid span – without irregularities –Open Frame 15m

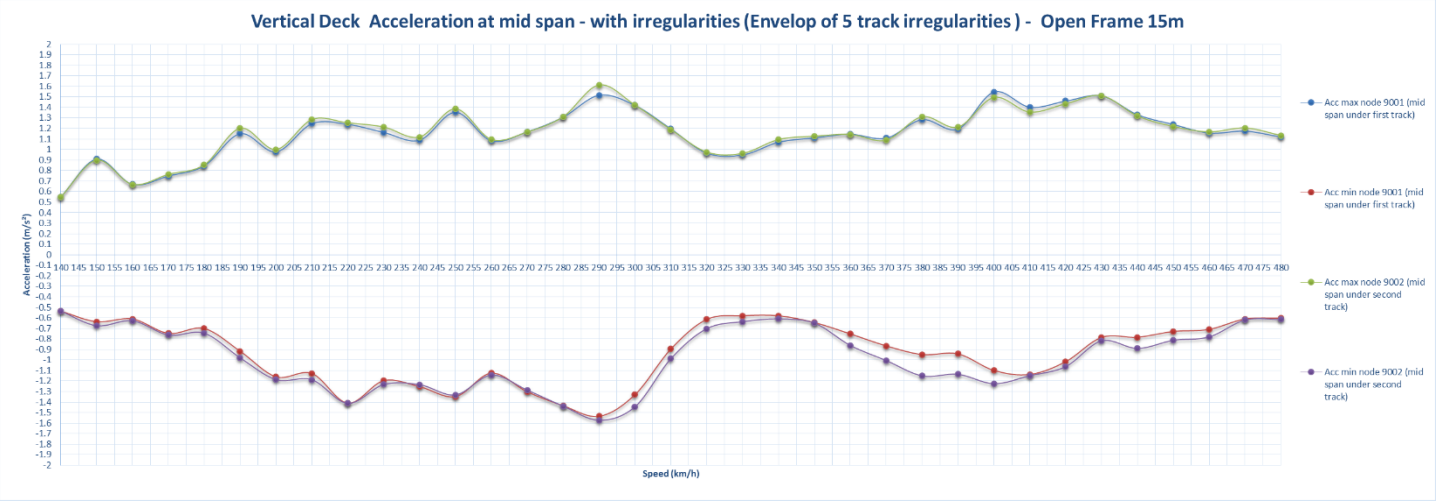

Figure 121. Vertical deck acceleration at mid span – with irregularities –Open Frame 15m

CLOSED FRAME 5M

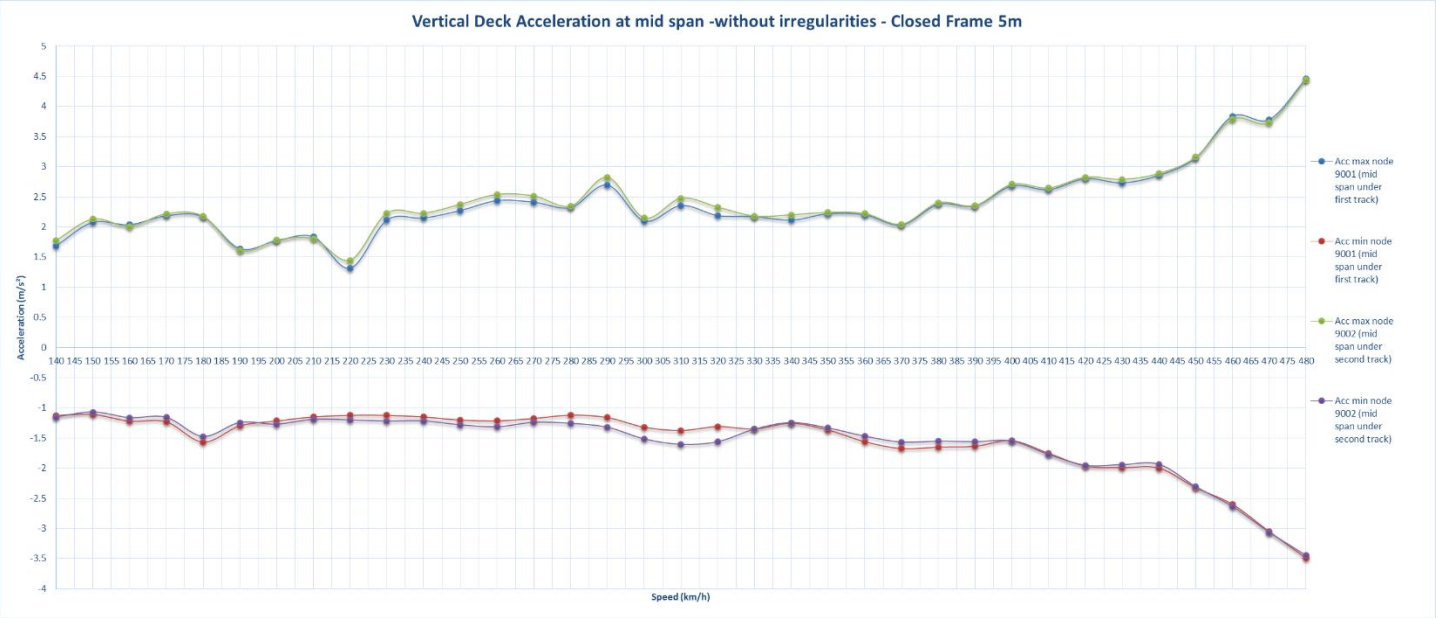

Figure 122. Vertical deck acceleration at mid span – without irregularities –Closed Frame 5m

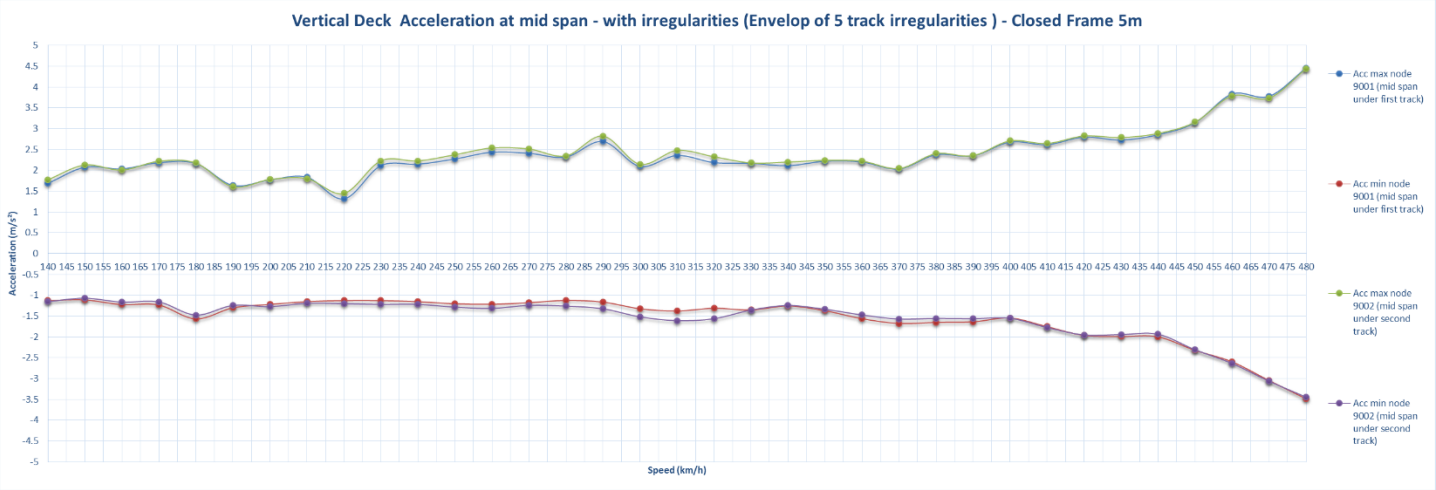

Figure 123. Vertical deck acceleration at mid span – with irregularities –Closed Frame 5m

CLOSED FRAME 10M

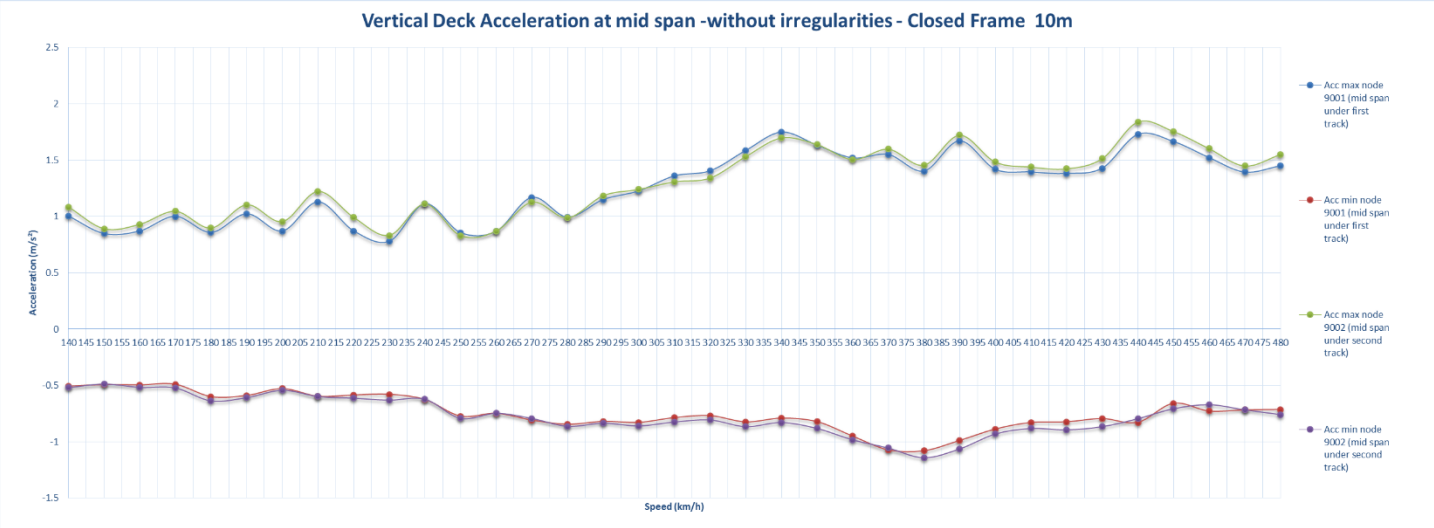

Figure 124. Vertical deck acceleration at mid span – without irregularities –Closed Frame 10m

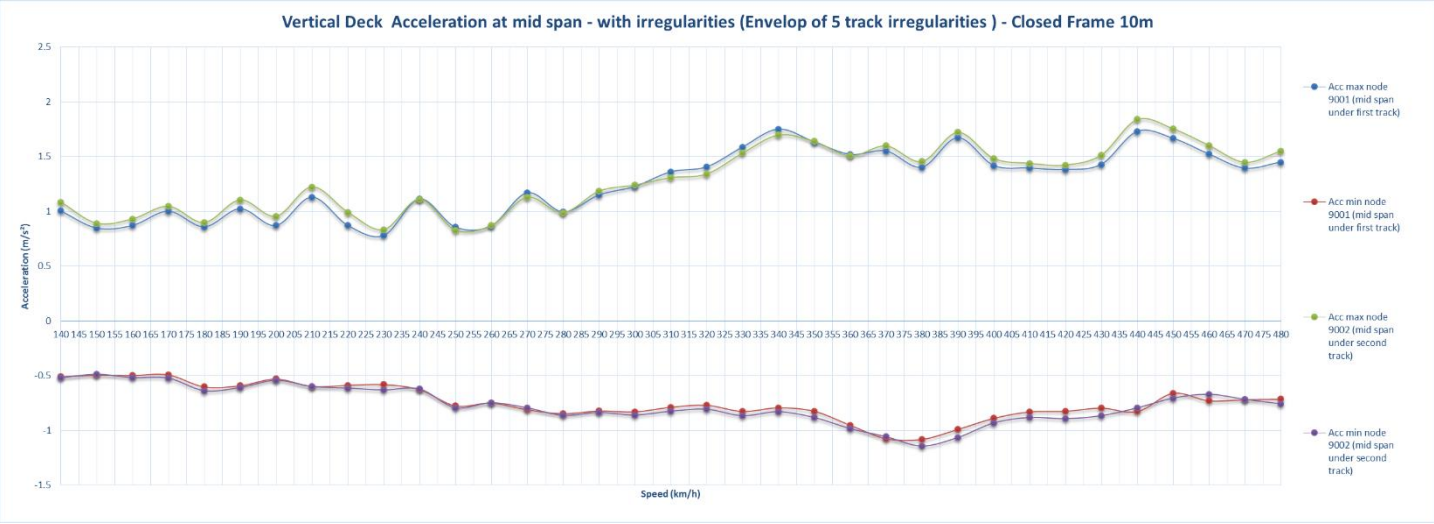

Figure 125. Vertical deck acceleration at mid span – witht irregularities –Closed Frame 10m

CONCLUSIONS

As anticipated, the track irregularities have no impact on the deck vertical acceleration. There are some local maxima of the deck vertical acceleration at critical speeds.

	Acc MAX [m/s2]	Speed [KM/h]	Acc MIN [m/s2]	Speed [KM/h]
Open Frame 10m	2.54	330	-2.52	340
Open Frame 15m	1.6	290	-1.6	290
Closed Frame 5m	4.5	480	-4.5	480
Closed Frame 10m	1.75	340	-1.15	380

az (m/s²)	Open frame 10 m	Open frame 15 m	Closed frame 5 m	Closed frame 10 m

Without irregularities	2.54	1.60	4.5	1.75
With irregularities	2.54	1.60	4.5	1.75

Figure 126. Comparison vertical acceleration in deck for 3D French TGV with and without Irregularities

Following the EN1991-2 Annex C, ϕ'' (dynamic enhancement to take into account track irregularities) has been calculated.

A comparison between the ratio az with irreugularities/az without irregularities and $1+0.5\,\phi''$ shows that the calculation with $1+0.5\,\phi''$ is conservative. The impact of track irregularities are negligible on deck vertical acceleration because the considered track irregularities for TGV are low.

az (m/s^2)	**Open frame 10 m**	**Open frame 15 m**	**Closed frame 5 m**	**Closed frame 10 m**
n_0	6.541	5.268	8.722	7.025
$L\phi$	10	15	5	10
ϕ''	0.135	0.054	0.259	0.159
$1+0.5\phi''$	1.135	1.054	1.259	1.159
Without irregularities	2.54	1.60	4.5	1.75
With irregularities	2.54	1.60	4.5	1.75
With irregularities/Without irregularities	1	1	1	1

4.3.6.3. 3D MODEL: VERTICAL PASSENGER ACCELERATION FOR FRENCH TGV WITH OR WITHOUT IRREGULARITIES

OPEN FRAME 10M

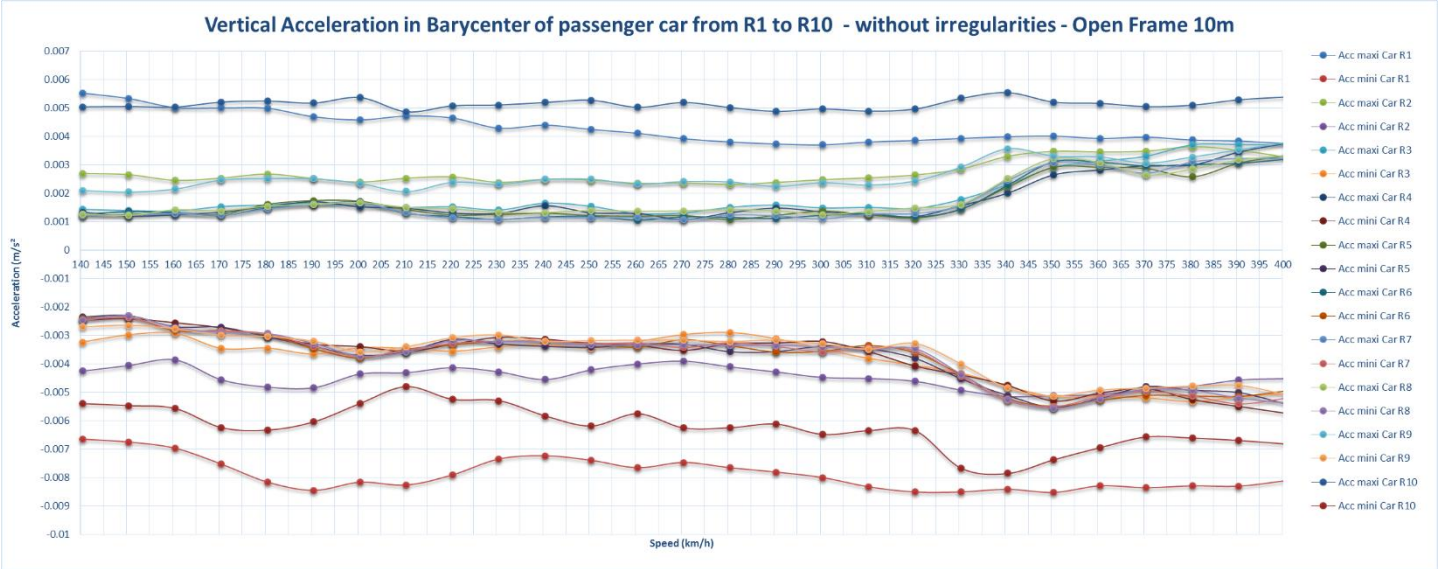

Figure 127. Vertical Acceleration in Barycenter of Passenger cars from R1 to R10 – without irregularities Open Frame 10m

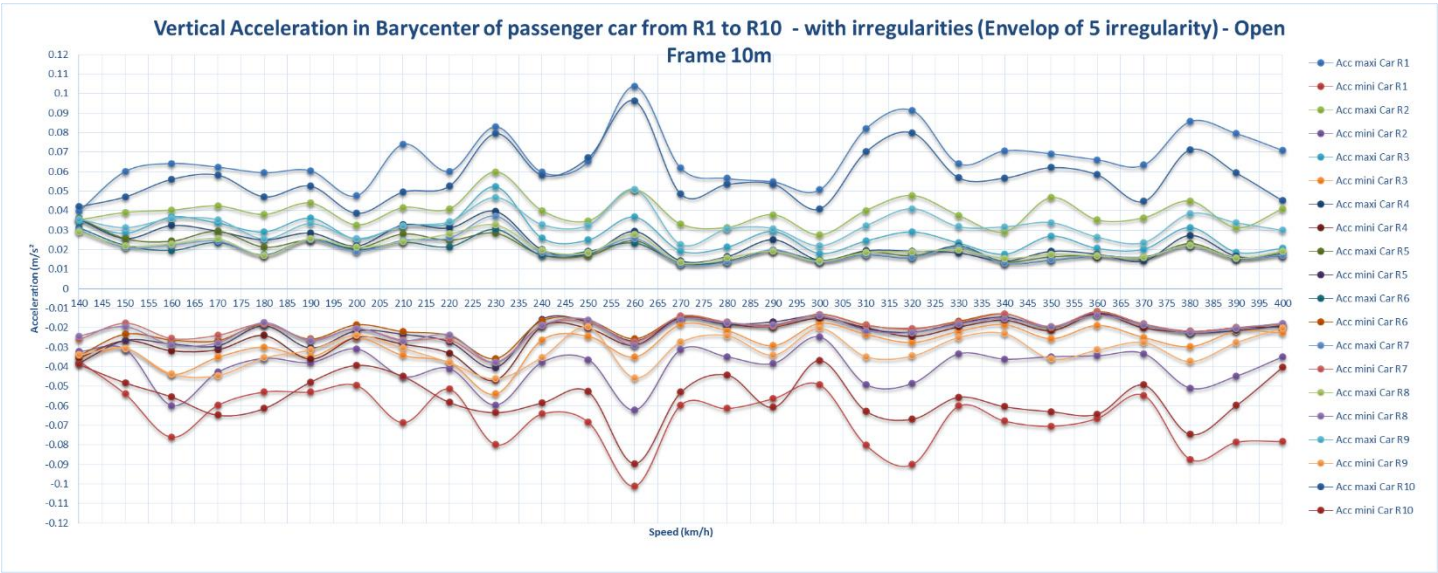

Figure 128. Vertical Acceleration in Barycenter of Passenger cars from R1 to R10 – with irregularities Open Frame 10m

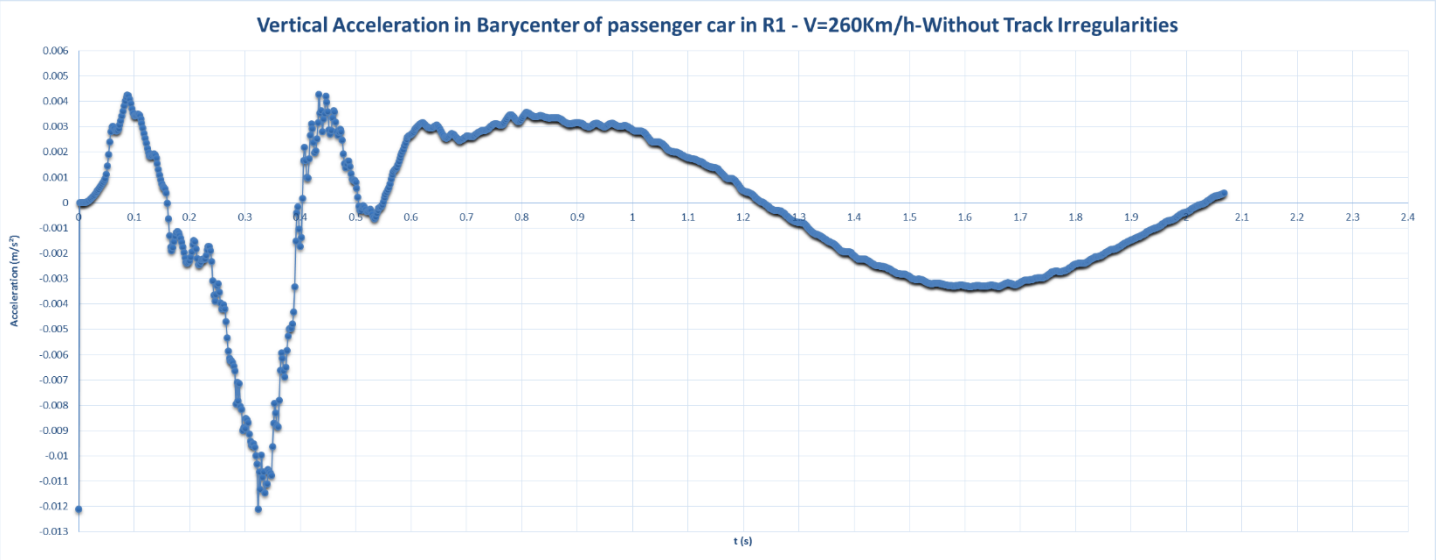

Figure 129. Vertical Acceleration in Barycenter of Passenger cars in R1 for a speed=260 Km/h

For maximum acceleration of Car 01 equal to 0.113m/s2 and for 5 types of track irregularities the mean, the standard deviation and the variance are calculated.

az (m/s²) Irregularity n°1	**az (m/s²) Irregularity n°2**	**az (m/s²) Irregularity n°3**	**az (m/s²) Irregularity n°4**	**az (m/s²) Irregularity n°5**
0.033	0.050	0.113	0.094	0.109

Figure 130. Vertical Acceleration in Barycenter of Passenger cars in R1 for a speed=260 Km/h, 5 types of track irregularities

$x = \frac{1}{n}\sum_i x_i = 0.08$ m/s² Mean

$\sigma = \sqrt{\frac{1}{n}\sum_i (x_i - x)^2} = 0.032$ m/s² Standard Deviation

$\frac{\sigma}{x} = 0.404$ Variation coefficient

This high variation coefficient means that it is necessary to perform the analysis with many irregularities profiles.

OPEN FRAME 15M

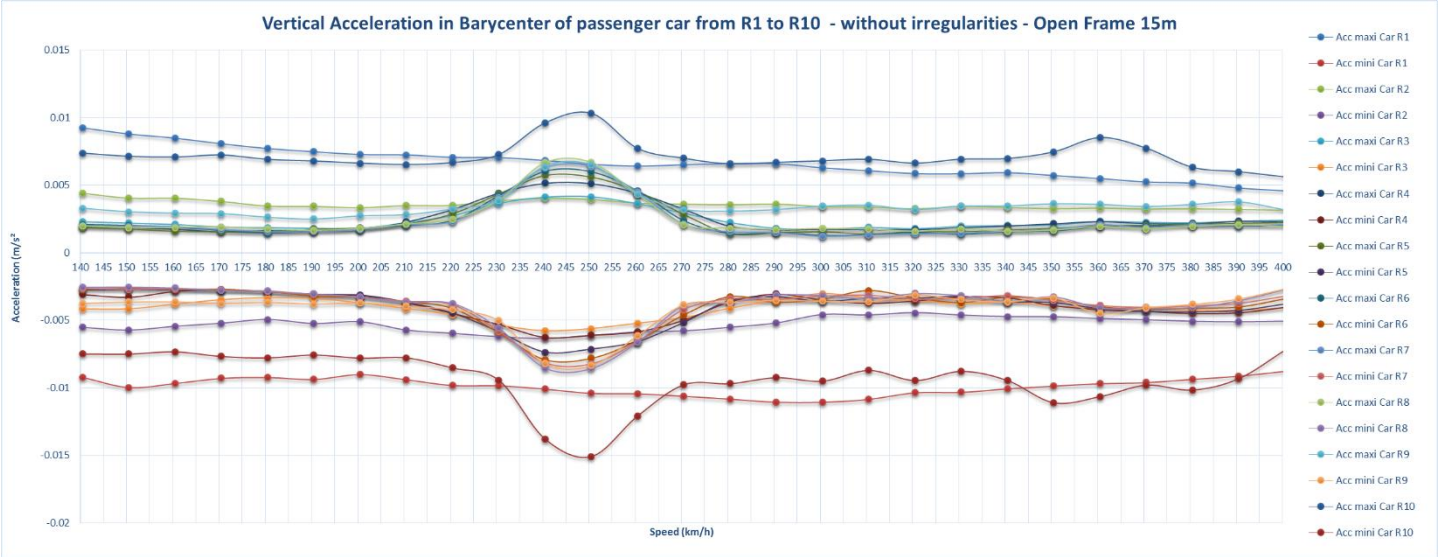

Figure 131. Vertical Acceleration in Barycenter of Passenger cars from R1 to R10 – without irregularities Open Frame 15m

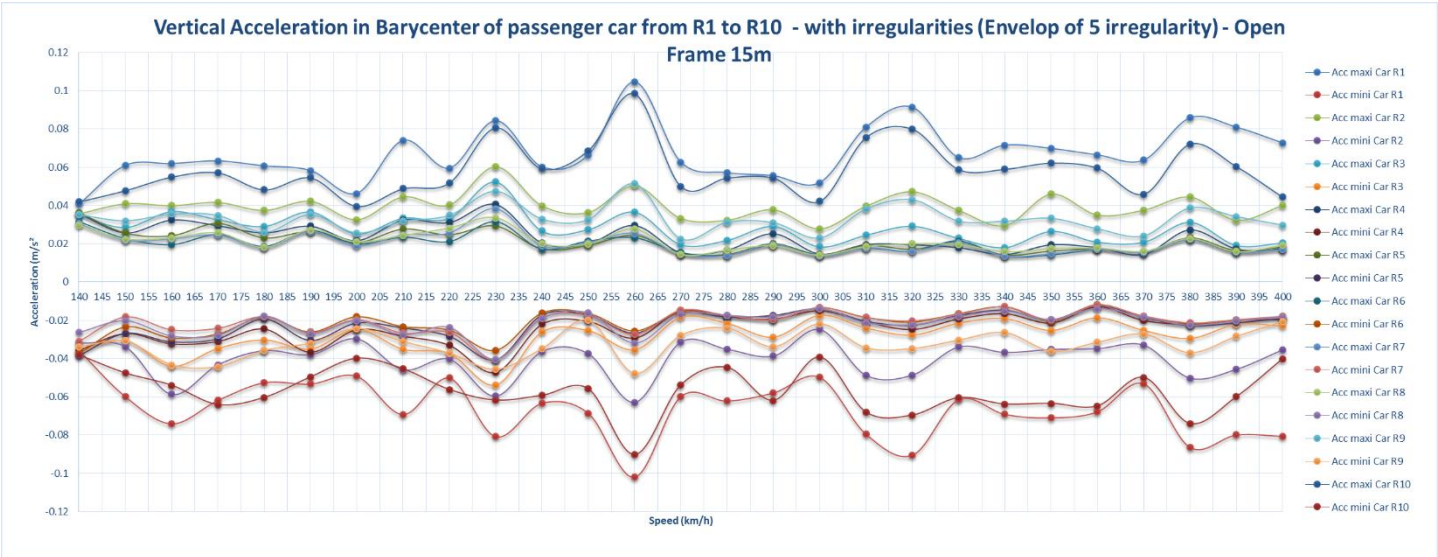

Figure 132. Vertical Acceleration in Barycenter of Passenger cars from R1 to R10 – with irregularities Open Frame 15m

CLOSED FRAME 5M

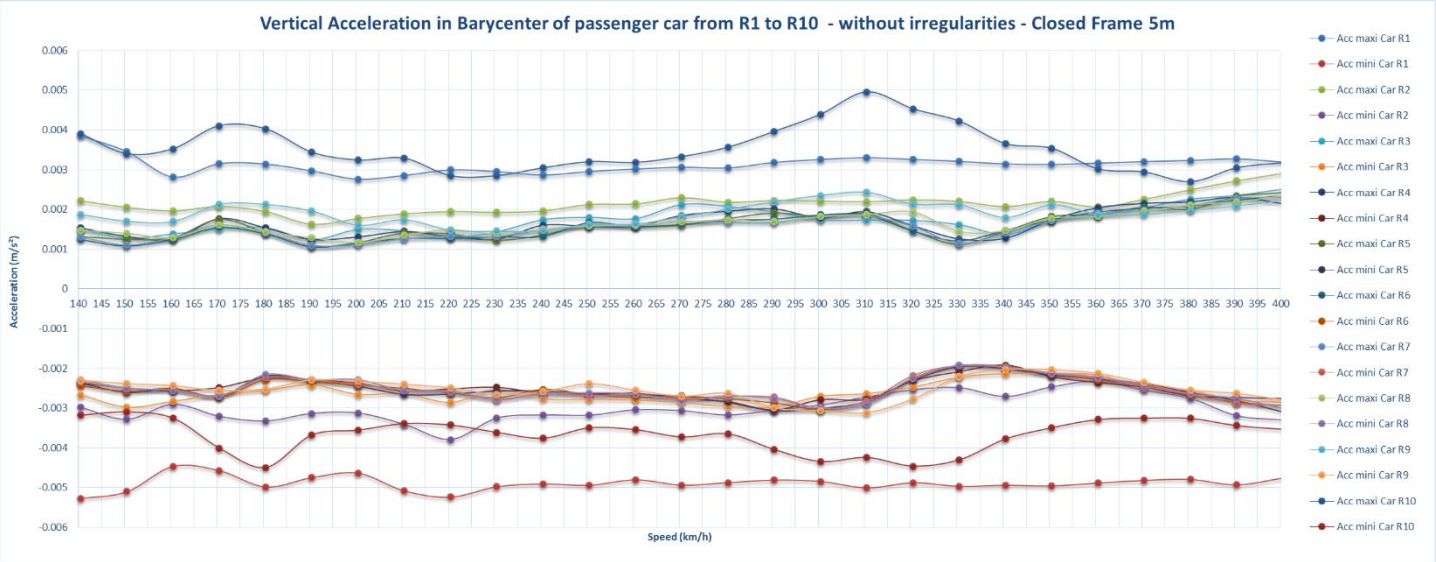

Figure 133. Vertical Acceleration in Barycenter of Passenger cars from R1 to R10 – without irregularities Closed Frame 5m

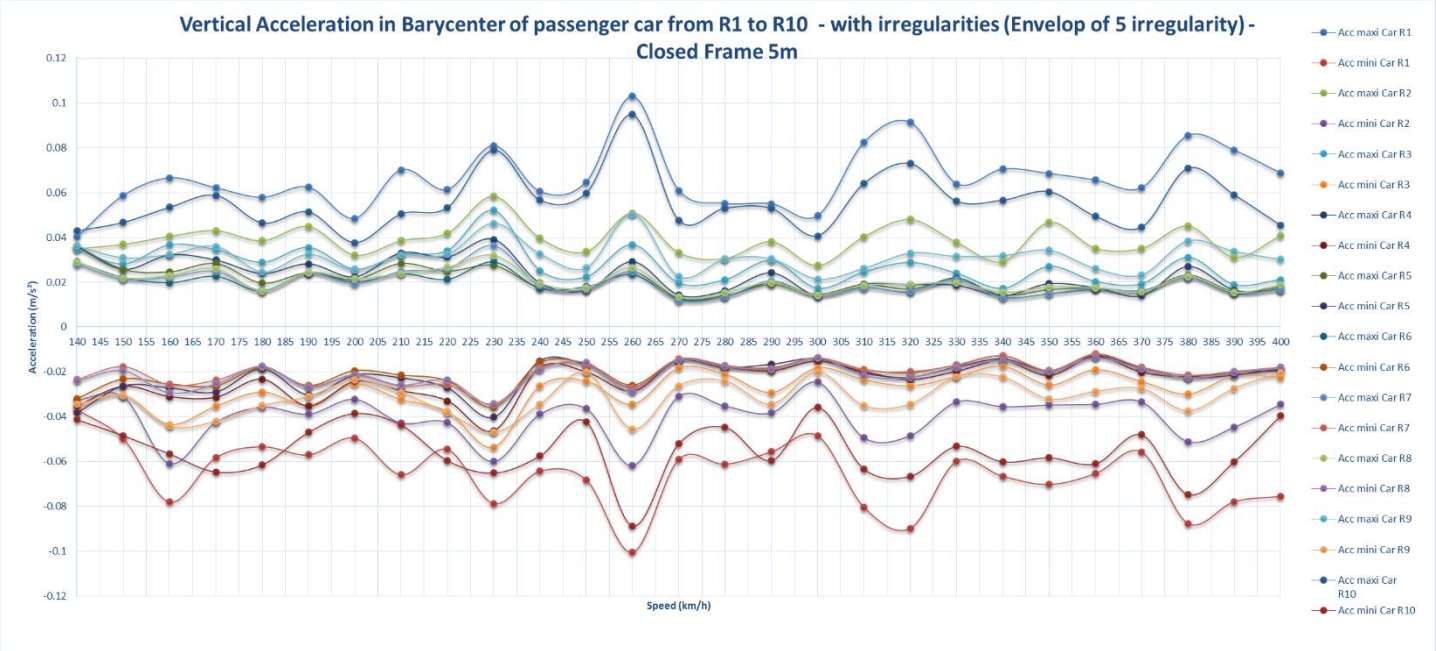

Figure 134. Vertical Acceleration in Barycenter of Passenger cars from R1 to R10 – with irregularities Closed Frame 5m

CLOSED FRAME 10M

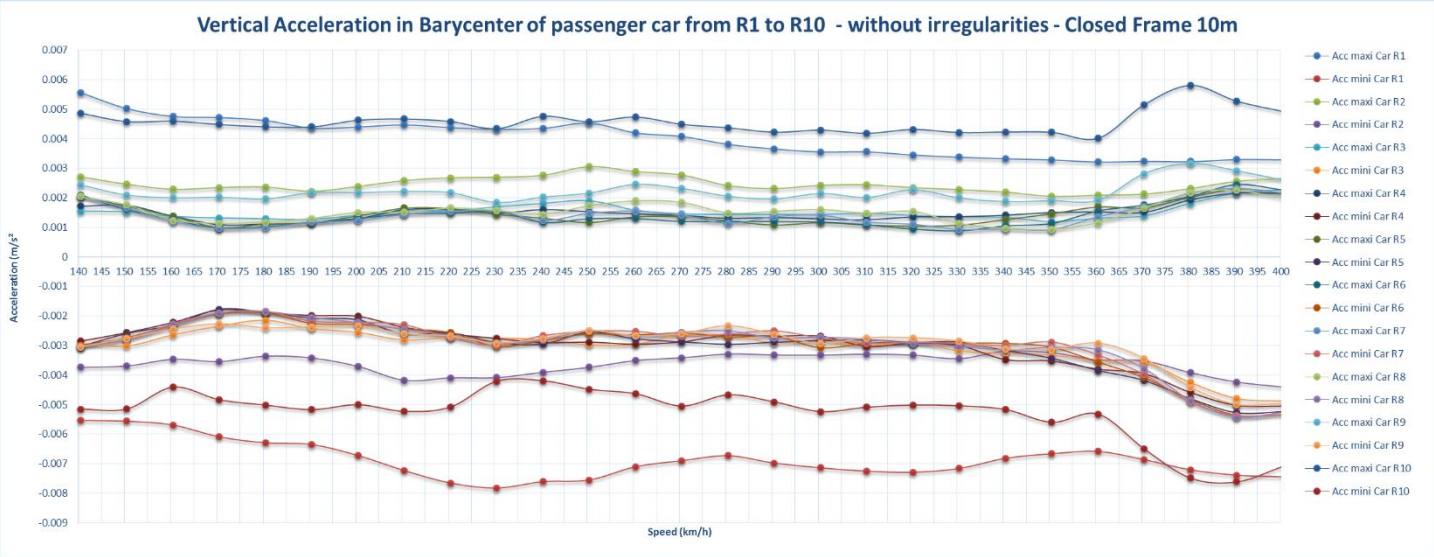

Figure 135. Vertical Acceleration in Barycenter of Passenger cars from R1 to R10 – without irregularities Closed Frame 10m

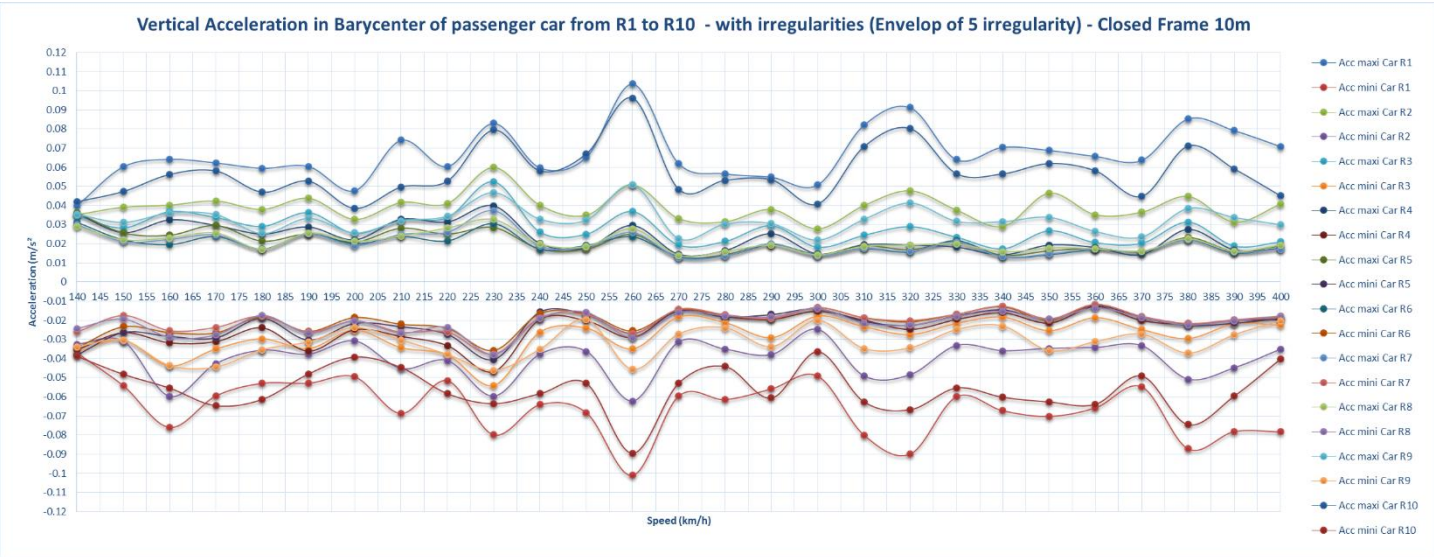

Figure 136. Vertical Acceleration in Barycenter of Passenger cars from R1 to R10 – with irregularities Closed Frame 10m

CONCLUSIONS

We noted that:

- The results of comfort analysis show that for the studied bridge, the values of acceleration are lower than the limit given by the Eurocode for good level of Comfort equal to 1 m/s2. Therefore for small span bridges comfort analysis is not critical.
- The results of dynamic analysis of bridge for French TGV show that for Closed Frame Bridge (5m), the vertical acceleration at mid span of the deck is higher than 3,5 m/s^2 given in the Eurocode. Therefore the vertical acceleration in the deck increases when the span length decreases.
- The passenger vertical acceleration due to track irregularities is governing.
- The train speed for which the passenger acceleration is maximum is generally not the same without track irregularities and with track irregularities.

az (m/s^2)	Open frame 10 m	Open frame 15 m	Closed frame 5 m	Closed frame 10 m
Without irregularities	0.009	0.015	0.005	0.008
With irregularities	0.1	0.1	0.1	0.1
Ratio: With irregularities/Without irregularities	11	7	20	13

4.3.6.4. 3D MODEL: TRANSVERSE PASSENGER ACCELERATION FOR FRENCH TGV WITH OR WITHOUT IRREGULARITIES

OPEN FRAME 10M

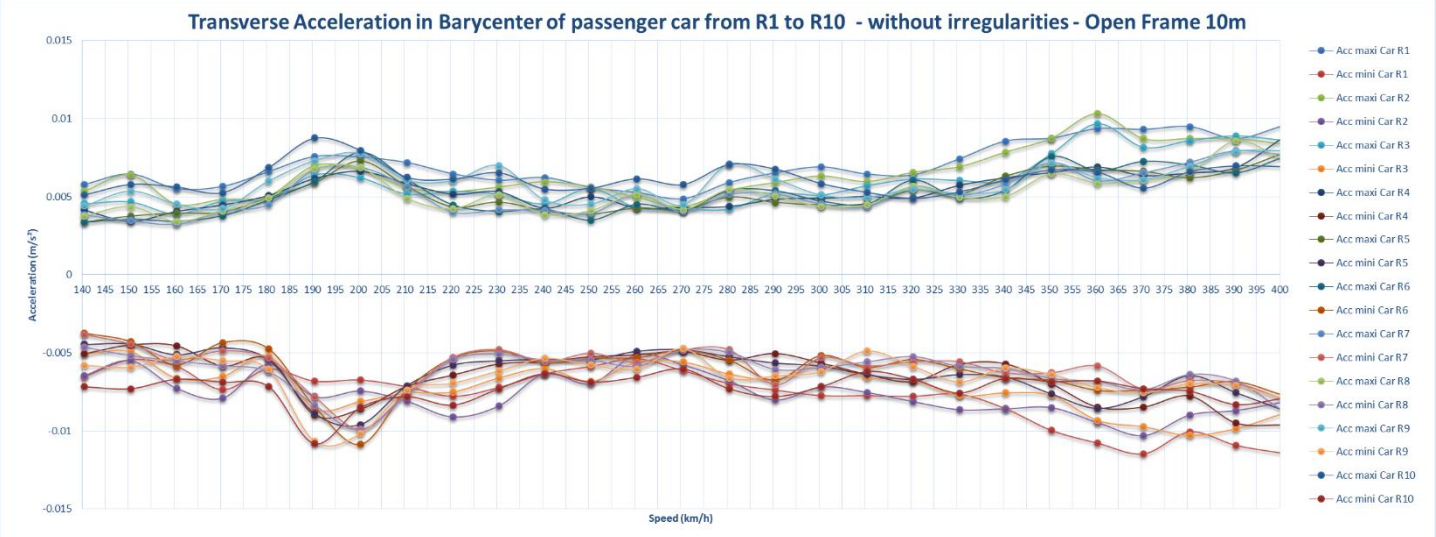

Figure 137. Transverse Acceleration in Barycenter of Passenger cars from R1 to R10 – without irregularities Open Frame 10m

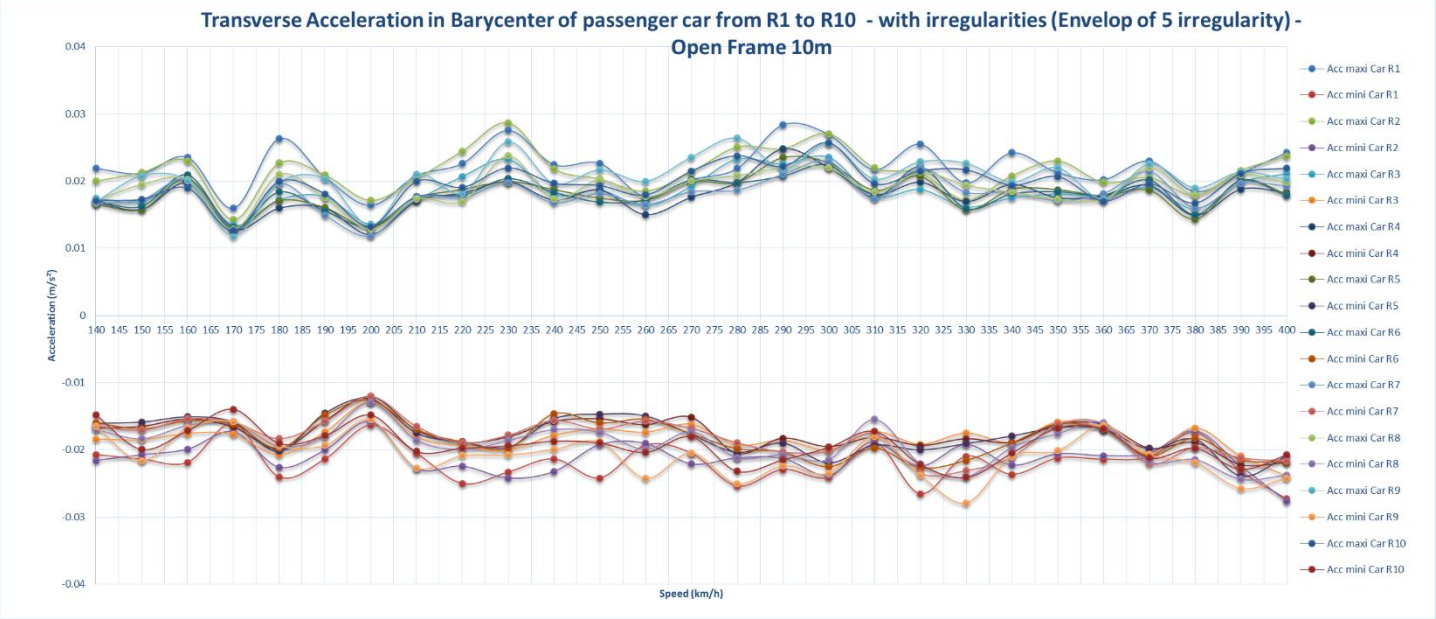

Figure 138. Transverse Acceleration in Barycenter of Passenger cars from R1 to R10 – with irregularities Open Frame 10m

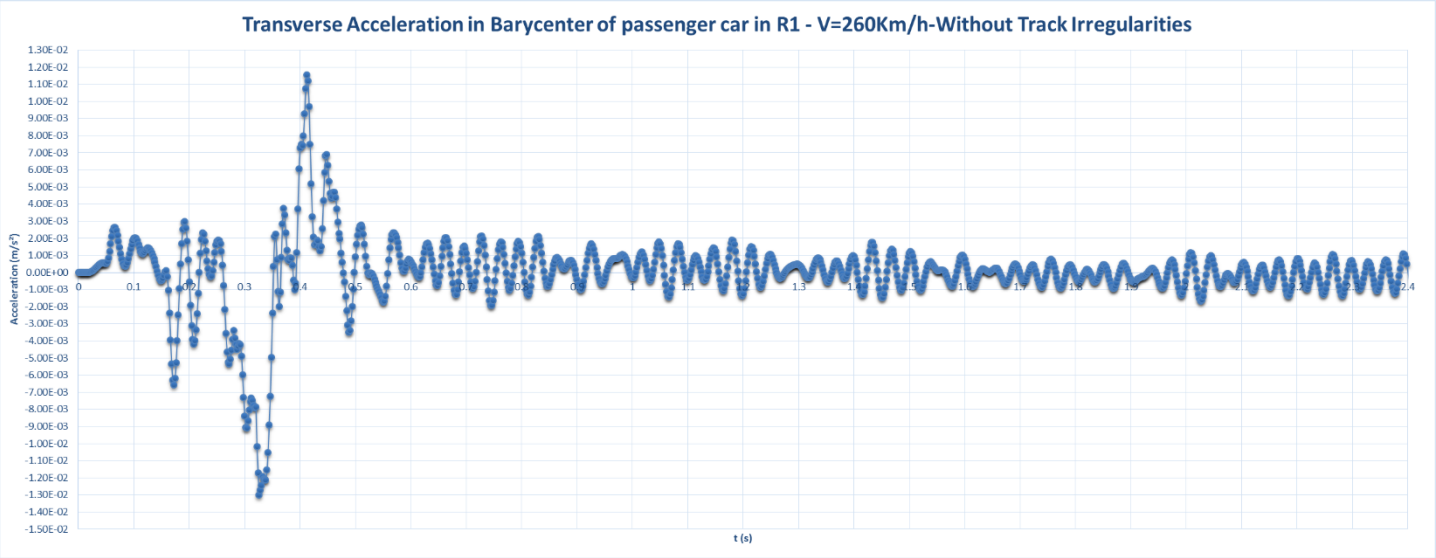

Figure 139. Transverse Acceleration in Barycenter of Passenger cars in R1 for a speed=260 Km/h

OPEN FRAME 15M

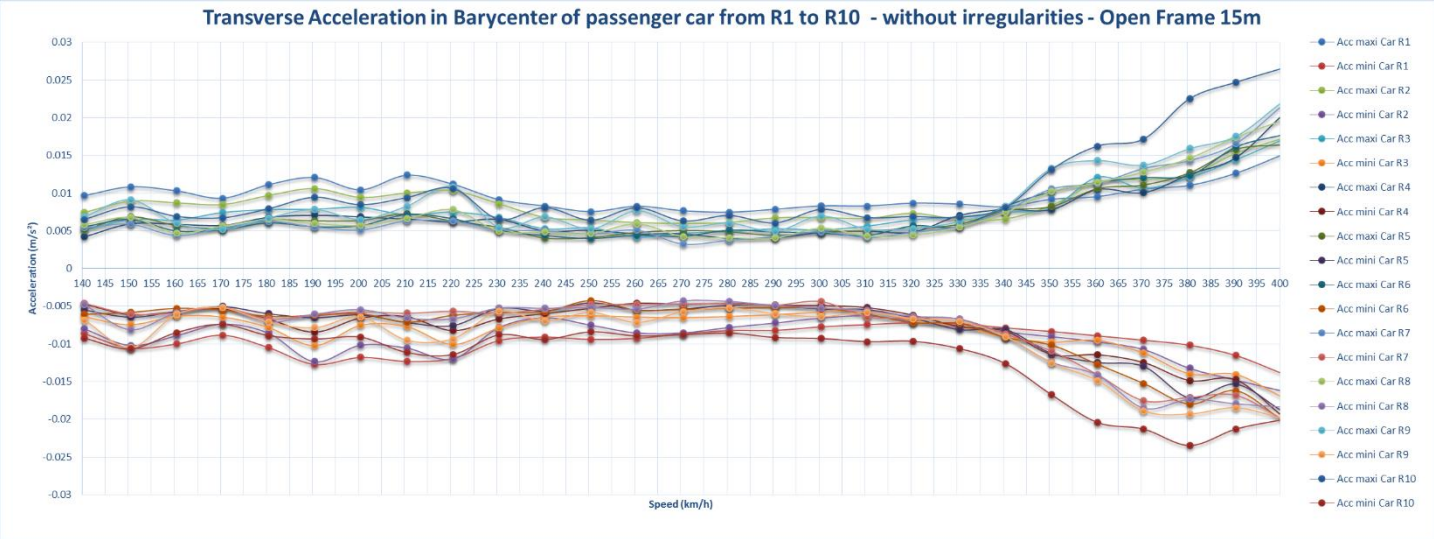

Figure 140. Transverse Acceleration in Barycenter of Passenger cars from R1 to R10 – without irregularities Open Frame 15m

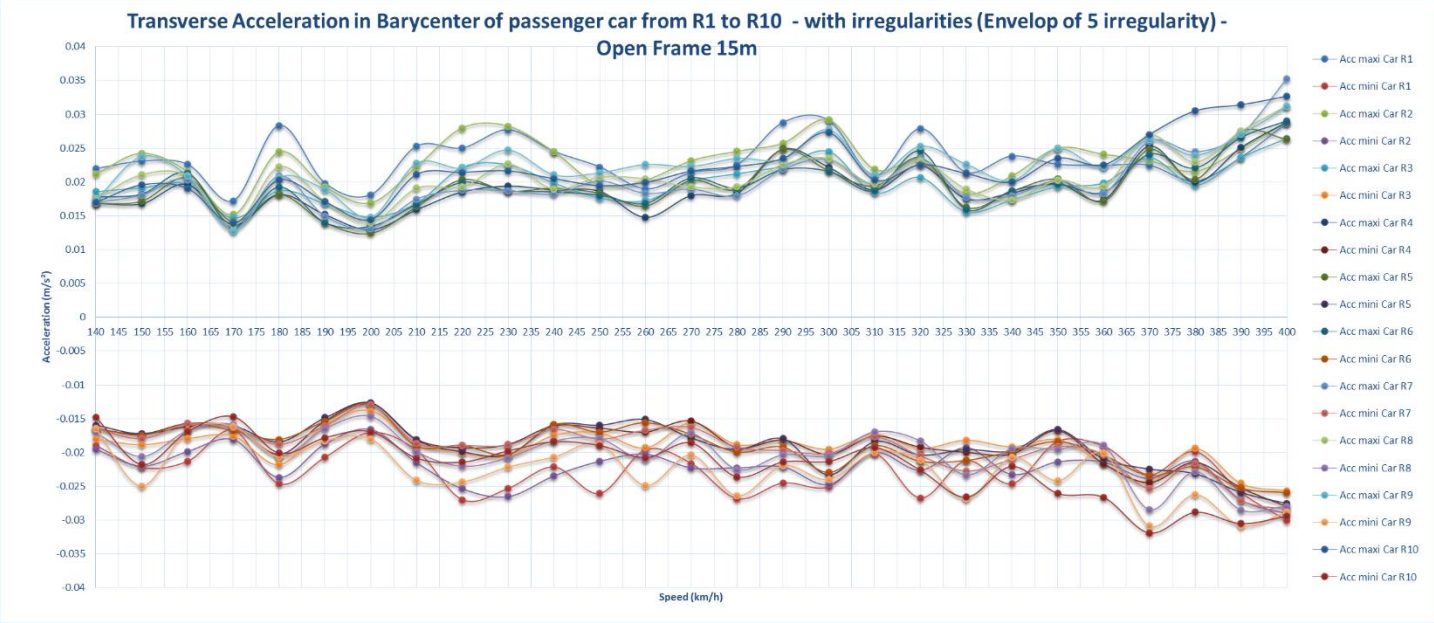

Figure 141. Transverse Acceleration in Barycenter of Passenger cars from R1 to R10 – with irregularities Open Frame 15m

CLOSED FRAME 5M

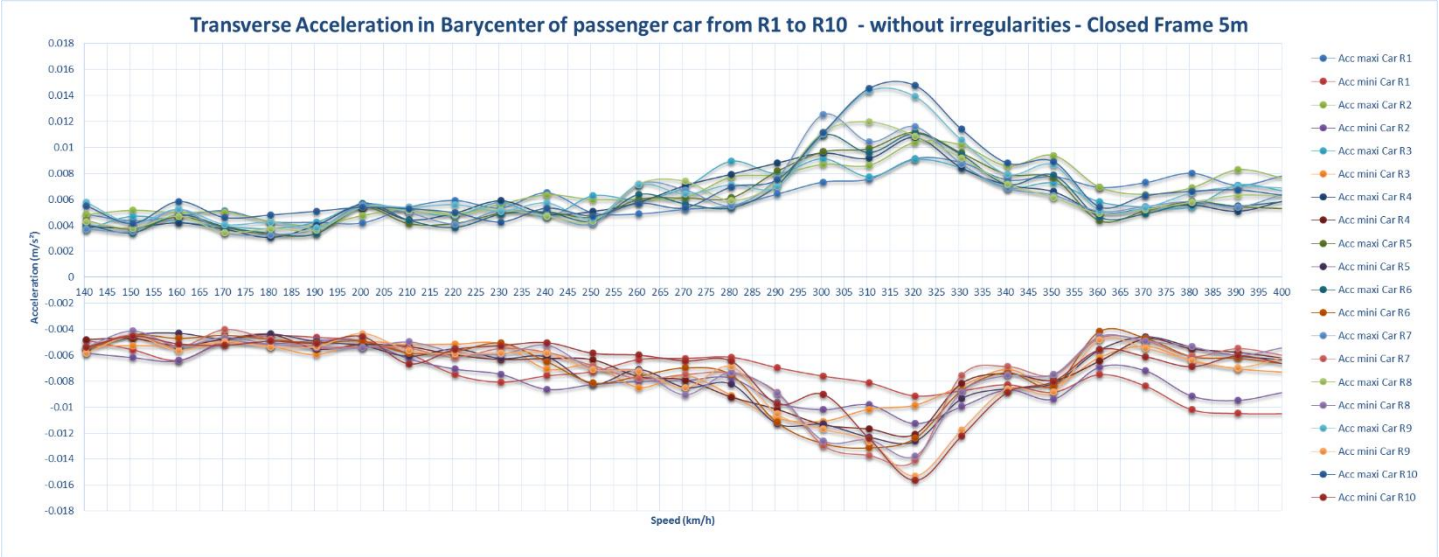

Figure 142. Transverse Acceleration in Barycenter of Passenger cars from R1 to R10 – without irregularities Closed Frame 5m

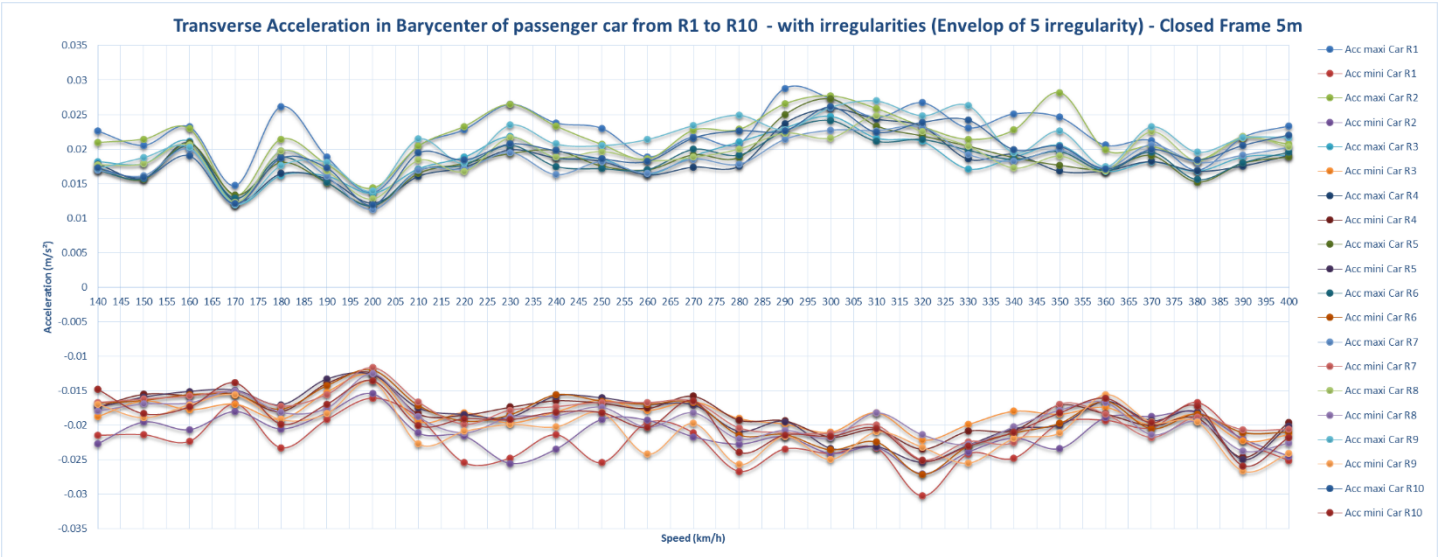

Figure 143. Transverse Acceleration in Barycenter of Passenger cars from R1 to R10 – with irregularities Closed Frame 5m

CLOSED FRAME 10M

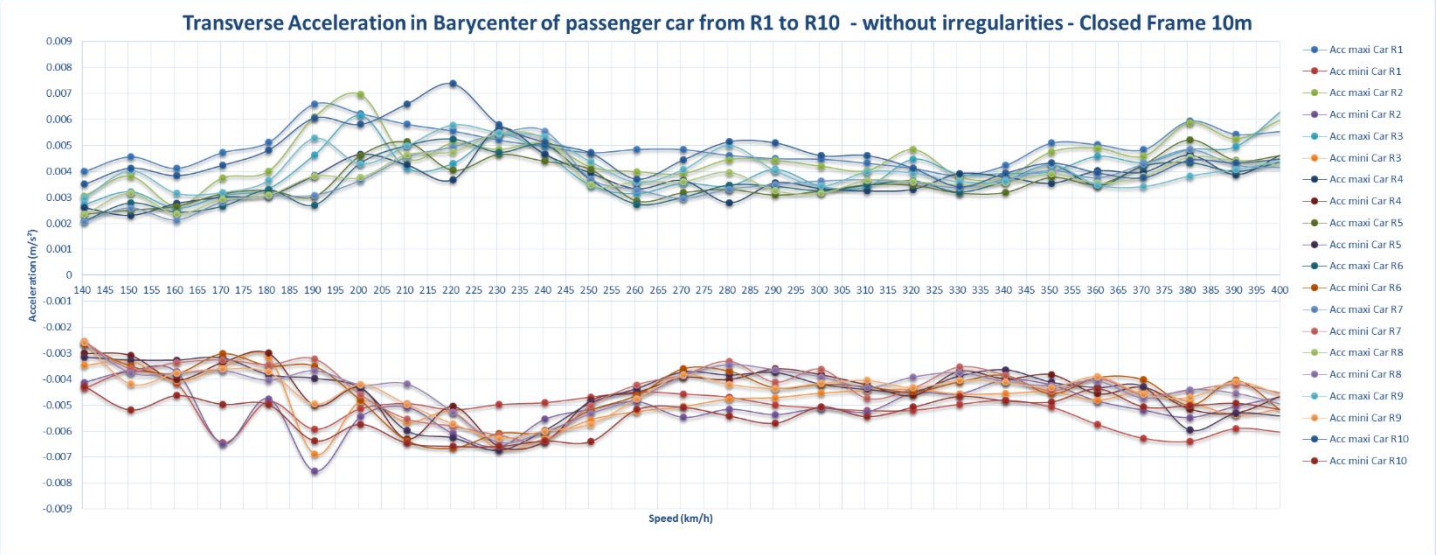

Figure 144. Transverse Acceleration in Barycenter of Passenger cars from R1 to R10 – without irregularities Closed Frame 10m

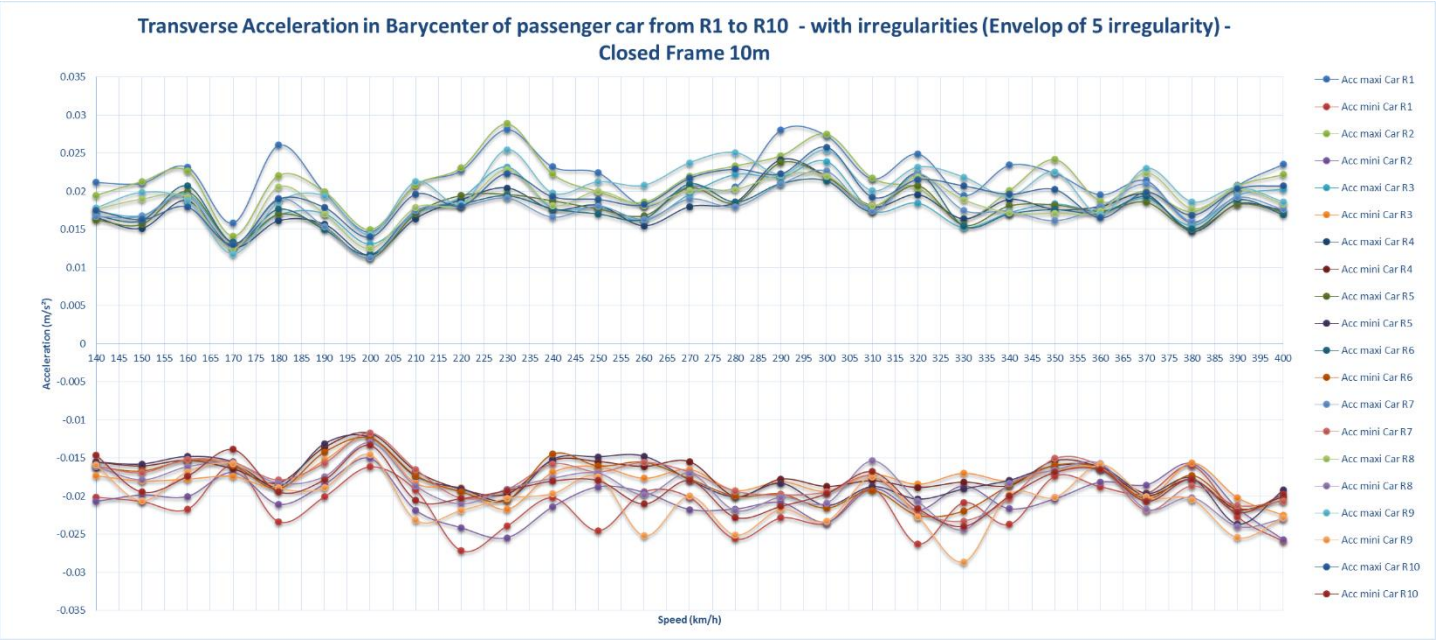

Figure 145. Transverse Acceleration in Barycenter of Passenger cars from R1 to R10 – with irregularities Closed Frame 10m

CONCLUSIONS

We noted that the transverse acceleration due to track irregularities is higher than the transverse acceleration without track irregularities.

The train speed for which the transverse passenger acceleration is maximum is generally not the same with and without track irregularities.

ay (m/s^2)	Open frame 10 m	Open frame 15 m	Closed frame 5 m	Closed frame 10 m
Without irregularities	0.012	0.025	0.015	0.008
With irregularities	0.028	0.035	0.030	0.011
Ratio: With irregularities/Without irregularities	2.33	1.4	2	1.37

Figure 146. Comparison Transverse Acceleration in Barycenter of Passenger with and without irregularities

4.3.6.5. 3D MODEL: WHEEL UNLOADING COEFFICIENT FOR FRENCH TGV

In the tables below are shown:

the ΔP max et min (wheel vertical load).
It corresponds to wheel vertical load variation = dynamic wheel load -static wheel load for the first 16 contact nodes (train axles).

OPEN FRAME 10M

	Speed / irregularities	ΔP maxi (KN)	Speed / irregularities	ΔP mini (KN)
Node n°1	230/5	2.99	230/5	-3.13
Node n°2	230/5	3.25	230/5	-3.12
Node n°3	230/5	3.09	230/5	-3.40
Node n°4	230/5	3.25	230/5	-3.38
Node n°5	200/5	4.04	225/4	-4.39
Node n°6	**200/5**	**4.24**	**225/4**	**-4.65**
Node n°7	200/5	3.94	200/5	-4.42
Node n°8	270/3	3.99	200/5	-4.61
Node n°9	265/5	2.86	265/5	-2.69
Node n°10	215/3	2.88	225/4	-2.69
Node n°11	265/5	3.96	260/3	-3.49
Node n°12	265/5	3.49	225/4	-3.47
Node n°13	260/5	3.10	265/2	-3.17
Node n°14	260/3	3.31	270/4	-3.05
Node n°15	260/2	3.46	215/3	-3.72
Node n°16	260/2	3.61	265/5	-3.85

Figure 147. Wheel unloading coefficient – Open Frame 10m

OPEN FRAME 15M

	Speed / irregularities	ΔP maxi (KN)	Speed / irregularities	ΔP mini (KN)
Node n°1	230/5	2.97	230/5	-3.13
Node n°2	230/5	3.32	230/5	-3.12
Node n°3	230/5	3.08	230/5	-3.40
Node n°4	230/5	3.31	230/5	-3.36
Node n°5	200/5	4.09	245/1	-4.86
Node n°6	200/5	4.31	**245/1**	**-5.24**
Node n°7	270/3	4.13	200/5	-4.48
Node n°8	**270/3**	**4.31**	270/2	-4.81
Node n°9	265/5	2.91	265/5	-2.70
Node n°10	215/3	2.90	225/4	-2.67
Node n°11	265/5	3.97	260/3	-3.50
Node n°12	265/5	3.51	225/4	-3.44
Node n°13	260/5	3.10	265/2	-3.18
Node n°14	260/3	3.33	265/2	-3.05
Node n°15	260/2	3.46	215/3	-3.73
Node n°16	260/2	3.63	265/5	-3.76

Figure 148. Wheel unloading coefficient – Open Frame 15m

Closed Frame 5m

	Speed / irregularities	ΔP maxi (KN)	Speed / irregularities	ΔP mini (KN)
Node n°1	230/5	3.02	230/5	-3.14
Node n°2	230/5	3.26	230/5	-3.14
Node n°3	230/5	3.12	230/5	-3.42
Node n°4	230/5	3.26	230/5	-3.41
Node n°5	200/5	4.00	200/5	-4.31
Node n°6	200/5	4.19	225/4	-4.56
Node n°7	140/2	4.00	145/2	-4.80
Node n°8	**140/2**	**4.37**	**145/5**	**-5.24**
Node n°9	265/5	2.84	175/4	-2.80
Node n°10	265/5	2.86	170/2	-2.74
Node n°11	265/5	3.79	260/3	-3.48
Node n°12	265/5	3.48	225/4	-3.49
Node n°13	260/5	3.10	265/2	-3.13
Node n°14	260/3	3.30	270/4	-3.06
Node n°15	260/2	3.45	215/3	-3.72
Node n°16	260/2	3.60	250/4	-3.74

Figure 149. Wheel unloading coefficient – Closed Frame 5m

Closed Frame 10m

	Speed / irregularities	ΔP maxi (KN)	Speed / irregularities	ΔP mini (KN)
Node n°1	230/5	3.00	155/3	-3.37
Node n°2	230/5	3.25	155/3	-3.49
Node n°3	230/5	3.10	230/5	-3.41
Node n°4	230/5	3.25	230/5	-3.39
Node n°5	200/5	4.03	175/4	-4.51
Node n°6	**200/5**	**4.23**	190/1	-4.80
Node n°7	200/5	3.93	215/4	-5.42
Node n°8	270/3	3.98	**215/4**	**-5.57**
Node n°9	265/5	2.85	265/5	-2.68
Node n°10	215/3	2.96	225/4	-2.70
Node n°11	265/5	3.96	260/3	-3.48
Node n°12	260/3	3.63	225/4	-3.47
Node n°13	260/5	3.10	265/2	-3.15
Node n°14	260/3	3.31	270/4	-3.05
Node n°15	260/2	3.46	215/3	-3.72
Node n°16	260/2	3.61	265/5	-3.85

Figure 150. Wheel unloading coefficient – Closed Frame 10m

CONCLUSIONS

ΔP max is equal to 5.57 kN for closed Frame 10 m.

ΔP max=5.57 kN corresponds to a maximum irregularity equal to 4mm generated for speed= 215 km/h.

The static load per axle corresponds to P = 85 kN.

We note that ΔP/P = 0.066 < 0.25 (Ma and Zhu, 1998)

Criteria	Description	Parameter	Limit	References
Unloading Coefficient	Axle load decrement ratio	ΔQ / Qs	0.25	Ma and Zhu, 1998

Figure 151. Wheel unloading coefficient - Limit

The train speeds which creates the maximum wheel unloading coefficient is generally not equal to the train speed which creates the maximum passenger vertical acceleration.

4.3.6.6. 3D MODEL: DERAILMENT COEFFICIENT FOR FRENCH TGV WITH OR WITHOUT IRREGULARITIES

In the tables below are shown:

the Y max and Y min. It corresponds to wheel horizontal load for the first 16 contact nodes (train axles).

OPEN FRAME 10M

	Speed / irregularities	Y maxi (KN)	Speed / irregularities	Y mini (KN)
Node n°1	265/4	1.04	270/2	-1.75
Node n°2	265/4	1.04	270/2	-1.74
Node n°3	265/4	1.04	270/2	-1.70
Node n°4	265/4	1.04	270/2	-1.78
Node n°5	270/4	1.56	**265/4**	**-2.95**
Node n°6	270/4	1.56	265/4	-2.93
Node n°7	270/4	1.56	265/4	-2.88
Node n°8	270/4	1.56	265/4	-3.00
Node n°9	**255/4**	**2.23**	185/4	-1.34
Node n°10	255/4	2.11	255/2	-1.39
Node n°11	255/4	2.18	185/4	-1.34
Node n°12	255/4	2.15	255/2	-1.37
Node n°13	185/2	2.27	245/5	-1.97
Node n°14	185/2	2.27	245/5	-1.95
Node n°15	185/2	2.27	185/4	-1.93
Node n°16	185/2	2.27	245/5	-2.00

Figure 152. Derailment Coefficient – Open Frame 10m

OPEN FRAME 15M

	Speed / irregularities	Y maxi (KN)	Speed / irregularities	Y mini (KN)
Node n°1	265/4	1.04	170/1	-1.91
Node n°2	265/4	1.04	170/1	-1.91
Node n°3	265/4	1.04	170/1	-1.91
Node n°4	265/4	1.04	170/1	-1.91
Node n°5	150/3	1.79	160/3	-3.13
Node n°6	150/3	1.75	160/3	-3.12
Node n°7	150/3	1.78	160/3	-3.10
Node n°8	150/3	1.76	**160/3**	**-3.15**
Node n°9	**190/4**	**2.61**	145/4	-1.69
Node n°10	190/4	2.56	145/4	-1.69
Node n°11	190/4	2.60	145/4	-1.69
Node n°12	190/4	2.58	145/4	-1.69
Node n°13	185/2	2.28	270/2	-2.30
Node n°14	185/2	2.28	270/2	-2.29
Node n°15	185/2	2.28	270/2	-2.28
Node n°16	185/2	2.28	270/2	-2.31

Figure 153. Derailment Coefficient – Open Frame 15m

Closed Frame 5m

	Speed / irregularities	Y maxi (KN)	Speed / irregularities	Y mini (KN)
Node n°1	150/3	1.18	250/3	-1.69
Node n°2	265/4	1.04	250/3	-1.67
Node n°3	150/3	1.12	250/3	-1.61
Node n°4	150/3	1.08	250/3	-1.76
Node n°5	255/4	1.53	265/4	-2.57
Node n°6	255/4	1.39	265/4	-2.56
Node n°7	255/4	1.48	265/4	-2.49
Node n°8	255/4	1.44	**265/4**	**-2.64**
Node n°9	**270/4**	**2.01**	225/3	-1.80
Node n°10	270/4	1.98	225/3	-1.78
Node n°11	270/4	2.00	225/3	-1.71
Node n°12	270/4	2.00	225/3	-1.87
Node n°13	185/2	2.28	225/3	-2.33
Node n°14	185/2	2.28	225/3	-2.31
Node n°15	185/2	2.28	225/3	-2.25
Node n°16	185/2	2.28	225/3	-2.40

Figure 154. Derailment Coefficient – Closed Frame 5m

Closed Frame 10m

	Speed / irregularities	Y maxi	Speed / irregularities	Y mini
Node n°1	265/4	1.04	255/2	-1.16
Node n°2	265/4	1.04	255/2	-1.15
Node n°3	265/4	1.04	270/3	-1.13
Node n°4	265/4	1.04	255/2	-1.18
Node n°5	270/4	1.07	265/4	-2.07
Node n°6	270/4	1.07	265/4	-2.06
Node n°7	270/4	1.09	265/4	-2.03
Node n°8	210/5	1.06	265/4	-2.10
Node n°9	180/2	1.71	185/4	-1.34
Node n°10	180/2	1.64	185/4	-1.34
Node n°11	180/2	1.69	185/4	-1.34
Node n°12	180/2	1.66	185/4	-1.34
Node n°13	185/2	2.28	170/1	-1.94
Node n°14	185/2	2.28	170/1	-1.94
Node n°15	185/2	2.28	170/1	-1.94
Node n°16	185/2	2.28	170/1	-1.93

Figure 155. Derailment Coefficient – Closed Frame 10m

CONCLUSIONS

Y max is equal to 3.15 kN for open Frame 15 m

Ymax=3.15 kN corresponds to a maximum irregularity equal to 4mm generated for speed= 160 Km/h

The dynamic load per axle corresponds to P_{dyn}=85 – 5.57 = 79.4 kN.

We noted that Y_{max}/P_{dyn}= 3.15 / 79.4 = 0.04 < 0.8

Criteria	Description	Parameter	Limit	References
Derailment Coefficient	Single wheel lateral to vertical force ratio	Y / Q	1.2	Elkins and Carter, 1993
Derailment Coefficient	Single wheel lateral to vertical force ratio	Y / Q	0.8 (average value on 2m)	UIC 518 art. 10.1.1.1
Derailment Coefficient	Wheelset lateral to vertical force ratio (axle)	Y / Q	0.8	Ma and Zhu, 1998
Derailment Coefficient	Bogie-side lateral to vertical force ratio (all wheels on one side of a bogie)	Y / Q	0.6	Elkins and Carter, 1993

Figure 156. Derailment Coefficient - Limits

4.3.7 SUMMARY OF RESULTS AND DISCUSSIONS

The results from parametric studies have shown that:

- The dynamic behaviour of bridges governs the design for small span and speed higher than 350 km/h.
  The maximum allowable train speed in order to fulfil the vertical deck acceleration criteria is lower than 480 km/h:

This means that the thickness of the slab has to be increased in order to fulfil the vertical deck acceleration criteria.

Figure 157. Maximum speed to check the acceleration limit (HSLM Trains)

- The passengers comfort does not govern the design of the bridges for small span bridges

az (m/s²)	**Open frame 10 m**	**Open frame 15 m**	**Closed frame 5 m**	**Closed frame 10 m**
Without irregularities	0.009	0.015	0.005	0.008
Limit	1	1	1	1

Figure 158. Vertical acceleration in passenger car

- Track irregularities create:
  - No increase of vertical deck acceleration
  - Large increase of vertical passenger acceleration

az (m/s²)	Open frame 10 m	Open frame 15 m	Closed frame 5 m	Closed frame 10 m
Without irregularities	0.009	0.015	0.005	0.008
With irregularities	0.1	0.1	0.1	0.1
Ratio: With irregularities/Without irregularities	11	7	20	13

Figure 159.Comparison Vertical Acceleration in Barycenter of Passenger cars with or without irregularities ϕ''

- Moderate increase of transverse passenger acceleration

- ay (m/s²)	Open frame 10 m	Open frame 15 m	Closed frame 5 m	Closed frame 10 m
Without irregularities	0.012	0.025	0.015	0.008
With irregularities	0.028	0.035	0.030	0.011
Ratio: With irregularities/Without irregularities	2.33	1.4	2	1.37

Figure 160. Comparison Transverse Acceleration in Barycenter of Passenger cars with and without irregularities

5. Ways of reducing acceleration levels

5.1 Effect of axle load spreading

In dynamic analyses of railway bridges, the train axle loads are often modeled as moving point forces. However, one effect of the ballast is to spread these point forces. This can lead to large reductions of the bridge response, especially for short span bridges. For this reason, Eurocode suggests to distribute the axle loads over three adjacent sleepers. In the work presented here, the axle load distribution is first studied using a plane finite element analysis and based on that, a triangular load distribution is proposed. Then, numerical simulations are performed to compare the effect of this load distribution with the Eurocode one. The work focuses on simply supported bridges with span lengths less than 10m. This work has also recently been presented in a journal paper where more information can be found [47].

5.1.1 Introduction

An alternative to a full train-track-bridge modelling is to use moving loads model [39] where the axle loads of the train are modelled as concentrated, moving forces of constant magnitudes. In this approach, the dynamic effect of the mass of the train (i.e. the train-track interaction) is not considered and the bridge is often modelled using 2D beams. The main effect of the track-bridge interaction is to spread the axle loads through the rails, sleepers and ballast. This effect can be easily introduced in the FE model by replacing the concentrated axle force with several point forces.

This issue has been studied in [40] and two approaches to model the load distribution are prescribed by the Eurocode [41]: in the first model, each axle load is represented by three point forces, with 50% of the axle load acting on the sleeper located underneath the axle and 25% on the two adjacent sleepers. In the second model, the three point forces are further distributed through the sleepers and the ballast with a height to width ratio of 4:1. However, it seems that the effect of these distributions on the dynamic response of bridges has not been studied carefully. For example, only the first model, using three point forces, was considered in [42,43]. A different approach was studied in [44,45]: each axle load is uniformly distributed over a length varying from 1m to 3m. But this distribution is not realistic. In [46], the load distribution is only considered at the abutment's vicinity.

In this study, a 2D static analysis of the track system if performed and based on that a more realistic load distribution than the ones prescribed in the Eurocode is proposed. Then, the accelerations obtained using this new triangular load distribution is compared to the ones obtained using the Eurocode load distributions. For each case, the load distributions are modelled as a number of point loads. Simply supported bridges with short spans ($L \leq 10$ m) are considered. These bridges present often difficulties to pass the requirements on vertical bridge deck acceleration. For simply supported bridges, the maximal accelerations are due to the resonant response caused by the passage of regularly spaced axle loads at a frequency coinciding with one of the natural frequencies of the structure.

5.1.2 FE Analysis of the load distribution through the ballast

The 2D finite element model of the track system is shown in Figure 161. The rails were modelled with Timoshenko beam elements and the sleepers and the ballast were modelled with plane stress isoparametric eight node elements using a 2x2 Gauss integration. Symmetry conditions were applied on the right vertical edge and the vertical translations are fixed at the interface between the ballast and the bridge (bottom horizontal edge). The ballast material was considered as linear elastic and the connection between the sleepers and the ballast were modelled with non-linear zero thickness joint elements which only transfer compression loads. Two ballast depths were studied: 0.40 m, which is the lowest acceptable ballast depth in Sweden, and 0.65 m, which is the average ballast height for several bridges in Sweden. Three values for the Young's modulus of the ballast were tested: 100, 200 and 350 MPa.

The stress distributions obtained at the interface between the ballast and the bridge superstructure are depicted in Figure 162 and Figure 163. In Figure 162 the stress distribution proposed by Eurocode is included. This comparison is not performed in Figure 163 since Eurocode considers only the case where the axle load acts on a sleeper. From these figures it can be seen that the value of the ballast stiffness has a small influence on the results, especially with a ballast depth of 0.65 m. It can further be seen that with a ballast depth of 0.65 m, a triangular stress distribution with a base of approximately three meters can be adopted.

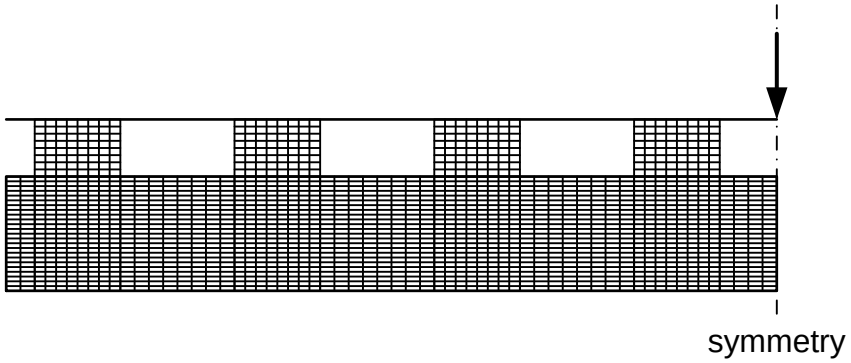

Figure 161. 2D FE Model of the rails, sleepers and ballast.

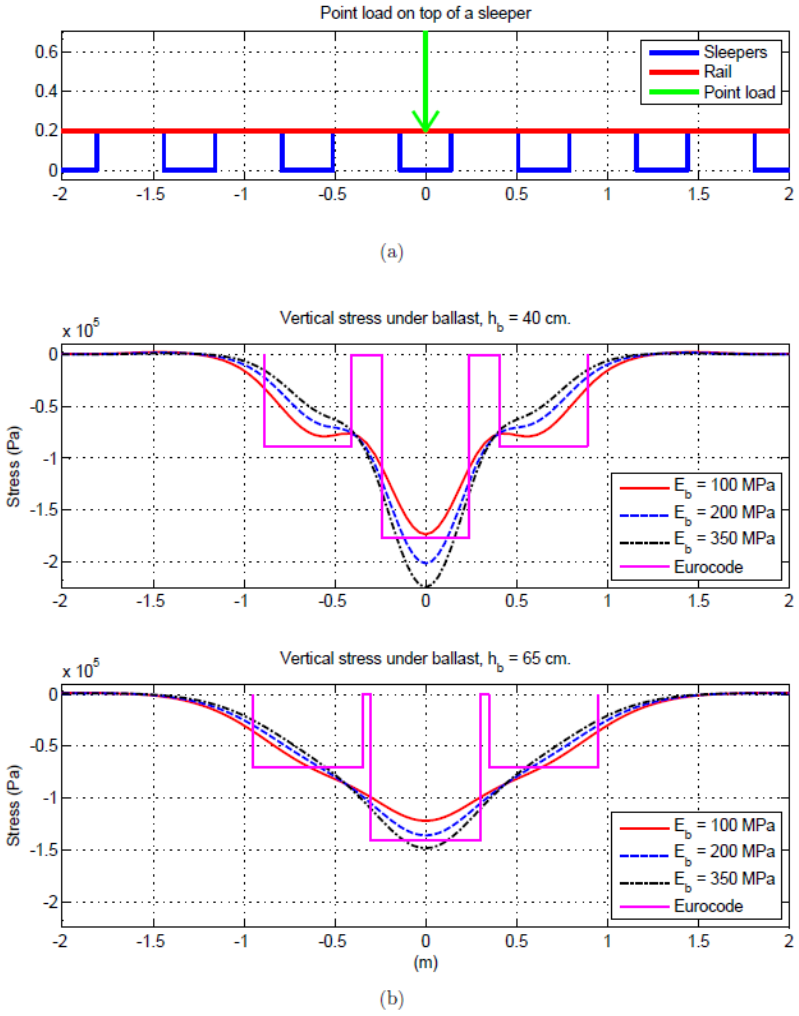

Figure 162. (a) Axle load on sleeper, (b) Stress distribution for different E_b and h_b.

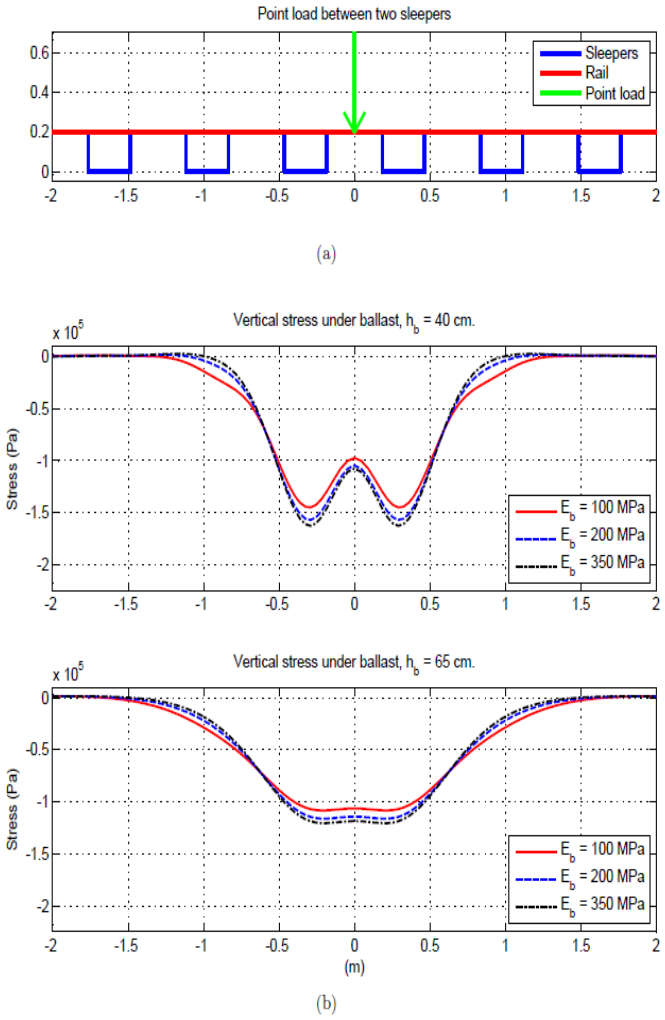

Figure 163. (a) Axle load between sleepers, (b) Stress distribution for different E_b and h_b.

5.1.3 Load distributions

Based on the above results, a triangular load shape with a base length of 3 m is adopted. This load shape provides a reasonable representation of the axle load distribution, especially for a ballast depth of 65 cm. This triangular load shape is modelled by using several point loads, as shown in Figure 164.

The load shapes proposed in Eurocode are also studied, both with and without ballast distribution, see Figure 165. When considering the ballast distribution, the spread through the ballast is performed according to Eurocode with a height to width ratio of 4:1 and by taking several point loads. For the Eurocode load without ballast distribution (*EC3*), the three point loads are acting on adjacent sleepers.

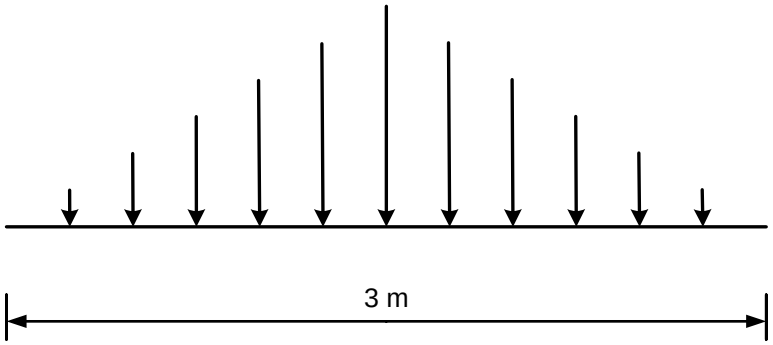

Figure 164. The triangular load shape with 11 point loads (Tri11).

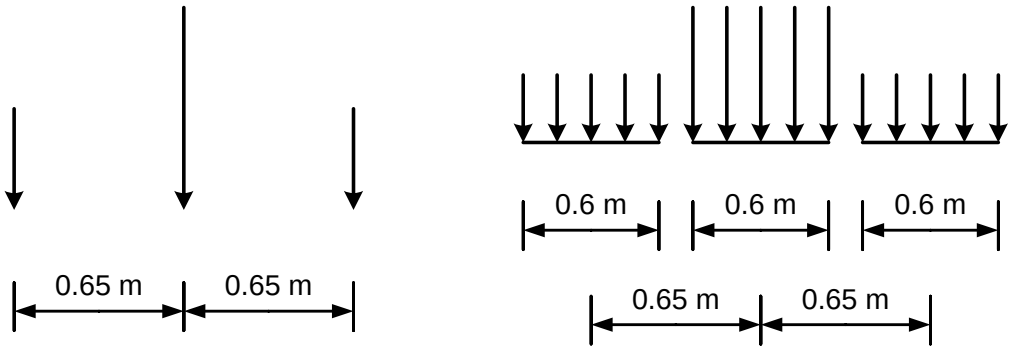

Figure 165. The Eurocode load shape. (a) without ballast distribution modelled as 3 point loads (EC3) acting on 3 adjacent sleepers, (b) with ballast distribution modelled as 15 point loads (EC15).

5.1.4 Bridge properties

Simply supported bridges are included in the study. The properties of the bridge models were determined based on an inventory of Swedish railway bridges carried out by the *Division of Structural Design and Bridges* at *KTH Royal Institute of Technology* [42]. Johansson et al. used a probabilistic method to determine, for each bridge length, realistic intervals for the fundamental frequency and the mass. Hence, for each bridge length, three property sets are tested: in the middle of the intervals (Set 2) and in the lower (Set 1) and higher (Set 3) boundary of the intervals. The Properties of the bridges included in the study are presented in Table 3.

The bridges were modelled with 2D Euler-Bernoulli beam elements. Numerical tests were conducted in order to determine the element length required to obtain converged results for all the bridges. Based on these tests, an element length of 0.05 m has been adopted. A Rayleigh damping, with a damping ratio of 1 % for the first and third modes, were adopted for all the bridges.

Table 3. Mass and fundamental frequency of the simply supported bridges.

	Bridge Length [m]	5	6	7	8	9	10
Set 1	m [kg/m]	5700	6400	7100	7800	8400	9100
	f1 [Hz]	55.3	41.4	32.4	26.3	21.8	18.5
Set 2	m [kg/m]	11100	11700	12400	13100	13800	14500
	f1 [Hz]	37.4	28.1	22.0	17.9	14.5	12.6
Set 3	m [kg/m]	16400	17100	17800	18400	19100	19800
	f1 [Hz]	25.3	19.0	15.0	12.2	10.1	8.6

5.1.5 RESULTS

Simulations of HSLM-A1 train passages were performed on all bridges with speeds varying from 50 to 300 km/h, with a step of 1 km/h. The objective was to obtain the maximum bridge acceleration for each train passage. The load models presented above were applied to each axle of the train. As prescribed by the Eurocode, modal superposition was adopted by considering the three lowest bending modes. For each mode, the average acceleration method was used, with a very small time step of 0.00005 s in order to ensure convergence for all the cases.

The maximum vertical accelerations of the 18 simply supported bridges included in the study have been calculated. For the Eurocode load with ballast distribution, it has been observed that, except for the last bridge with the highest fundamental frequencies, load models with 9 point loads (*EC9*), 15 points loads (*EC15*) and 60 point loads (*EC60*) give almost the same results and that with 60 point loads convergence is obtained for all the bridges. For the triangular load with ballast distribution, it has been observed that, except for the last bridge with the highest fundamental frequencies, load models with 11 point loads (*Tri11*), 17 points loads (*Tri17*) and 51 point loads (*Tri51*) give almost the same results and that with 51 point loads convergence is obtained for all the bridges.

A comparison between the results obtained with EC3 (Eurocode without ballast distribution) EC60 and Tri51 is shown in Figure 166. It can be seen that the triangular load distribution gives the lowest maximum accelerations for all bridges and that *EC3* load gives the highest maximum accelerations for all the bridges. Furthermore, for some bridges the choice of load distribution is vital for whether the acceleration criterion is fulfilled or not. An example of such a bridge is shown in Figure 167.

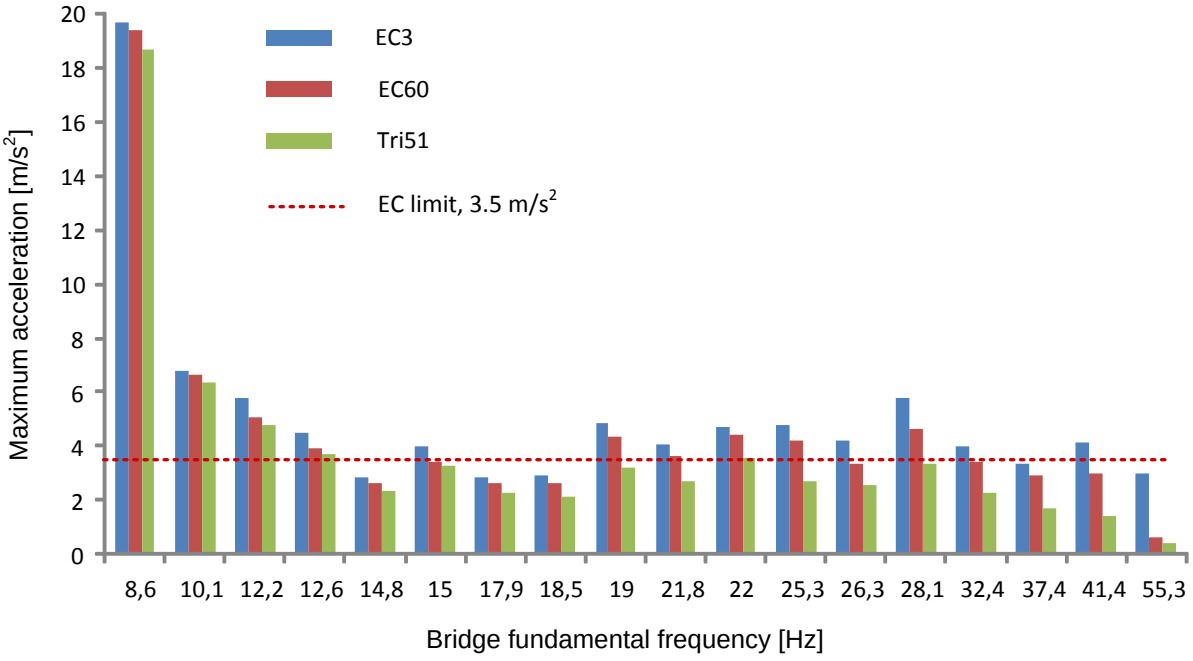

Figure 166. Maximum vertical accelerations for the 18 simply supported bridges using Eurocode and triangular distributions.

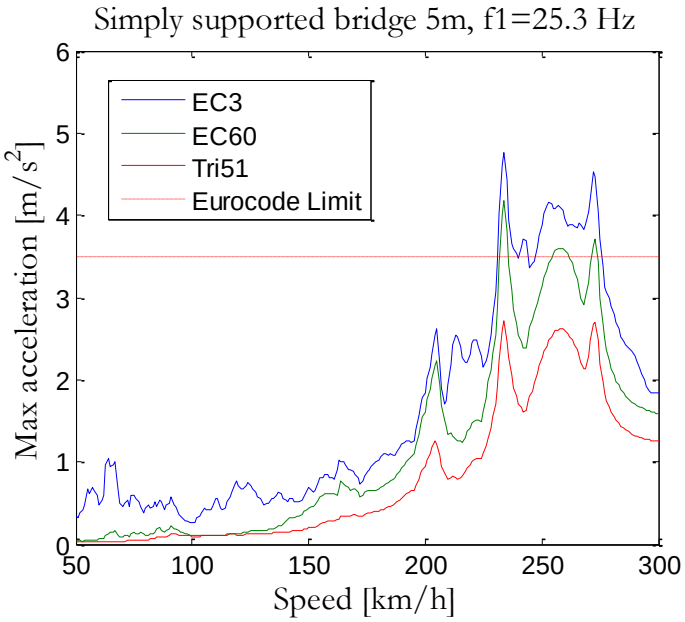

Figure 167. Bridge acceleration-train speed graph for bridge number 12.

5.1.6 Discussion and concluding remarks

The following conclusions can be made from the above study:

- Ballast distribution is important for short span simply supported bridges (especially the ones with high fundamental frequency). The accelerations in these bridges are reduced significantly when ballast distribution is considered.
- The ballast distribution can be easily introduced in FEM analyses by replacing each point force corresponding to an axle load by a number of point forces. However, in that case, spurious acceleration peaks can be obtained and to avoid that the number of point forces must be large enough.
- Two ballast load distribution shapes should be envisaged: the Eurocode one and the triangular one. The triangular one is more realistic, especially with a ballast height of 0.65 m, and gives lower accelerations in the bridges than the Eurocode one.

5.2 Soil-Structure-Interaction (SSI)

Despite of considerable research about the influence of soil-structure interaction (SSI) on seismic response of bridges (see Sextos 2014 [48] for a summary), little studies have been published about the effect of SSI on the train-induced vibration of railway bridges. Recent numerical investigations [49-52] have shown that the modal damping ratios of short-span railway bridges are much higher than the recommended design values (1.5%-2.5%) [53], due to the substantial energy dissipation at the boundaries. Hence, neglecting the effect of the soil-structure interaction in the train-induced vibration analysis of short span bridges may lead to conservative and unrealistic results at resonance regime.

The most straightforward approach to model dynamic soil-structure interaction analysis is to numerically model the entire structure-foundation-soil system [54] using commercially available finite element software. However, due to expensive computational costs related to the FE modelling of unbounded soil medium, alternative method involve kinematic and inertial decoupling of structure and soil medium has been developed, see Figure 168. In this method, the foundation-soil system is replaced by the impedance (dynamic stiffness) functions which have been derived for different foundation types (surface, embedded, piled), and subsoils condition (uniform or layered half-space, stratum over rock) by pioneers in the field of soil dynamic [55-62].

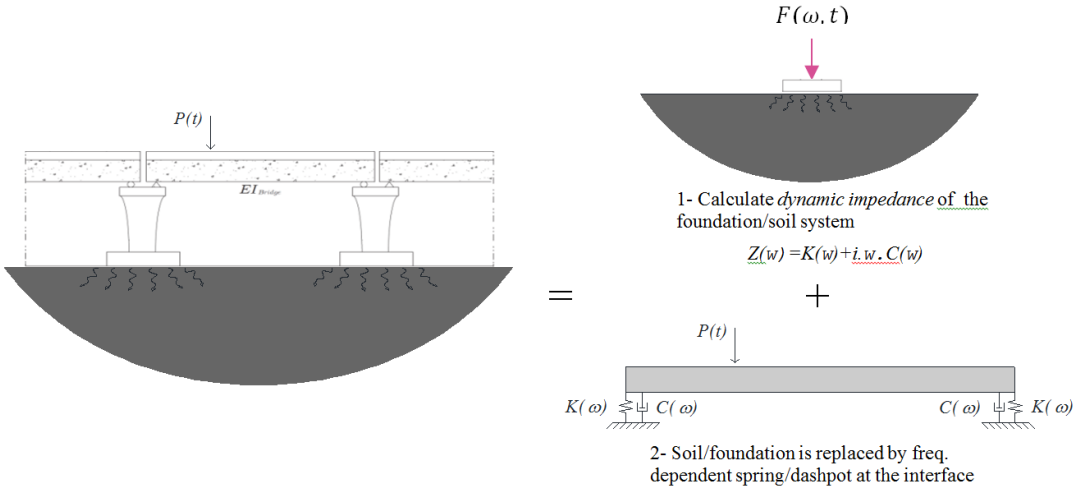

Figure 168. Principal of substructuring method for inertial soil-structure interaction analysis.

5.2.1 Beam Bridges

Based on the research studies on the effect of soil–structure interaction analyses of railway bridges [49-51, 63], two general conclusions can be drawn for short-span simply supported beam bridges: (1) elastic deformation in the soil lowers the fundamental natural frequency and consequently the resonance speed, and (2) geometric damping in the soil, also known as radiation damping, reduces the amplitude of the vibrations at resonance. Figure 169(a) & (b) illustrate the fundamental frequency shortening (Ratio between the natural frequencies of system considering SSI and a fixed-fixed system) and additional modal damping ratio (Due to radiation of waves) of a beam bridge considering SSI. As it can be seen the fundamental frequency shortening and radiation damping ratio are considerable for a short-span (stiff) beam supported by a soft foundation. Both parameters decrease with decreasing structure/soil relative stiffness.

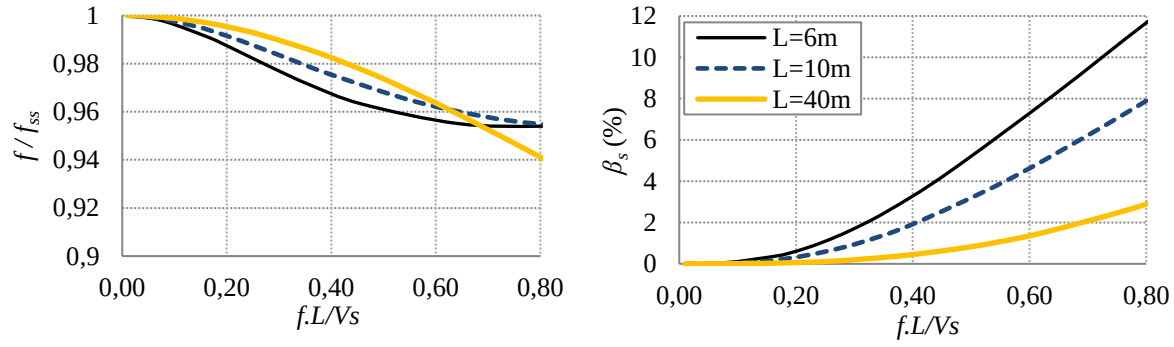

(a) (b)

Figure 169. (a) Frequency shortening ratio, (b) Modal damping ratio due to radiation at boundaries; for simply supported beam bridges.

5.2.2 PORTAL FRAME BRIDGE

The effect of surrounding soil on the dynamic response of short-span portal frame (integral) bridges is more pronounced (providing additional stiffness, mass and damping). There are no detailed recommendations in the Eurocode [53] on how to account for this and the behaviour at very high speeds are not readily known. The numerical studies show that the dissipative capacity of the backfill could lead to an increase in the global damping of the system and consequently reduce the amplitude of resonant response of bridges [65]. The presence of backfill soil may provide an additional stiffness to the system which leads to an increase in the fundamental natural frequency and consequently shifts the critical resonant speed to a higher value.

The effect of the surrounding soil conditions on the vertical dynamic response of a portal frame bridge is investigated both numerically and experimentally at KTH [52]. In this study, a controlled vibration test has been performed on a full-scale portal frame bridge to determine the modal properties of the bridge-soil system by using a hydraulic bridge exciter [66]. The hydraulic exciter was developed by KTH within the IP2-In2Track European project. The significant features of the bridge, surrounding soil and arrangement of the exciter and accelerometers are shown in Figure 170. A simplified FE model which involves the inertial decoupling of the structure and surrounding soil was used for FE model calibration based on the measured data, see Figure 171. Finally, the calibrated FE model was used to highlight the influence of SSI on the dynamic response of the bridge.

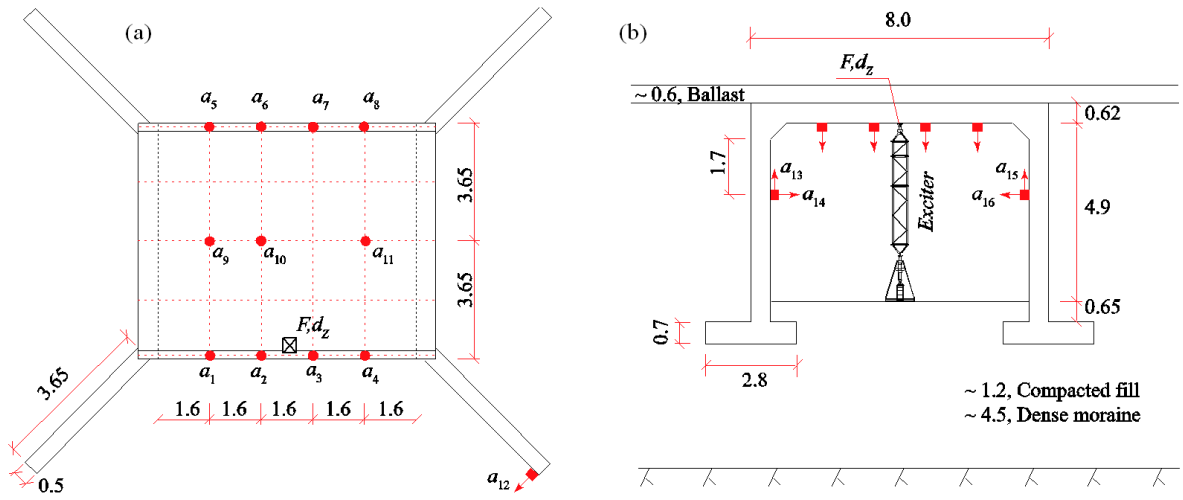

Figure 170. Geometry and instrumentation (a) Plan (b) Elevation. All units in m.

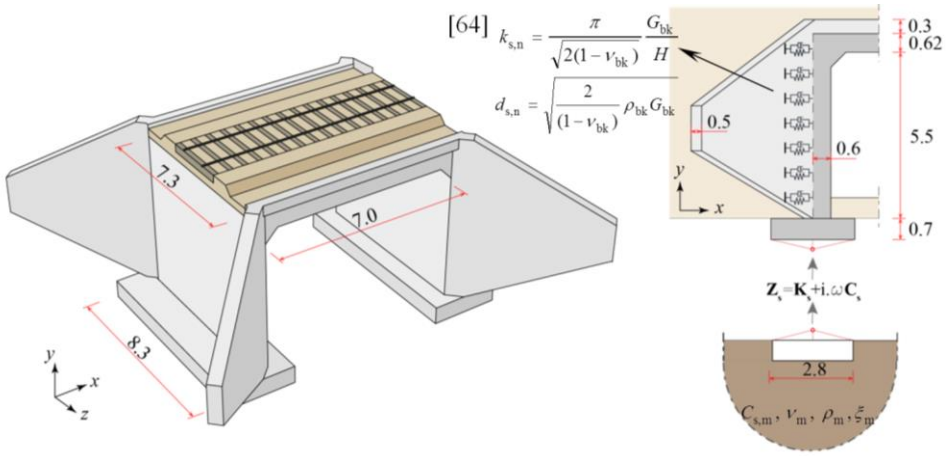

Figure 171. Configuration of the FE model & boundary conditions.

In order to identify the influence of the surrounding soil on the dynamic response of a portal frame bridge, a comparison is performed between estimated modal properties and train-induced resonance response of the system for the following cases: (1) calibrated model, (2) calibrated model without SSI. The estimated modal properties are presented in Table 4. The envelope of calculated maximum acceleration due to passage of HSLM trains is shown in the Figure 172.

Table 4. Natural frequencies and damping ratios for different cases.

			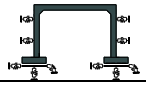		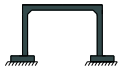	
	Test		Case 1 (Calibrated)		Case 2 (No SSI)	
Mode	f (Hz)	ξ (%)	f (Hz)	ξ (%)	f (Hz)	ξ (%)
1st bending	29.8	16.4	29.2	13.9	26.5	2.6

The experimental results show that the vertical bending of the deck involved substantial horizontal movement of the sidewalls. Hence, the presence of the backfill soil leads to an increase in the natural frequency and damping ratio of the longitudinal bending modes as it can be seen in the Table 4. The comparison between case 1 and case 2 reveals that neglecting the effect of SSI in the train-induced vibration analysis of this type of bridges might be significantly conservative. The damping ratio of the fundamental vertical bending mode in the calibrated FE model is almost 5 times higher than the model without SSI which can lead to considerably lower resonant amplitudes, see Figure 172. Moreover, the presence of backfill soil leads to 10% higher natural frequency of the fundamental mode which consequently shifts the critical resonant speed to a higher value.

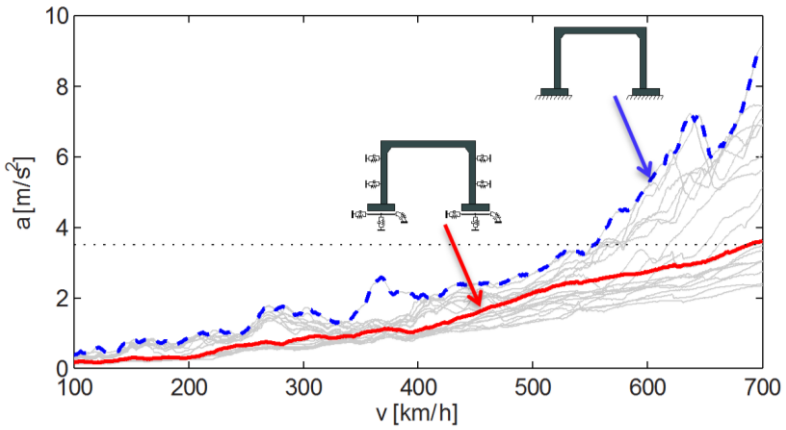

Figure 172. Calculated maximum acceleration at bridge's mid-span; Envelope of all HSLM trains.

5.3 DAMPING DEVICES

Increasing the damping can be an interesting solution in order to decrease the vibrations level, without increasing too much the quantities of construction materials, and then the bridge cost. Various damping strategies are available, such as tuned mass dampers, fluid viscous dampers and visco-elastic dampers, which proved efficient in recent practical critical cases (pedestrian lightweight bridges submitted to dense pedestrian crowds).

In cases where the deck vertical acceleration exceed the limits given by the codes, use of tuned mass dampers (TMD) is possible to reduce the acceleration. A tuned mass damper (TMD) is a mass connected to the structure through a spring and a damper.

A judicious choice of the added mass, as well as its own frequency and damping, makes possible to reduce the peak value of the dynamic impact coefficient (dynamic deflection/static deflection).

In the book published by BACHMANN H., WEBER B *Tuned vibration absorbers for « lively » structures,* graphs are given allowing the choice of the value m_t / m_h, as a function of the desired dynamic coefficient impact and of the damping coefficient of the structure.

In which:

- m_t is the mass of the considered mode of the structure
- m_h is the mass of the TMD

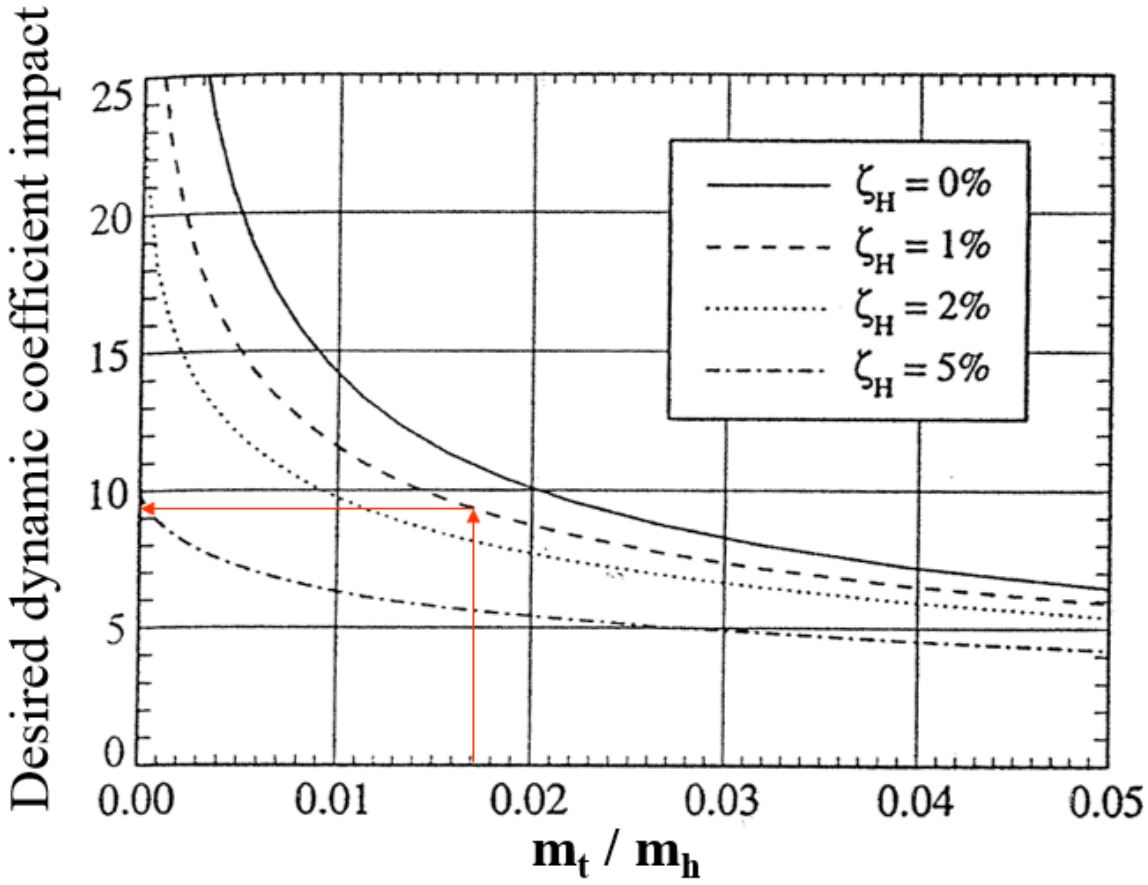

Figure 173. Desired Dynamic coefficient Impact

For the open and closed frames that have been studied by Systra in section 4.3, Systra tried to size a TMD using the graphs given above. However, they realized that for this kind of structures the abacus is not applicable as the desired dynamic coefficient impact does not exceed five.

The mass of the TMD must be determined in another way, as by testing different masses.

5.3.1 Fluid viscous dampers (FVD)

A type of damper that has attracted attention recently is the fluid viscous damper (FVD). The advantages of FVDs are, mainly, the robustness and reliability of the passive damping system. Several studies [67-71] have focused on structural mitigation of high-speed railway bridges using FVDs connected between the load-carrying beam and an auxiliary beam. The results from the studies show that the dynamic response could be substantially reduced using this retrofit method.

The scope of this section includes investigations concerning the influence of a fluid viscous damper retrofit on the dynamic response of a simply supported steel-concrete composite girder bridge. Mainly, the aim is to reduce the maximum vertical acceleration of the bridge deck and investigate the effect

of changing different parameters connected to the FVDs, without using any auxiliary beam system. An extended version of the presented results is found in [72].

MODELLING FRAMEWORK AND NUMERICAL PROCEDURE

To find the dynamic response of the bridge prior to and after installation of the FVDs, the finite element method is applied. Additionally, the bridge is modelled as a 2D Euler-Bernoulli beam subjected to moving point loads with dashpot elements corresponding to the FVDs. Moreover, the FVDs are installed to the bridge deck and connected rigidly to the fixed abutments, resulting in an inclination of the dampers which is shown in Figure 174. The eccentricity from the neutral axis of the bridge to the connection points of the FVDs and the supports are modelled as rigid links. By solving the equation of motion at each time step using numerical direct integration (Newmark's average acceleration method), the maximum vertical bridge deck acceleration is obtained for all train speeds.

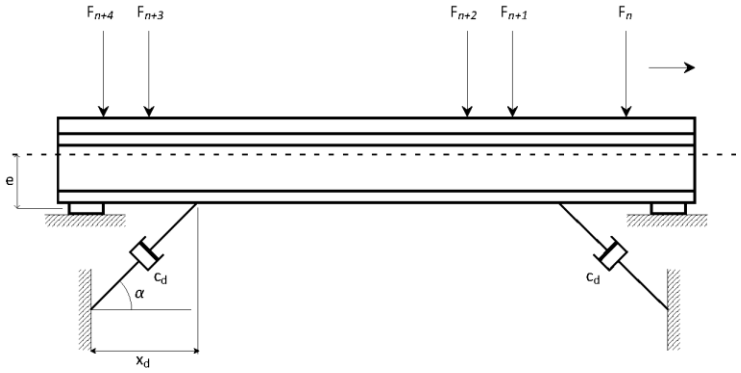

Figure 174. A visualisation of the beam-damper model, in which c_d is the damping coefficient, α is the damper inclination, x_d is the distance from the support to the damper connection, e is the eccentricity from the neutral axis to the damper connection and F_n is the load from the *n*th train axle.

Further, the influence of some parameters on the efficiency of the dampers is investigated. The damper inclination α, the distance from the supports to the connection point of the dampers x_d and the damping coefficient c_d are varied simultaneously, in order to evaluate how the maximum vertical bridge deck acceleration is affected.

5.3.2 CASE STUDY

The presented model is applied to an existing bridge that has shown to be problematic from a dynamical point of view, even for speeds below the design value. The concerned bridge is the Banafjäl Bridge, which is located along the Bothnia Line in Sweden. Table 3 shows the properties of the ballasted, single-track Banafjäl Bridge, where E is the modulus of elasticity, I is the second area moment of inertia, m is the mass per unit length, L is the span length, e is the eccentricity and ξ is the damping ratio of the bridge, respectively.

Table 5. Properties of the Banafjäl Bridge.

E (GPa)	I (m^4)	m (kg/m)	L (m)	e (m)	ξ (%)
200	40	18400	42	2.2	0.5

In the analyses, the bridge is subjected to the high-speed load models (HSLM) A1-A10 that are given in [73].

5.3.3 Results

In order to perform the simulations, the critical HSLM train must be determined. Figure 175 shows the maximum vertical deck acceleration of the Banafjäl Bridge subjected to the HSLM-A1-HSLM-A10 trains travelling at speeds ranging from 100 km/h to 300 km/h. The FVD parameters are chosen as $\alpha = \pi/4$ radians, $x_d/L = 0.024$ and $c_d = 1.8$ MNs/m, since this is one combination that reduces the deck acceleration below the requirement for all HSLM trains. The solid and dashed lines correspond to the acceleration level of the bridge prior to the installation of the FVDs and after the FVD retrofit, respectively. As seen in the figure, the HSLM-A4 is the most critical train model for both cases. Hence, the subsequent results are based on simulations with the HSLM-A4 train.

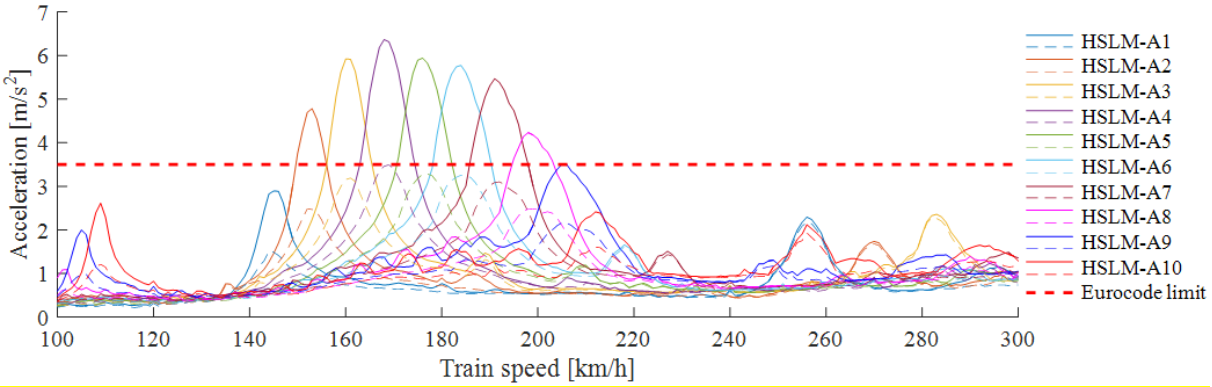

Figure 175. The acceleration envelope of all HSLM trains within the relevant train speed range prior to (solid lines) and after installation (dashed lines) of fluid viscous dampers with $c_d = 1.8$ MNs/m, $x_d/L = 0.024$ and $\alpha = \pi/4$ radians.

Figure 176 shows the combinations of x_d/L, α and c_d that are necessary for reducing the acceleration level in the Banafjäl Bridge below the requirement for ballasted tracks (3.5 m/s^2) [73]. Naturally, the required damping coefficient increases as x_d/L decreases. However, for dampers located close to the supports, c_d is reduced for smaller values of α. Conversely, for larger values of x_d/L, optimal damping is obtained for increased inclinations of the dampers. This is due to the eccentricity, which increases the rotation of the beam cross-section with decreasing distance to the supports.

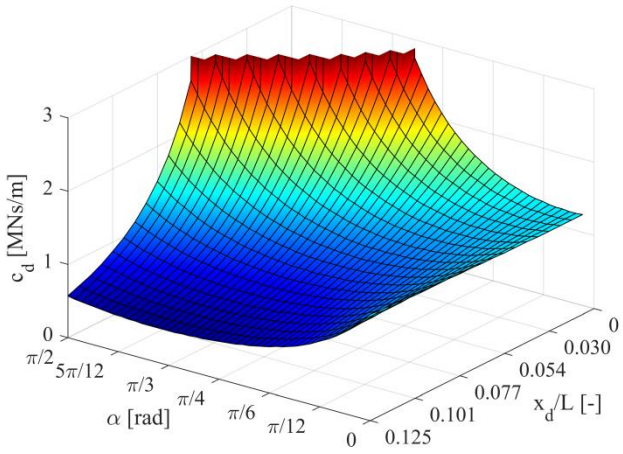

Figure 176. The required damping coefficient c_d for reducing the maximum vertical deck acceleration below 3.5 m/s^2 for different values of the damper inclination α and ratio x_d/L of the distance from the supports to the damper connections x_d and the span length of the bridge L.

5.3.4 Discussion and concluding remarks

From the presented results, it can be concluded that the acceleration of the bridge deck is substantially reduced after the FVD retrofit. From Figure 175, it is clear that it is possible to reduce the acceleration level of the bridge deck below Eurocode limit for ballasted tracks (3.5 m/s^2).

The damping coefficient c_d, damper inclination α and distance from the supports to the damper connections x_d have an impact on the dynamic behaviour at resonance. Figure 176 shows that the required damping coefficient increases with increasing damper inclination and decreasing distance between the supports and damper connections.

For further reading within this subject, please refer to [74].

6. Verification by full scale test

6.1 General

Experimental data serve as valuable input in understanding the real structural manner of action of the bridges and for updating or revising the proposed structural models. The main characteristics to be determined consist of natural frequencies, mode shapes and damping ratios. See section 3.2 for few case studies. In the following chapter, a comprehensive test performed, within the Capacity4Rail project work package WP1.2 subtask T.1.2.3, on a frame bridge in Spain is presented.

6.2 Test on Viaduct PI024

The following section present results from the bridge PI024. The bridge is designed as a portal frame bridge and is located on the high-speed line between Madrid and Barcelona, km 072+068 (40°38'40"N 3°4'53"W).

Ineco, Cedex and Adif performed full-scale tests in November 2015. The instrumentation consisted of accelerometers, strain gauges and displacement transducers. The response from passing trains was measured. The data has partially been analysed and compared with numerical models by Munõz (2016) [75]. See also Appendix A for more information.

In this section, the response from recorded passages is analysed, with speeds ranging from about 200 to 360 km/h. The analysis consists of:

- determine modal parameters (f, ζ, ϕ) based on free vibrations,

- propose a 3D FE-model based on a model updating algorithm,

- compare the measured response from passing trains with the FE-model,

- use the FE-model to predict maximum acceleration based on Eurocode regulations,

- draw conclusions on the dynamic structural manner of action.

6.2.1 The Bridge

A photo of the bridge is shown in Figure 177. The span length is 8.0 m and the width 14.2 m, carrying two ballasted railway tracks. The drawings are presented in Figure 178, Figure 179and Figure 180.

The bridge deck and walls consist of pre-fabricated elements, Figure 181. The walls are 2.4 m wide and the deck elements 1.2 m wide. The upper surface of the deck is casted in-situ, forming a casted joint at the connection with the wall, see Figure 181c. The total deck thickness is 0.95 m (of which 0.4 m is pre-casted). A similar bridge during construction is shown in Figure 182.

FIGURE 177. Photo of the bridge PI024, during passage of a CAF Alvia S-120 train.

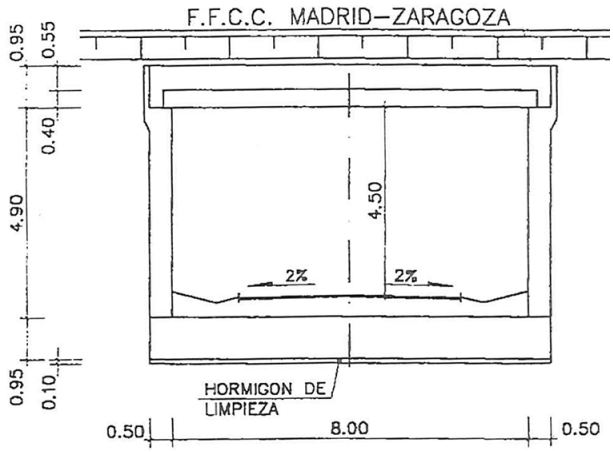

Figure 178. Bridge PI024, cross-section B-B along the bridge.

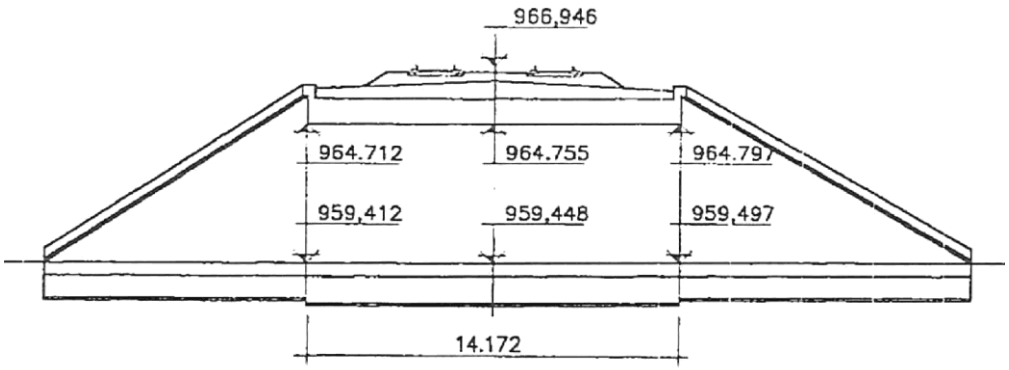

Figure 179. Bridge PI024, cross-section A-A across the bridge.

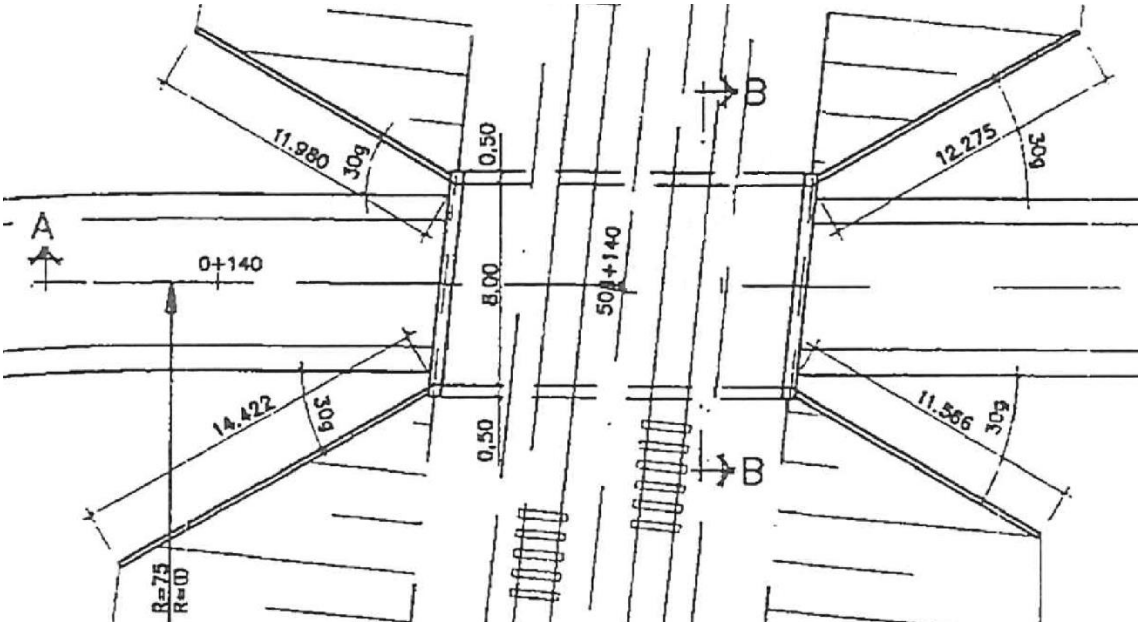

Figure 180. Bridge PI024, plan.

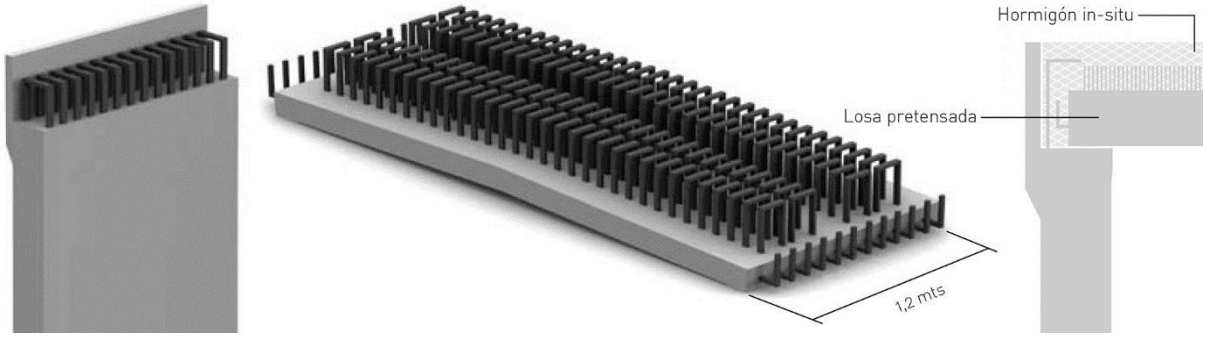

a) b) c)

Figure 181. Details of the pre-fabricated bridge elements, a) upper part of the wall, b) the deck, c) the wall-to-deck connection, Forte (2010).

Figure 182. View of a similar bridge during construction, Forte (2010).

6.2.2 INSTRUMENTATION

The instrumentation by INECO is shown in Figure 183. The following sensors were installed:

- P01-P04, vertical deck displacement at the deck soffit.
- A01-A03, A11-A15, A21-A23, vertical deck acceleration at the deck soffit.
- AT1, AT2, vertical acceleration on the sleepers.
- G11-G13, G22, strain gauges at the bridge soffit.
- GC1, GC2, GF1, GF2, strain gauges at the rail foot.

The sensors P01-P04 consisted of extensometers at the ground level, connected to the deck soffit by a wire in tension. All sensors were collected using a sample rate of 2000 Hz.

The recorded train passages is presented in Table 6. Train passages denoted TP01 – TP04 was performed with a dedicated Talgo Avril train at very high speeds. Train passages denoted TC01 – TC12 was performed under regular traffic at regular speed. The train speed and train characteristics were determined using the strain gauges on the rail.

The Talgo Avril train is shown in Figure 184. The train consists of motor cars in each end and 12 intermediate wagons with a shared single axle configuration, in total 21 axles. The axle load is 17 ton/axle. The Talgo S103 train is shown in Figure 185, with the highest axle load of 15.5 ton/axle and a total of 32 axles.

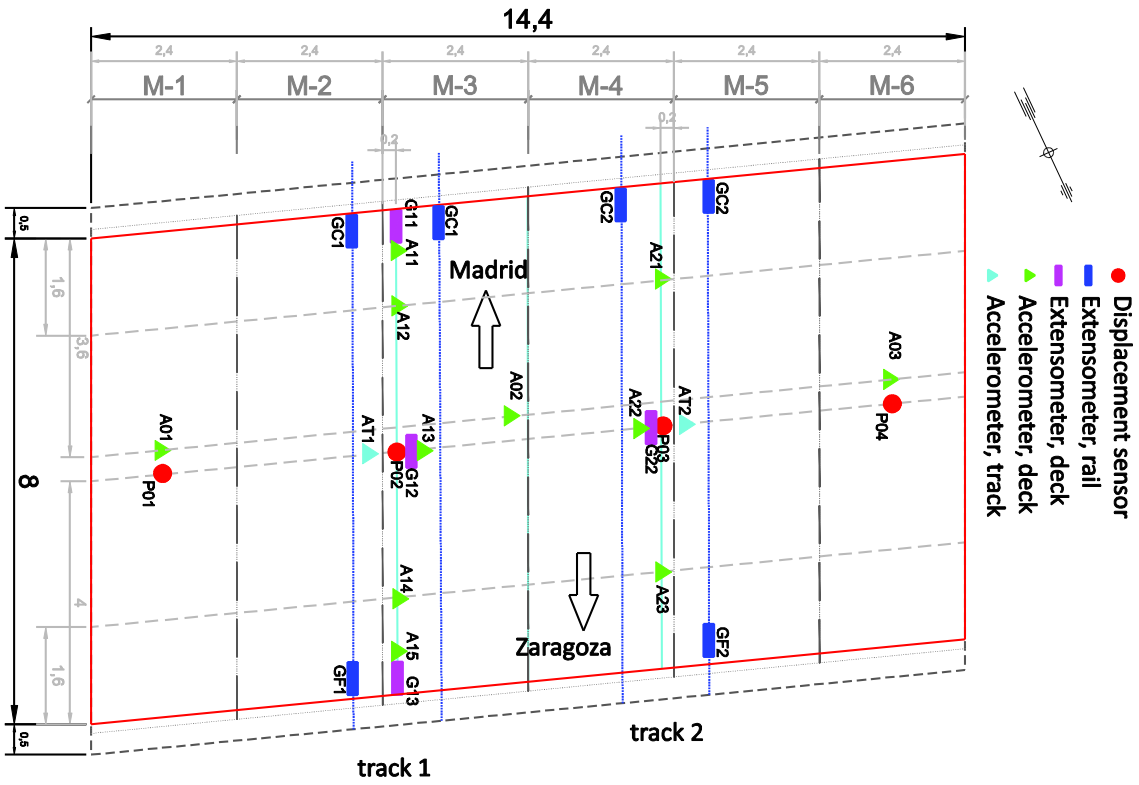

Figure 183. Instrumentation, Ineco (2015).

Table 6. Measured train passages and peak deck acceleration (A01 – A23) and deck displacement (P01 – P04), LP-filtered at 40 Hz.

File	Train	Direction	v (km/h)	track	amax (m/s2)	dmax (mm)
TP01	Talgo Avril	Madrid - Barcelona	317	1	0.98	0.19
TP02	Talgo Avril	Barcelona - Madrid	358	1	1.49	0.18
TP03	Talgo Avril	Madrid - Barcelona	313	2	0.81	0.20
TP04	Talgo Avril	Barcelona - Madrid	317	2	0.82	0.20
TC01	Velaro S103	Madrid - Barcelona	277	1	0.79	0.17
TC02	Velaro S103	Madrid - Barcelona	252	1	0.42	0.19
TC03	Velaro S103	Barcelona - Madrid	198	2	0.41	0.18
TC04	Velaro S103	Madrid - Barcelona	252	1	0.47	0.22
TC05	unknown	Barcelona - Madrid	-	2	1.11	0.35
TC06	Velaro S103	Madrid - Barcelona	218	1	0.36	0.21
TC07	unknown	Madrid - Barcelona	-	1	0.34	0.32
TC08	unknown	Barcelona - Madrid	-	2	0.55	0.38
TC09	Velaro S103	Madrid - Barcelona	288	1	0.71	0.24
TC10	Talgo S102	Barcelona - Madrid	241	2	0.82	0.23
TC11	Velaro S103	Barcelona - Madrid	272	2	0.74	0.15
TC12	Velaro S103	Madrid - Barcelona	288	1	0.76	0.19

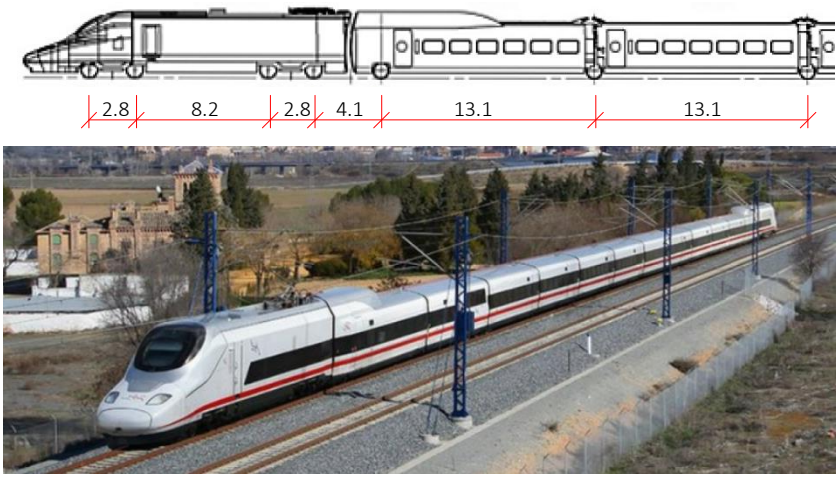

Figure 184. The Talgo Avril train.

Figure 185. The Siemens Velaro S103 train.

6.2.3 Experimental Results

Figure 186 and Figure 187 present the recorded time response from TP01, passing on track 1 at a speed of 317 km/h. The largest vertical deck displacement is less than 0.2 mm and about 0.05 mm under the adjacent track. The largest displacement is caused by the motor wagons, due to the axle distance in the bogie. The largest deck acceleration at A13 is about 0.7 m/s2, caused by a transient from the motor wagon. The corresponding acceleration due to the intermediate wagons is about 0.3 m/s2. The last axle leaves the bridge after 4.7 s and a free decay of less than 1 s is visible.

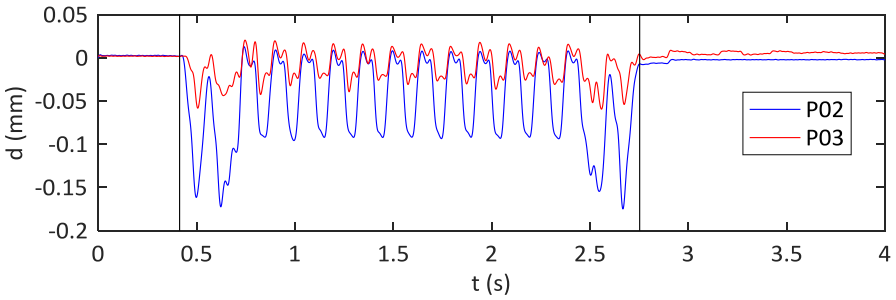

Figure 186. Vertical displacement of the bridge deck, train 1.

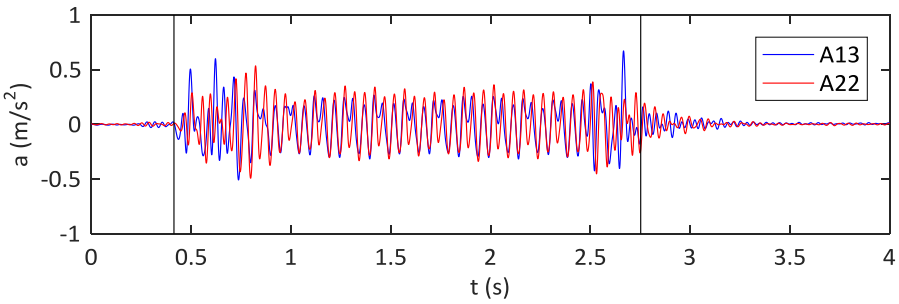

Figure 187. Vertical acceleration of the bridge deck, train 1, 30 Hz LP-filter.

An energy frequency spectrum of sensor A13 is presented in Figure 188, using Welch method with 30% windows size and no overlap. The signal is separated in forced vibration during train passage and the

following free vibrations. To enable a comparison in the same plot, each signal is normalized to unity. The estimated frequencies are presented in Table 7**Erreur ! Source du renvoi introuvable.**. The first 4 natural frequencies of the bridge are clearly visible.

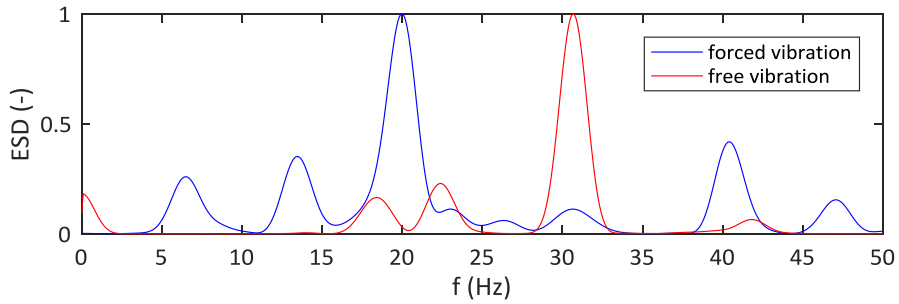

Figure 188. Normalized energy spectrum using Welch method, for the forced and free vibration of sensor A13.

Table 7.Estimated frequencies from the energy spectrum in Figure 188.

(Hz)	f_1	f_2	f_3	f_4	f_5
free vibration	18.5	22.4	30.7	41.8	-
forced vibration	6.5	13.5	20.0	26.2	30.6
f_F	6.6	13.2	19.8	26.5	30.9

The forced vibration frequency f_F is given by Equation **(6.1)**, where v is the train speed and λ the axle distance. The speed of train 1 was 317 km/h, corresponding to v = 88 m/s. The first four forced vibration frequencies are given as multiples of the coach axle distance as 88/13.1 = 6.7 Hz, the fifth frequency is given by the bogie distance as 88/2.8 = 31 Hz.

$$f_F = v/\lambda\,,\quad \lambda = d/i\,,\quad i = 1,2,3,\ldots \tag{6.1}$$

In Figure 189, estimated of the first four eigenmodes of the bridge deck is presented. The circles denote sensor positions and the surfaces are obtained by cubic interpolation of the acceleration response. Each mode is isolated by band-pass filtering of the free vibration response.

The damping ratio is estimated using the logarithmic decrement of the free vibrations after the train passage. In addition to band-pass filtering, the modes are further separated by facilitating the phase angle between different sensors. Mode 1 and 3 are symmetric and the signal A = A1+A3 is used. Mode 2 is antisymmetric and the signal A = A1-A3 is used. Finally, A = A3+A13 was found to give reliable results for mode 4. The results are summarised in Table 8, comprising all four train passages. The results are generally consistent between the train passages, indicating higher damping for the first mode and second mode compared to the third and fourth. As comparison, following EN 1991-2 would result in a damping ration of 2.3%.

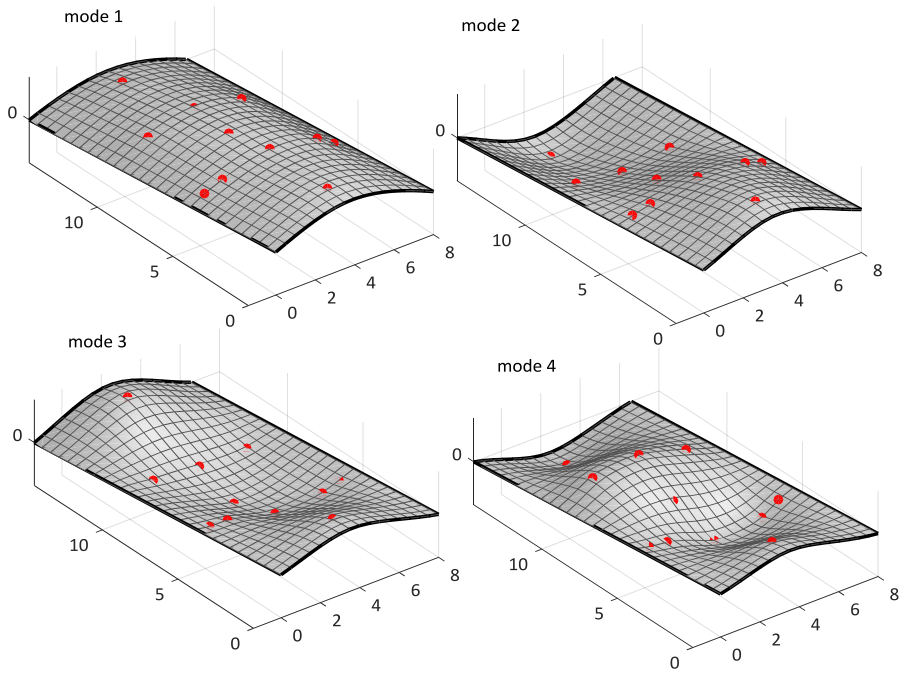

Figure 189. The first four eigenmodes, based on free vibrations from train TP01.

Table 8. Estimated natural frequencies and damping ratios, based on free vibrations.

	f_1 (Hz)	ζ_1 (%)	f_2 (Hz)	ζ_2 (%)	f_3 (Hz)	ζ_3 (%)	f_4 (Hz)	ζ_4 (%)
TP01	18.2	4.9	22.7	4.3	31.0	2.3	42.1	2.2
TP02	18.4	5.3	23.2	3.4	30.7	2.3	41.3	2.1
TP03	18.6	5.1	23.2	4.2	30.6	2.8	41.2	2.3
TP04	18.6	4.1	22.7	2.0	30.6	2.1	41.3	2.3

6.2.4 Numerical Results

The bridge deck is modelled with 9-nodes shell elements. The span length is 8.5 m, the width 14.4 m, the skewness 1.4 m and thickness 0.95 m. the connection with the support walls is modelled with vertical and rotational springs, denoted K_v and K_r. The deck is assumed to have an evenly distributed mass, estimated to $\rho_c = 4000$ kg/m^3 including the concrete deck, ballast and track. The reference value for the concrete Young's modulus is $E_c = 35$ GPa. The bridge deck is initially assumed isotropic, but due to the prefabricated elements a better fit is found when assuming orthotropic behaviour with a significantly lower stiffness E_{c2} in the transverse direction. The Poisson's ratio is assumed $v = 0.2$. The model is updated to fit the first four eigenfrequencies estimated from the experiments, taken as the average from Table 9. The Pattern-Search optimization algorithm in Matlab is used with the objective function in Equation **(6.2)**.

$$f_{obj} = \sum \left(1 - \frac{f_{FEM}}{f_{exp}}\right)^2 \tag{6.2}$$

A total of four different models are studied as listed below. The resulting mode shapes are similar in all four models. The result from model 4 is shown in Figure 190. The optimal parameters from the different models are summarized in Table 9.

- Model 1, isotropic material, simply supported, updating E_c and ρ_c.
- Model 2, orthotropic material, simply supported, updating E_c E_{c2} and ρ_c.
- Model 3, orthotropic material, flexible supports, updating E_c E_{c2}, ρ_c.and K_v.
- Model 4, orthotropic material, flexible supports, updating E_c E_{c2}, ρ_c, K_v. and K_r.

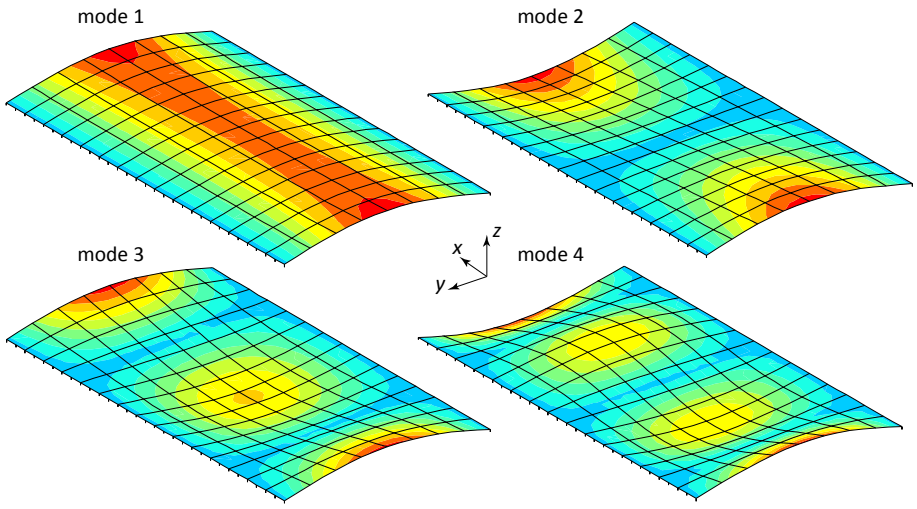

Figure 190. The first four eigenmodes, updated 3D-model, f1 = 18.6 Hz, f2 = 22.6 Hz, f3 = 31.3Hz, f4 = 41.3 Hz.

Table 9. Results from model updating, updated parameters and resulting frequencies.

model:	E_c (GPa)	E_{c2} (GPa)	ρ_c (kg/m^3)	K_v (GN/m)	K_r (GNm/rad)	f_1 (Hz)	f_2 (Hz)	f_3 (Hz)	f_4 (Hz)
1	30.8	-	4200	-	-	16.0	19.8	31.0	49.4
2	41.9	3.6	4280	-	-	18.3	22.3	31.3	42.1
3	43.4	3.8	4200	130	-	18.6	22.6	31.3	41.3
4	43.5	3.7	4200	129	0	18.6	22.6	31.3	41.2

Based on the optimal results from model 4, a uni-variable analysis is performed to study the influence of K_v and K_r, Figure 191. The model shows that the supports can be assumed near fully fixed in vertical direction and fully hinged in rotation. The results are however rather ill-conditioned, since a large increase in either parameter would result in a minor change in natural frequencies.

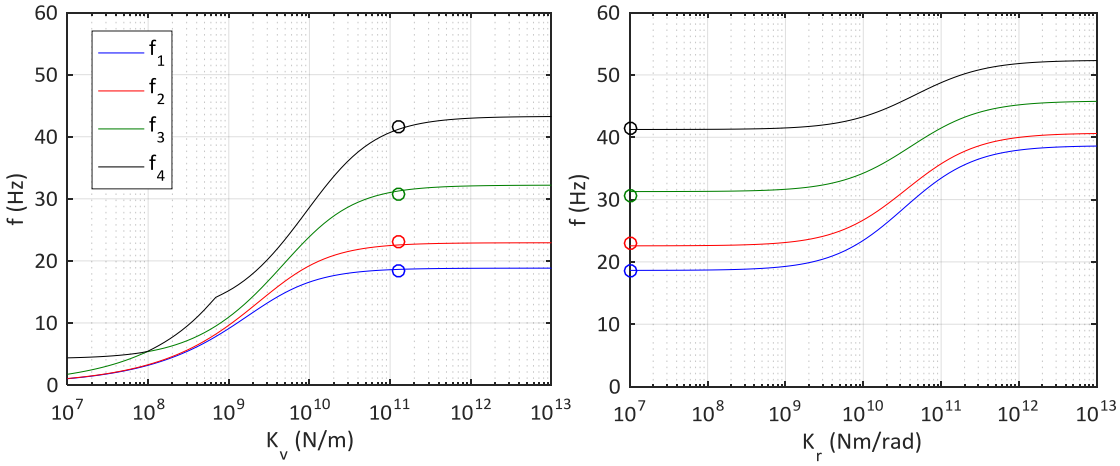

Figure 191. The first four eigenfrequencies as function of the vertical stiffness K_v and rotational stiffness K_r, based on model 4. The circles denote experimental frequencies.

Based on model 4, dynamic simulations of passing trains are performed. The train is modelled with vertical loads on the bridge deck. The load from each axle follows a triangular distribution with length of 2.0 m along the track and a rectangular distribution with a length of 3.0 m across the track. All other interaction with the train and the track is neglected. The analysis is performed using modal superposition of the first four eigenmodes presented in Figure 190 and with the modal damping according to Table 8. The analysis is performed with a sample frequency of 400 Hz.

The time response is compared with train TP01 in Figure 192 and Figure 193. Very good agreement is found for both the deck displacement and deck acceleration.

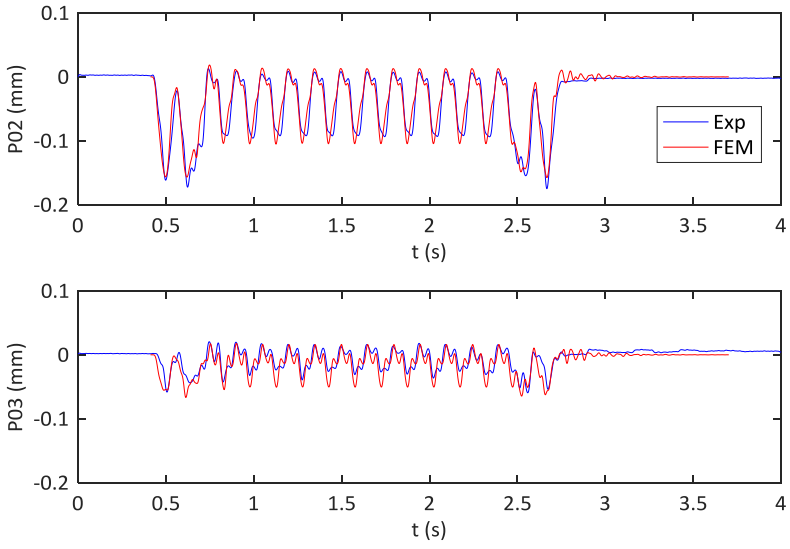

Figure 192. Deck displacement at point P02 and P03, comparison between experiments and FE-results, train TP01.

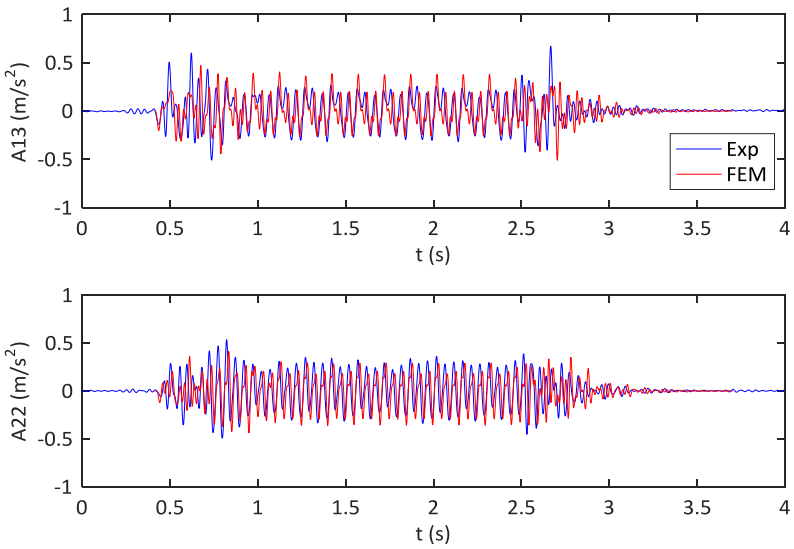

Figure 193. Deck acceleration at point A13 and A22, comparison between experiments and FE-results, train TP01.

The response from the train model HSLM A1-A10 according to EN 1991-2 is compared with similar analysis of the trains Talgo Avril and Siemens S103. For each train passage, the peak deck displacement and peak deck acceleration is calculated. Two different set of simulations are studied; with the modal damping according to Table 8 and with modal damping according to EN 1991-2, corresponding to 2.3% in all modes. The results are presented in Figure 194 and Figure 195, where the shaded areas represent the range between the two cased of damping. For the HSLM results, the envelope of train A1-A10 is presented. The circles correspond to the experimental results, according to Table 6.

The peak deck displacement in Figure 194 does not show any significant risk of resonance. The scatter from the experimental results appears to be larger than the variation in either speed or damping. A more detailed study of the displacement signal from train TC10, corresponding to a Talgo Bombardier S-102 at 241 km/h, revealed that the signal was afflicted with significant disturbance and may therefore be overestimated.

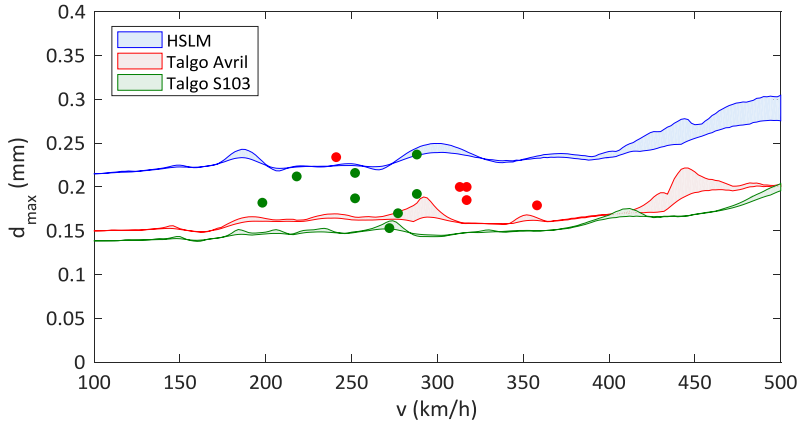

Figure 194. Peak deck displacement as function of the train speed. Shaded areas from FE-results (low/high damping), circles from experiment.

The corresponding peak deck acceleration is presented in Figure 195. All results are well below the design limit of 3.5 m/s^2 according to EN 1990. The simulations show that the response from the Talgo Avril train may be higher than the HSLM train load at some speeds. The experimental results are generally higher than the simulated counterparts, even for the case of low damping. The largest difference is found for train TP02 at the speed of 358 km/h, having a peak acceleration of 1.5 m/s^2 at sensor A01. The corresponding time response is shown in Figure 196.

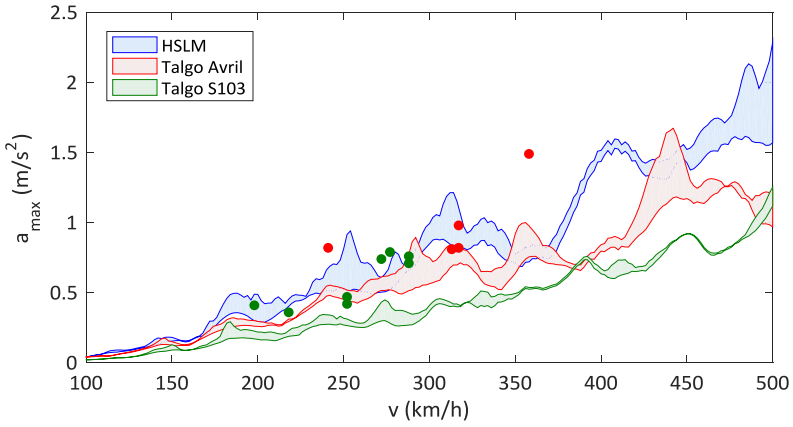

Figure 195. Peak deck acceleration as function of the train speed. Shaded areas from FE-results (low/high damping), circles from experiment.

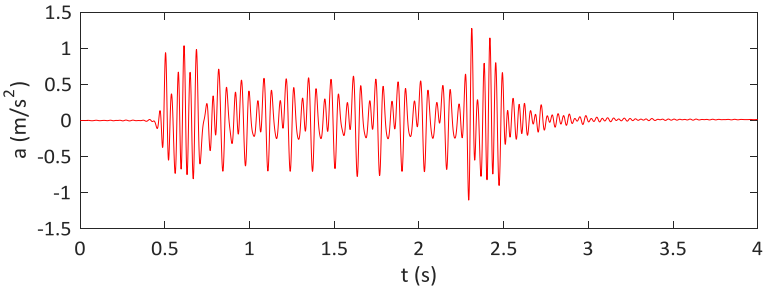

Figure 196. The time response from sensor A01 during train passage TP02.

6.2.5 Discussion and concluding remarks

From the performed analysis of the case study bridge, the following is concluded.

- The experimental from passing trains show a peak deck acceleration of 0.5 – 1.5 m/s^2 and a peak deck displacement of merely 0.2 mm.
- The first four modes can be obtained from the free vibration response, consisting of one bending mode and three plate modes.
- Based on the free vibrations, the modal damping is estimated to 5% for the first mode, 4% for the second mode and about 2.5% for the third and fourth mode.

- A 3D FE-model is updated based on the experimental modal properties. The model proposes that the stiffness in the transverse direction is very low, likely due to the prefabricated elements.
- The simulated response from passing trains is generally in good agreement with the experimental results.

7. Conclusions

In this report, different aspects of railway bridge dynamics have been presented and discussed. The success in predicting the real dynamic response highly depends on the choice of structural model. An increased level of detail may improve the results, but reliable input data for such models are not always available. On the other hand, simplified models may prove sufficient and sometimes with similar accuracy as far more complicated models, provided that the main governing features of the real response can be described.

The dynamic response of railway bridges on high-speed lines is limited by a set of serviceability criteria. Some of these, e.g. the vertical deck acceleration, may sometimes be over conservative. More accurate design limits may result in the use of slender bridges and enabling upgrading of more existing bridges to higher speeds, with a required safety limit.

Increased understanding of the real dynamic manner of action by experimental testing can hopefully result in more accurate predictions of the dynamic response and model updating and hence less need for safety margins in the models.

The main aim of the study presented in this report is to investigate, both numerically and experimentally, the dynamic behaviour and requirements for load bearing structures intended for very high speed trains (i.e. for speeds up to 480 km/h) focusing on common types of railway bridges.

Some of the main conclusions drawn from this study are:

- The analyses on short two-span and three-span beam bridges show that their dynamic behaviour need to be studied carefully in the speed range between high speeds (up to 350 km/h) and very high speeds (up to 480 km/h). Double-track two-span bridges, as well as single-track three-span bridges, may have acceleration levels above or close to the Eurocode acceleration limit 3.5m/s^2 for very high speeds.
- The dynamic analysis on portal frame bridges shows:
    - For closed frame bridges, the lower is the span length, the higher is the resonance risk for high speed. The vertical acceleration at mid span for 5m closed frame bridge is higher than acceleration for 10m closed frame bridge.
    - For open frame bridges, the lower is the span length, the higher is the resonance risk for high speed. The vertical acceleration at mid span for 10m open frame bridge is higher than acceleration for 15m open frame bridge.
    - The results of studied bridges are higher than limit of 3.5 m/s2 for ballasted track or 5 m/s2 for track without ballast. To respect these limitations for speed up to 480 km/h we have redesigned and increased the thickness of the deck.
- The effect of track irregularities was found to compare well with the Eurocode factor (1+0.5 ϕ''), for track irregularities corresponding to EN 13848-6 track quality class A.
- At the presence of track irregularities, significant high-frequency content was observed in the bridge deck acceleration for some of the case study bridges. There is a need for further research on the

behaviour of ballast at different frequencies of vibration in order to give thorough recommendations on the choice of cut-off frequency.

- The results of comfort analysis and track irregularities for portal frame bridges shows:
  - The passengers comfort does not govern the design of the bridges for small span bridges
  - Track irregularities create:
    - No increase of vertical deck acceleration
    - Large increase of vertical passenger acceleration
    - Moderate increase of transverse passenger acceleration.

8. References

[1] Shift2Rail Masterplan 2014.
[2] European Commission, Roadmap to a Single European Transport Area, COM(2011) 144 final.
[3] J. Bién, L. Elfgren, J. Olofsson, SusB. D9.3 (2007).
[4] ERRI, D214/RP8 (1999).
[5] Guo, W., Xia, H., Karoumi, R., Zhang, T., Li, X., Wind and Structures vol. 20. No. 2 (2015).
[6] RTRI, Displacement Limits (2007).
[7] ERRI, D214/RP9 (1999).
[8] Johansson, C., Andersson, A., Wiberg, J., Ülker-Kaustell, M., Pacoste, C., Karoumi, R., TRITA-BKN/R-139-SE (2010).
[9] ERRI, D214/RP6 (1999).
[10] Johansson, C., Pacoste, C., Karoumi, R., Comp.& Struct. 119 (2013).
[11] Johansson, C., Arvidsson, T., Martino, D., Solat Yavari, M., Andersson, A., Pacoste, C., Karoumi, R., TRITA-BKN/R-141-SE (2012).
[12] Johansson, C., Andersson, A., Pacoste, C., Karoumi, R. TRITA-BKN/R-145-SE (2013).
[13] Gazetas, G., J. Geotech. Eng. 117(9) (1991).
[14] Ülker-Kaustell, M., Karoumi, R., Pacoste, R., Eng.Struct 32(2010).
[15] Zangeneh Kamali, A., KTH (2015).
[16] CEN European committee for standardization: "EN 1991-2 Eurocode 1: Actions on structures - Part 2: Traffic loads on bridges", 2003.
[17] T. Arvidsson, TRITA-BKN Bulletin 122, Licentiate Thesis (2014).
[18] ERRI, D214/RP4 (1999).
[19] ERRI, D214/RP2 (1999).
[20] M. Baeßler, J. Bronsert, P. Cuéllar & W. Rücker. Bridge Maintenance, Safety, Management and Life Extension (2014).
[21] Ülker-Kasutell, M., Karoumi, R., J. Rail Transp. 1(4) (2013).
[22] Gonzales, I., Ülker-Kaustell, M., Karoumi, R., Eng.Struct 57 (2013).
[23] Ülker-Kaustell, M., Karoumi, R., Eng.Struct 33 (2011)
[24] García, A. L., TRITA-BKN/EX-320-SE (2011).
[25] Fröidh, O., KTH Railway Group 12-01 (2012).
[26] Andersson, A., Sundquist, H., Karoumi, R., Rydzyna 23-24.04.2012 (2012).
[27] Mellat, P., Andersson, A., Pettersson, L., Karoumi, R., Eng. Struct 69 (2014).
[28] Andersson, A., Ülker-Kaustell, M., Borg, R., Dymén, O., Karoumi, R., EVACES'15 (2015).
[29] Borg, R., Dymén, O., TRITA-BKN/EX-460-SE (2015).
[30] Cantero, D., Arvidsson, T., OBrien, E., Karoumi, R.: "Train–track–bridge modelling and review of parameters" submitted to Structure and Infrastructure Engineering, 2015.
[31] Zhai W, Wang K, Lin J.: "Modelling and experiment of railway ballast vibrations" J Sound Vib. 2004, 270(4–5), 673–683.
[32] Doménech, A., Museros, P., Martínez-Rodrigo, M.D.: "Influence of the vehicle model on the prediction of the maximum bending response of simply-supported bridges under high-speed railway traffic" Engineering Structures, 2014, 72, 123–139.
[33] CEN European committee for standardization: "EN 13848-6 Railway applications - track - track geometry - part 6: characterisation of track geometry quality", 2014.
[34] Guo, WW., Xia, H., De Roeck, G., & Liu, K.: "Integral model for train-track-bridge interaction on the Sesia viaduct: dynamic simulation and critical assessment" Computers and Structures 2012, 112, 205-216.

[35] CEN European Committee for Standardization: “EN 13848-5 Railway applications - Track - Track geometry quality - part 5 - Geometric quality levels - Plain line”, 2010.
[36] CEN European Committee for Standardization: “EN 14363 Railway applications - Testing for the acceptance of running characteristics of railway vehicles - Testing of running behaviour and stationary tests”, 2005.
[37] CEN European Committee for Standardization: “EN 14067-6 Railway Applications - Aerodynamics - Part 6: Requirements and Test Procedures for Cross Wind Assessment”, 2010.
[38] ERRI D214. RP 5 Rail bridges for speeds >200 km/h – numerical investigation of the effect of track irregularities at bridge resonance. Utrecht: European Rail Research Institute, 1999.
[39] Frýba L. Vibration of Solids and Structures under Moving Loads. London: Thomas Telford, 1999.
[40] ERRI D 214/RP 9 Rail bridges for speed > 200km/h. European Rail Research Institute 1999
[41] CEN/TC 250. Eurocode 1: Actions on structures - Part 2: Traffic loads on bridges. EN 1991-2 2002. Brussels: CEN.
[42] Johansson C, Arvidsson T, Martino D, Yavari M S, Andersson A, Pacoste C, Karoumi R. 2011. Höghastighetsprojekt bro – inventering av järnvägsbroar för ökad hastighet på befintliga banor. Stockholm: KTH, Division of Structural Design and Bridges. 2011 (In Swedish)
[43] Goicolea JM, Antolin P. The dynamics of high-speed railway bridges: a review of design issues and new research for lateral dynamics. International Journal of Railway Technology 2012; 1:27-55
[44] UIC Code 776-2. Design requirements for rail-bridges based on interaction phenomena between train, track and bridge, International Union of Railways 2009, 2nd edition
[45] Museros P, Romero ML, Poy A, Alarcón E. Advances in the analysis of short span railway bridges for high-speed lines. Computers and Structures 2002; 80:2121-2132
[46] Martinez-Rodrigo MD, Lavado J, Museros P. Dynamic performance of existing high-speed railway bridges under resonant conditions retrofitted with fluid viscous dampers. Engineering Structures 2010; 32:808-828
[47] Erik A, Annelie S, Mahir Ü.K., Jean-Marc B. Effect of axle load spreading and support stiffness on the dynamic response of short span railway bridges. Structural Engineering International 2014; 24, 4 457-465.
[48] A. Sextos, ICT applications for new generation seismic design, construction and assessment of bridges, Struct. Eng. Int., 24(2), 173–183 (2014).
[49] M. Ülker-Kaustell, R. Karoumi, C. Pacoste, Simplifed analysis of the dynamic soil-structure interaction of a portal frame railway bridge, Engineering structures 32 (11) (2010) 3692-3698.
[50] A. Romero, M. Solís, J. Domínguez, P. Galvín, Soil-structure interaction in resonant railway bridges, Soil Dynamics and Earthquake Engineering 47 (2013) 108-116.
[51] C. Svedholm, C. Pacoste, R. Karoumi, Modal properties of simply supported railway bridges due to soil-sturcture interaction, in: Conference of 5th ECCOMAS Thematic Conference on Computational Methods in Structural Dynamics and Earthquake Engineering, COMPDYN 2015; 25-27 May 2015, 2015 pp. 1709-1719
[52] A. Zangeneh, C. Svedholm, A. Andersson, C. Pacoste, R. Karoumi, Dynamic Stiffness Identification of Portal Frame Bridge–Soil System using Controlled Dynamic Testing, to be presented in Conference of EURODYN 2017;10-13 September 2017, 2017
[53] EN1991-2, Eurocode 1, Actions on Structures. Part2: Traffic loads on Bridges, 2003.
[54] J. P. Wolf, Soil-structure interaction analysis in time domain, Nucl. Eng. Des., 111 (3) (1989), 381–393.

[55] Veletsos, A. S., and Wei, Y. T. (1971). “Lateral and rocking vibrations of footings.” J. Soil Mech. Found. Div., 97(SM9), 1227–1248.
[56] Wong, H. L., and Luco, J. E. (1985). “Tables of impedance functions for square foundations on layered media.” Int. J. Soil Dyn. Earthquake Eng., 4(2), 64–81.
[57] G. Gazetas, Formulas and charts for impdances of surface and embedded foundations, J. of Geo. Eng., 117(9) (1991), p. 1363-1381
[58] Dominguez, J., and Roesset, J. M. (1978). “Dynamic stiffness of rectangular foundations.” Research Rep., R78-20, Massachusetts Institute of Technology, Cambridge, MA.
[59] A. Kaynia, E. Kausel, Dynamic response of pile groups, in: 2nd International conference on numerical method in offshore piling, Austin, TX, 1982, pp. 509-532.
[60] M. Novak, M. Sheta, Dynamic response of piles and pile groups, in: 2nd International conference on numerical method in offshore piling, Austin, TX, 1982
[61] G. Gazetas, K. Fan, A. Kaynia, E. Kausel, Dynamic interaction factors for floating pile groups, Journal of Geotechnical Engineering 117 (10) (1991) 1531-1548
[62] L. Padrón, J. Aznárez, O. Maeso, M. Saitoh, Impedance functions of end-bearing inclined piles, Soil Dynamics and Earthquake Engineeirng 38 (2012) 97-108.
[63] A. Doménech, M.D. Martínez-Rodrigo, A. Romero, P. Galvín, On the basic phenomenon of soil-structure interaction on the free vibration response of beams: Application to railway bridges, Engineering Structures 125 (2016) 254–265.
[64] A. Veletsos, A. Younan, Dynamic soil pressures on vertical walls, in: Proceedings: 3rd Int. Conf. on Recent Advances in Geotechnical Earthquake Engineering and Soil Dynamics, (1995) Volume Ill, St. Louis, Missouri
[65] J. Vega, A. Fraile, E. Alarcon, L. Hermanns, Dynamic response of underpasses for high-speed train lines, Journal of sound and vibration 331 (2012) 5125-5140.
[66] A. Anderson, M. Ülker-Kaustell, R. Borg, O. Dymén, A. Carolin, R. Karoumi, Pilot testing of a hydraulic bridge exciter, in: MATEC Web of Conferences, Vol. 24, EDP Sciences, 2015, p. 02001.
[67] Museros P., & Martínez-Rodrigo M.D. “Vibration Control of Simply Supported Beams under Moving Loads using Fluid Viscous Dampers” Journal of Sound and Vibration 2002; 300(1): 292-315.
[68] Martínez-Rodrigo M.D., Lavado J., & Museros P. “Dynamic Performance of Existing High-speed Railway Bridges under Resonant Conditions Retrofitted with Fluid Viscous Dampers” Engineering Structures 2010; 32(3) 808-828.
[69] Martínez-Rodrigo M.D., & Museros P. “Optimal Design of Passive Viscous Dampers for Controlling the Resonant Response of Orthotropic Plates under High-speed Moving Loads” Journal of Sound and Vibration 2011; 330(7): 1328-1351.
[70] Lavado J., Doménech A., & Martínez-Rodrigo M.D. “Dynamic performance of existing high-speed railway bridges under resonant conditions following a retrofit with fluid viscous dampers supported on clamped auxiliary beams” Engineering Structures 2014; 59: 355-374
[71] Luu M., Martínez-Rodrigo M.D., Zabel V., & Könke C. “H∞ optimization of fluid viscous dampers for reducing vibrations of high-speed railway bridges” Journal of Sound and Vibration 2014;333(9):2421-2442.
[72] Rådeström S., Karoumi R., Ülker-Kaustell M., Tell V., & Andersson A. “Structural control of high-speed railway bridges by means of fluid viscous dampers” 19th IABSE Congress Stockholm: Challenges in Design and Construction of an Innovative and Sustainable Built Environment September 2016.

[73] CEN European committee for standardization: “EN 1991-2 Eurocode 1: Actions on structures - Part 2: Traffic loads on bridges”, 2003.
[74] Rådeström S., Ülker-Kaustell M., Andersson A., Tell V., & Karoumi R. “Application of fluid viscous dampers to mitigate vibrations of high-speed railway bridges” International Journal of Rail Transportation 2016;1-16.
[75] Munõz, J., J. S., 2016. Study of accelerations in short-span bridges on high-speed lines. MSc. Thesis, Technical University of Madrid, UPM (in Spanish).
[76] Forte, 2010. Obra Civil, product catalogue, www.forte.es.
[77] ERRI D 214/RP 4 (December 1999)- Rail Bridges for Speeds> 200 KM/h - European Rail Research Institute 1999
[78] ERRI D 214.2/RP 1 (April 2002)- Use of universal trains for the dynamic design of railway bridges - European Rail Research Institute 1999
[79] ERRI D 214/RP 9 (December 1999)- Rail Bridges for Speeds> 200 KM/h – Final Report - European Rail Research Institute 1999
[80] ERRI D 214/RP 6 (December 1999)- Rail Bridges for Speeds> 200 KM/h – Calculation for bridges with simply-supported beams during the passage of a train. - European Rail Research Institute 1999
[81] M.Olmos, M.A.Astiz. Analysis of the lateral dynamic response of high pier viaducts under high-speed train travel. Engineering Structures 56 (2013) 1384-1401
[82] Mécanique de la voie. SNCF octobre 1981
[83] D.Herron, C.Jones, D.Thompson. Characterising the high-frequency dynamic stiffness of railway ballast. ICSV16, Poland, 5-9 July 2009
[84] W.M.Zhai, K.Y.Wang, J.H.Lin. Modelling and experiment of railway ballast vibrations. Journal of Sound and Vibration 270 (2004) 673-683
[85] Vehicle-bridge interaction dynamics, Y.B. Yang, J.D. Yau, Y.S. Wu, World Scientific, 2004

9. Appendix A

IN-SITU TEST CAMPAIGN

HIGH SPEED LINE MADRID-BARCELONA

PK 72+000

TRAIN PASS-BY MEASUREMENTS

(NOVEMBER - 2015)

CEDEX

Table of contents

Introduction

This document has been prepared in the frame of Task 1.2.3 “Structures dynamical effects due to very high speed” for the European collaborative project CAPACITY4RAIL of the 7th Framework Programme.

The main objective of this in-situ campaign is to obtain real data to verify calculation methods and models to study the dynamical effects in structures due to the pass-by of trains.

In this report an overview of the in-situ test campaign carried out by CEDEX in the High Speed Line Madrid-Barcelona PK 72+200 on 1st and 2nd of November, 2015 is presented. Figure 197 shows a photograph of the test site. In this location, there is a span bridge of 8 m long with its corresponding transition zone of 27 m long as shown in Figure 198.

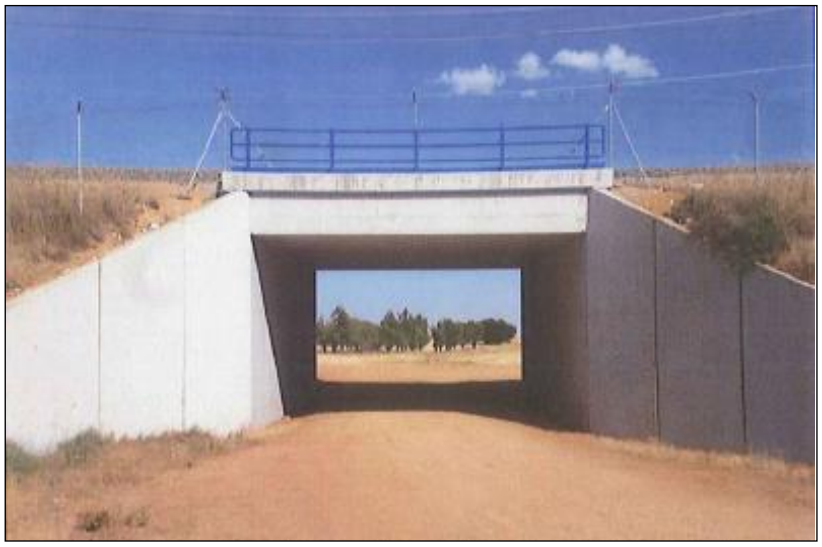

FIGURE 197: PHOTOGRAPH OF THE STRUCTURE SITUATED IN THE TEST SITE

The first and second chapters contain information related with the position of the installed sensors and the recorded trains, respectively. In Chapter 3 there is a description of the protocol used to analyze the signals as well as some examples of the results that can be obtained.

All the raw data recorded in this campaign are collected in the annexed CD for other C4R partners to use them in their tasks.

Besides that, data recorded in this in-situ test campaign can be compared with those acquired by ADIF and can also be used as a source to validate test results obtained in CEDEX Track Box and, finally, could help to calibrate the models proposed by KTH in the frame of Sub-Task 1.2.3.1.

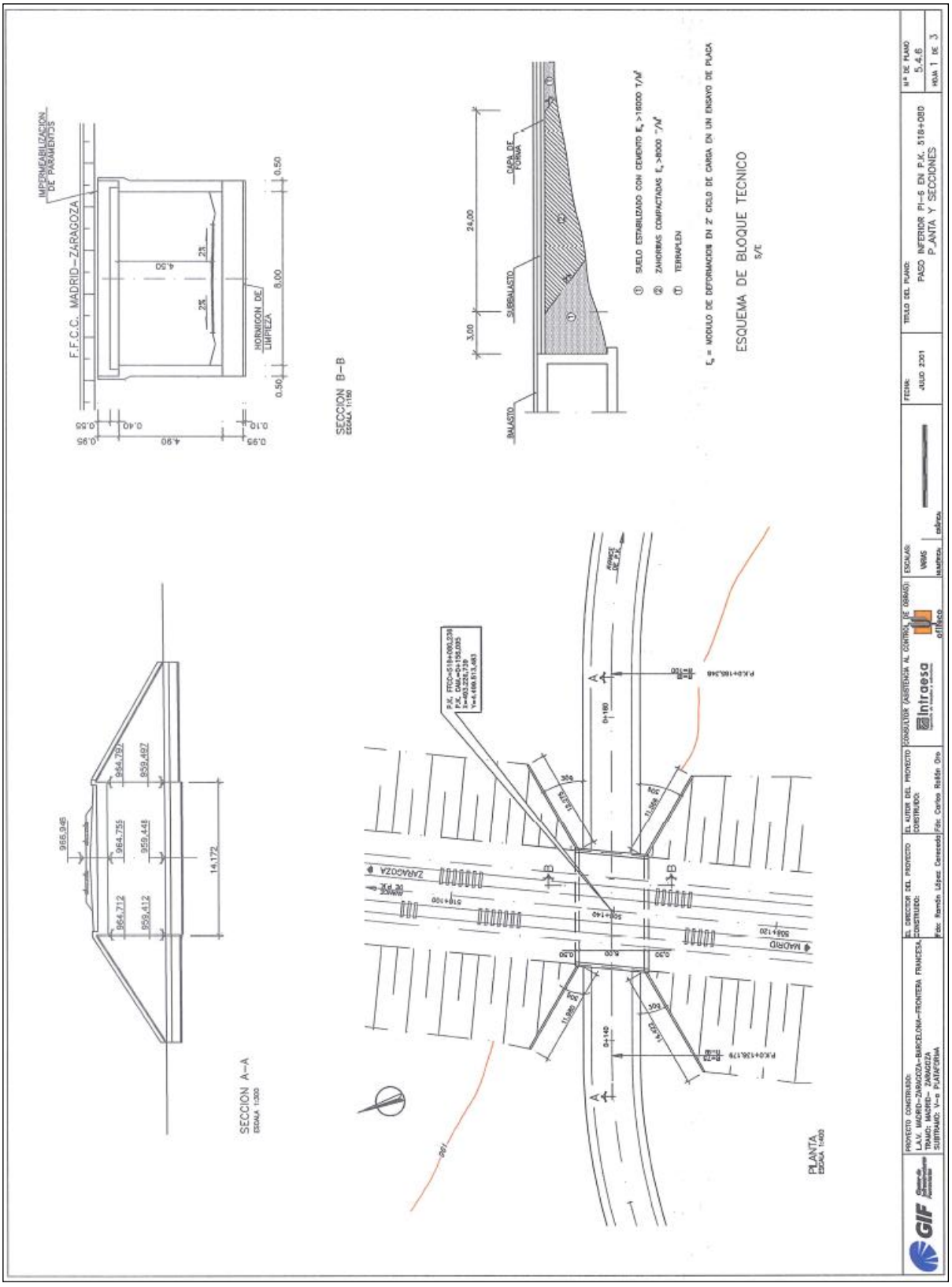

Figure 198: Sketch of the test site, bridge structure and transition zone

Instrumentation

The aim of this field test campaign was to study the transition zone between the structure and the embankment. The position of the installed sensors is presented in Figure 199.

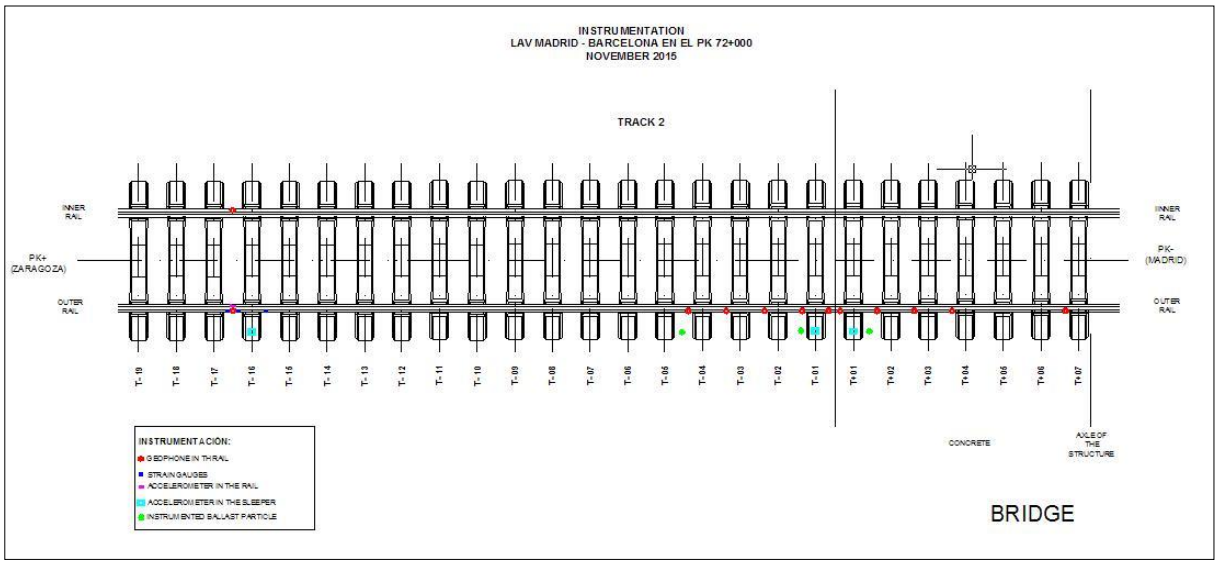

FIGURE 199: SKETCH OF THE INSTRUMENTED SECTION

- Strain gauges are represented by dark-blue squares. The gauges are glued at the level of the neutral fibre of the rail in order to measure only shear strain. Loads are obtained using the pair placed at the span between two sleepers. The pair located at both sides of the sleeper can be used to calculate the reaction of the sleeper.
- 2Hz geophones installed in the rail are marked with red spots. They are used to measure the velocity of the vibration in the rail produced by the trains pass by. To obtain the deflections integrating these velocity signals is also possible.
- Vertical accelerometer stacked in the rail is shown with a fuchsia rectangle.
- Accelerometers stacked in the outer side of the sleeper are represented by light-blue squares.
- Triaxial accelerometers installed inside different ballast particles are presented with green spots.

Figure 200 and Figure 201 are zooms of the left and right side of Figure 199. Figure 200 shows the sensors installed at 10 m from the beginning of the bridge and Figure 201 shows the sleepers involved in the transition zone between the structure and the embankment. In both figures, the configuration of the instrumentation installed can be observed more clearly.

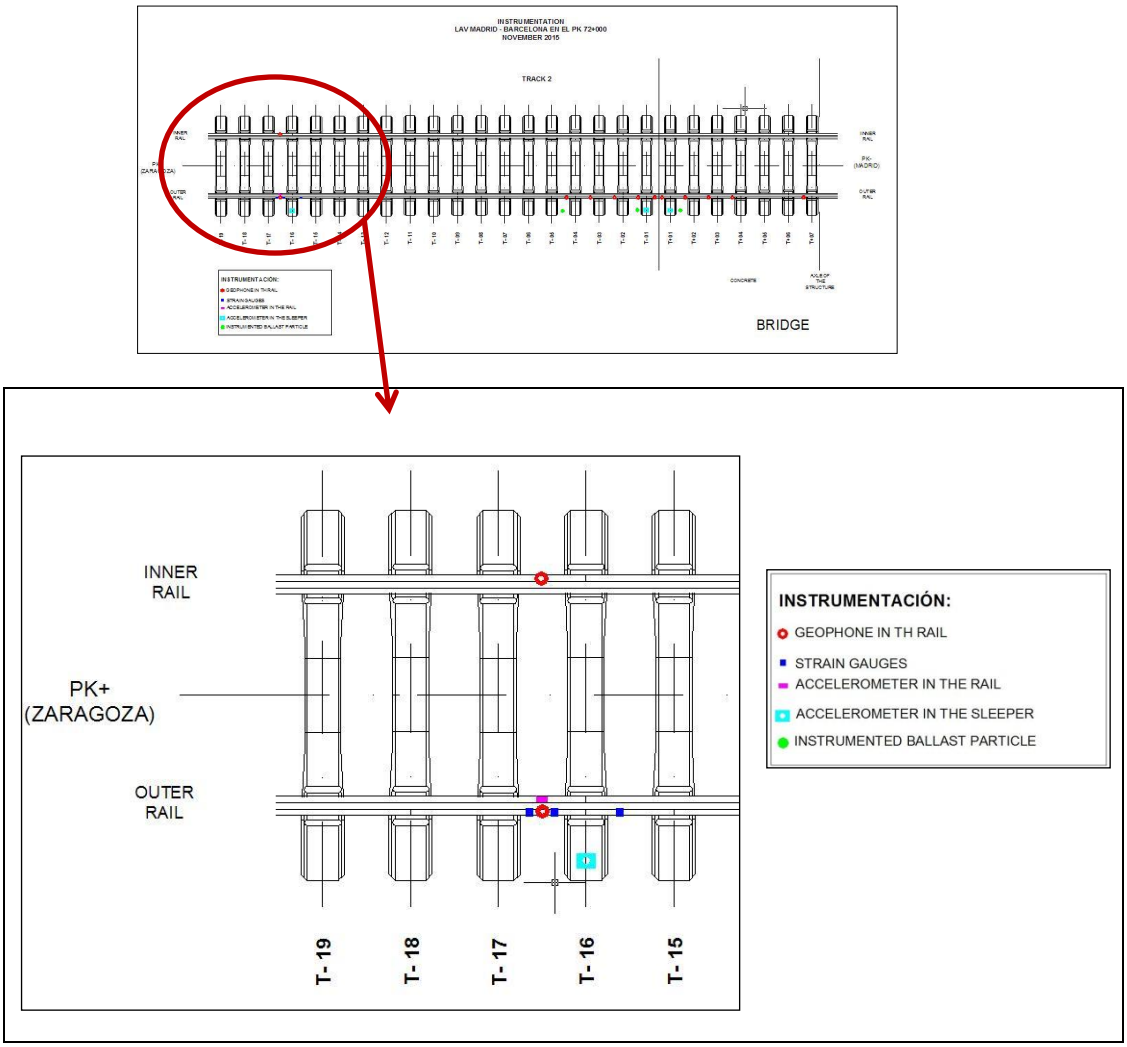

FIGURE 200: SKETCH OF THE INSTRUMENTED SECTION LOCATED AT 10 M FROM THE BRIDGE

Sleepers T-16 and T-17 are placed at the embankment, 10 m far away from the beginning of the bridge which begins between sleepers T+1 and T-1.

The instrumentation installed in this section of the test site consisted on:

- one accelerometer in the sleeper T-16,
- another accelerometer stacked at the rail between T-16 and T-17,
- three strain gauges and two geophones between T-16 and T-17 (in the inner and outer rail). It was decided to measure the loads at that position in order to be a bit far away from the transition zone between the embankment and the bridge, trying to avoid a possible anomalous effect there due to the transition zone.

The deflection of the rail was obtained by the integration of the signal of the geophone placed between the strain gauges what makes it easy to calculate the track stiffness track at that site. This

measurement makes it possible to compare these results with others obtained in other sites studied before. The two geophones were installed, one in each rail, to determine the influence of the small curve existing at that point. The accelerometer in the rail offers redundant information as it is used to confirm the geophone measurements. The accelerometer in sleeper T-16 can be used to compare the accelerations measured in the bridge area.

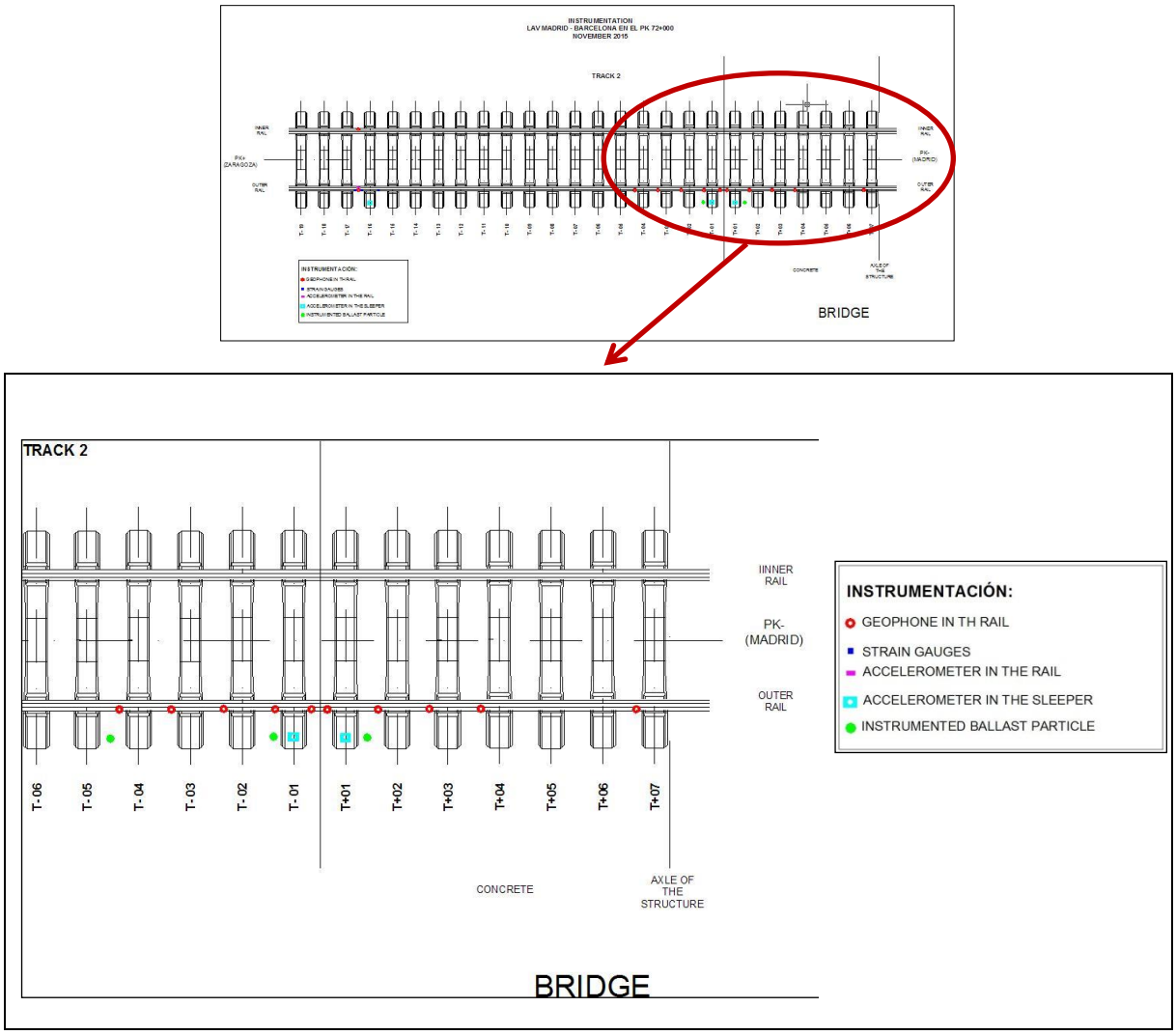

FIGURE 201: SKETCH OF THE INSTRUMENTED SECTION SITUATED IN THE TRANSITION ZONES AND ON THE BRIDGE

This sub-section contains the transition zone and the bridge. The bridge begins between T-1 and T+1, so sleepers at the right side are over the structure. The sleeper T+7 is situated at the central axle of the bridge.

The instrumentation installed consisted on:

- Ten geophones to study the vertical rail velocities and their variation along the transition zone and the bridge.
- Two accelerometers stacked at sleepers T-1 and T+1, and
- Three instrumented ballast particles, buried between two sleepers at a depth of 20 cm below the rail which implies around 5 cm over the sleeper base level.

In the next photographs (Figure 202 to Figure 204) the distribution of the sensor in each sub-section can be observed.

FIGURE 202: PHOTOGRAPH OF THE INSTRUMENTATION IN T-16 AND T-17: SOME STRAIN GAUGES AND A GEOPHONE IN THE RAIL AND ONE ACCELEROMETER, IN THE LEFT SLEEPER

FIGURE 203. PHOTOGRAPH OF THE INSTRUMENTATION BETWEEN T-5 AND T+7. GEOPHONE SPREAD IN THE RAIL CAN BE OBSERVED

FIGURE 204. PHOTOGRAPH OF THE INSTRUMENTED BALLAST PARTICLE PLACED CLOSE TO T-5

Recorded trains

During the test campaign eight trains were recorded:

- during the afternoon, six commercial trains that were currently operating in this track and
- during the night, two passes of a test train (AVRIL) that is able to reach velocities up to 350km/h.

Table 10 compiles information regarding the registered trains:

- The date and time (which is also the name of the file),
- the train type,
- the passing-by direction, and
- the speed.

As it can be observed in Figure 199, all the sensors were installed at Track 2 (trains travelling with direction to Madrid) because it was thought that the test train could reach the highest speed in that track, but unfortunately for different reasons it did not happen. It is important to take into account that the AVRIL test train passed-by in the two different directions as the general track behaviour can

be different when the train passes from the bridge to the embankment than from the embankment to the bridge.

TABLE 10: RECORDED TRAINS

DATE & TIME	TRAIN TYPE	DIRECTION	SPEED (km/h)
01/11/2015_17:20	Siemens S-103	Madrid	295±10
01/11/2015_18:07	S-120	Madrid	240±10
01/11/2015_18:31	Talgo S-102	Madrid	295±10
01/11/2015_18:34	Siemens S-103	Madrid	255±10
01/11/2015_18:46	Siemens S-103	Madrid	290±10
01/11/2015_19:19	Siemens S-103	Madrid	300±10
02/11/2015_02:12	AVRIL	Barcelona	310±10
02/11/2015_03:17	AVRIL	Madrid	310±10

Signal analysis procedure

This chapter describes the way to process the raw data for each kind of sensor. For all the time signal obtained, the first step is to calculate the Fast Fourier Transform (FFT) to visualize the frequency domain and then to decide the filter which must be applied in case it was considered necessary. In general for this kind of studies, the most used filter is the Low Pass Filter (LPF) which cuts off frequencies above the range of interest in each particular case.

TRIAXIAL ACCELEROMETER INSIDE BALLAST PARTICLES

Three instrumented ballast particles were installed inside the ballast layer, buried between two sleepers at a depth of 20 cm below the rail, as it was said in the previous chapter. These stones have a triaxial accelerometer inserted in them as can be seen in Figure 205.The stone has a flat surface that allows the electronical board of the accelerometers placed inside the particle to stay in a horizontal position.

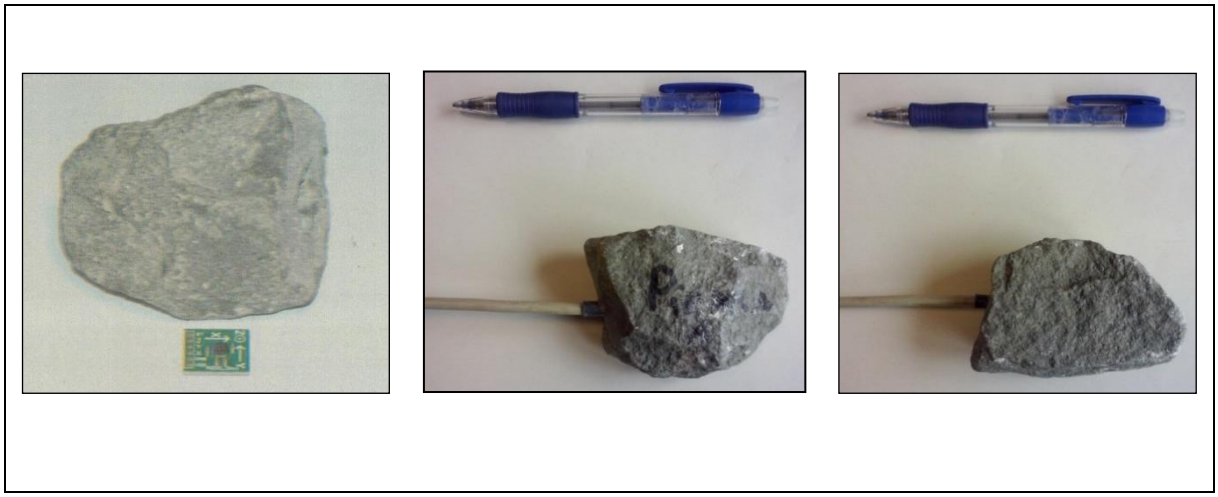

FIGURE 205: PHOTOGRAPHS OF THE TRIAXIAL ACCELEROMETER BEFORE (LEFT) AND AFTER (MIDDLE AND RIGHT) BEING INSTALLED INSIDE THE BALLAST PARTICLE. THE FLAT SURFACE OF THE STONE CAN BE SEEN THE RIGHT PHOTOGRAPH.

To install the ballast particle in the track is necessary to remove previously the ballast until the desired depth. Once it has been done, the ballast particle must be placed very carefully trying to leave the flat surface of the stone in a horizontal plane and to orientate the cable perpendicular to the rail and parallel to the sleeper. With that arrangement, the axes of the accelerometer will be orientated as follows: Z-axis in the vertical direction and X and Y axis orientated parallel and perpendicular to the rail, respectively. With this procedure and if the particle only suffers small displacements from its original position, to analyse the signal comes to be very easy as no correction of rotation is needed.

The following figures show the time signal of the three different components of the acceleration measured in two of the ballast particles when one S-103 train passed at 18:34 (data in the file named as 011115_183453).

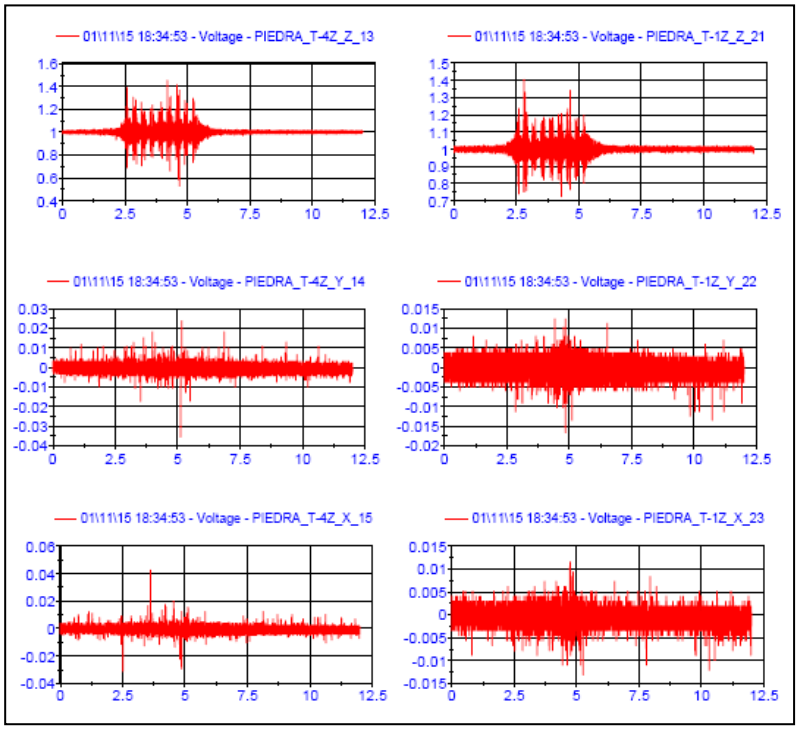

FIGURE 206: COMPONENTS Z, X AND Y OF ACCELERATION MEASURED IN THE BALLAST PARTICLES PLACED AT T-4 (LEFT) AND T-1 (RIGHT)

In Figure 206 it can be observed that the stones installed in T-4 and T-1 have almost all the acceleration in the vertical component while horizontal accelerations are close to zero. This behaviour did not appear in the particle placed at T+1, shown in Figure 207. In that stone, all components have influence in the total acceleration, so a rotation correction is needed. An unexpected presence of high noise in the signals can also be observed.

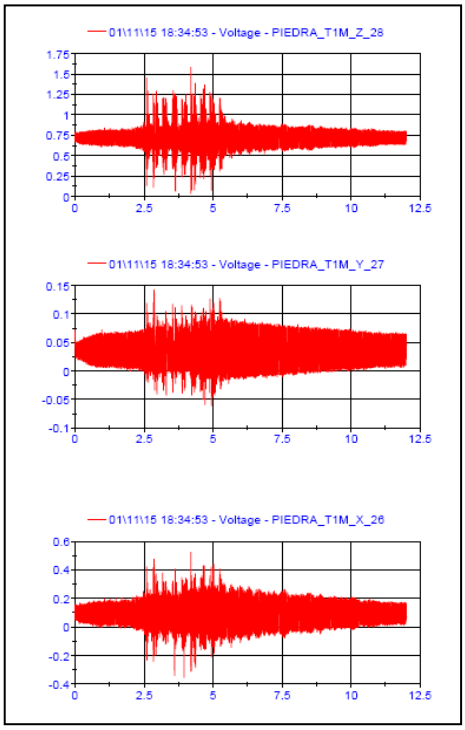

FIGURE 207: ACCELERATION COMPONENTS OF THE ACCELERATION MEASURED IN THE BALLAST PARTICLE PLACED AT T+1

The following figures are presented as examples of the display of a signal in the time and frequency domain (Figure 208) and the effect of applying different filters to the same signal (Figure 209). In this case, the vertical component of the acceleration measured in the particle located at T-4 for the test train that passed at 03:17 (data in the file named as 021115_031742) is shown.

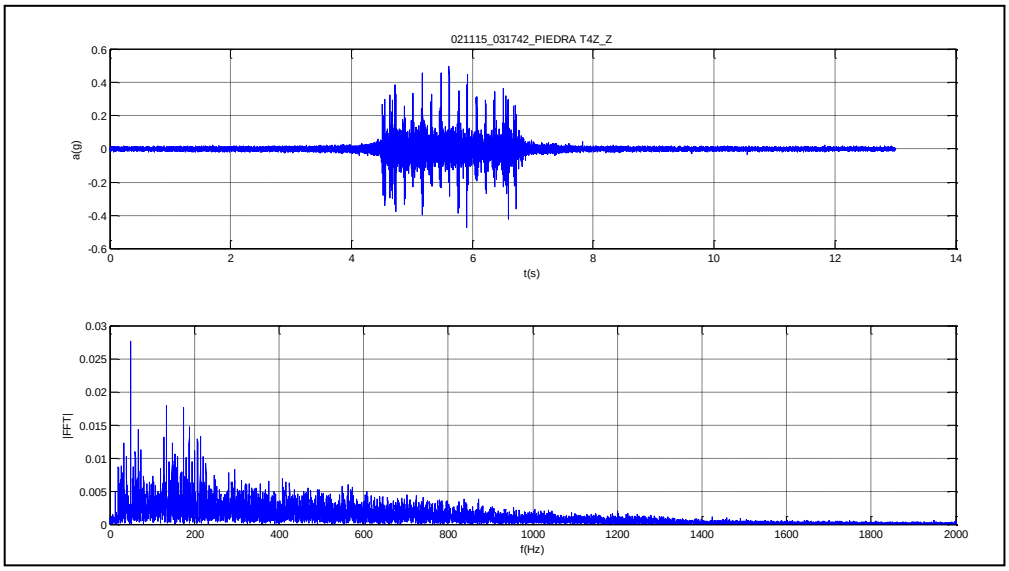

FIGURE 208: TIME SIGNAL (ABOVE) AND SPECTRUM (BELOW). (TEST TRAIN AT 03:17)

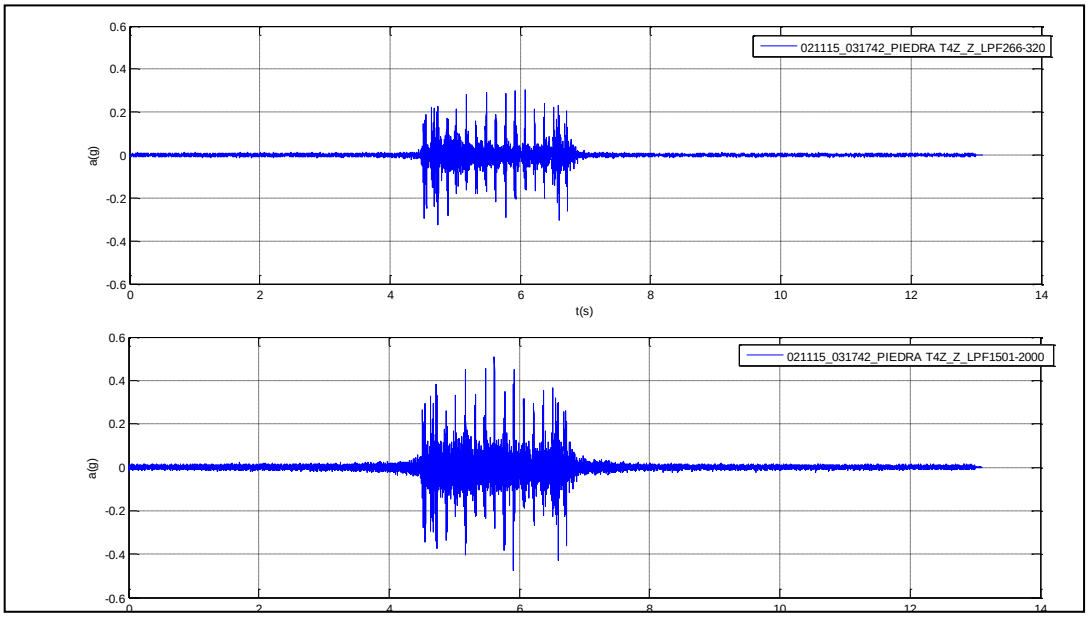

Figure 209: Signal after applying a LPF of 265Hz (above) and after applying a LPF of 1500Hz (below) (Test train at 03:17)

The spectrum in Figure 208 reveals that the bulk influence of the train pass-by in the particle acceleration is below 250 Hz while above 1500 Hz there is no signal. Therefore, the raw signal and the one obtained after applying a 1500Hz LPF are almost the same.

On other hand, according to the procedure followed by ADIF, it is possible to evaluate the maximum acceleration registered calculating the average of the positive and negative peaks.

As an example of that, the following figures are presented: Figure 210 shows the raw time signal and its spectrum of the vertical component of the sensor put close to T-4 for the test train recorded at 02:12 (data in the file named as 02112015_021207).

Figure 211 is a zoom of that raw signal that can be used to estimate the average of the peaks.

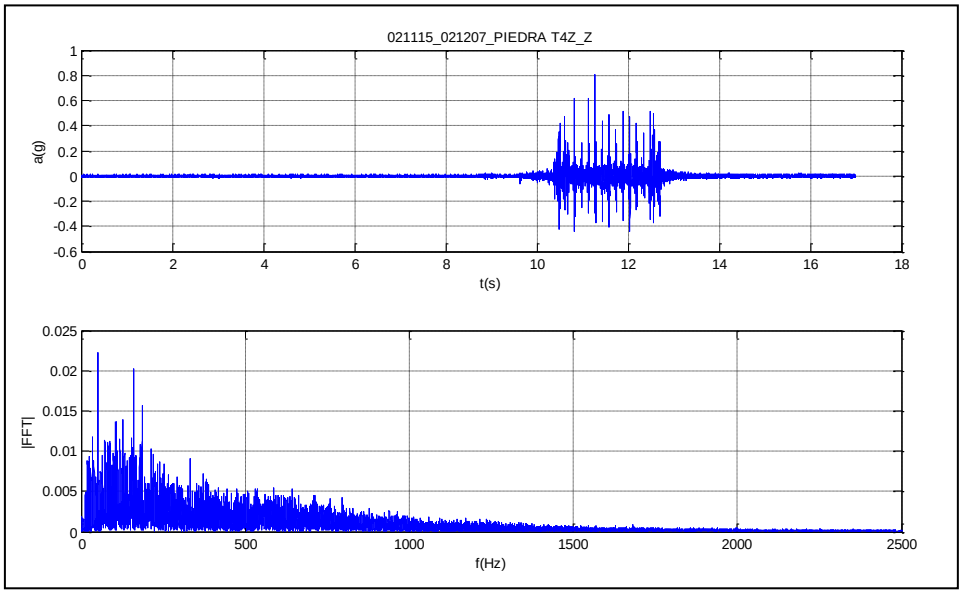

Figure 210: Time signal and spectrum of the test train passed at 02:12

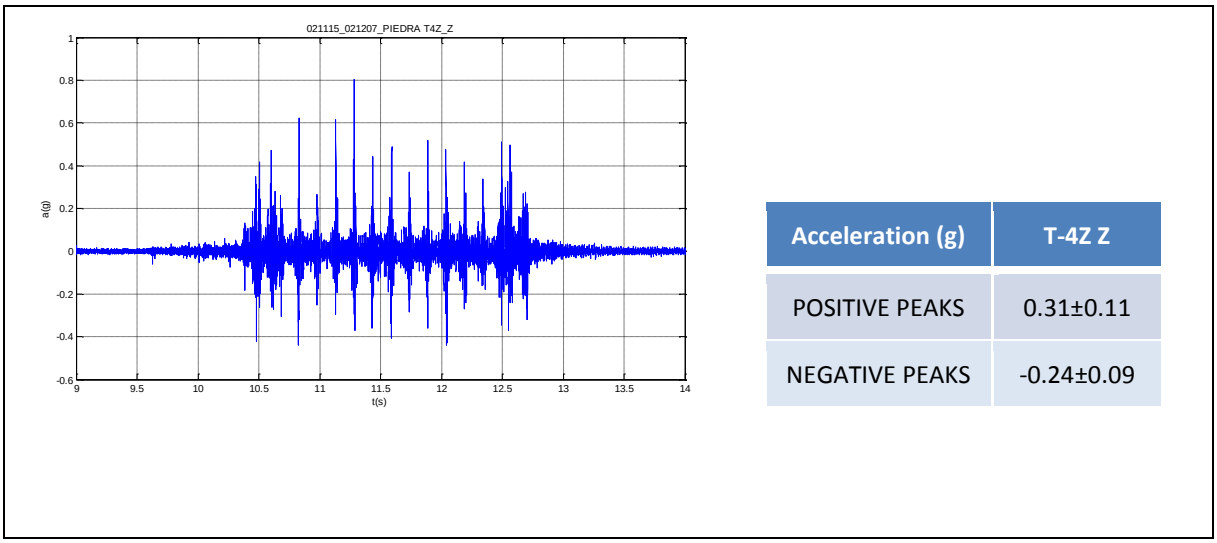

Acceleration (g)	T-4Z Z
POSITIVE PEAKS	0.31±0.11
NEGATIVE PEAKS	-0.24±0.09

Figure 211: Zoom of the time signal of the test train passed at 02:12 (left). Average of the maximum and minimum peaks of this raw signal (right)

There are other methods to evaluate the acceleration signals, for instance in the frequency domain, that can also be used.

Finally, these raw data can be compared with those ones obtained by ADIF in the same in-situ campaign.

VERTICAL ACCELEROMETERS

Four vertical accelerometers were installed: three stacked at different sleepers and one in the rail between the strain gauges, as can be seen in Figure 200. FFT is calculated for each signal and then applied the appropriate LPF.

Figure 14 shows the filtered data of the accelerometer placed in the rail for the AVRIL test train that passed at 02:12 (data in the file named as 02112015_021207).

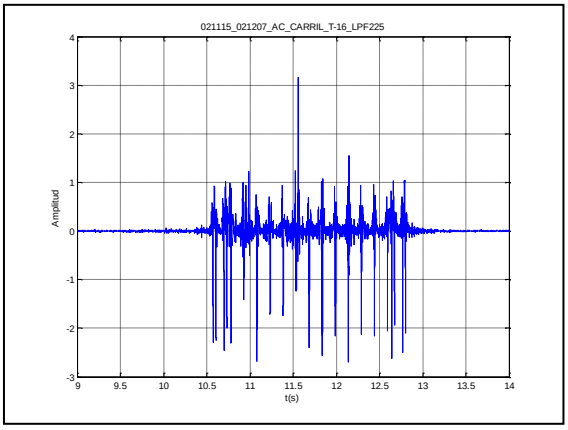

Figure 212 Filtered signal of the vertical accelerometer in the rail (Test train at 02:12)

As it will be shown later, this rail acceleration can be integrated to obtain the rail velocity and then compared with the velocity signal obtained with the geophone placed at the same position (Figure 217).

Figure 213 shows the different signals obtained with the accelerometers placed in the sleepers.

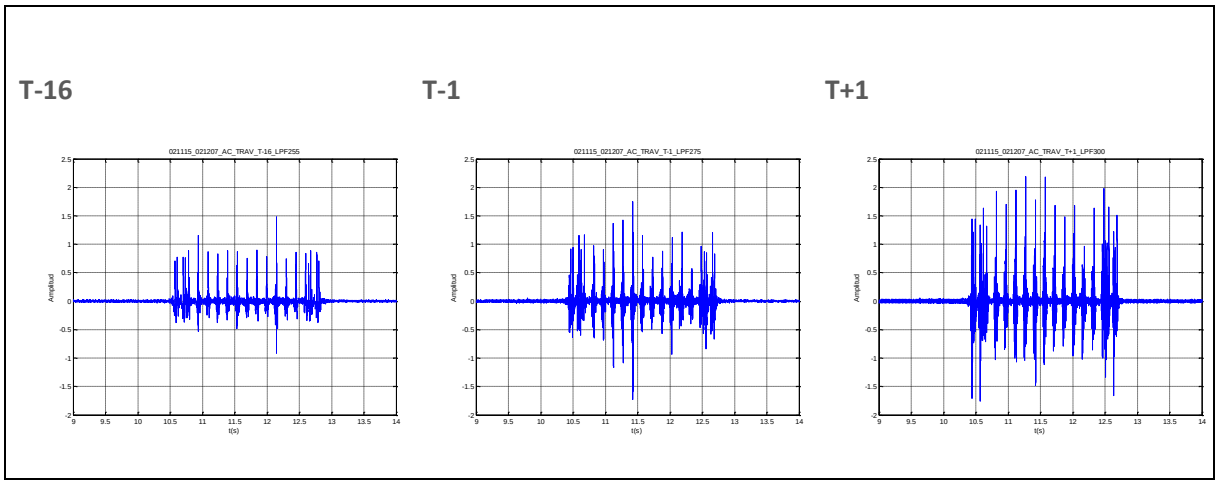

Figure 213: Filtered signals of vertical accelerometers installed in different sleepers (Test train at 02:12)

At a first sight, when looking at raw accelerograms, it is not possible to see the influence of the wheel loads in the rail or the sleeper due to the presence of a high noise, but using a 250 Hz Low Pass Filter (LPF) the signals reveal that influence. As examples, Figure 214 shows the signal of the accelerometer placed in the rail and Figure 215 the one placed in a sleeper, for the second pass of the AVRIL test train. The peaks in the green lines represent the accelerations produced by the wheel passing-by.

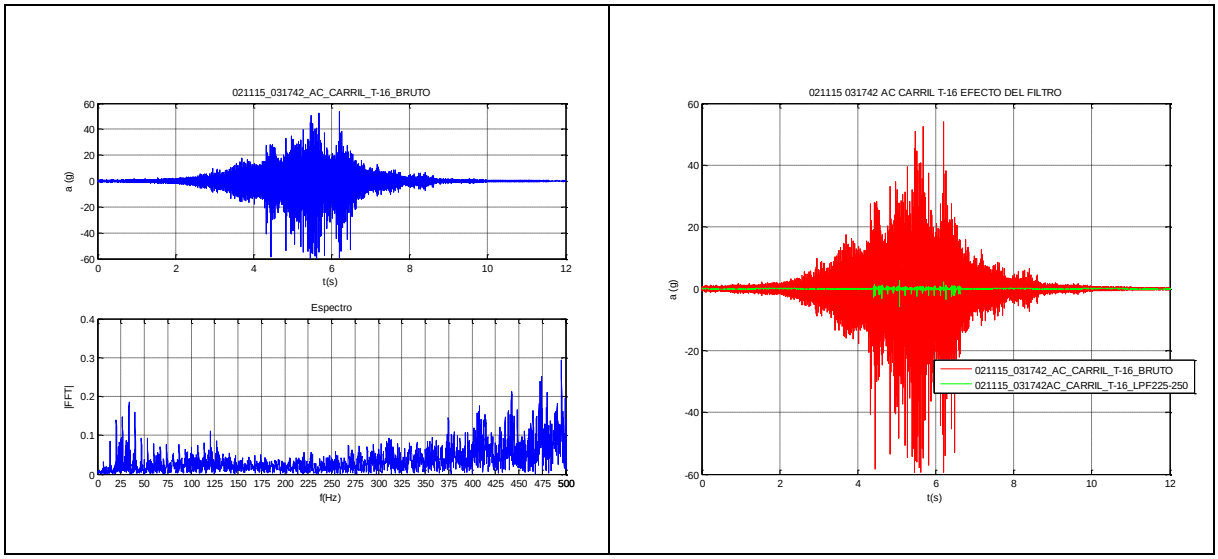

Figure 214: Rail acceleration for the AVRIL train at 03:17. Left: Raw signal and spectrum. Right: Effect of applying a 225 Hz LPF

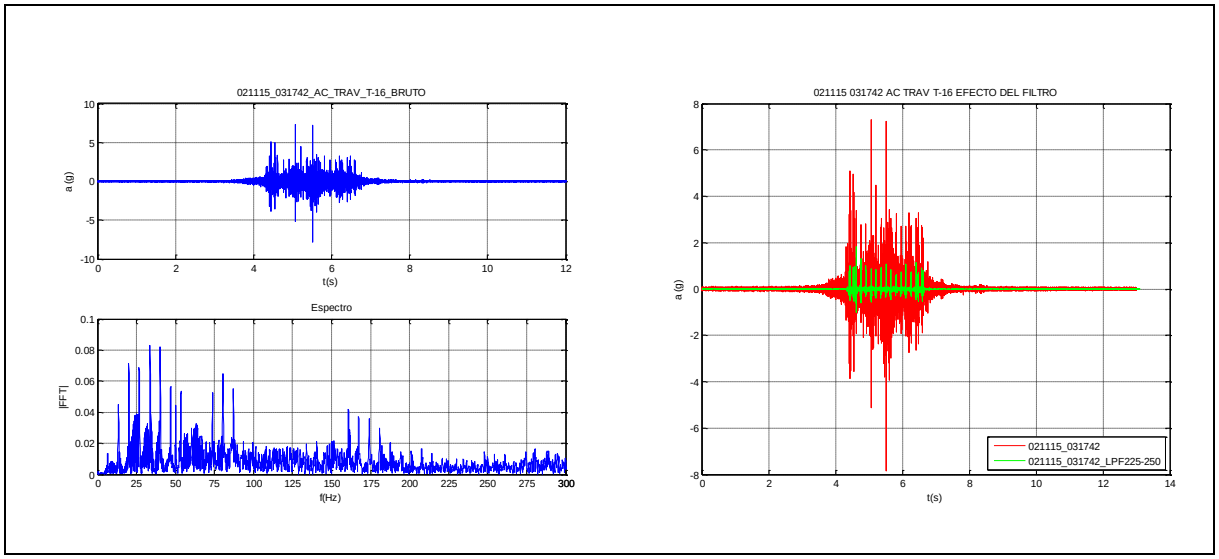

Figure 215: T-15 sleeper acceleration for the AVRIL train at 03:17. Left: Raw signal and spectrum. Right: Effect of applying a 225 Hz LPF

GEOPHONES

The same procedure applied to the accelerometers is used to analyse geophones. First FFT is calculated for each signal and then the appropriate LPF is applied. Furthermore it is possible to integrate the geophone signals to obtain rail deflections. This is particularly important for the geophone placed in the outer rail between the strain gauges in T-16 - T-15, because it will be used to obtain the track stiffness.

Figure 216 shows an example of the velocity values obtained in different positions.

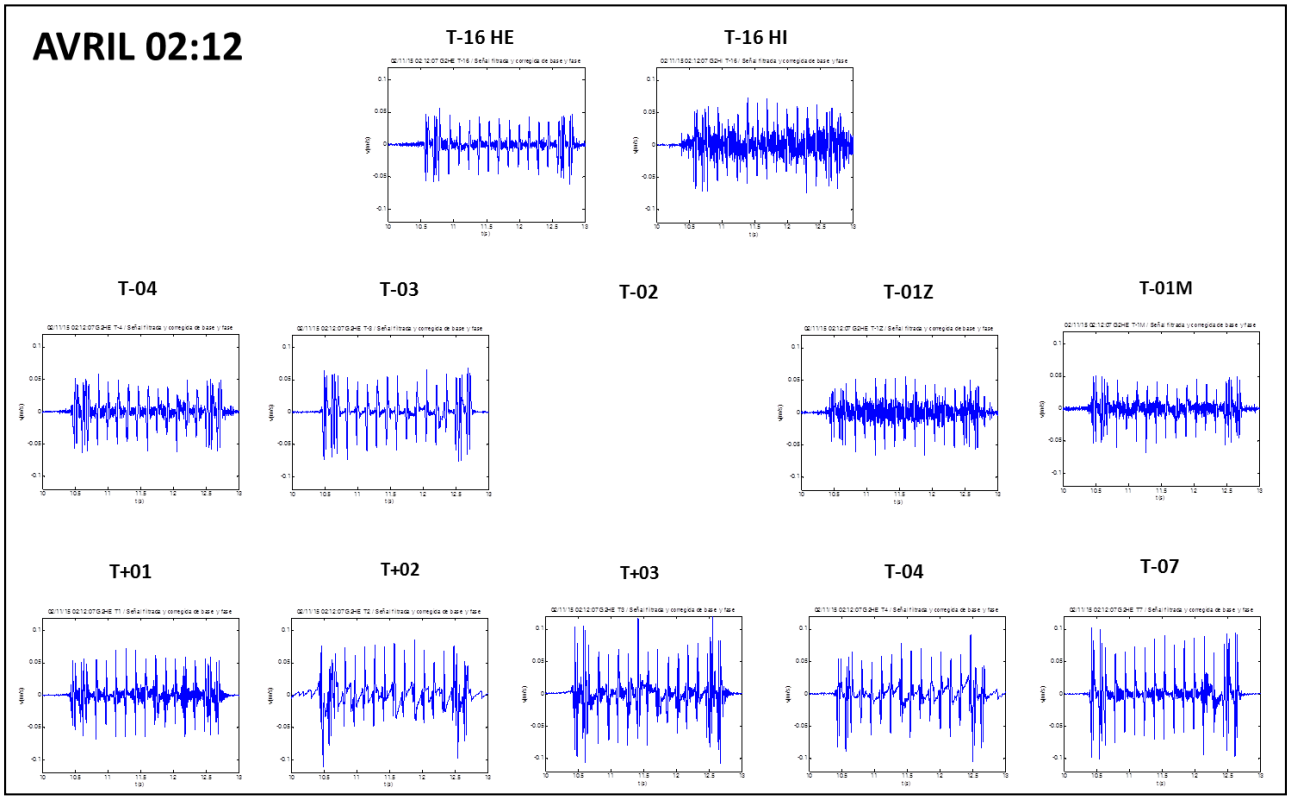

Figure 216: Velocities registered with the different geophones (AVRIL test train at 02:12)

Figure 217 shows the comparison of the velocity signal obtained directly with a geophone and the calculated one by the integration of the acceleration obtained with an accelerometer placed at same site. The deflection obtained integrating the geophone velocity signal can be observed in Figure 218.

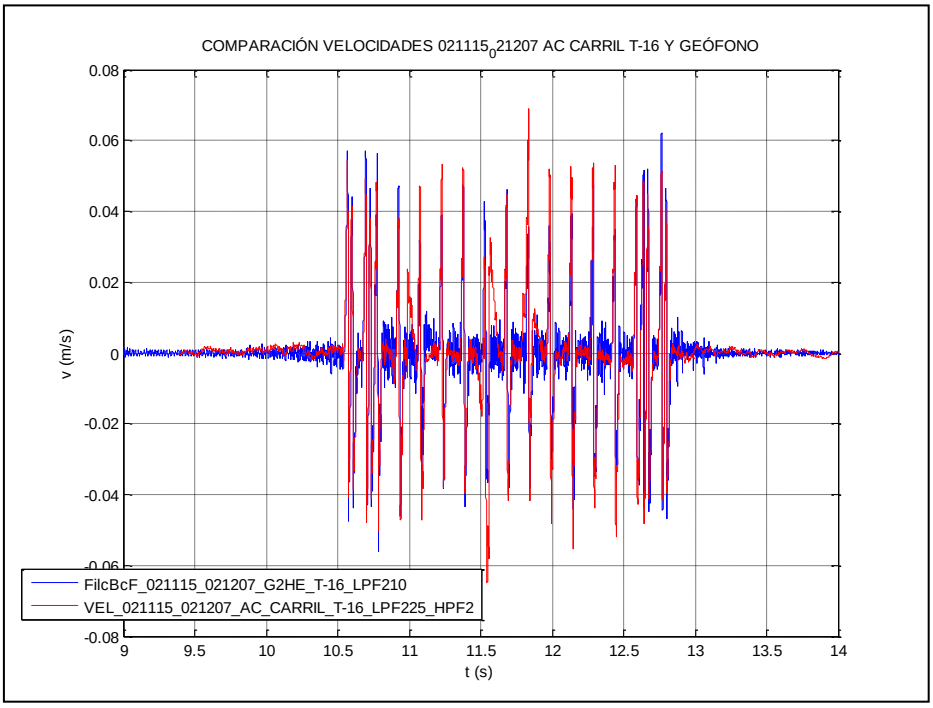

Figure 217: Comparison of the velocities obtained directly by the geophone and the integrated signal of the accelerometer; both sensors placed between the strain gauges in the outer rail T-16 T-15 (AVRIL train at 02:12)

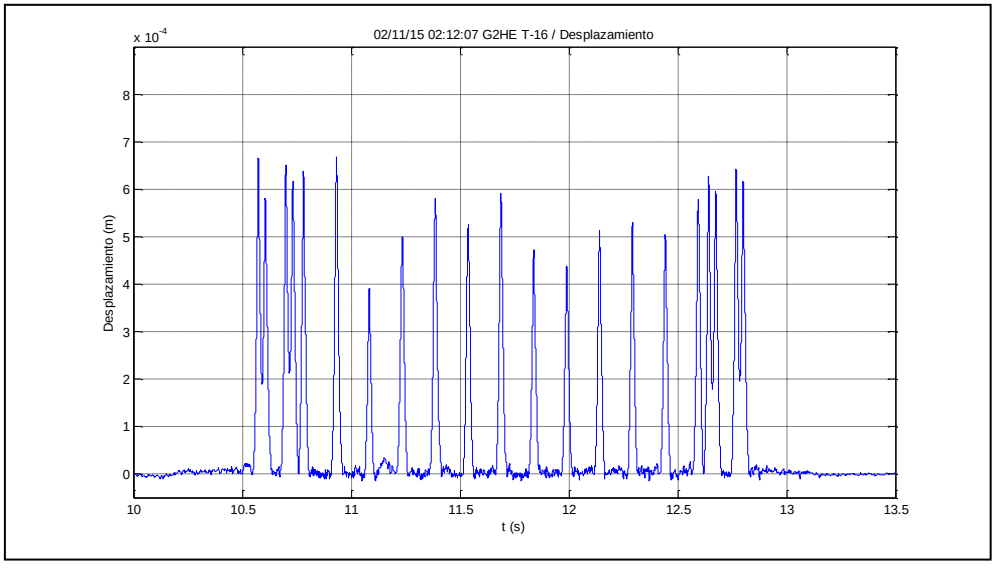

Figure 218: Rail deflections obtained from the integration of the velocity registered by the geophone placed between T-16 T-15 in the outer rail (AVRIL train at 02:12). Despite rail movement is downwards, the peaks are presented as positive.

LOADS

The measurement of wheel loads were made, as sketched in Figure 219, by finding the difference between the two shear forces induced in two points of the rail, 0,30 m apart, situated between two consecutive sleepers, by a travelling wheel passing over them.

First the shear stress is calculated multiplying the microstrain values recorded by the strain gauges by a constant that depends on the geometry of the rail. In this case the constant is:

$$k = (2 * 10^6 * 0.17344)\frac{kN}{\mu\varepsilon} = 346880\ \frac{kN}{\mu\varepsilon}$$

After that, the FFT of the signal is calculated and the appropriate filter is applied. Finally, the shear forces values are subtracted to obtain the load.

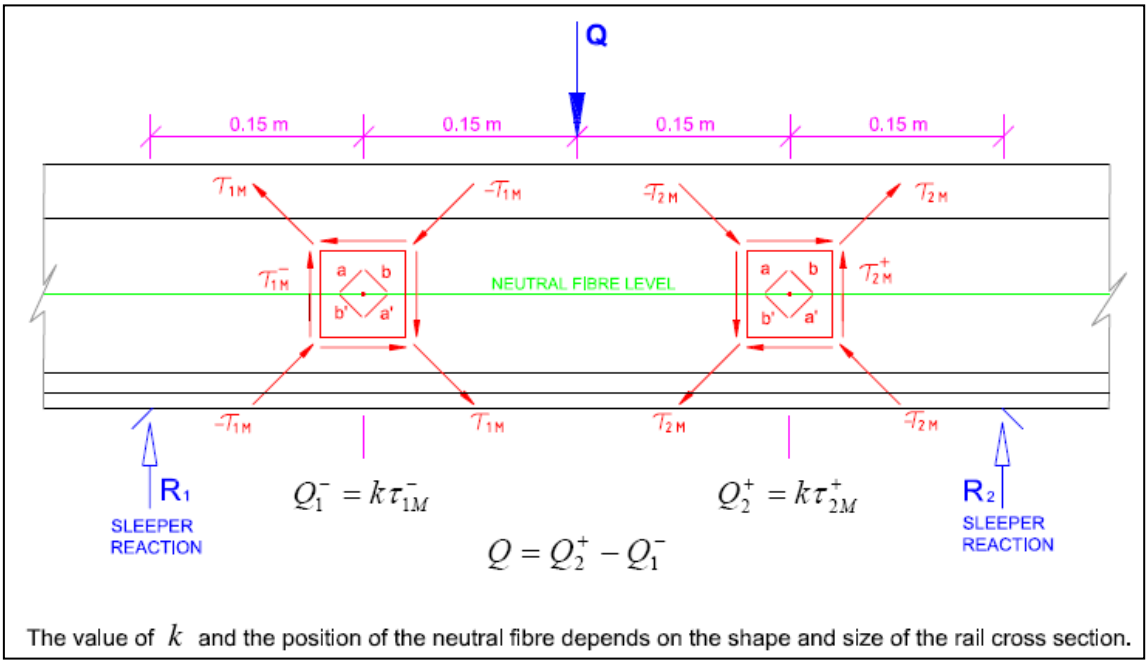

Figure 219: Schematic arrangement of strain gauge gridlines for measuring wheel loads

Figure 220 is an example of the load time history obtained for the AVRIL test train that passed at 02:12.

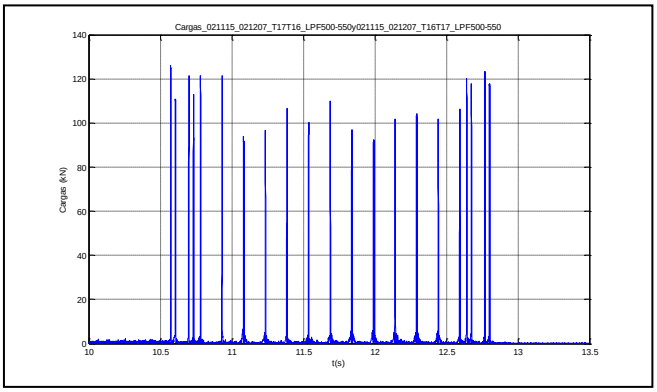

Figure 220: Load calculated signal (AVRIL test train at 02:12)

It is possible to obtain the track stiffness by dividing the calculated loads and deflections, as it is shown in Figure 221.

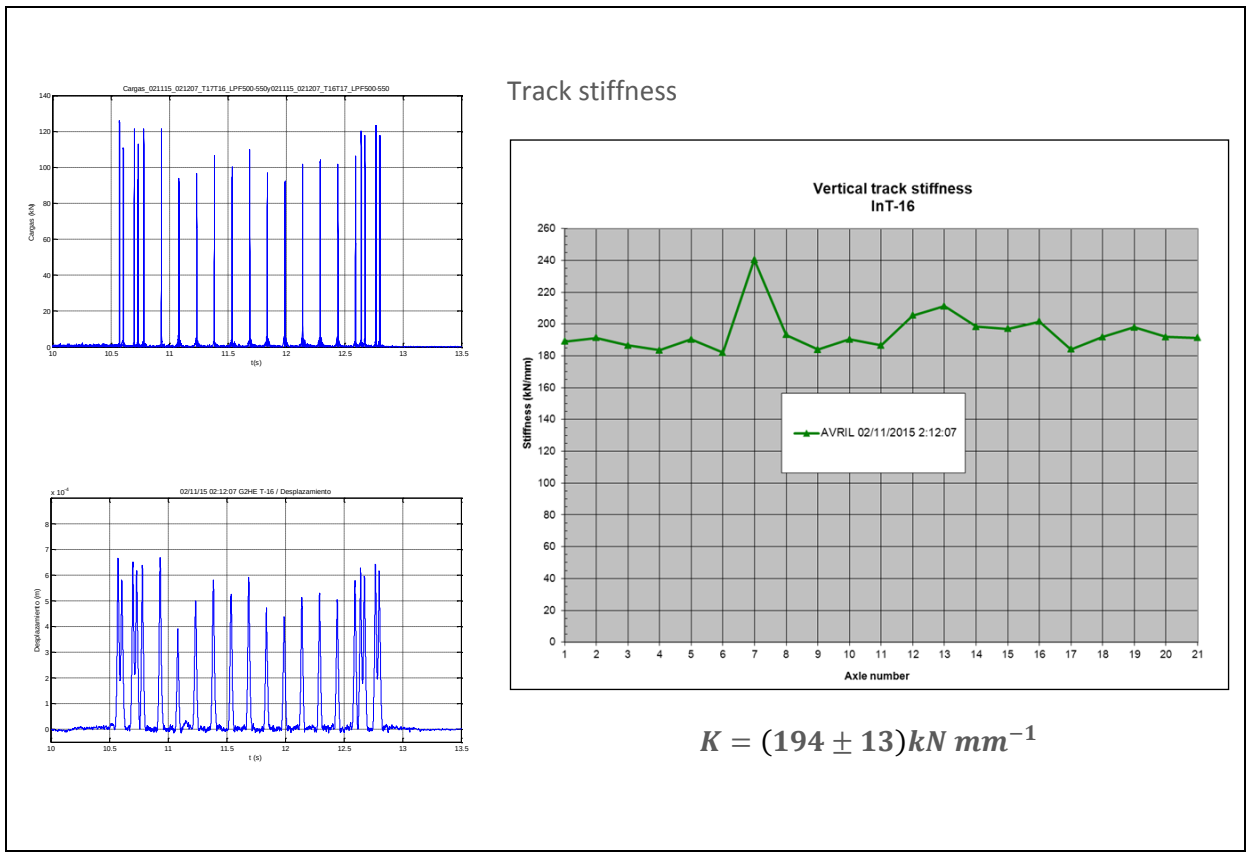

Figure 221: Track stiffness (AVRIL test train at 02:12) calculated for each wheel. The mean value and the standard deviation have also been obtained

Track stiffness seems to be higher than in regular tracks without bridges. The existing strain gauges are 10 m far from the beginning of the structure and there the embankment is still affected by the

transition zone are the materials used are stiffer than in conventional embankments far from transition zones. Because of that it has been proposed to install a new strain gauge set a bit far away from the bridge in the next in-situ campaign.

Summary

CEDEX and ADIF performed an in-situ test campaign in PK 72+000 of the High Speed Line Madrid-Barcelona to obtain real data to verify calculation methods and models to study the dynamical effects in structures due to the pass-by of trains.

In the test site there is a span bridge of 8 m long with its corresponding transition zone of 27 m long.

The instrumentation installed in this test site consisted on:

- Strain gauges to measure the wheel loads
- 2 Hz geophones installed in the rail to measure the velocity of the vibration in the rail produced by the trains pass by. To obtain the deflections integrating these velocity signals is also possible.
- Vertical accelerometer stacked in the rail.
- Accelerometers stacked in sleepers.
- Triaxial accelerometers installed inside different ballast particles.

Some of the data obtained has been analyzed to be used as examples of the results obtained using the protocol developed by CEDEX. The possibility of obtaining track stiffness from the measurements must be highlighted.

All the raw data recorded in this campaign is collected in the annexed CD for other C4R partners to use them in their tasks.

Besides that, data recorded in this in-situ campaign can be compared with those acquired by ADIF, can also be used as a source to validate information obtained in CEDEX Track Box and, finally, could help to calibrate the models proposed by KTH.

ADIF and CEDEX are planning to carry out a new in-situ test campaign to study other effects produced by the pass-by of trains. The new in-situ campaign is expected to be developed in May or June 2016.